FOG

Freiberg Online Geology

FOG is an electronic journal registered under **ISSN 1434-7512**

2006, VOL 16

Nadir Eraifej

Gas Geochemistry and Isotopic Signatures in the deep Thermal waters in Jordan

256 pages, 77 figures, 53 tables, 210 references

Acknowledgment

The author is indebted to his supervisor Prof. Dr. habil Broder Merkel, Dean of the Faculty Geosceinces, Geo-engineering and Mining; Head of the Geology Department and Chair of Hydrogeology for his invaluable guidance, encouragement, patience that have taught me not only the scientific research but also the ethics of being a professional scientist also great thanks for his financial support for this study, with out this support this research could not come to the light.

I would like to express my gratitude to Katholic Academic Foreigner Service (Katholischer Akademischer Ausländer Dienst-KAAD) for the finance of my German language course, the scholarship that I was given for the period of my study and the financial support of my field trips to Jordan. Many thanks also go to the DFG-PHD program for the considerable financial support during the fieldwork in Jordan.

I would like to thank Prof. Dr. habil Detlef Hebert for his fruitful discussion, efforts for helping in interpretations of the isotope analysis and the analysis of the tritium isotopes. Special thanks goes to Dr. Marion Tischomirowa for the fruitful discussion and supplying with the isotopes literature. Many thanks go to Prof. Dr. Klaus Peter Seiler from the GSF for the analysis of stable isotopes.

I would like to express my deepest thanks to Dr. Nizar Abu-Jaber for his fruitful discussion, for providing the field equipments and continuous encouragement. I am indebted to Prof. Dr. Elias Salameh, who gave me the chance to continue my postgraduate studies in Germany, continuous support and encouragement through the years of my study. I would like to acknowledge the help of Prof. Dr. Omar Rimawi for his advise, providing the facilities and transportation for the research in Jordan. Special thanks goes to B.A.Chem. Ahmad El-Barishi for his help and supervision in the water chemical analysis in Jordan.

The author would like to express his grateful to the staff and colleagues of the Hydrogeology department, TU Bergakademie Freiberg: Dr. Britta Planer-Friedrich, Dipl.Geol. Susane Stadler, Dr. Christian Wolkersdorfer, Dipl. Chem. Peter Volke, Mrs Heike Kluge, Dr. habil. Peter Dietrich, Dr. Volkmar Dunger and Dipl. Chem. Hans-Joachim Peter who helped and advised me through the course of my study and research.

Many Thanks goes to the Ministry of Water and Irrigation in Jordan and their workers especially Eng. Nidal Khaliefeh and Eng. Zakaria Zohdy for supplying me with the different literature, which was very useful in my research. Special thanks goes to the Natural Resources Authority staff: M.Sc. Julia Sahawaneh, Dr. Ali Sawarieh and M.Sc. Emad Akawai.

Many thanks go to my special friends Dipl. BWL Tatjana Simukova, Dr. Ziad Makhamreh, Dipl. Min. Manuela Junghans, Dipl. Eng. Abdulkader Kadauw, M.Sc. Min. Nima Nezafati, and Dr. Jihad Almahamid for their support and encouragement through out the research time.

A words of appreciation and love goes to my family: father, mother, brother Hyatham and his family Julina, Munir and Talar for their support, words of encouragement and patience. Without this support it would have been impossible to complete my dissertation.

ABSTRACT

The hydrochemistry and isotopic signatures of the thermal waters along the eastern side of the Dead Sea Transform (DST) in Jordan were investigated. The main objectives of this study were: to determine the origin and mean residence time of the thermal waters along the DST, to determine depth and nature of ground water circulation in the DST and to determine the possible source for the chemical and gaseous constituents along with the other relative parameters.

The area of investigation contains geological formations ranging between the Late Proterozoic and recent age. The thermal waters tap two aquifers: the upper cretaceous limestone aquifer (B2/A7) and the lower sandstone aquifer (Zarqa and Kurnub).

A new sampling methodology to trap the natural gases H_2S, CO_2 and CH_4 were developed, tested and verified in the field. Two sampling campaigns were carried out to sample the thermal water springs and wells. The samples were collected for the chemical analysis, Rare Earth Elements (REE) and the isotopes: ^{3}H, $\delta^{18}O_{water}$, δD_{water}, $\delta^{34}S_{sulfate}$ and $\delta^{18}O_{sulfate}$ $\delta^{13}C_{CO2}$, Helium and Neon.

The water types of each aquifer were determined by means of chemical criteria and compared with the location and the salinity. A statistical approach using cluster analysis supported by Kruskal-Wallis and Mann-Whitney tests classified the thermal waters into two main groups: A and B. Group A consist of two subgroups: A_1 and A_2. Group A_1 includes the fresh water wells and springs that have the lowest salinity of the studied thermal waters and consist of two subgroups: A_{1a}, which represent the thermal waters that tap the Kurnub aquifer but their chemical characteristics are similar to the B2/A7 waters; group A_{1b} which includes the thermal waters that tap the B2/A7. Group A_2 includes the brackish wells and springs that taps the Kurnub aquifer plus two thermal waters from the B2/A7 aquifer: Abu-Zyad and Abu-Thableh, which have a high percent of Kurnub water contribution. Group B includes the thermal waters that tap the Zarqa aquifer.

The Quartz, Quartz steam loss and the Isotope SO_4-H_2 geothermometer (after Kuskabe (1975)) were found to be suitable for calculating the reservoir temperatures. The K/Mg geothermometer was found to be suitable for the B2/A7 aquifer but not for the lower sandstone aquifer because it gives a very low reservoir temperature. Depending on the Quartz geothermometers the water circulation depth were calculated.

On the $\delta^{34}S_{Sulfate,}$ $\delta^{18}O_{Sulfate}$ diagram, the thermal waters plot on a mixing line between two end members: the evaporites and the oxidation of sulphides. Most of the sulfate is caused by the dissolution of evaporites from the rock matrix. Three samples are more affected with the second end member: Al-Kafreen, Afra/Sawna and Afra/Maqla.

By comparing the $\delta^{13}C_{CO2}$ values with the $\delta^{13}C_{HCO3}$ values, the system was found to be not in equilibrium, which means that the CO_2 have other sources. The CO_2 seems to be derived from oxidation-reduction processes of the organic matter present in the rock matrix.

The thermal waters are Tritum free, which indicates, that all those water components are old and the recharge have occurred before 1952 or the share of younger water (recharged after 1952) is very small

The $^{3}H/^{3}He$ age determination method was not suitable to give mean residence time estimation due to additional helium (not a tritium decay product), which has invaded the system. The excess helium is assumed to be coming from the mantle exhalation bounded more or less to the deep faults in the Dead Sea Transform.

The B2/A7 thermal waters are associated with the Mediterranean meteoric water line (MMWL). This indicates that those waters occurred under climatic conditions that are dominating Jordan and the surrounding areas those days. The thermal waters of the lower sandstone aquifer are distributed in three groups on the δD-$\delta^{18}O$ diagram: the first group is associated with the Global Meteoric Water Line (GMWL), indicating that the pure lower sandstone aquifer thermal waters are not being affected by the evaporation effect; the second group are located below the GMWL, indicating that the lower aquifer waters were affected by evaporation during precipitation; the third group is located between the GMWL and the MMWL representing the lower aquifer thermal waters that are mixed in different ratios with other water sources.

ZUSAMMENFASSUNG

In der vorliegenden Arbeit wurden die Hydrochemie und die Isotopensignale von Thermalwässern entlang der östlichen Seite des Dead Sea Transform (DST) in Jordanien untersucht. Die Hauptziele dieser Untersuchungen waren: die Bestimmung der Herkunft und der mittleren Verweilzeiten von Thermalwässern entlang des DST, die Bestimmung der Tiefe und Art der Grundwasserzirkulation im DST und die Ermittlung der möglichen Quelle für chemische und gasförmige Bestandteile sowie anderer Parameter.

Das Untersuchungsgebiet beinhaltet geologische Formationen seit dem späten Proterozoikum bis heute. Die Thermalwässer stehen mit zwei Aquiferen in Verbindung: der Kalksteinaquifer aus der Oberen Kreide (B2/A7) und der darunterliegende Sandsteinaquifer (Zarqa und Kurnub).

Eine neue Probenahmemethode zur Fixierung der natürlichen Gase H_2S, CO_2 und CH_4 wurde entwickelt und im Feld gestestet. Zwei Probenahmekampagnen fanden zur Beprobung von Thermalquellen und Brunnen statt. An diesen Proben wurden die Hauptinhalstoffe, Spurenelemente incl. seltene Erden Elemente (SEE) und die folgenden Isotopie bestimmt: ^{3}H, $\delta^{18}O_{Wasser}$, δD_{Wasser}, $\delta^{34}S_{Sulfat}$ and $\delta^{18}O_{Sulfat}$ $\delta^{13}C_{CO2}$, Helium und Neon.

Die Wassertypen in den einzelnen Aquiferen wurden mit Hilfe chemischer Kriterien bestimmt und anschließend mit den Lokalitäten und der Salinität am Standort abgeglichen. Statistische Auswertung mittels Clusteranalyse, Kruskal-Wallis und Mann-Whitney Test ergaben eine Klassifikation der Thermalwässer in zwei Gruppen (A und B). Gruppe A besteht aus zwei Untergruppen: A_1 and A_2. Gruppe A_1 beinhaltet Süßwasserbrunnen und Quellen, die die niedrigste Salinität der untersuchten Thermalwässer aufweisen. Diese bestehen wiederum aus zwei Untergruppen: A_{1a} beschreibt Thermalwässer im Kontakt mit dem Kurnub Aquifer, ihre wasserchemischen Eigenschaften ähneln den B2/A7 Wässern. Gruppe A_{1B} beinhaltet Thermalwässer, die in Kontakt mit B2/A7 stehen. Gruppe A_2 besteht aus Brackwasserbrunnen und Quellen des Kurnub-Aquifers und zwei Thermalwässern des B2/A7 Aquifers: Abu-Zyad und Abu-Thableh, die stark durch Kurnub Wasser beeinflußt sind. Gruppe B beinhaltet die Thermalwässer des Zarqa Aquifers.

Die Quarz, Quarz-Entgasung und die SO_4-H_2 Isotopen-Geothermometer (nach Kuskabe, 1975) erwiesen sich als geeignet für die Berechnung der Reservoirtemperaturen. Das K/Mg Geothermometer eignete sich für den B2/A7 Aqufer, aber nicht für den unterliegenden Sandsteinaquifer, da es sehr niedrige Reservoirtemperaturen berechnet. In Abhängigheit der Quarz-Geothermometer wurden die Wasserzirkulationstiefen berechnet.

In dem $\delta^{34}S_{Sulfat,}$ $\delta^{18}O_{Sulfat}$ Diagramm liegen die Thermalwässer auf einer Mischungslinie zwischen zwei Endgliedern: Den Evaporiten und der Sulfidoxidation. Ein Großteil der Sulfate stammt aus der Lösung von Evaporiten aus der Gesteinsmatrix. Drei Proben waren stärker durch das zweite Englied beeinflusst: Al-Kafreen, Afra/Sawna und Afra/Maqla.

Durch den Vergleich der $\delta^{13}C_{CO2}$ Werte mit den $\delta^{13}C_{HCO3}$ Werten wurde sichtbar, daß das System nicht im Gleichgewicht steht, was bedeutet, daß das CO_2 andere Quellen hat. Das CO_2 ist möglicherweise das Ergebnis von Redoxreaktionen des organischen Kohlenstoffes in der Gesteinsmatrix.

Die Thermalwässer beinhalten kein Tritium. Dies bedeutet, daß alle Wasserkomponenten alt sind, Neubildungsprozesse von 1952 stattgefunden haben oder daß der Jungwasseranteil (nach 1952 neugebildet) sehr gering ist.

Die $^3H/^3He$ Datierungsmethode erwies sich als nicht anwendbar, da zusätzliches Helium (nicht aus dem Zerfall von Tritium) vorhanden war, das in das System eingedrungen ist. Der Heliumüberschuß ist vermutlich der Mantelexhalation zuzuordnen, die an die tiefgreifenden Störungen in dem Dead Sea Transform gebunden ist.

Die B2/A7 Thermalwässer liegen auf der “Mediterranean meteoric water line” (MMWL). Dies weist auf ein Entstehen dieser Wässer unter den bestehenden klimatischen Bedingungen Jordaniens und der Umgebung an. Die Thermalwässer des unteren Sandsteinaquifers bilden drei Gruppen im δD-$\delta^{18}O$ Diagramm: Die erste Gruppe steht mit der “Global Meteoric Water Line” (GMWL) in Verbindung und zeigt, daß die rein aus dem Sandstein stammenden Thermalwässer nicht durch Evaporation beeinflußt sind. Die zweite Gruppe liegt unterhalb der GMWL und weist auf Evaporationsprozesse während der Niederschlagsbildung hin. Die dritte Gruppe liegt zwischen der GMWL und der MMWL und ist repräsentativ für die Thermalwässer des unteren Aquifers, die in in verschiedenen Anteilen Mischung mit anderen Wässern erfahren haben.

TABLE OF CONTENTS

LIST OF FIGURES

LIST OF TABLES

LIST OF APPENDICES

ABBREVIATIONS

#	Number
%	Percentage
<	Less than
>	More than
±	Plus Minus
≤	equal or less than
≥	equal or more than
^{12}C	Carbon-12
^{13}C	Carbon-13
^{14}C	Carbon-14
^{14}N	Nitrogene-14
^{16}O	Oxygen-16
^{17}O	Oxygen-17
^{18}O	Oxygen-18
1^{st}	First
^{20}Ne	Neon-20
^{22}Ne	Neon-22
^{238}U	Uranium-238
2^{nd}	Second
^{32}S	Sulfur-32
^{33}S	Sulfur-33
^{34}S	Sulfur-34
^{36}S	Sulfur-36
^{3}He	Helium-3
^{3}H	Tritium
^{4}He	Helium-4
$^{o}/_{oo}$	Per mil
^{o}C	Degree centigrade
α	Fractionation factor
β	Beta
δ	Delta
μmohs/cm	Micro Mohs per Centimetre
μS/cm	Micro Siemens per centimetre
τ	Tao
A1/2	Naur Formation
A3	Fuheis Formation
A4	Hummar Formation
A5/6	Shuaib Formation
A7	Wadi Es Sir Formation
AHP	Al-Hasa Phosphortite Formation
Al	Alluvim
AM	Ain Mousa Formation
AR	Abu Rweis Formation

ASL	Above sea level
AZ	Azab Group
B1	Wadi Umm Ghudran Formation
B2	Amman Formation
B3	Muwaqar Formation
B4	Rijam Formation
B5	Shallala Formation
B	Baslat
BDS	Burj Dolomite Shale Formation
BP	Before present
BSL	Below sea level
Cc	Cubic Centimeter
CFC	Chloro Floro Carbon
Ct	Calcrete
Cu	Cupper
DC	Dana Conglomerate Formation
D	Deuterium
DH	Dahab Formation
DI	Disi Formation
DO	Dissolved oxygen
DR	Dardour Formation
DS	Dead Sea
DST	Dead Sea Transform
EC	Electrical conductivity
E_H	Redox potential
ESCWA	Economic and Social Commission for Western Asia
F	Fuheis Formation
F/H/S	Fuheis/Hummar/Shuaib undifferentiated
g/l	Gram per Liter
GMWL	Global Meteoric Water Line
GPS	Global Positioning System
GR	Ghor Al-Katar Formation
HA	Hammam Formation
He_{equi}	Equilibrium Helium
He_{excess}	Excess Helium
He_{prim}	Primordial Helium
He_{rad}	Radiogenic Helium
He_{trit}	Tritiogenic Helium
H	Hummar Formation
HI	Hihi Formation
HL	Husban Limestone Formation
HS	Hanneh Siltstone member
i.e	That is
IAP	Ion Activity Product
ICP-MS	Inductivley-coupled Plasma-Mass Spectrometry

IN	Umm Ishrin Formation
IR	Irkheim Formation
JGMP	Jordan Geology Mapping Project
JISM	Jordan Institution for Standards and Metrology
JV	Jordan Valley
K/T	Cretaceous/Tertiary
K1	Arda Formation
K2	Subeihi Formation
Ka	Kilo Anom
Km^2	Squared Kilometer
Km^3	Cubic Kilometer
Km	Kilo Meter
Ksp	Solubility product
L/Km^2	Liter per Squared Kilometer
LM	Lisan Marl
LSI	Langlier Saturation Index
m^2/d	Squared Meter per Day
m^2/s	Squared Meter per Second
MCM	Muwaqar Chalk Formation
meq/l	Milliequivalent per Liter
mg/l	Milli Gram per Liter
MK	Mukheiris Formation
ml	Milli Liter
m	Meter
MMWL	Mediterranean Meteoric Water Line
MN	Ma'in Formation
MUG	Mughaniya Formation
Myr	Million Year
ND	Numayri Dolomite member
NL	Naur Limestone Formation
N	Neutron
NRA	Natural Resources Authority
NR	Nimr Formation
pH	Acidity value
QU	Quani Diorite Formation
r	correlation coefficient
REE	Rare Earth Elements
RM	Ramla Formation
RSC	Residual Sodium Carbonate
SAR	Sodium Adsorption Ratio
SB	Salib Formation
SC	Sarmouj Conglomerate
SF	Saham Formation
SHC	Shagur Conglomerate Formtaion
SI	Saturation Index

SL	Silal Formation
S	Shuaib Formation
s	Soils
SSP	Soluble Sodium Percent
$T_{1/2}$	Half life
TDS	Total Dissolved Solids
TH	Total Hardness
TL	Tayyiba Limestone Formation
Tr	Travertine
TS	Tayan Siltstone member
T	Temperature
TU	Tritium Unit
UI	Umm Irna Formation
URC	Umm Rijam Chert Formation
UT	Umm Tima Formation
V-PDB	Vienna Pee Dee Belemnite
WC	Waqas Conglomerate Formation
WG	Wadi Umm Ghudran Formation
WHO	World Health Organisation
WSC	Wadi Shallala Chalk Formation
WSL	Wadi Es Sir Formation
Z1	Ma'in Formation
Z2	Hmui Formation

1 INTRODUCTION

Thermal waters in Jordan are characterized by an average temperature of at least 5°C above the mean annual air temperature of its locality. They range in temperature from 31 to 60°C (Salameh and Rimawi 1984).

Thermal waters are found on both sides along the Dead Sea Transform (DST); the eastern part and the western part. The behavior of the groundwater systems at both sides of the rift are different (Arad and Bein 1986); because of the separation caused by a juxtaposition of aquifer on the flank with aquitards across the fault in the Rift Valley (Gvirtzman et al. 1997).

This study focuses on the thermal waters of the eastern part of the DST. In Jordan there are about 200 thermal springs, which are generally restricted to the rift zone between the southern end of the Dead Sea (DS) and the Yarmouk River in the north. The main springs are El-Hamme, North Shuneh well, Abu-Zyad Well, Waqas Well, Abu Thableh, Deir Alla (Abu El-Zeeghan) wells, Kafrain wells, Ma'in springs, Zara springs, Potash company wells, Iben Hammad spring, Burbaita spring, and Afra springs. The elevated temperature of many spring waters is the result of deep circulation under normal geothermal gradients (Salameh and Rimawi 1984). In the south, the thermal springs are restricted to Lower Cretaceous sandstones, whereas in the north the springs issue from Upper Cretaceous limestones and dolomitic limestones, (Salameh and Rimawi 1984).

1.1 Geography

The area of study (Fig. 1.1) is located along the eastern part of the Dead Sea Transform (DST); west of Jordan between 40-240 Palestin grid north (PGN) and 200 and 220 Palestine grid east (PGE). Table 1.1 shows the studied thermal waters, their coordinates in Palestine grid (PG) and tapping aquifers.

1.2 Geomorphology

In general, Jordan consists of different distinctive geomorphological and topographic features (Fig. 1.2) trending in north-south direction. These units are related to rifting along the Jordan Valley-Dead Sea-Wadi Araba-Red Sea line, which was formed in the last few tens of millions of years. The rift was formed along the same line (Salameh 1996).

The rift valley lies in the western part of the country. Generally it trends south north from the Gulf of Aqaba through the Dead Sea to lake Tiberias. According to Neev and Emery (1967), the elevation of the bottom of the valley ranges from sea level in Aqaba at the shores of the Red Sea to around 240 m ASL at a distance of 80 km to the north. From that point it drops gradually to about 417 m BSL (in the year 2005) at the shores of the Dead Sea and 750 m BSL at the bottom of the Dead Sea, then to the north of Dead Sea floor the elevation arises to about 210 m BSL at the shores of lake Tiberias.

The rift valley has a length of 375 km. Its width decreases from about 30 km in Wadi Araba area in the south to about 4 km in lake Tiberias area in the north.

The high lands of Jordan, which are located east of the rift valley, rise to elevations of more than 1000 m ASL in Ajloun and Balqa in the north and to more than 1200 m ASL in Shoubak. At the eastern toes of the high lands one find the steppe or the plateau, which ranges in elevation from 1000 m ASL in the south to about 700 m ASL in the northeast. The southern desert is a flat area intersected by partly deep incised wadis, in the southeast it rises to 1000 m ASL that is the Aqaba mountains. The Ras El-Naqab escarpment is another feature, which drains to the Dead Sea; this part of Jordan is called the southern desert.

Table 1.1: The thermal waters studied, their coordinates in Palestine grid (PG) and tapping aquifers.

No	Well/spring	Type	PGN	PGE	Aquifer
1	EL-Mokhybeh	Well	235.071	215.860	Upper aquifer (B2/A7)
2	El-Hmmeh/Maqla	Spring	234.500	214.500	Upper aquifer (B2/A7)
3	El-Hammeh/Bajeh	Spring	234.548	214.504	Upper aquifer (B2/A7)
4	North Shuneh hot	Well	224.360	208.141	Upper aquifer (B2/A7)
5	Waqas	Well	216.200	209.160	Upper aquifer (B2/A7)
6	Abu-Zyad	Well	212.200	208.600	Upper aquifer (B2/A7)
7	Abu-Thableh	Spring	208.000	208.600	Upper aquifer (B2/A7)
8	Abu El-Zeeghan/1	Well	177.830	211.540	Lower aquifer (Zarqa)
9	Abu El-Zeeghan/2	Well	177.694	211.341	Lower aquifer (Zarqa)
10	Al-Kafreen	Well	140.511	214.722	Upper aquifer (B2/A7)
11	Zara/Istraha	Spring	112.094	203.481	Lower aquifer (Kurnub)
12	Zara/Maghara	Spring	112.102	203.670	Lower aquifer (Kurnub)
13	El-Seel El-Hami	Spring	109.112	203.381	Lower aquifer (Kurnub)
14	Tal El-Rojom	Spring	108.652	209.460	Lower aquifer (Kurnub)
15	Ma'in/El-Mabkhara	Spring	112.600	209.600	Lower aquifer (Kurnub)
16	Ma'in/El-Ameer	Spring	113.200	207.300	Lower aquifer (Kurnub)
17	Ma'in/El-Shallal	Spring	113.300	207.100	Lower aquifer (Kurnub)
18	TA1	Well	077.300	202.500	Lower aquifer (Kurnub)
19	TA2	Well	077.700	203.300	Lower aquifer (Kurnub)
20	Iben Hammad	Spring	078.300	203.200	Lower aquifer (Kurnub)
21	Burbyta	Spring	043.75	214.000	Lower aquifer (Kurnub)
22	Afra/Sawna	Spring	041.883	211.278	Lower aquifer (Kurnub)
23	Afra/Maqla	Spring	041.873	211.350	Lower aquifer (Kurnub)

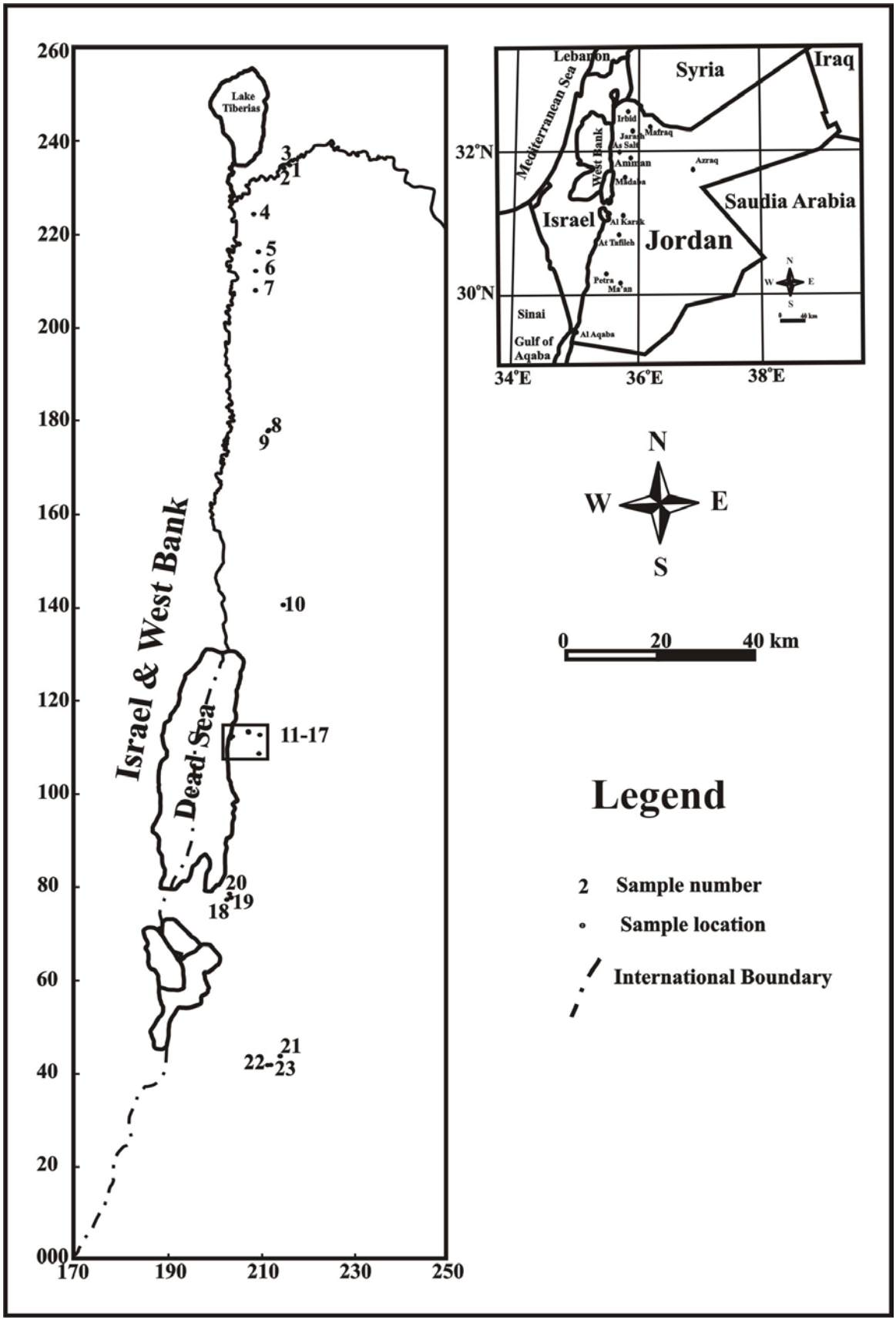

Fig. 1.1: Map of the thermal water sampling sites in Jordan.

The area of study and the neighbouring areas consist of four major distinctive topographic zones trending in general North-South. Those zones are:

1. High lands (above 800 meters);
2. Escarpment (0 ~ 800 meters);
3. Foot hills (-200 ~ 0 meters);
4. Rift valley (-417 ~ -200 meters).

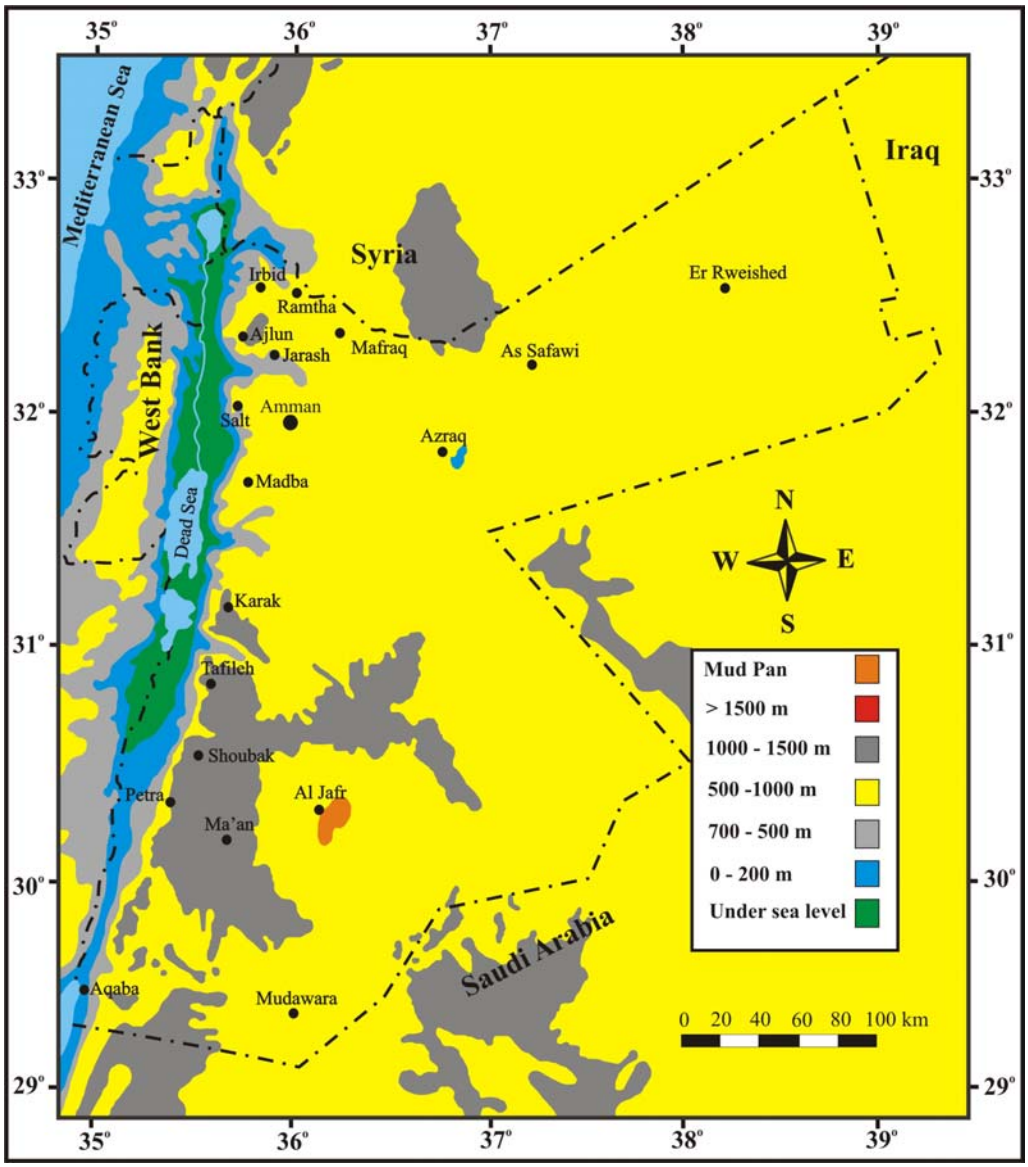

Fig. 1.2: Topographic map of Jordan (RJGC 2004).

The highlands form the eastern-central part of the study area around Salt city where the elevation ranges from 800 to 1000 meters ASL with a gradient of 0 to 10 degrees. The escarpment covers a wide area on the east slope of the Jordan Valley with an elevation of about Sea level to +800 meters; slopes in this zone are about 10 to 35 degrees. The foothills are at the feet of the mountains, which form the escarpment; the elevation of this zone varies from about –200 meters to Sea level with a slope of about 3 to 10 degrees. The rift valley is around 10 km wide in the north of the Dead Sea and narrows to about 2 km in

the Jordan Rift Valley, which consist of the flood plains of the Jordan River and the Jordan Valley floor. The Jordan valley floor occupies most of the rift valley and the elevation of the floor ranges from about –300 meters at the Kureiyma area to about –415 meters in the Dead Sea area.

1.3 Objectives and bibliography

1.3.1 Previous studies

Many authors have studied the thermal springs in Jordan. Schumacher (1886) reported the discharge of the thermal springs along the Jordan rift valley and he described the thermal spring of El-Hammeh (Roman Amatha near Gadara). Noetling (1887), Friedman (1913) and Lachmann (1933) have also descriped and analysed these thermal springs; they have reported that most of these springs occur north of the Yarmouk River in the Syrian Territory and that in the Jordanian Territory one spring is used for feeding and as a bathing pool and that the temperature of the different springs vary between 48 ^{o}C (in Hammet Selim) and 34.1 ^{o}C (in Hammet Er-Rih) (Friedmann 1913).

Blankenhorn (1912a) described the warm spring Hammet Abu-Thableh that is located 2 km northeast of Tabqat Fahl, the Roman city of Pella. He described it as a basin with muddy water that tastes and smells of H_2S of 37 ^{o}C at an air temperature of about 22 ^{o}C. The water of this spring was analysed by Dr. F.Grüneberg (German Geological Mission in Jordan 1961-1966 (1966)). Also Blankenhron (1912a) have recorded the warm spring of El-Machruk, which lies southeast of Deir Alla from fluviatile gravels. He recorded that it has a temperature of 34 ^{o}C at 27 ^{o}C air temperature also the same author mentioned the 36 ^{o}C warm spring of Ain El-Hammam from the Wadi Al-Kafrin 15 km north-east of the Dead Sea. In 1964 the Central Water Authority described the mineral springs of Ain Suweimeh, which discharges from a thick travertine cover and they have analysed the main spring (Ain Hirri). Jacoby (1905) described the thermal springs of Zarqa Ma'in. Lartet (1876), Blankenhorn (1912a), Schrötter (1924) and Lachmann (1933) have published some data about the Zara springs. Lachmann (1933) have studied a hot spring called Ain Sbeh and most probably it is Hammam El-Maghara in Wadi Ibin Hammad. Rofe and Rafetty (1963) have studied Ain Fashkha, which is located at the western shore of Dead Sea.

Bender (1968, 1974) studied most of the thermal springs in Jordan and he made a literature review for most of the previous works. He analyzed the water of the Zarqa Ma'in and sketched a geological map for the Zarqa Ma'in area and proposed answers for some open questions for the Zarqa Ma'in thermal waters. Bender has explained the reason of the high temperature by the intermediate vicinity to the basalt extrusions in the area that are of Middle Pleistocene or younger age and proposed a low geothermal gradient for the area. He questioned the origin of the high iodine and bromine contents and inferred it to the Dead Sea water migration into the sandstone successions, which reaches the surface together with juvenile thermal water. Furthermore he proposed that sedimentation ($CaCO_3$) have closed the lower morphological outlets, which forced the waters to appear at higher levels. He reported that the major springs in Zarqa Ma'in yield between 15 and 35

l/s while the Zara springs yield between 15 and 25 l/s. Nir (1967) made isotopical analysis for the thermal springs in Afra and Burbyta area.

Truesdell (1979) concluded that the Zarqa Ma'in and Zara springs are fed by waters circulating deep within the paleozoic sandstone aquifers and receiving the heat from normal geothermal gradient. He suggested that these waters exist at a maximum temperature of 110 ^{o}C at depth and that they are cooled during their ascent by mixing.

Rimawi (1980) divided Jordan into 5 areas and studied the thermal springs in each area. He analyzed the water chemically and for stable isotopes and tritium concluding that the thermal waters result from mixing between meteoric water and Dead Sea water following the stable isotopes equation: $\delta D = 4.15\ \delta^{18}O - 17.94$.

Lloyd (1980) studied environmental isotope data from the sandstone and limestone aquifers in eastern Jordan. He found that the stable isotopes ($\delta^{18}O$ and δD) in the sandstone groundwater have largely been depleted; he concluded that the infiltrating water was subject to evaporation. Although his ^{14}C data indicated some modern recharge, the tritium data showed evidences of only localized recharge. This research could not provide quantitative information on the area and did not estimate the amount of direct recharge.

Abu Ajamieh (1980) reported major exploration exercises using a variety of exploration techniques that was carried out by the National Resources Authority (NRA) in the Zarqa Ma'in-Zara thermal area in the period between 1977 and 1978; he concluded that an important geothermal reservoir is indicated in the area of springs, most propably heated by Hammamat Umm Hasan basalt plug.

Mabey (1980) studied the previous data of the Zarqa Ma'in-Zara area and recommended an investigation program for this area. The program proposed included interpretation of magnetic data, developing of a geological model, undertaking of gravity and geochemical survey, micro earthquake survey, thermal gradient studies, resistivity surveys, and deep drilling.

Hakki and Teimeh (1981) carried out a detailed geological study of the Zarqa Ma'in-Zara area. They assumed that the hottest springs evidence is related to the highest intensity of shearing in the area.

McEwen and Holocombe (1982) applied a terrain correction to the resistivity data of Abu Ajamieh (1980). They suggested that four areas of lower resistivity exist in the Zarqa Ma'in-Zara area, but non had the lateral extent normally characterizing of high temperature geothermal reservoirs.

Flanigan and El Kaysi (1984) reported on preliminary Audio-Magnetotelluric studies in the Zarqa Ma'in-Zara area and concluded that the rocks in the area range between moderately conductive to very conductive.

Salameh and Rimawi (1984) studied the hydrochemistry and isotopes of the thermal springs along the eastern side of the Jordan-Dead Sea-Wadi Araba rift valley. They concluded that water precipitating on the mountainous areas infiltrates through the bedrocks flows in an easterly direction through out several aquifers and then flows westerly to discharge along the Dead Sea escarpment. They concluded that the dissolved solids are derived primarily from the upper cretaceous sediments that cover the infiltrate area. Those waters mix with hypersaline waters present in the lower Cretaceous or even older rocks. They attributed the high temperatures of some springs to the deep circulation under normal geothermal gradient. They stated that the ground water of the surface aquifers lies isotopically between the Mediteranean Meteoric Water Line and the Global Meteoric Water Line and that the isotopic composition of the southern samples is shifted closer to the Global Meteoric Water Line. They proposed mixing at the interface between the fresh groundwater and the Dead Sea water between the two later mentioned waters under normal geothermal gradient to produce thermal waters that have an isotopic composition following the equation: $\delta D = 3.97\ \delta^{18}O - 16.9$.

Salameh and Udluft (1985) studied the hydrodynamic pattern of the central part of Jordan. They determined the measurable and non-measurable discharge along the western slopes of the Dead Sea as $91.4 \cdot 10^6$ m^3/yr and $78.8 \cdot 10^6$ m^3/yr respectively. They determined the permeability of the different sandstone aquifers from pumping tests and they assumed the average permeability of aquitards to be $1.3 \cdot 10^{-9}$ m/s. The average filter and horizontal straight-line velocities of the aquicludes was calculated to be $2.2 \cdot 10^{-10}$ m/s and $2.2 \cdot 10^{-8}$ m/s respectively. They also calculated the average time needed for water to penetrate vertically through the individual aquifers and aquitards until reaching the lower sandstone aquifer and then flowing horizontally and discharging at the western slopes near the Dead Sea to be around 3500 years.

Galanis and others (1986) reported that the heat flow in the Zarqa Ma'in-Zara area is high (472 mW/m^2) and that the area of heighest heat flow is associated with Zarqa Ma'in fault zone rather than the local basaltic eruptions.

Rimawi and Salameh (1988) studied the hydrochemistry and groundwater system of the Zarqa Ma'in-Zara thermal fields. They presented a groundwater flow model through the different geological successions from the upper Cretaceous, the lower Cretaceous sandstone and older units. They concluded that the Zara thermal waters represent discharge from the upper part of the aquifer, where the water flows horizontally through recent fault surfaces to neighboring ones to discharge finally along the Zara slopes. The water of the Zara Ma'in area flows vertically through older faults and fractures to reach almost near the fresh water-Dead Sea water interface. At surface and along upper parts of the fault planes, the sandstone pores are clogged by secondary Aragonite, which precipitates as soon as the groundwater comes in contact with the atmosphere. Along some faults the pressure and velocity of the artesian flowing water doesn't allow consolidation of Aragonite, also individual Aragonite grains are eroded and transported by water flowing out the fault space. They concluded that the thermal waters discharging from Zarqa Ma'in-Zara area consist of three end members mixed in different ratios with a component of old thermal water which is undersaturated with respect to carbonate minerals and containing hundreds

of milligrams per liter of CO_2. They attributed the elevated temperatures to a heat-storing layer topping the aquifer.

Sawarieh (1990) reported the presence of thermal water in the shallow boreholes near Queen Alia airport, which result from mixing between the thermal water of the lower aquifer and the fresh cold water of the upper aquifer (B2/A7). He related the heat source in the Zarqa Ma'in area to the deep circulation process along the Zarqa Ma'in fault.

El-Naser (1991) studied the groundwater resources of the Lower aquifer systems in NW-Jordan. In his conceptual hydrodynamic model he showed, that an upward leakage from the lower aquifer (Kurnub) to the upper aquifer (B2/A7) is taking place. He also quantified the amount of upward leakage as well as the thermodynamics of both aquifers, and built a quasi three-dimensional groundwater flow model. He used the hydrogeochemical modeling delineated by the use of natural traces like Br and Cl to determine the mixing ratios between the upper and the lower aquifer. He found that the mixing ratios increase with the increase in the confinement degree of the aquifer. The mixing of the two end members is always understaurated with respect to calcite and dolomite. This aggressive water enlarges the water flow paths.

Sawarieh and Massarweh (1993) studied the thermal springs in Wadi Iben Hammad and concluded that the heat source is more likely to be due to the heat storage in the saturated sandstone complex resulting in higher geothermal gradient.

In his book "Water quality degradation in Jordan", Salameh (1996) divided the thermal waters into waters with low salinity and high temperatures (Afra spring, Iben Hammad spring, North Shuneh well) and waters with high salinity and elevated temperatures (Zarqa Ma'in springs, Deir Alla spring, Abu Thableh and Abu Zyad well) and described them chemically.

Abu-Jaber and Wafa (1996) studied the hydrochemistry of aquifers in the southern Dead Sea area. They discussed the Dhiraa water field and concluded that with in this field exist three water types. The Tritium and Oxygen isotope analysis indicated that the waters are old. The authors left an open question: the possibility of groundwater renewability. They indicated that there is no evidence of Dead Sea water intrusion in the aquifer.

Sawarieh and Massarweh (1996) studied the geothermal water in Zara and Zarqa Ma'in area and reported that the origin of the heat is more likely to be due to deep circulation process rather than magmatic origin and that the deep faults mainly Zarqa Ma'in fault may act as a conduit for rapid ascent of hot waters from the deep confined lower aquifer. They also concluded that the water is driven toward the surface by hydraulically induced forced-convection.

Bajjali et al. (1997) studied the artesian thermal groundwater of northern Jordan. They suggested, that all ground waters are characterized by a late Holocene (modern) stable isotope signature. The groundwater from upper B2 aquifer (El-Mokhybeh wells) have a

$\delta^{18}O/\delta D$ composition demonstrating recharge in the B2 outcrop region east of Irbid area while the deeper A7 aquifer (Jordan Rift Valley wells) are recharged at a lower elevation in the rift valley margin. They stated that the deepest strata (A1 to A6) contain the isotopically most depleted waters and they probably recharged from the highest landscape of northern Jordan. This work recommended sampling of chemical and isotopic data from the Syrian side to shed a light on the geochemical evolution of the ground water from the recharge area to the discharge zone and sampling of environmental isotopes for the gases at the thermal sites for a better understanding of the mantle contribution in the thermal waters.

Sawarieh and Massarweh (1997) studied the geothermal water in El-Mokhybeh and North Shuneh areas; they reported that the heat source of the thermal waters in these areas is related to the mixing process taking place between the two aquifers (B2/A7 and Kurnub sandstone).

Salameh and Rimawi (1997) studied the curative thermal–mineral water of Jordan. In their Bulletin the following studies were carried out: the origin and temperature of the waters, source of mineralization and complete chemical analysis of the following locations: Ma'in, Jordan Ghor springs, Hisban spring, Wadi Al Kafraen wells, North Shuneh well, El-Hammeh, and south Jordan Springs (Afra).

The chemical modeling of the Dead Sea brines carried out by Abu-Jaber (1998) indicated that the evolution of the waters could be explained by simple mixture and evaporation model. The model requires the input of $50 \cdot 10^6$ m^3/yr of hot spring waters similar to those emanating at Zohar with an evaporation factor of around 50. This model suggests that the Dead Sea salts have accumulated over the past 5000 years. He also reviewed the data of the springs, which are responsible for the chemical nature of the Dead Sea. He suggested that these waters are meteoric-continental origin, which have experienced deep circulation in the rift system before discharging at the surface due to convective forces operating in the rift.

Wagner and Geyh (1999) studied the application of isotope methods for groundwater in the ESCWA region. They reviewed the data of Mazor et al. (1973), Bajjali (1994) and Bjjali et al. (1997). They related the stable isotope composition in the Yarmouk and upper Jordan river basin to altitude effect. They suggested that the δD values of the A7 aquifer indicate recharge from areas at higher elevation of those of the B2 aquifer. The depleted $\delta^{18}O$ values suggest a Pleistocene recharge that characterizes the groundwater of deeper Kurnub aquifer. They assumed that the ^{14}C decrease is caused by secondary hydrochemical process in the aquifer, which are SO_4 reduction by oxidation of fossil organic matter and subsequent $CaCo_3$ dissolution. They suggested that Al-Mokhybeh water residence time ranges between 4200-7000 a. The authors recommended the following studies for the ESCWA region by the use of isotope hydrologic methods: determination and quantify of groundwater recharge, the occurrence of renewable groundwater recharge, the origin of the water resources, the regional ground water movement, the mixing of different groundwater resources, and the paleohydrogeologic conditions of groundwater recharge.

Salameh and El-Naser (1999) quantified the effect of the Dead Sea level decline on the precious groundwater resources of the surrounding aquifers. They analyzed the historic and predevelopment inflows and outflows of the Dead Sea basin resulting in a water balance. They analyzed the present situation to quantify groundwater inflows to the Dead Sea as a result of drop of the Dead Sea level. They found that effect of the present day level declines on the fresh groundwater/saltwater interface indicate that considerable amounts of groundwater are driven into the Dead Sea. The result is seaward migration of the freshwater/saline water interface.

Salameh and El-Naser (2000) studied the reaction of the freshwater/saltwater interface driven by the Dead Sea level changes. The study was carried out using the inflows into the Dead Sea and outflows caused by evaporation, artificial discharge and hydrographic registration of the Dead Sea. Their analysis showed that the interface seaward migration resulted in a groundwater discharge of $423 \cdot 10^6$ m^3 per meter drop of the Dead Sea level in the 1994-1998 period and $525 \cdot 10^6$ m^3/m in the 1930-1937 period. $51 \cdot 10^6$ m^3 per one square kilometer of shrinkage in the Dead Sea area is the additional amount of groundwater that joins the Dead Sea due to the interface migration in the 1930-1937 periods and $91 \cdot 10^6$ m^3/km^3 in the 1994-1998 periods. $370 \cdot 10^6$ m^3 of freshwater is lost nowadays to the Dead Sea per year.

El-Naser and Subah (2000) studied the hydrochemistry and isotopes of the ground waters in the eastern area of the Dead Sea (DS) to determine the groundwater source of Ain Maghara spring. They analyzed the waters of both TA1 and TA2 wells and they calculated the mean residence time of water from those two wells through ^{14}C. The authors have recommended the following: measuring chemistry and isotopic composition of water discharging from the spring throughout the year, evaluate the changes in mean residence time compared to the discharge of the waters and using CFC's to measure mean residence time of young water resources.

Salameh (2001) studied the source of water salinities in the Jordan Valley. He concluded that the evaporites with in the Jurassic and Triassic rocks as well as those of deposits of the ancestors of the Dead Sea (DS) extending along the whole length of the Jordan Valley are the main contributors to the water chemistry encountered in the eastern side of the Jordan Valley. He recommended isotope analysis to calculate the mixing ratios of the end members, which result in present hydrochemical composition of each site in the Jordan Valley.

Cappaccioni et al. (2003) studied the origin of thermal waters from the eastern flank of the Dead Sea rift valley. He concluded that the thermal waters which are located in northeast part of the Dead Sea Rift Valley are recharged with present day meteoric waters while the Ma'in thermal waters are recharged by meteoric water contaminated with saline waters. He assumed further that the saline waters could represent residual pockets of ground waters in equilibrium with those waters that filled the Dead Sea depression before the retreat of Lake Lisan (17-15 ka BP) or with ancient seawater of the Sedom Lake (early Pleistocene). He

concluded that there is no significant evaporation processes for those waters and suggested that they are chemically and isotopically modified by rock water interaction processes.

Swarieh (2005) studied the heat source of the groundwater in the Zara-Zarqa M'in-Jiza area. He concluded that the Zara-Zarqa Ma'in area hot springs that tap the lower aquifer are hydraulically connected with the Madba-Jiza region that discharge from the upper aquifer. This connection is caused by the presence of many faults of different trends. The hydrological, chemical and simulation studies showed that heat is transported to the thermal wells by water up-flow movement via faults forming the heat source for these thermal wells. Thus, to find higher temperatures, the thermal water should be intercepted in the faults (conduits) before it reaches the upper aquifer. This study recommended further chemical and isotopic specialized researches such as noble gas measurements and the drilling of deep wells of about 1200 m in depth to investigate the lower aquifer.

1.3.2 Statement of problem and objectives

Even though a lot of research has been done concerning the thermal springs in Jordan, data related to the origin, movement of the waters and the source of the dissolved gases and constituents are missing. Also many questions related to the hydrogeological situation, source of heat and balneological investigations are still open.

Because there is still a debate about the source of salinity and water movement in the Dead Sea Transform area, there is a need in further basic research being part of this work.

This research may help to determine the geohydrological and geohydrochemical history, determine the paleoclimate in the study area, hydrocarbon potentials and to give an idea about the development of water chemistry with in the Dead Sea Transform (DST) system.

This research aims to:

- Determine the origin and mean residence time of the thermal waters along the Dead Sea Transform (DST);
- Calculate the thermal waters temperature at depth;
- Determine depth and nature of ground water circulation in the DST;
- Test the quality of different geothermometers for the available geological and hydrogeological conditions;
- Determine the possible source for the chemical and gaseous constituents;
- Applying and evaluation of new techniques;
- Developing, testing, and verifying of new sampling methodologies (gas trapping unit).

The study of $\delta^{18}O$, δD, Tritium, δHe, δNe and ^{14}C isotopes were used to determine the origin and mean residence time of the thermal waters. Both solute and the isotope geothermometers were used to calculate the thermal waters temperatures at depths. By using the geothermometer diagrams, the comparison with the saturation indices and the

previous literature; the quality of the different geothermometers were tested to determine the best geothermometers in such geological and hydrogeological situation. $\delta^{34}S_{SO4,}$ $\delta^{18}O_{SO4}$, δHe, δNe and $\delta^{13}C_{CO2}$ in addition to the physical and chemical parameters of the thermal water were used to determine the possible source for the chemical and gaseous constituents of the thermal waters. The physical and chemical parameters were as well used to evaluate the suitability of the thermal waters for domestic and agricultural purposes.

2 METHODOLOGY

2.1 Data management

Data have been collected through the literature review, fieldwork, laboratory analysis and the analysis of different isotopes.

All scientific papers, technical reports, maps, M.Sc. Theses, Ph.D. dissertations as well as unpublished reports dealing with the geology, hydrogeology and hydrochemistry of the thermal springs and wells, the Dead Sea Transform area and the Dead Sea were gathered and evaluated.

All references were entered in a reference management system. Relevant data from bibliography and data collected in this study were entered in data base system using Microsoft Access program. A relational database were build, which consist of tables that is connected with each other through the ID number of each spring, the built database tables are:

1. Chemical analysis obtained in the first sampling campaign;
2. Chemical analysis obtained in the second sampling campaign;
3. Average chemical analysis of both of the sampling campaigns;
4. Rare earth elements;
5. Tritium isotope analysis (^{3}H);
6. Stable isotopes of water ($\delta^{18}O$, δD);
7. Sulfate isotopes ($\delta^{34}S_{SO4}$ and $\delta^{18}O_{SO4}$);
8. Helium and Neon isotopes;
9. Calcualted geothermometers;
10. Saturation indices;

2.2 Sampling and Laboratory analysis

2.2.1 Development of gas trapping unit

A new methodology has been developed in order to trap the gases that emerge from the thermal springs and wells. The principle idea is to precipitate Hydrogen sulphate (H_2S), Carbon dioxide (CO_2) and Methane (CH_4) in chemical solutions in order to prepare them for further isotopic analysis. The new methodology was developed in the hydrogeology laboratories at the TU Bergakademie Freiberg.

2.2.1.1 Laboratory design

In the laboratory, a gas-developing unit was developed to produce gases and to inject them into the water (Fig. 2.1). This step was designed to simulate thermal waters that contain different natural gases (CO_2, H_2S and CH_4). The Methane (CH_4) was not injected in the laboratory because of the explosion danger and safety measurements. This part was applied in the Physikalische Chemie Laboratory at the TU Bergakademie Freiberg.

In the gas-developing unit, the H_2S was developed by the reaction of HCl with the Na_2S while the CO_2 was developed by the reaction between HCl and the limestone (marble). The

developed gases were transported from the gas-developing unit to the water container by the help of nitrogen gas as an inert carrier.

The next step was to degas the water by bubbling nitrogen through water. In order to trap the gas, a hose from the water container was connected with three gas washing bottles; the first gas wash bottle contains a solution of $PbNO_3$ (which is prepared by dissolving 5 g $PbNO_3$ in 500 ml distilled water and the pH adjusted to ~ 3 by adding HNO_3) the second and the third gas wash bottles contain a over saturated $Ba(OH)_2$ solution. In the first bottle the H_2S is being trapped as PbS while in the second gas wash bottle the CO_2 is being trapped as $BaCO_3$. The CH_4 is being passed over a catalyst in a heated quartz pipe in order to transform it to CO_2 and trap it as $BaCO_3$ in $Ba(OH)_2$ solution (see Fig. 2.1).

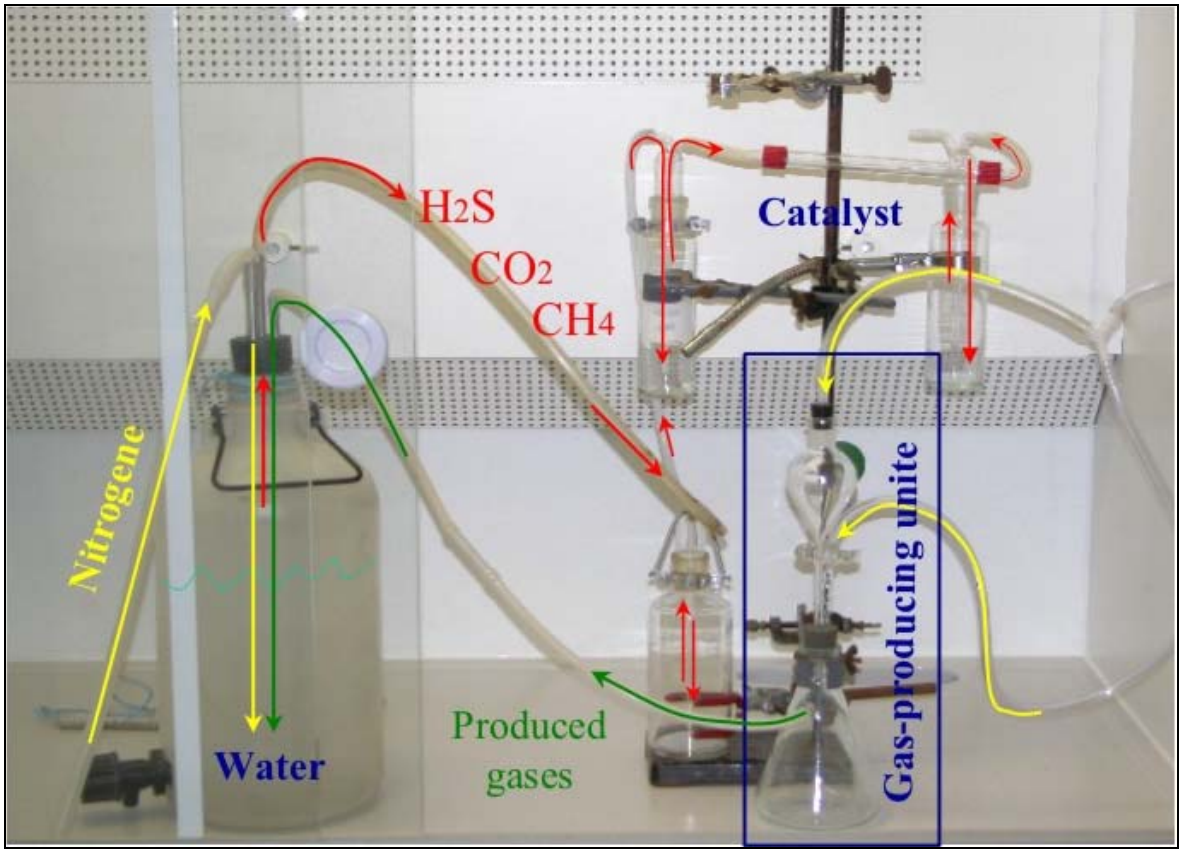

Fig.2.1: Laboratory design. To the right the gas-developing unit, to the left the degassing unit and the precipitating unit composed of three gas wash bottles.

2.2.1.2 Catalyst Description

In order to burn the CH_4 to CO_2, the CeO_2-ZrO_2-Y_2O_3 mixed oxides was used as described by Fraga et al (2002). The catalyst was prepared in the laboratory as follows:

1. The mixed oxides were obtained by dissolving cerium (IV) ammonium nitrate, zirconium nitrate and yttrium nitrate. The mixing ratio was: Ce (75%), Zr (20%) and Y (5%).
2. By adding excess ammonium hydroxide, the hydroxides were coprecipitated;

3. The solid were then filtered and washed with distilled water until constant pH of about 7;
4. The solid from the third step was calcined at 500°C for 1 hour in a muffle furnace;
5. The catalyst was prepared by mixing the resulted from previous step oxide mixture (CeO_2, ZrO_2 and Y_2O_3) with an aqueous solution of $Pd(NO_3)_2$;
6. The sample was then dried overnight at 110°C and calcined at about 500°C under airflow for 5 hours;
7. The resulted catalyst was then grinded by the use of agate mortar.

The catalyst was tested in the laboratories of the Institut für Physikalische Chemie of the TU-Bergakademie Freiberg (it was used for a methane-air-mix with a 3% methane content applying 2.6 mg of the catalyst in a quartz tube with a flow rate of 5 ml/min). It was found that the catalyst performed a 80% efficiency at about 480°C (Fig. 2.2).

In the experiment several chemical solutions were tested like NaOCl, PbNO3, $CaHCO_3$ and $Ba(HCO_3)_2$ in order to reach the best result with regard to precipitating the gasses. The chemicals shown in the afore mentioned experimental design were found to perform best: $Pb(NO3)_2$ to precipitate the H_2S and $Ba(HCO)_2$ to precipitate the CO_2 and CH_4.

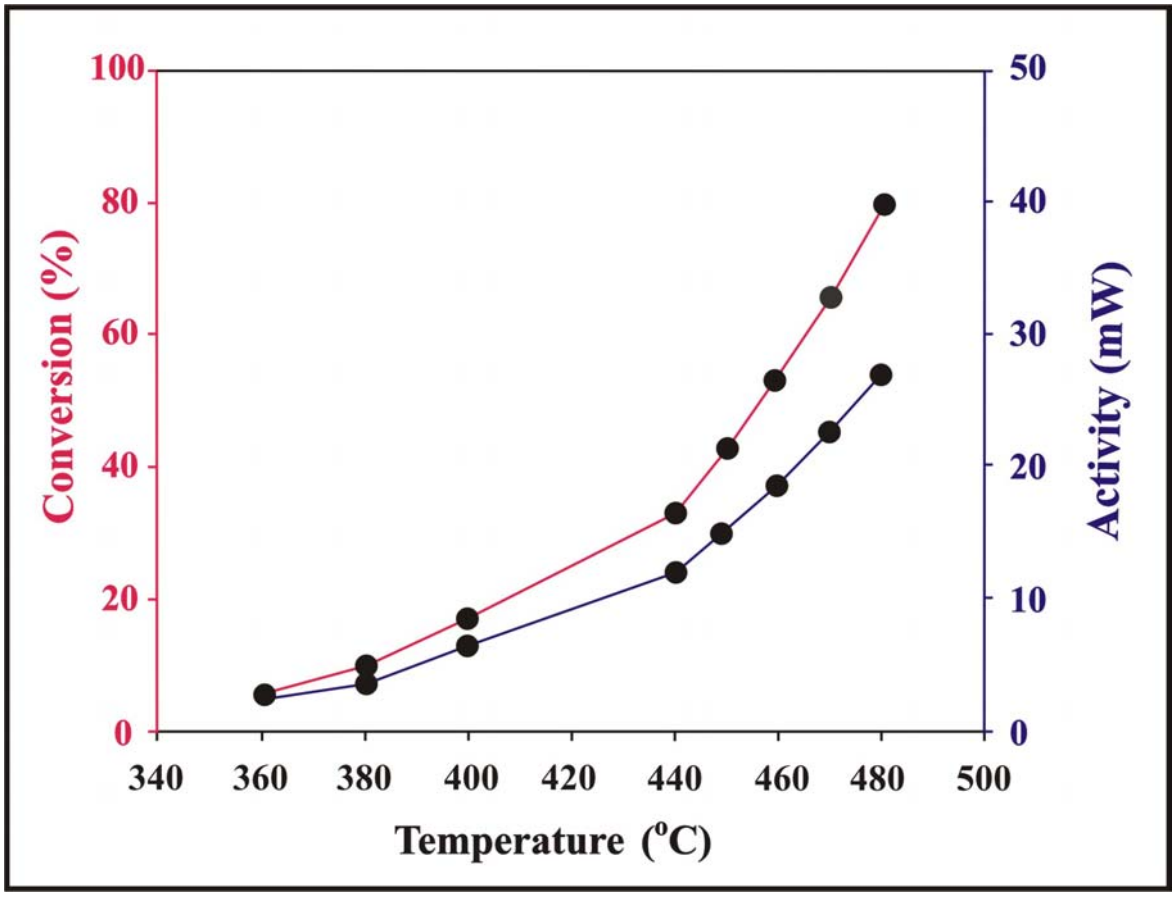

Fig. 2.2: Relation ship between the temperature and both of the conversion and the activity.

2.2.1.3 Application in the Field

Fig. 2.3 shows the construction and arrangement of the field setup. Nitrogen bottle (1) is used to degas the thermal waters that were beforehand pumped into the water container (2). H_2S, CO_2, and CH_4 are degassed together with all other gases (O_2, N_2) from the water. The H_2S is precipitated as PbS in the first gas wash bottle (3) containing $Pb(NO_3)_2$ solution. CO_2 is precipitated as Barium carbonate in the second gas wash bottle (4) containing $Ba(HCO_3)_2$ solution. CH_4 is converted to CO_2 in the quartz tube (6) by means of the previous described catalyst. The catalyst is being heated with a gas pistol (7) to maintain 480 ^oC. The produced CO_2 is being precipitated as barium carbonate in the third gas wash bottle (5) that contain $Ba(HCO_3)_2$ solution.

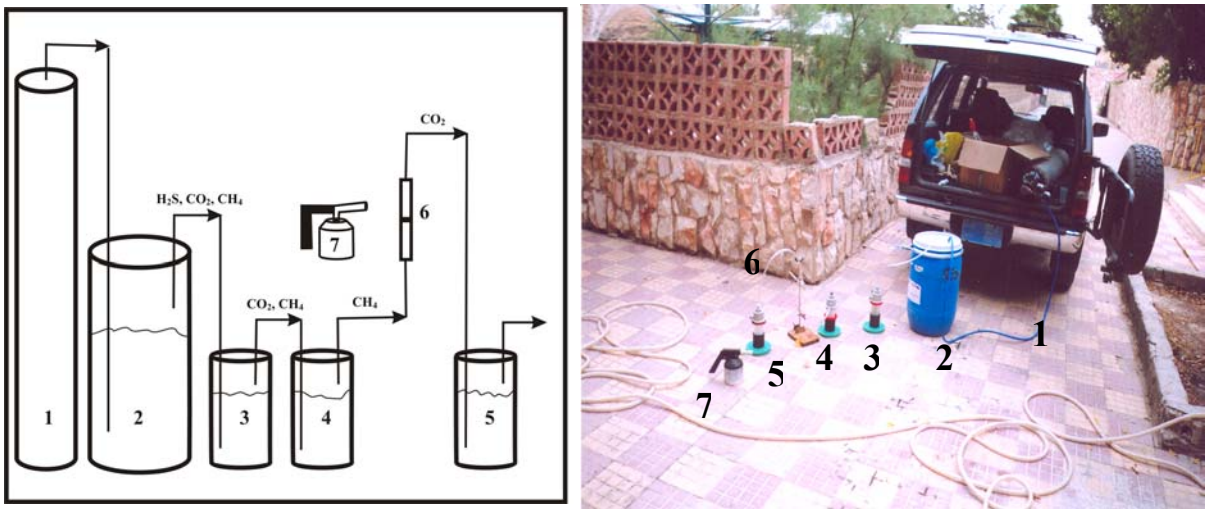

Fig.2.3: Field design of the gas-sampling device. (1) Nitrogen bottle; (2) Water container; (3) Gas wash bottle contains $Pb(NO_3)_2$; (4) and (5) gas wash bottle contains $Ba(HCO_3)_2$, (6) Quartz tube that contains the catalyst; (7) Gas-pistol (heat source).

2.2.2 Fieldwork

A field survey was carried out to detect the locations of the thermal springs and wells. The field survey was followed by two sampling campaigns. The following is a brief description of the sampling campaigns, collected samples, used devices, sampling techniques, and special treatment.

- **Sampling campaigns:** two sampling campaigns were carried out. They extended from 20/2/2005 to 5/5/2003 and from 5/5/2004 to 1/8/2004 respectively.

- **Collected samples:**
  - 46 samples (1 Liter Polyethylene bottle) for the chemical analysis;
  - 46 samples (250 ml Polyethylene bottle) for Rare Earth Element (REE) analysis;
  - 32 samples (0.5 Liter Polyethylene bottle) for the ^3H isotopic analysis;
  - 32 samples (250 ml dark glass bottle) for the $\delta^{18}O$ and δD analysis;
  - 23 samples (3 Liter Polyethylene bottle) for sulfate precipitation for determination of $\delta^{18}O_{SO4}$ and $\delta^{34}S_{SO4}$;

- 4 samples (40 cc copper tube, 3 duplicates) for the δHe and δNe analysis;
- 4 samples ($BaCO_3$ precipitant) for the $\delta^{13}C_{CO2}$ analysis.

- **Devices used:**
  - WTW-Multilinie and WTW-electrodes for the measurement of the physical properties (temperature (T) and electrical conductivity (EC)) and chemical properties (dissolved oxygen (DO), redox potential (E_H) and pH.
  - Global positioning system (GPS) device to determine the locations in Palestine grids.

- **Sampling techniques:** the T, pH and EC were continuously measured and when those 3 parameters showed constant values; the waters were then sampled. The rare earth elements (REE) samples were filtered using 200 nm pore-sized filter and acidified with 1 ml concentrated analytical nitric acid (supra pure).

- **Special treatments:** the O_2 and pH devices were calibrated using relative methods of calibration while the correction of the sensors and devices of T, EC and E_H were checked. The water samples were cooled during storage and transportation.

2.2.2.1 Sampling groundwater for noble gas analysis

The extremely light noble gasses Helium and Neon and their isotopes ^3He, ^4He, ^{20}Ne and ^{22}Ne have a high diffusion potential. Thus, most materials cannot be used as sampling-containers. Copper (Cu) tubes have proved to be a good choice, because samples can be stored for years after being filled with water and squeezed at their ends.

The quality of the analysis depends very much on avoiding contamination with atmospheric air during the sampling procedure. Usually the isotopes concentration can be measured with a precision better than 0.5% and an air bubble of 2 mm^3 contains such quantities of gasses.

One should take care that during filling of the copper tube no air bubbles will be released from the pumping line. This can be monitored by connecting a transparent hose between the pumping line with the copper tube (Figs. 2.4 and 2.5).

To avoid possible degassing, one has to maintain a water pressure in the copper tube, which is higher than the hydrostatic pressure of sampling depth. This can be obtained by connecting a backpressure valve to the outlet of the copper tube and if that is not available one can put a hose clip onto the hose to increase the pressure (Figs. 2.4 and 2.5).

Perfect sampling is usually done in closed boreholes because groundwater in open wells is in equilibrium with the atmosphere to a large extent. Borehole, copper tube and hoses should be flushed for some period of time. From each borehole 3 copper tubes were filled in order to check for reproducibility.

The collection of the water samples for the $^3H/^4He$ age determination and $^3He/^4He$ for helium origin determination was done in the first sampling campaign. The sampling

equipments and procedures were provided by the Institut für Umwelphysik-Abteilung Ozeanographie Dienstleistung in Bremen University.

The following procedure was applied in the field to sample noble gasses:

1. The well is pumped until T, pH and EC are constant;
2. A transparent hose is used to connect the copper tube with the pumping line (Figs. 2.4 and 2.5);
3. A short transparent hose and backpressure valve is connected to the other end of the copper tube (outlet) in order to increase the water pressure;
4. The copper tube (1mm wall thickness) outlet is raised by approximately 45^{o} to assure that gas bubble-if present-will be completely flushed;
5. The copper tube (40 cc) is then flushed at least 10 times and meanwhile the aluminum rack is hit frequently with a stiff tool (ratchet wrench) to release air bubbles from inner walls of the tube;
6. The clamps are then screwed tightly (cold welded) first outlet then inlet (Fig. 2.6). The clamps are prepared in a manner so the copper will be squeezed down to 0.7 mm;
7. The planar surface of the clamps must rest on back-to-back;
8. The ends of the tubes should not be bended or squeezed;
9. The tubes are then labeled.

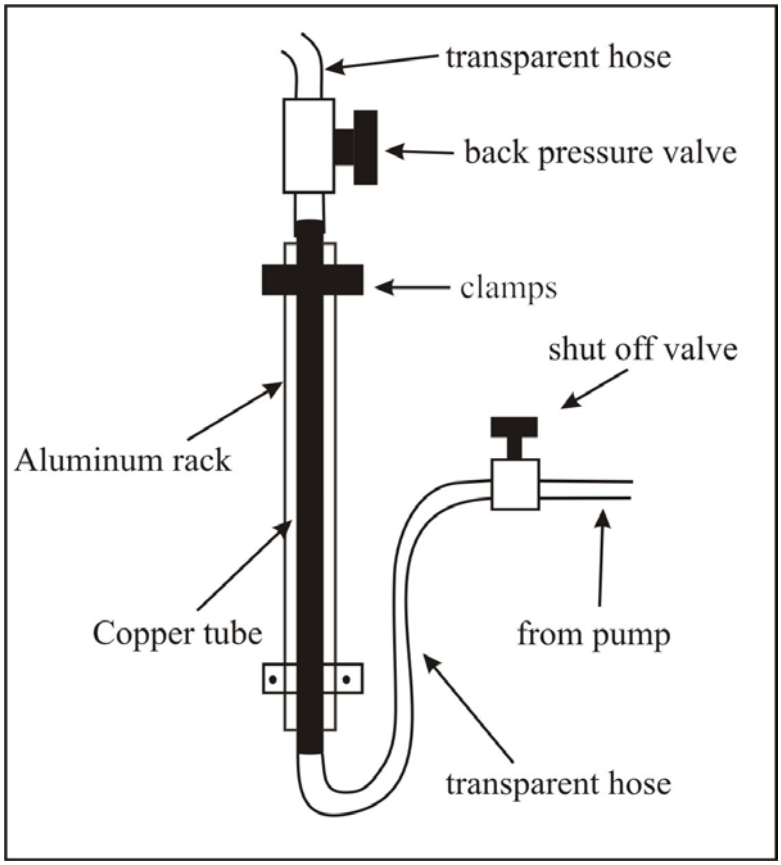

Fig. 2.4: Sketch of the copper tube in the aluminum rack with transparent hoses and backpressure valve attached.

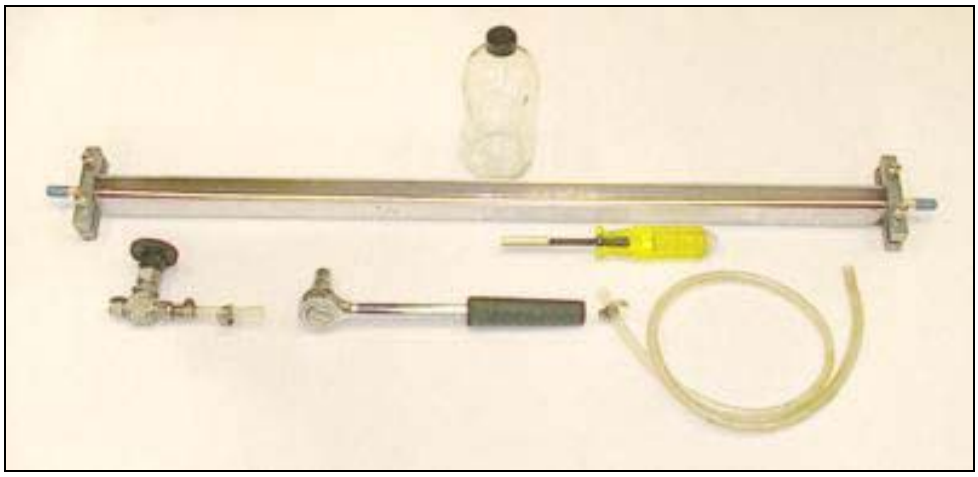

Fig. 2.5: The copper tube attached on aluminum channel with a backpressure valve, transparent hoses, and stiff tool (ratchet wrench).

Fig. 2.6: Properly cold welded copper tube.

2.2.3 Chemical analysis

2.2.3.1 Inorganic constituents

According to the standards of the American Public Health Association (1995) the major ions (Ca^{2+}, Mg^{2+}, Na^{+}, K^{+}, HCO_3^{-}, Cl^{-}, SO_4^{2-}, NO_3^{-}, PO_4^{3-}) were determined in the Geology department laboratories in the university of Jordan. Temperature, conductivity (EC), and pH were measured in the field by using Field Multi Electrode Meter (WTW-Multilinie). Alkalinity (CO_3^{2-} and HCO_3^{-}) was determined by titration with HCl using Phenolphthalin and Bromocresol-green indicators. Sulfate (SO_4^{2-}) was determined by precipitation of $BaSO_4$ and then measuring the absorbency with a spectrophotometer at λ=420 nm. Chloride (Cl^{-}) was determined by titration with $AgNO_3$ using Potassium

chromate indicator. Sodium (Na^+) and Potassium (K^+) were determined by flame photometer. The total hardness (Ca^{2+}+ Mg^{2+}) was determined by titration with Na_2-EDTA using Erichrome black-T indicator while the Calcium (Ca^{2+}) was determined by using Murexide indicator. Nitrate (NO_3^-) was determined by using UV-spectrophotometry at λ=220 nm. Phosphate (PO_4^{3-}) was determined by adding Stannous Chloride and then measuring the absorbency with a spectrophotometer at λ=700 nm. The Rare Earth Elements (REE) were determined by using ICP-MS in the ACTLAB in Canada. Table 2.1 shows the detection limits for the major analyzed hydrochemical parameters in this study.

Table 2.1: The detection limit of the hydrochemical Parameter.

Hydrochemical parameter	Detection limit	Hydrochemical Parameter	Detection limit
Ca	1.0 mg/l	HCO_3	10.0 mg/l
Mg	0.5 mg/l	SO_4	0.1 mg/L
Na	0.5 mg/l	Cl	1.0 mg/l
K	0.5 mg/l	SiO_2	1.0 mg/l

2.2.3.1.2 Precipitation of sulfate for isotope determination

For the determination of both $\delta^{34}S_{SO4}$ and $\delta^{18}O_{SO4}$ on $BaSO_4$, sulfate was precipitated according to Carmody et al. (1998):

1. The water sample is filtered with a 0.45 µm filter paper to remove all impurities from the water;
2. The pH is then measured, if it is not between 3 and 4, 1 molar HCL is then added in order to adjust the pH;
3. The sample is then heated to 80°C;
4. A super saturated $BaCl_2$ solution is then added while continuously mixing;
5. The sample is filtered a second time by 0.45 µm to separate the water from the precipitate;
6. The Cl is then washed from the precipitant by the use of distilled water;
7. The sample with the filter paper is heated at 49°C;
8. After being dried the sample is grinded using agate mortar and stored in small containers.

2.2.3.2 Isotopes

2.2.3.2.1 Sulfate isotopes ($\delta^{34}S_{SO4}$ and $\delta^{18}O_{SO4}$)

Sulfur and oxygen isotope ratios were determined by isotope ratio mass spectrometer in the (Mineralogy department) laboratories at the TU Bergakademie Freiberg. Canyon Diablo Triolite (V-CDT) was used as a standard for $\delta^{34}S$ and Standard Mean Ocean Water (V-SMOW) was used as a standard for $\delta^{18}O$.

The $\delta^{34}S_{SO4}$ were determined by a continuous flow isotope ratio mass spectrometer using Finigan MAT DELTA plus/EA at 1020°C. The $\delta^{34}S_{SO4}$ values are being determined with a precision of ± 0.3 $^{o}/_{oo}$, while $\delta^{18}O_{SO4}$ where measured by a continuous flow isotope ratio mass spectrometer using Finigan MAT DELTA plus/Pyrolysis at 1450°C with a precision of ± 0.5 $^{o}/_{oo}$.

2.2.3.2.2 Helium and Neon isotopes

The noble gasses (Helium-3, Helium-4, Neon-20 and Neon-22) were measured at the Instiut für Umweltphysik, Abteilung Ozeanographie in Bremen University (Abteilung Ozeanographie 2000). The measuring system is calibrated by defined quantities of gas standads. Additionally blank and linearity measurements are accomplished. The Ne concentration determination precision is better than 1%, for the $^{3}He/^{4}He$ and He/Ne ratio is better than 0.5%.

2.2.3.2.3 Environmental isotope analysis ($\delta^{18}O$, δD and ^{3}H)

The complete analysis and separation of the stable isotopes ($\delta^{18}O$ and δD) were carried out in the laboratory of GSF-institute for hydrology in Neuherberg. The Standard Mean Ocean Water (V-SMOW) was used as a standard for both $\delta^{18}O$ and δD. The $\delta^{18}O$ was determined with a precision of ± 0.1 $^{o}/_{oo}$ while δD are determined with a precision of ± 1 $^{o}/_{oo}$.

The Tritium (^{3}H) was analysed in the Institut für Angewandte Physik labratories at the TU-Bergakademie Freiberg with a precision of ± 0.3 TU.

2.2.4 Accuracy of analysis

Reliability of water analysis can be detected by electrical balance. Normally the major cations: Ca, Mg, Na and K and the major anions: HCO_3, SO_4, Cl, and NO_3 are taken as meq/l. two equations are common:

$$\textbf{Error \% =100* (}\sum\textbf{Cat-}\sum\textbf{An)/ (}\sum\textbf{Cat+}\sum\textbf{An)} \qquad \textbf{(1)}$$

$$\textbf{Error \% =100* (}\sum\textbf{Cat-}\sum\textbf{An)/0.5 (}\sum\textbf{Cat+}\sum\textbf{An)} \qquad \textbf{(2)}$$

Eqution 2 is common in Germany, while equation 1 is common by many other countries. PhreeqC offers a more precise method by taking into account all positive and negative charged complexes. Different criteria of reliability can be found in the literature (1, 2, 5 and 10%) for equation 1 and 2. In this study the electrical balance error calculated by PhreeqC was used and evaluation of data was with respect to a 5% criteria.

2.2.5 Electrical conductivity

It measures the ability of water to conduct an electric current. It is directly related to the total dissolved salts (ions) in the water. It is abbreviated as EC and is reported in

microSiemens per centimeter (µS/cm). EC is not independent from temperature since EC increases if temperature increases. This can be expressed with a linear regression function: an increase or decrease by 1 ^{o}C will cause an increase or decrease of about 2% in EC. More precise correction is possible by means of non-linear functions. Modern EC meter offer the choice of both linear and non-linear correction. In certain cases it is recommended to report the true EC and not the transformed EC at 25 ^{o}C. Furthermore old data sometimes are true EC or even EC transformed to 20 ^{o}C (was standard for some time). Most modern probes automatically correct for temperature and standardize all readings to 25°C and then refer to the data as specific EC. Electrical Conductivity (EC) estimates the amount of total dissolved salts (TDS), or the total amount of dissolved ions in the water.

2.2.6 Total dissolved solids

Water is a good solvent and picks up impurities easily. Pure water is tasteless, colorless, and odorless. It is often called the universal solvent. Dissolved solids refer to any minerals, salts, metals, cations or anions dissolved in water. Total dissolved solids (TDS) comprise inorganic salts (principally calcium, magnesium, potassium, sodium, bicarbonates, chlorides and sulfates) and some small amounts of organic matter that are dissolved in water. The water could be classified according to its TDS value into four types: fresh, brackish, saline, and brine (Caroll 1962) (Table 5.1).

Table 2.2: Groundwater classification according to Caroll (1962).

Water Category	TDS (mg/L)
Fresh	0-1000
Brackish	1000-10000
Saline	10000-100000
Brine	>100000

2.3 Classification and statistics

2.3.1 Classification of the hydrochemical data

In order to classify water samples into groups graphical and statistical methods were used. Piper, Durov, Schoeller, Langeleir-Ludwig comes with Aquachem version 3.7.42, Dendrogram cluster analysis was performed SPSS 11, while bar chart were drawn with Plotchem version 7.7.

The main purpose of the **Piper diagram** is to cluster the samples that have similar chemical composition. Piper (1944) proposed this diagram where it plots the major ions (as percentage of milli-equivalents) within two triangles at the base. The total cations and anions are set equal to 100%. The data points in the two base triangles are projected onto an adjacent diamond grid. Fig. 2.7 and Table 2.3 shows the water classifications according to Furtak and Langguth (1967).

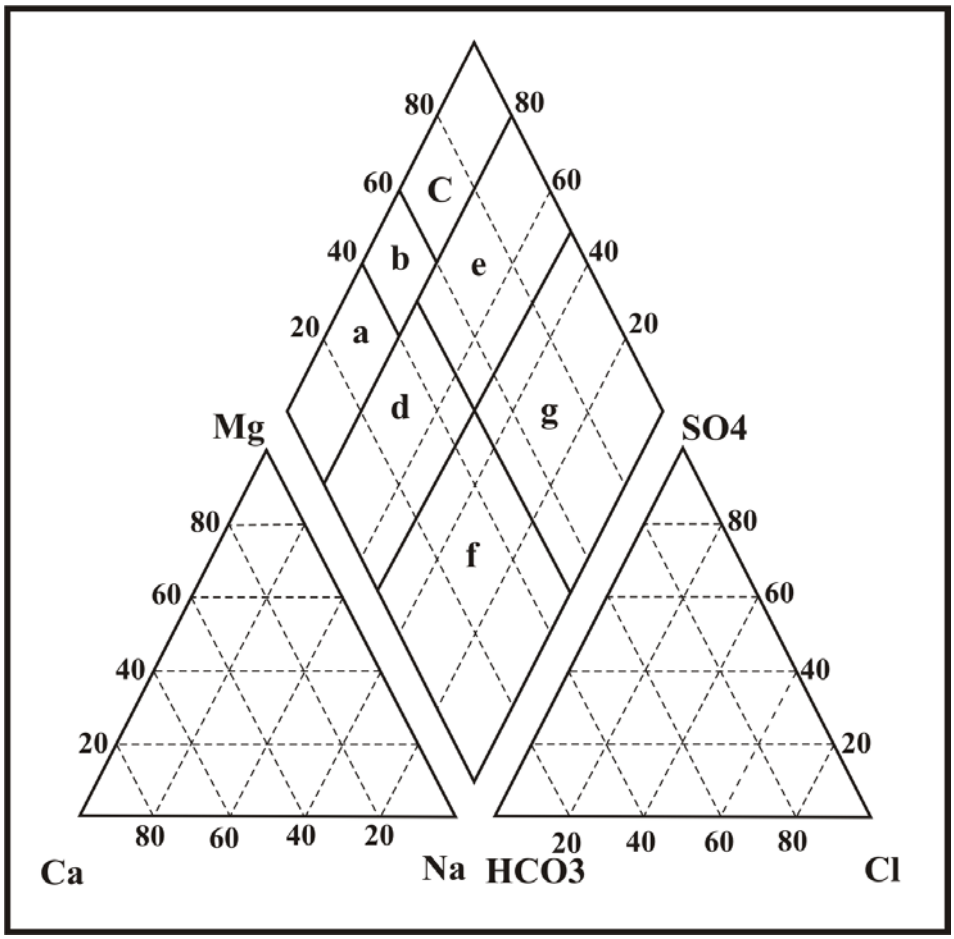

Fig. 2.7: Piper diagram (for explanation seeTable 2.3).

Table 2.3: Classification of Ground waters after Furtak and Langguth (1967).

Water Types	**Field (See Fig.2.7)**
Normal earth alkaline water	
With prevailing bicarbonate	a
With prevailing bicarbonate and sulfate or chloride	b
With prevailing sulfate or chloride	c
Earth alkaline water with increased portions of alkalis	
With prevailing bicarbonate	d
With sulfate and chloride	e
Alkaline water	
With prevailing bicarbonate	f
With prevailing sulfate-chloride	g

The main purpose of the **Durov diagram** is to cluster the data points indicating the samples with similar chemical composition as well as to reveal a useful relationships and properities for a large sample groups. It plots the major ions (as a percentages of milli-equivalents) with in two triangles, where the total cations and anions are set equal to 100%. The points in the two triangles are then projected onto a square grid that is perpendicular to the third axis of each triangle. Fig. 2.8 and Table 2.4 illustrates the classification of Lloyd and Heathcoat (1985).

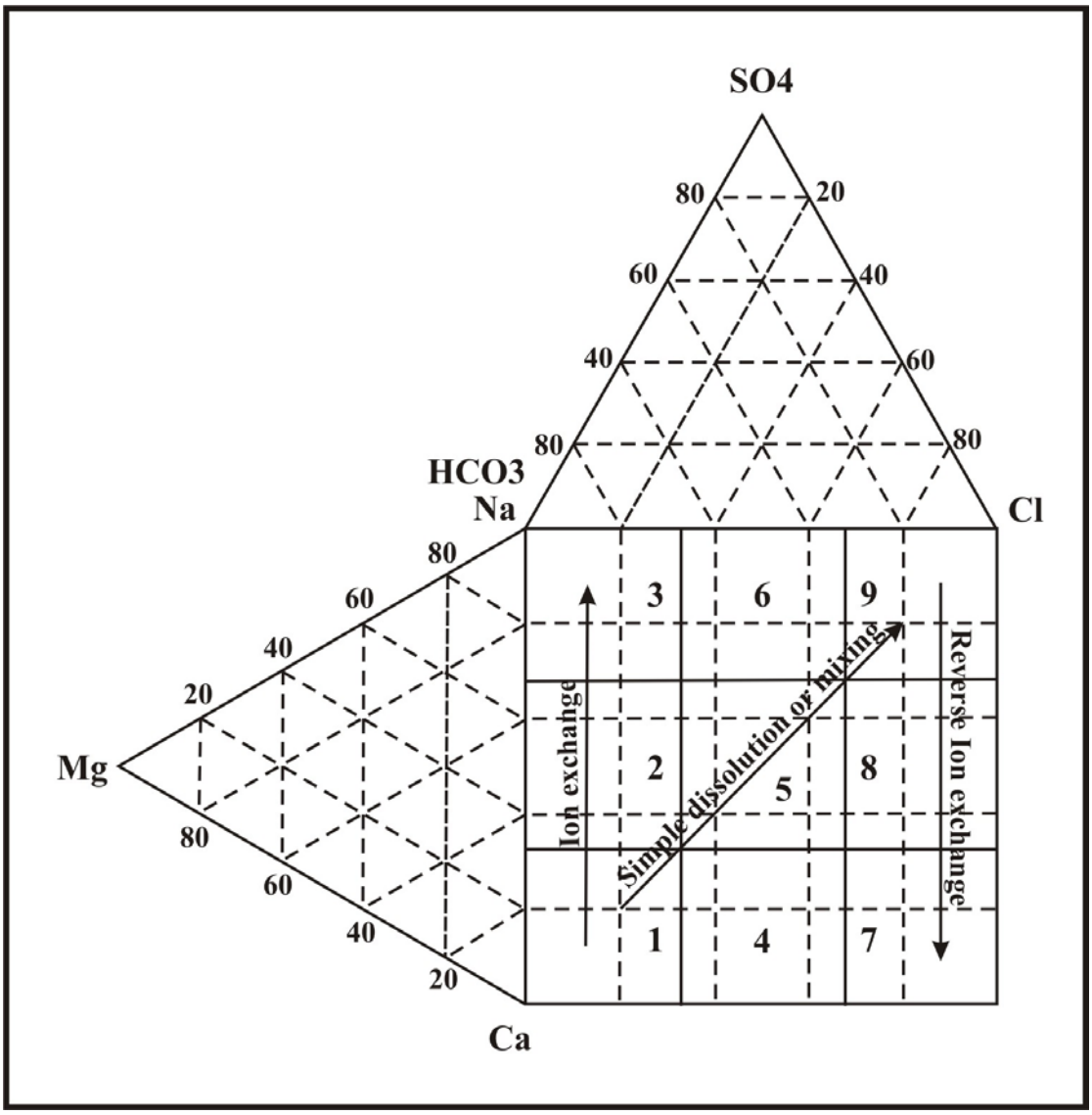

Fig. 2.8: Durov diagram for major cations and anions (for explanation see Table 2.4).

Table 2.4: Water classification and geochemical processes that could affect the water genesis after Lloyd and Heathcoat (1985).

Water type	Field (see Fig. 2.8)
HCO_3 and Ca are dominant, frequently indicates recharging water in limestone, sandstone, and other aquifers.	1
Water dominated by Ca and HCO_3 ions with presumed association with dolomite if Mg is significant. However, an important ion exchange is presumed if the Na is significant.	2
HCO_3 and Na are dominant which indicates an ion exchanged water, although the generation of CO_2 at depth can produce HCO_3 where Na is dominant under certain circumstances.	3
SO_4 dominates, or anion discriminant and Ca dominant, Ca and SO_4 dominant, frequently indicates a recharge water in lava and gypsiferous deposits, otherwise a mixed water or water exhibiting simple dissolution might be indicated.	4
No dominate anion or cation, which indicates water exhibiting simple dissolution or mixing.	5
SO_4 is dominant or anion discriminant and Na dominant; which is a water type that is not frequently encountered and indicates probable mixing influence.	6
Cl and Na are dominant, which is frequently encountered unless cement pollution is present other wise the water may result from reverse ion exchange of Na-Cl waters.	7
Cl is a dominant anions and Na dominate the cations, which indicates that the ground waters can be related to reverse ion exchange of Na-Cl waters.	8
Cl and Na dominant frequently indicate end-point waters.	9

Schoeller plots are semi logarithmic diagrams, which were developed by Schoeller (1962) to represent the analysis of major ions in milliequivelant per liter (meq/l) and in order to demonstrate the different hydrochemical water types on the same diagram (Fig. 2.9). It has the advantage that actual sample concentration are displayed and compared, but the number of analysis that can be illustrated at one time is limited.

Bar charts present the relative major ion composition in milliequivelant per liter (meq/l). In this study the Cations (Ca^{2+}, Mg^{2+}, Na^{+}, K^{+}) are plotted on the left of the diagram while the anions are plotted on the right ($HCO3^{-}$, Cl^{-}, SO_4^{2-}) (Fig. 2.10).

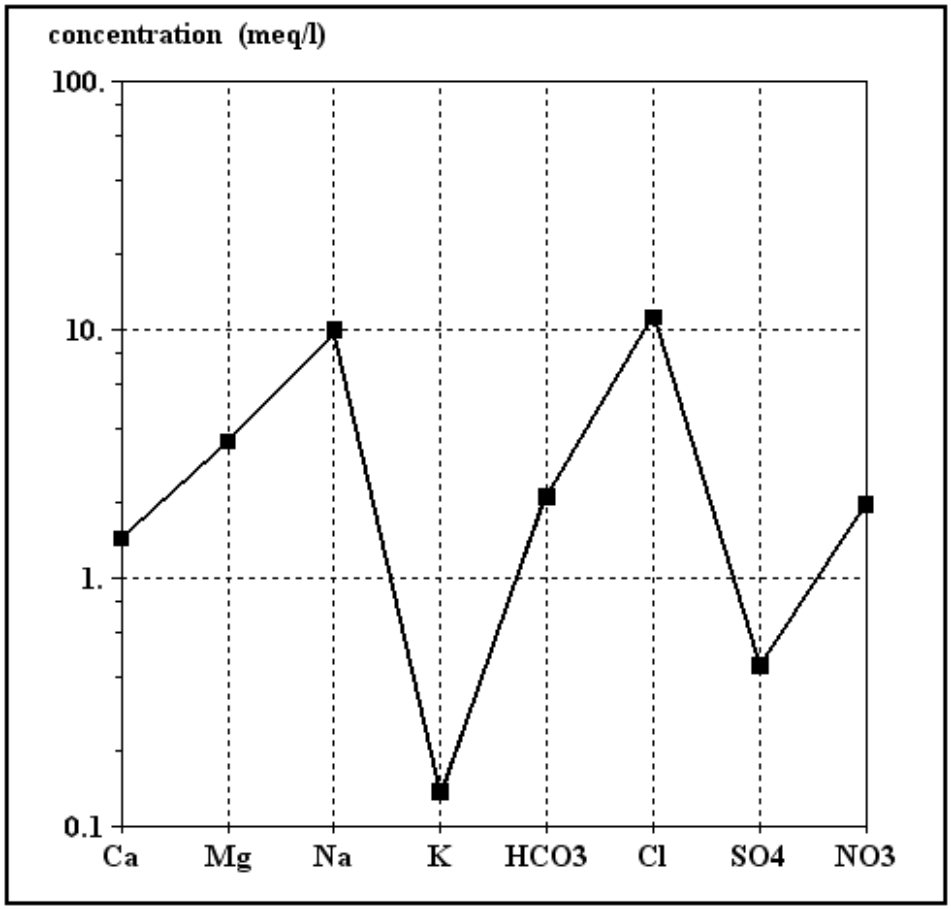

Fig. 2.9: Semi-logarithmic Schoeller plot.

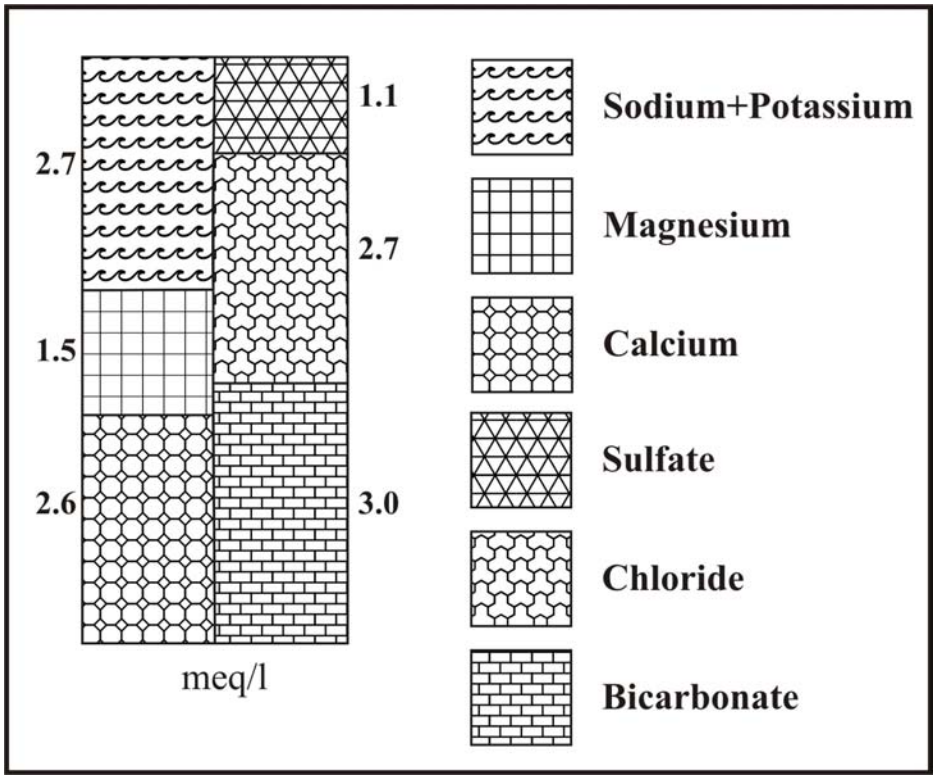

Fig. 2.10: Bar charts presenting the major cations and anions in meq/l.

2.3.2 Statistical evaluation of the hydrochemical parameters

The statistical analysis was done using SPSS 11. The minimum, maximum, mean and standard deviations were calculated for each parameter. Frequency diagrams were drawn to detect if the distribution of the variables were normal or not, then this was tested with Kolomogorov-Smirnov test for the goodness of fit. If the calculated significance value (α) is higher than the proposed significant level (α=0.05) this indicates a normal distribution of the studied parameter. Since most of the variables are not normally distributed; the nonparametric Spearmans rank correlation analysis was adopted to calculate the correlation coefficient.

Mann-Whitney test was applied to determine if the average of the results of the two sampling campaigns could be used for further statistical analysis. To group the samples into clusters according to their major chemical constituents; a Dendrogram was drawn trying different clustering methods and measure intervals. The Ward's method with the Euclidean distance was found to give the best Dendrogram that could be reasonably interpreted and represent the actual hydrochemical situation. Kruskal-Wallis and Mann-Whitney tests were applied to test the significance of the differences between the groups found by cluster analysis.

2.4 Geothermometers

Ground water chemistry provides a guide to determine the temperature at depths from which water is derived from. Geothermometery is considered to be one of the most important geochemical tools for exploration and development of geothermal resources.

2.4.1 Geothermometers types

According to D'Amore and Arnorsson (2000) geothermometers have been classified into three groups:

1. Water or solute geothermometers: They were developed between mid-1960s to the 1980s. The most important ones are the silica (quartz and chalcedony), Na/K and Na-K-Ca geothermometers. The others that have been developed are based on Na/Li, Li/Mg, K/Mg ratios and Na-K-Mg relationships.

2. Steam or gas geothermometers: They are used when the geothermal field consist only of hot ground, acid surface waters and fumaroles. In these fields the thermal groundwater table is subsurface. In such cases water geothermometers cannot be applied. There are three types of steam geothermometers:

a. Gas-gas equilibria;
b. Mineral-gas equilibria involving H_2S, H_2 and CH_4 but assuming CO_2 to be externally fixed according to empirical methods;
c. Mineral-gas equilibria.

3. Isotope geothermometers: Fractionation of light elements isotopes between compounds is significant and temperature dependent; this has made so the distribution of the stable isotopes of H, C and O between aqueous and gaseous compounds as geothermometers. Temperature is determined based on the calculated fractionation (α) between two compounds A and B using the formula:

$$\mathbf{1000 ln\alpha_{AB} = \delta_A - \delta_B}$$

where δ_A and δ_B designate the respective isotopic ratios in compounds A and B.

2.4.2 Principle and theory

Geothermometers are used to estimate the original subsurface reservoir temperature of ascending ground waters, which underwent conductive cooling during their ascent. They reflect the temperature dependence of individual rock water reactions. Reactants, which remain metastable dissolved while ascending to the surface are proportional to their original aquifer temperatures. For example SiO_2 (Quartz or chalcedony dissolution) or Na/K for albitisation.

Geothermometers are generally derived from the Van't Hoff equation and have the form:

$$\mathbf{T(^oC) = a/b + log(k) + 273}$$

Where a, b: are constants describing a straight line in the 1000/T-log(K) plot. K: depends on the reaction used for the geothermometer, for example it is SiO_2 for all SiO_2 thermometers, Na/K for the Na/K thermometer etc.

It should be noted that the geothermometres don't take the impact of pressure into account and don't correct the mineral solubility according to the pressure. The effect of pressure on the minerals saturation index is explained in section (4.5.5).

The difficult part in using geothermometry is that applying geothermometer to the same water samples furnishes different results. This is referred to:

1. That each geothermometer has its certain conditions, which should be fulfilled if a meaningful value is expected;
2. The residence time of water at depth was not sufficient to reach equilibrium;
3. The aquifer composition is different from the one assumed by the geothermometer;
4. The mineral used is present in the rock.

2.4.3 Geothermometers formulas

In order to determine which are the best geothermometers for these thermal springs and wells, different types of geothermometer were calculated. The following list shows the formulas that were used to calculate each geothermometer in this study:

1.Amorphus Silica: **$t(^oC)=[720/(4.52-\log(SiO_2))]-273.15$** (Fournier 1977);

2. Cristobalite Alpha: **$t(^oC)=[1000/(4.78-\log(SiO_2))]-273.15$** (Fournier 1977);

3.Cristobalite Beta: **$t(^oC)=[781/(4.51-\log(SiO_2))]-273.15$** (Fournier 1977);

4.Chalcedony: **$t(^oC)=[1032/(4.69-\log(SiO_2))]-273.15$** (Fournier 1977);

5.Quartz: **$t(^oC)=[1309/(5.19-\log(SiO_2))]-273.15$** (Fournier 1977);

6. Quartz steam loss: **$t(^oC)=[1522/(5.75-\log(SiO_2))]-273.15$** (Fournier 1977);
where:
SiO_2 is the concentration of silica as SiO_2 in mg/kg.

7. K/Mg: **$t(^oC)=[4410/(14-\log(K^2/Mg))]-273.15$** (Giggenbach 1988);

8. Na/K: **$t(^oC)=[777/(0.7-\log(Na/K))]-273.15$** (Fournier 1973);

9. Na/K: **$t(^oC)=[856/(0.857-\log(Na/K))]-273.15$** (Truesdell 1976);

10. Na/K: **$t(^oC)=[1180/(1.31-\log(Na/K))]-273.15$** (Fournier & Potter1979);

11. Na/K: **$t(^oC)=[1217/(1.483-\log(Na/K))]-273.15$** (Fournier 1979);
where:
Na and K are concentration of dissolved sodium and potassium in mg/kg.

12. Na-K-Ca: **$t(^oC)=1647/\{\log(Na/K)+\beta[\log(Ca/Na)+2.06]+2.47\}-273.15$** (Fournier 1979)
where:
Na, K, Ca are the ionic concentration in mg/kg of the sodium, potassium and calcium in the hot water;
$\beta=1/3$ for $T>100^oC$;
$\beta=3/4$ for $T<100^oC$.

13. Na-K-Ca (Mg corrected) (Fournier 1979)

This geothermometer is based on a variable, which is **R**
Where:

$$\mathbf{R=\{C_{Mg} / C_{Mg}+00.61C_{Ca}+0.31C_k\}*1000}$$

where C_x represent the concentration in ppm of the component x
For $1.5 < \mathbf{R} < 5$, the Mg Correction (Δt_{Mg} in ^oC) is:

$$\mathbf{t_{Mg}=-\Delta 1.03+59.971\log R+145.05(\log R)^2-36711(\log R)^2/T-1.67*10^7\log TR/T^2}$$

For $5 < \mathbf{R} < 50$, the Mg Correction (Δt_{Mg} in ^oC) is:

$$\Delta t_{Mg}=10.66-4.7472\log R+325.87(\log R)^2-1.032*10^5(\log R)^2/T-1.968*10^{71}\log R/T^2+1.605*10^7(\log R)^3/T^2$$

where the Δt_{Mg} is substracted from the Na-K-Ca geothermometer value. The Mg correction will not be applied if Δt is negative or R<1.5 and if R<1.5 the measured spring temperature is being selected and T represent the calculated Na-K-Ca temperature in Kelvin.

14. Isotope SO_4-H_2O: **$1000\ln\alpha= 3.88(10^6/T^2)-3.4$** (Lloyd 1968);
where: $\alpha= (1000+\delta^{18}O_{SO4})/(1000+\delta^{18}O_{H2O})$
T in Kelvin.

15. Isotope SO_4-H_2O: **$1000\ln \alpha =3{,}01(10^6/T^2)-7.3$** (Kusakabe1974);
where: $\alpha= (1000+\delta^{18}O_{SO4})/(1000+\delta^{18}O_{H2O})$
T in Kelvin.

16. Isotope SO_4-H_2O: **$1000\ln\alpha=2.88(10^6/T^2)-4.1$** (Mizutani and Rafter 1969);
where: $\alpha= (1000+\delta^{18}O_{SO4})/(1000+\delta^{18}O_{H2O})$
T in Kelvin.

2.4.4 Giggenbach triangle

To assess the degree of water-rock equilibrium, Giggenbach (1988) suggested a new method named Giggenbach triangle (Fig. 2.11). It combines the fast responding K/Mg geothermometer with the slowly re-equilibriating Na/K geothermometer. In this Na-K-$Mg^{1/2}$ triangle, the two systems are being presented by two sets of lines and they are constant Na/K ratio and $K/Mg^{1/2}$ ratios, which radiate from the $Mg^{1/2}$ vertex and the Na vertex respectively. Since each value of the Na/K ratio and $K/Mg^{1/2}$ ratio corresponds with a unique temperature value, each of these lines is an isotherm. The intersection of the isotherms of each Na/k and K/Mg ratio, which refers to the same temperature, corresponds to water compositions in equilibrium with the mineral phases controlling both geothermometers and delineates the full equilibrium curve.

Giggenbach triangle is composed of three main zones (immature waters along the base, partially equilibriated waters in the middle and fully equilibriated waters along the upper curve) (Fig. 2.11). The extent of rock-water equilibrium can be determined from the sample plots on the triangle that depends on the concentration of K, Mg and Na.

Giggenbach triangle is considered to be a useful tool because it allows an immediate distinction between waters, suitable or unsuitable for the application of ionic solute geothermometry; it also allows the assessment of deep equilibrium temperature and evaluation of re-equilibriation and mixing effects on a large number of water samples (Marini 2000).

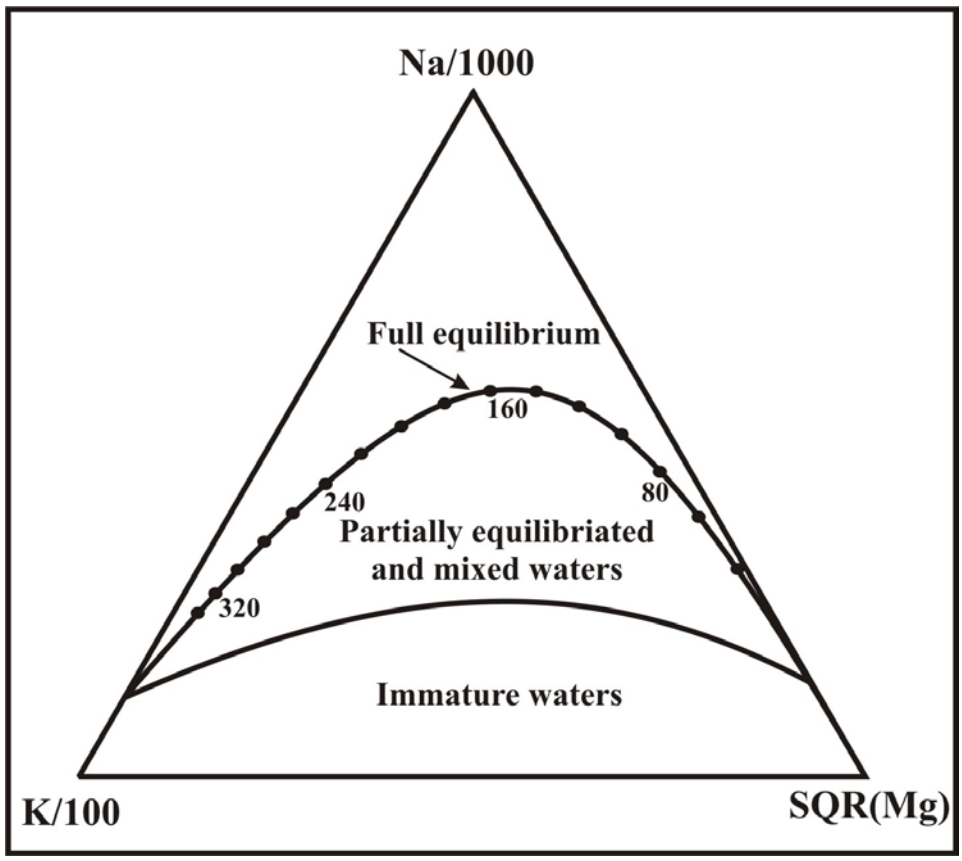

Fig. 2.11: Giggenbach triangle.

2.5 Geochemical modeling

The hydrochemical parameters were modeled with PhreeqC version 2.10.03, Solomineq88 and Aquachem version 3.7.42 with its PhreeqC interface. The modeling included geochemical speciations, saturation indices calculations, mixing water samples, and reverse modeling.

The Aquachem software package deals with the graphical analysis as well as modeling of aqueous geochemical data. It covers a variety of functions and calculations for interpreting and comparing hydrochemical data. It features a built-in graphical interface to PhreeqC to perform some of PhreeqC's simulation capabilities.

The PhreeqC is based on an ion dissociation aqueous model (Parkhurst and Appelo 1999) and was used to calculate equilibrium concentrations (activities) of the chemical species in the solution and the saturation indices of solid phases in equilibrium with the solution as well as the reverse modeling

2.5.1 Saturation index

The saturation index (SI) is used to express whether a solution is in equilibrium with a solid phase or if it is under or over saturated in relation to a solid phase respectively. The degree of water saturation with respect to a mineral is expressed by:

$$\mathbf{SI = Log(IAP/K_{sp})}$$

where IAP is the ion activity product and K_{sp} is the solubility product.

Practically, SI value ranging between -0.2 and 0.2 indicates equilibrium (Merkel and Planner-Friedrich 2005). SI value of more than 0.2 indicates water that is super saturated to the corresponding mineral. SI value of less than -0.2 indicates water that is under saturated with respect to the corresponding mineral.

2.5.2 Inverse mass balance modeling

Garrels and Mackenzie (1967) introduced the inverse mass balance modeling for the first time. Inverse mass balance modeling attempts to determine sets of mole transfers of phases that account for changes in water chemistry between one or a mixture of initial water compositions and a final water compositions (Parkhurst and Appelo 1999).

The major advantage of PhreeqC inverse modeling is its capability to include uncertainties in the analytical data that are in the inverse modeling calculation; this capability produces a robust model-calculated mole transfers.

According to Zhu and Anderson (2002) the applicability of the inverse mass balance modeling hinges on a number of assumptions and they are:

1. The two water analysis of the initial and final wells or springs should represent volumes of water that flow along the same path;
2. Dispersion and diffusion do not significantly affect solution chemistry;
3. A chemical steady state prevailed during the time considered;
4. The mineral phases, which are used in the calculation, are or were present in the aquifer.

2.6 Scale forming and corrosivity

The thermal waters have been tested to determine whether they are corrosive or scale forming. The Langlier saturation index (ΔpH) was calculated in order to determine whether the waters are corrosive or scale forming. The ΔpH can be calculated by:

$$\mathbf{\Delta pH = pH\text{-}pHs}$$

where the pH is the measured pH value. The pHs was calculated using PhreeqC, where it is the pH value at equilibrium with calcite. According to German standards, the permissible limit is when ΔpH range between –0.2 and 0.2. When the ΔpH > 0.2; the water is considered to be scale forming. When the ΔpH < -0.2; the water is considered to be aggressive (Merkel and Planner-Friedrich 2005).

The thermal waters were also classified based on the calcite saturation index, which is considered as another corrosion or scale forming indicator. The Wilex University (2004)

classification was used in this study where the saturation index (SI) ranges between -5 (severe corrosion) to 4 (severe scale forming).

2.7 General review of the isotopes used in this study

2.7.1 Tritium

Tritium (^3H) is a radioactive hydrogen isotope, which decays by β-decay to ^3He. It has a half-life ($T_{1/2}$) of 4500±8 days where 8 days corresponds to one standard uncertainty which equals 12.32 years (Lucas and Unterweger 2000) with a decay constant:

$$\lambda = \ln(2)/T_{1/2} = 0.05626\ yr^{-1}$$

Tritium (^3H) natural abundance is usually expressed in Tritium units (TU) where 1 TU = 1 ^3H atoms per 10^{18} H atoms and 1 TU = 0.118 $Bq.kg^{-1}$. Tritium is introduced to the hydrological cycle by both natural and human sources. It is formed in the atmosphere when the nitrogen is bombarded by cosmic rays according to the following reaction:

$$^{14}N + n \rightarrow {}^3H + {}^{12}C$$

Where n is a neutron from the cosmic radiation. About 3-5 % of all neutrons in the upper atmosphere react with Nitrogen to form ^3H (Ferronsky and Polyakoc1982).

According to Nir (1964) the natural concentration of Tritium is estimated to be between 4 to 25 TU depending on the location. Man introduced Tritium through the atmospheric nuclear testing. Between 1954–1958 and 1961–1962 large amount of tritium were released to the atmosphere. The other sources of Tritium (^3H) are weapon-producing industries, digital watch manufactures (which is being released to the atmosphere directly and to the hydrologic cycle) and nuclear power plants and in particular nuclear reprocessing plants.

Tritium (^3H) is used for dating of ground water because atomic weapon testing influenced its concentration in the precipitation. According to Clark and Fritz (1997) the concentration of tritium in precipitation is being affected by the following parameters:

1. Hemispherical and latitudinal effect;
2. Continental effects;
3. Altitude effect;
4. Seasonal effects.

Tritium is often used as a general guide to distinguish between Pre-bomb and post- bomb, which means recharge that happened before and after the atomic nuclear testing. The general rule to identify pre-bomb in ground water is: < 4 TU in high continental latitude and > 4 TU in low continental latitude (Fontes et al. 1979).

Also in ground water studies one would adopt the following as a general guide:

1. No Tritium, i.e. background of gas counting technique after electrolytic enrichment, indicates water older than 50 year;
2. Detectable Tritium means mixing with recent (past1952) waters (Fontes 1980).

2.7.2 Tritium/Helium-3 ($^3H/^3He$) method

This method was introduced for the first time in 1997 (Torgersen et al. 1979). In the literature this method is described to be suitable for dating ice with an age up to 100 a. It is possible to estimate the time since deep groundwater has been contact with the atmosphere (Geyh and Schleicher 1990).

By measuring tritium (^3H) together with its daughter Helium-3 (^3He), the true ages can be determined through calculation, which don't rely on complicated tritium input function (Clark and Fritz 1997).

2.7.2.1 Basic concept

Since the tritium-dating concept have lost some of its significance because of the anthropogenic tritium as a result of atomic tests which have masked the initial ^3H activity which have changed the tritium level in the rain, for example since the beginning of the 1970 the rain and snow in the northern hemisphere have a tritium specific activity in a narrow limits 20-40 TU and this content is maintained by nuclear power plants.

Also the natural input into the hydrogeological reservoirs (through precipitation, vapor exchange and river runoff) which varies from year to year and place to place and water might be a mixture from old and a new water which affects the tritium content and its always subjected to seasonal fluctuation, for example rain water in summer have more tritium than snow, and because of that the tritium helium technique was developed to solve the problem of varying tritium input.

According to Sultenfuss and Massman (2004) the following conditions must be fulfilled so that the Tritium/Helium-3 age determination could be looked as a time difference between the sampling and the last contact of the water with the atmosphere:

1. All helium sources has to be quantified;
2. The helium in the groundwater aquifer does not exchange with the atmosphere after the entry of the ^3H;
3. The dispersion transport in the aquifer must be neglectably small compared to the advection transport.

Beside the Tritiogenic Helium (He_{trit}), their are four sources of Helium. Helium which results from the exchange between the water and the atmosphere, this source could be divided into two types: (i) Equilibrium Helium (He_{equi}), which is a part that represent the solution mass balance; (ii) Excess Helium (He_{excess}), which represent the excess part. Two other types of Helium are not atmospheric. They are: (iii) Radiogenic Helium (He_{rad}),

which result from the Uranium and Thorium decay; (iv) Primordial Helium (He_{prim}), which comes from the earth's mantle (Sultenfuss and Massman 2004).

2.7.2.2 Tritium helium systematic

According to Clark and Fritz (1997), the decay of Tritium (^3H_t) from its initial concentration (^3H_o) after some time (t) is being predicted by the following equation:

$$^3H_t = {}^3H_o.e^{-\lambda t} \quad (1)$$

where λ is the decay constant $\lambda = \ln 2/T_{1/2}$

So in order to determine (t), it requires the knowing of (^{3}Ho) and because the decay of Tritium leads to ingrowths of (^{3}He) and the formula is then:

$$^3He_t = {}^3H_o(1-e^{-\lambda t}) \quad (2)$$

And by combining both of the equations (1) and (2), the dependency on the input concentration of tritium (^3H_o) could be cancelled, so the equation becomes:

$$^3He_t = {}^3H_t(e^{-\lambda t} - 1)$$

The Helium concentration at time (t) is being expressed in Tritium units (TU).

The measured ^{3}He value, which represents the ^{3}He ingrown from ^{3}H decay, and is then used in the following dating equation:

$$\tau = T_{1/2}/\ln 2 \,*(\ln 1 + [^3He_t][^3H_t])$$

where the $[^3He_t][^3H_t]$ is the concentration ratio of these two isotopes expressed in tritium units.

2.7.2.3 Age calculation

The following discusses the derivation of the equations in more details:

In a ground water (Fig. 2.12), which is being recharged by rainwater at time (t_o) and in the time of sampling (t), the age (τ) is being calculated as the difference between the time of the sampling and the time of recharge as follows:

$$\tau = t - t_0$$

At the time of recharge (t_0):

$$[^3H] = [^3H]_o \text{ and } [^3He] = 0$$

While at the time of sampling (t):

$$[^3H] = [^3H]_t = [^3H]_o \,.\, \exp\left(\frac{-\ln 2}{T_{1/2}} \,.\, \tau\right) \quad \textbf{(1)}$$

and

$$[^3He]_t = [^3H]_o - [^3H]_t \quad \textbf{(2)}$$

From the second equation, $[^3H_o]$ is being extracted, where both $[^3He]_t$ and $[^3H]_t$ are being measured as follows:

$^3H_o = {}^3He_t + {}^3H_t$

so the value of $[^3H]_o$ is being taken and substitute it in the first equation in order to calculate τ,

The first equation $^3H_t = {}^3H_o \,.\, \exp\left(\frac{-\ln 2}{T_{1/2}} \,.\, \tau\right)$ becomes:

$$^3H_t = (\,^3He_t + {}^3H_t\,).\, \exp\left(\frac{-\ln 2}{T_{1/2}} \,.\, \tau\right)$$

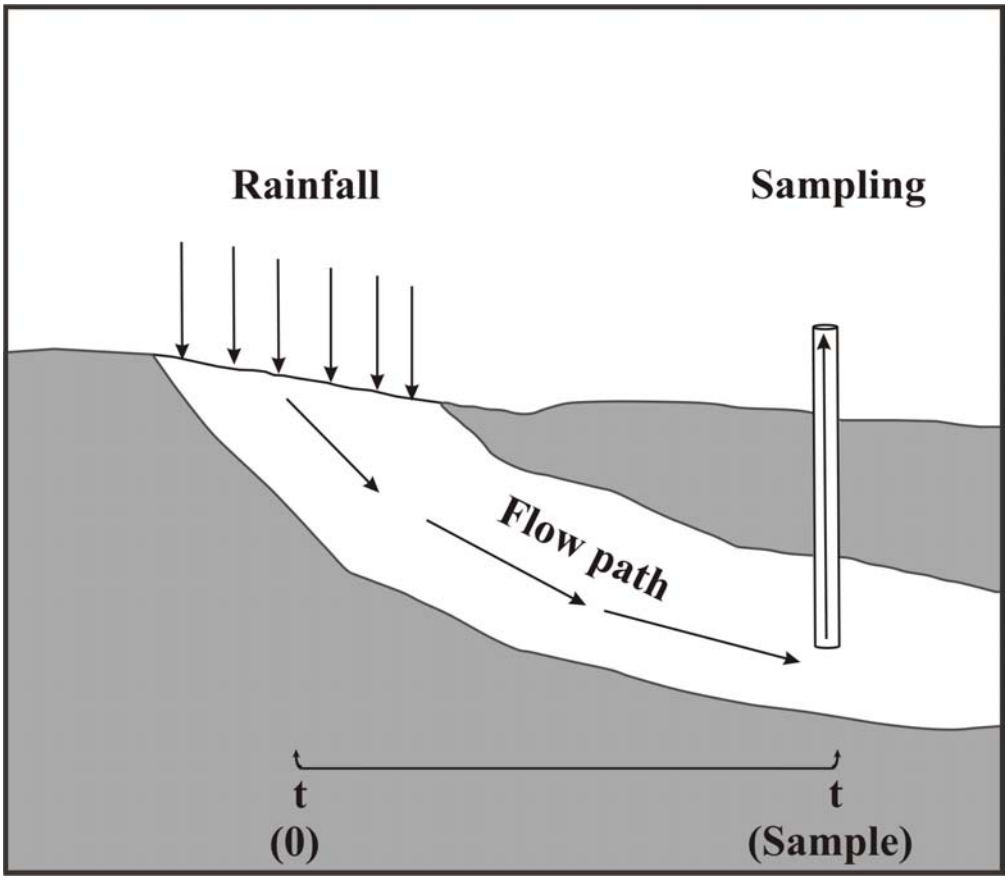

Fig. 2.12: Schematic diagram for the calculated component in the tritium helium age determination method.

By rearranging the equation, it becomes:

$$\exp\left(\frac{+\ln 2}{T_{1/2}} \cdot \tau\right) = 1+\frac{[^3\mathrm{He}]_t}{[^3\mathrm{H}]_t}$$

By another rearrangement for the equation, the final equation that will be used for age calculation will be as follows:

$$\tau = \frac{T_{1/2}}{\ln 2} \cdot \ln\left(1+\frac{[^3\mathrm{He}]_t}{[^3\mathrm{H}]_t}\right)$$

2.7.3 Identifying the Helium source in the samples

According to Centre for isotope geochemistry (2004), the noble gasses especially the Helium and the Neon are considered to be an excellent tracer for the fluid origins and the reservoir processes for the following reasons:

1. They are chemically inert and therefore they behave conservatively in the water-rock system;
2. They are moderately soluble in water and their solubility in water is a function of temperature (known up to the critical point for water);
3. There are three terrestrial reservoirs:

A.The earths mantle: it is believed that the earth's mantle to be partially or non-degassed and enriched in an indigenous or primordial noble gas component, which was inherited from meteoric materials through accretion during the earth's formation. The noble gas composition of the mantles reservoir of the present day is defined by the composition of the Mid-Ocean Ridge Basalt (MORB) and the Ocean Island Basalts (OIB). This reservoir is characterized by a $^3He/^4He$ ratio of 1.2 to $4.8 \cdot 10^{-5}$ (Centre for isotope geochemistry 2004).

B. The earth's crust: the processes which is involved in the formation of earth's continental and oceanic crusts result in a general enrichment of the incompatible lithophile elements such as K, U and Th, a depletion of noble gases and therefore a contaminant enrichment in the K/Ar and the (U+Th)/He ratios. Therefore old crustal materials tend to be enriched with respect to radiogenic noble gasses, which is produced by decay of naturally occurring radioactive isotopes like ^{40}K, U and Th, and tend also to be enriched in nucleogenic noble gasses, which is produced by nuclear interactions induced by natural radioactivity. From the nuclear theory, the theoretical composition of crustal noble gases can be calculated by using an average crustal elemental composition. The theoretical calculation has been confirmed by the noble gas isotope and abundance of hydrocarbon fluids from crustal region void of any recent magmatic/volcanic/mantle involvement. The earth's crust is characterized by a $^3He/^4He$ ratio of a bout $2 \cdot 10^{-8}$.

C. The Atmo-Hydrosphere: it represents an integrated mixture of noble gasses from the mantle and crust over 4.6 billion years of the earth's history. The one exception is the atmospheric abundance of helium. The atmosphere is strongly depleted with respect to helium relative to the other noble gasses because helium is very light and the earth's gravitational field is not able to retain He-isotopes from escaping the atmosphere. It is characterized by a $^3He/^4He$ ratio of $1.4 \cdot 10^{-6}$.

Table 2.5 shows the helium concentration, $^3He/^4He$ and R/R_{air} for the atmosphere, surface water, crustal fluids and mantle Helium (Clark and Fritz 1997).

Table 2.5: The helium abundance and isotope ratio in different reservoirs after (Clark and Fritz 1997).

Source	He concentration	$^3He/^4He$	R/R_{air}*
Atmosphere	5.24 ppmv	$1.38 \cdot 10^{-6}$	1
Surface water	4.5*10-8 Cm^3 STP/g	$\sim 1 \cdot 10^{-6}$	~1
Crustal fluids	10^{-7} to $<10^{-4}$ Cm^3 STP/g	$\sim 10^{-8}$ to $<10^{-10}$	0.007 to 0.022
Mantle Helium	up to $2.7*10^{-5}$ Cm^3 STP/g	1 to $3 \cdot 10^{-5}$	7 to 21

* $R=^3He/^4He$ and $R_{air}=1.4*10^{-6}$

2.7.4 Water stable isotopes ($\delta^{18}O$ and δD)

The two stable isotopes of water ($\delta^{18}O$ and δD) have proved to be an excellent proof for the water recharge and variable different conditions. The isotopic composition have also proved in different parts of the world to be a potential source of the information on climatic conditions of the past especially in the arid areas like the Middle East (Bajjali and Abu-Jaber 2001). The comparison of ground water data with present day precipitation can lead to conclusion on the climatic conditions that prevailed the area in the past and shed more light about the climatological conditions, which could have affected the precipitation.

There are many factors that affect the stable isotopes signatures. Those parameters are usually derived from the climate and they are mainly: precipitation temperature, the climatological conditions that is available during the condensation, and the relationship between the oxygen and deuterium stable isotopic content (Gat 1980). Also there is a good positive relation between $\delta^{18}O$ of the rainwater and the temperature of precipitation (Fricke and O'Neil 1999).

The base line relationship of the $\delta^{18}O$ and δD that is called Global Meteoric Water Line (GMWL) (Fig.2.13) defined by (Craig 1961) as:

$$\delta D = 8\delta^{18}O + 10$$

In eastern Mediterranean, this relationship is called Mediterranean Meteoric Water Line (MMWL) (Fig. 2.13) defined by Gat and Carmi (1970) as:

$$\delta D = 8\delta^{18}O + 22$$

A slope of 8 is reflecting the standard relationship of pure un-evaporated rainwater. According to Gat (1980) rainwater partial evaporation causes the slope to decrease while an intercept of 10 in the GMWL and 22 in the MMWL reflects the conditions of the source of evaporation (Gat 1996). Deuterium excess is a function of relative humidity and wind speed at the evaporation source (Merlivat and Jouzel 1979), although the recharge through the vadose zone doesn't alter the isotopic composition of the water and thus the change in slope of the $\delta D/\delta^{18}O$ ratio may cause a decrease in the intercept of the regression line (Ayalon et al. 1998).

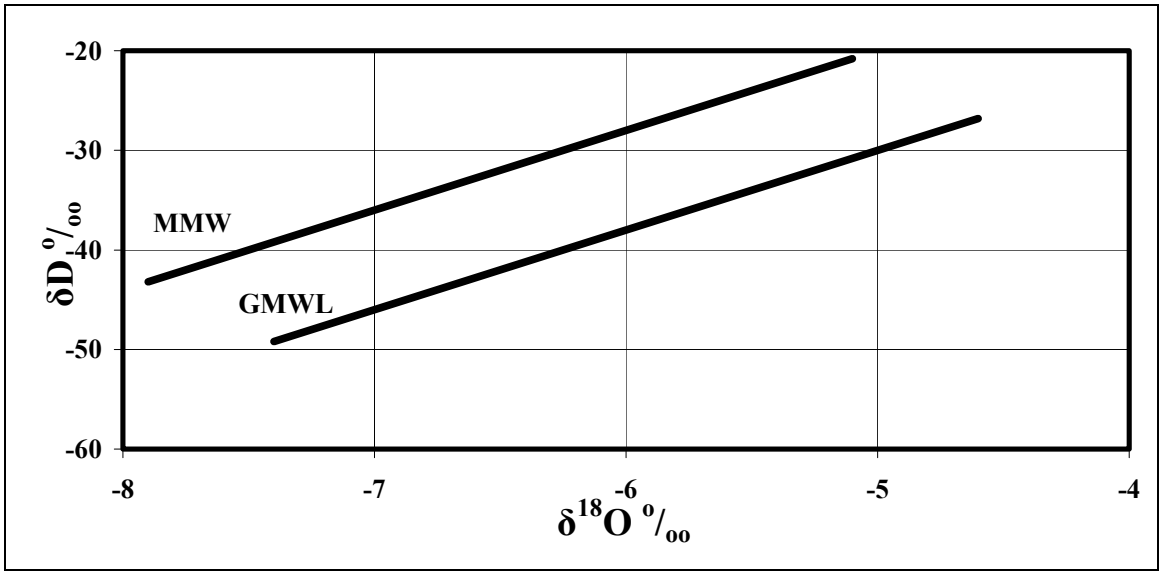

Fig. 2.13: The Mediterranean Meteoric Water Line (MMWL) compared to the Global Meteoric Water Line (GMWL) on the δD -$\delta^{18}O$ diagram.

The intercept (d) value was defined by Dansgard (1964) as:

$$d = \delta D - 8\delta^{18}O$$

The d-value or sometimes called the d-excess is a measure of the deuterium enrichment that exceed the $\delta^{18}O$ value by more than 8 times (Clark and Fritz 1997). It is also considered to be a measure of evaporation to form vapor effect during primary evaporation when the water is being evaporated to form a vapor mass and during secondary evaporation. A high d-value indicates low humidity and rapid kinetic evaporation effects on isotopes and secondary evaporation might happen during rainfall in a hot dry column and in this case causes low d-value, which is usually negative (Clark and Fritz 1997).

3. AREA OF INVESTIGATION

3.1 Climate

Jordan is classified as a semi desert area; the temperature varies across this area according to the latitude, the altitude and the physiographic provinces. The hilly areas of the high lands and plateau enjoy a Mediterranean climate, which is characterized by hot dry summers and cool winters with short transitional seasons.

According to Exact (2004), the average mean temperature (in Amman) for January ranges from 7 to 9 ^{o}C and in summer the average mean temperature is about 24 ^{o}C. The average daily mean temperature in the Jordan Valley rift area ranges from 15.6 ^{o}C in winter to 32.5 ^{o}C in summer but the average temperature is 24 ^{o}C (Salameh 1996). The temperature in the region might drop to below the freezing point when the air comes from cold polar regions. The area suffers also during spring and autumn from very hot days called (Khamasini) which might produce temperature rises from 10 to 20 ^{o}C above average and reaches 45 ^{o}C (Exact 2004).

3.1.1 Precipitation

Precipitation in Jordan occurs mainly as rainfall. Snowfall happens once or twice every year on the highlands. The rainfall usually extends from October until April and the highest amount of precipitation occurs in January and February.

The climate characteristics exhibit large changes from one area to another and across the seasons and the years as shown in the rainfall map (Fig. 3.1). The average rainfall decreases from the west to the east and from north to the south. Ranging from 600 mm to less than 50 mm in the desert area. The high lands of Ajloun, Balqa, Karak, and Shoubak receive a long term annual average of about 600, 550, 350 and 300 mm respectively (Salameh 1996). Moving eastward or westwards the precipitation decreases noticeably and reaches 250 mm in the Jordan Valley 10 km west of Ajloun and to 50 mm 30 km west of Shoubak.

3.1.2 Relative Humidity

In general, in Jordan the relative air humidity is low with about 50-60% in winter and dropping sometimes in summer to about 15% (Salameh1996). In the southern part of the study area the relative humidity is very low with a long term daily mean of about 64% in the coldest periods of the year (January and February) decreasing to about 27% in the hot summer months, while it ranges from 30% in summer to about 70% in winter in the northern parts of the study area (Salameh 2001).

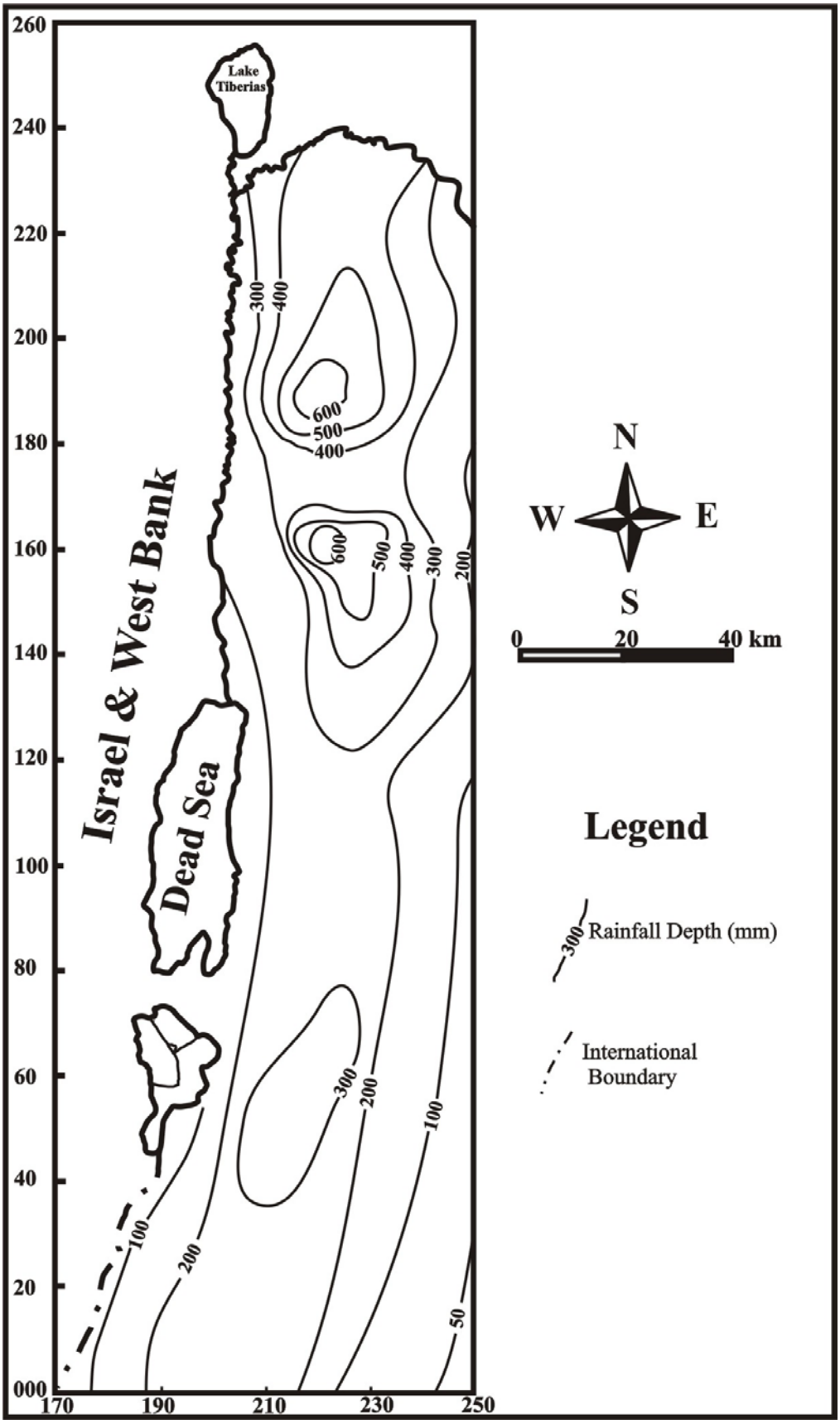

Fig. 3.1: Rainfall distribution in the area of study (mm/year) (modified after MWI 1996).

3.1.3 Evaporation

Generally, the potential evaporation in Jordan ranges between 1600 mm/year in the northwestern part to more than 4000 mm/year in the southern and eastern parts like Aqaba and Azraq areas (Salameh 1996).

Due to high temperatures and low relative humidity the Rift Valley potential evaporation ranges from 2000 m/year in the north to about 2400 mm/year at the Dead Sea Shores and increases further to the south to peak with 4000 mm/year in Aqaba area (Salameh 1996, 2001).

3.2 Geology

3.2.1 Stratigraphy

The outcropping rocks in the study area consist from the late Pre-Cambrian basement in Wadi Araba to Quaternary deposits in the Jordan valley. Fig. 3.2 shows the outcropping map of Jordan. Fig. 3.3 shows a detailed outcropping map of the Dead Sea Tranosform (DST). Figs. 3.4, 3.5, 3.6 and 3.7 shows cross sections in North Shuneh (A-A`), As Salt (B-B`), Al Karama (C-C`), Ma'in (D-D`), Ar Raba (E-E`-E``-E```) and Al Karak (F-F`) provinces.

The adopted terminology in this work is based on the Jordan Geological 1:50,000 Mapping Project (JGMP). Previous litostratigraphical nomenclature is shown in Table (3.1).

3.2.1.1 Late proterozoic (Safi group)

Sarmouj Conglomerate formation (SC): This formation is well exposed near the southern end of the Dead Sea to the east of Ghor El-Safi. It forms very rugged terrain cut by westward draining wadis (Powell 1988 and Jarrar 1991). It consist of well rounded boulders set in strongly consolidated arkosic cement; these dominated beds are being separated by well defined bands up to several meters thick of less strongly cemented limestone (Bender 1974, Powell 1988 and Jarrar 1991). Jarrar (1991) determined the age of Sarmouj of about 595-600 million year. The formation is intruded by the Quani Diorite (QU) in the southeastern part of the Dead Sea, which is Cambrian coarse-grained monzodiorite with biotite and large plagioclase laths.

3.2.1.2 Paleozoic sediments (Ram Group)

The Paleozoic sediments consist of four formations: Salib, Burj, Umm Ishrin and Disi.

- **Salib formation (SB)** is a complete sequence unconformably overlying the Sarmouj conglomerate. It is exposed east of the southern part of the Dead Sea and north of Wadi Al-Hasa. This formation consist of white, yellow-brown and purple, medium to coarse-grained arkosic and sub arkosic sandstone. It is of lower Cambrian age.

➢ **Burj Dolomite Shale formation (BDS)** forms a step cliff between the Salib formation and Umm Ishrin formation. This formation consists of two silicatic members separated by carbonate member; Tayan siltstone (TS), Numayri Dolomite (ND) and the Hanneh siltstone (HS) (Powell 1988). It crops out 11 km north of Wadi Zarqa Ma'in with a thickness of 74 m and in the southeastern part of the Dead Sea. It is from lower middle Cambrian (Shawabkeh 1998).

➢ **Umm Ishrin Sandstone formation (IN)** is equivalent to Quwiera Sandstone of Quennel (1951) and Burdon (1959) (Table 3.1). It keeps its characteristics throughout its outcrops from the Ram area to the southeast tip of the Dead Sea and it exposes in the deeply incised wadis and along the Dead Sea (Moh'd 1988). This formation is considered to be as an index formation.

Umm Ishrin formation crops out at the north of Wadi Al-Hasa and eastern part of the Dead Sea near Wadi Al-Hidan. This formation consists of medium to coarse grained, massive weathered sandstone and from lenticular bedding. The ideal thickness of Umm-Ishrin formation is 300-350 m. Its depositional environment starts as low braided low sinuosity, then changing into meandering of intermediate sinuosity (Amiereh et al. 1994). It is from the middle-late Cambrian.

➢ **Disi Sandstone formation (DI)** is defined by uncomfortable overlying with the Kurnub Sandstone. It consists of white, rounded, medium grained, massive quartz arenite sandstone. Amierh (1993) found that the Disi formation persists until Wadi Numeirah to the east of Potash factory. The Disi formation displays the normal spherical or dome-like weathering morphology, overturned and contorted cross bedding and the presence of dispersed quartz pebbles throughout (Amiereh 1993). Its age is from the upper Cambrian to lower Ordovician.

3.2.1.3 Triassic

Triassic rocks crop out in the area between Zarka Ma'in (Ma'in springs) and Wadi Al-Kafreen. The thickness of these rocks increases toward Wadi Husban to the north.

The Triassic rocks consist of eight formations: Umm Irna, Ma'in, Dardour, Ain Musa, Husban, Mukeiris, Umm Tina and Abu Rweis.

➢ **Umm Irna Sandstone formation (UI)** is outcropping adjacent to the Dead Sea shorelines as cliffs. It consists of two parts; lower thin-bedded clastic unit and upper thick-bedded clastic unit of sandstone upward fining sequences. It is of Permo-Triassic age (Bandel and Khoury 1981).

➢ **Ma'in Sandstone formation (MN)** consist of sandstone, siltstone, clay stone with carbonate rocks with a thickness of about 74 m. It outcrops along the eastern shoreline of the Dead Sea and in deep wadis between Wadi Mukheiris to the north and Al-Mamaleh to the south. Its age is Scynthian (Cox 1932).

Table 3.1: Previous lithostratigraphic nomenclature for the study area compared to the presenrt scheme (modified after Powell 1988).

<table>
<tr><th rowspan="2">Stratigraphy</th><th rowspan="2">Masri (1963)</th><th rowspan="2" colspan="2">MacDonald (1965)</th><th rowspan="2">G.G.M. (1961-1966) Bender (1974)</th><th rowspan="2" colspan="2">Parker (1970)</th><th colspan="2">1:50,000 Geological Mapping Project</th></tr>
<tr><th>Group</th><th>Formation</th></tr>
<tr><td>Quaternary</td><td></td><td colspan="2"></td><td></td><td colspan="2"></td><td colspan="2">Lisan Marl</td></tr>
<tr><td rowspan="2">Tertiary</td><td rowspan="2"></td><td colspan="2">Jordan Valley Conglomerate</td><td>Upper Synctonical Conglomerat Lower</td><td colspan="2">Dana Conglomerate</td><td rowspan="5">Balqa Group</td><td>Dana Conglomerate</td></tr>
<tr><td colspan="2">Chalk Limestone & Chert Unit (B3)</td><td>Chert Limestone Unit</td><td colspan="2">Rijam Formation</td><td>Um Rijam Chert Limestone</td></tr>
<tr><td rowspan="5">Upper Cretaceous</td><td>Muwagar Formation</td><td colspan="2">Chalk & Marl Formation '(B3)</td><td>Chalk-Marl Unit</td><td colspan="2">Muwagar Formation</td><td>Muwagar Chalk Marl</td></tr>
<tr><td rowspan="2">Amman Formation</td><td colspan="2">Silicified Limestone & Phosphate Formation (B2a & B2b)</td><td rowspan="2">Phosphorite Unit & Silicified Limestone Unit</td><td colspan="2" rowspan="2">Amman Formation</td><td>Al Hisa Phosphorite</td></tr>
<tr><td colspan="2" rowspan="2">Chalk, Marl, Chert & Sand Formation (B1a & B1c)</td><td>Amman Silicified Limestone</td></tr>
<tr><td>Wadi Es Sir Formation</td><td colspan="2">Marly Limestone Limestone Marly Limestonoe (A7a-A7c)</td><td>Sandy Limestone unit and Massive Limstone Unit</td><td colspan="2">Wadi Ghudran Formation</td><td>Wadi Umm Ghudran</td></tr>
<tr><td>Shueib Formation</td><td colspan="2" rowspan="3">Sandstones, Sandy limestones, Shales, Marls Marly Limestonoe (A3-A6)</td><td rowspan="2">Echinoidal Limstone Unit</td><td colspan="2">Wadi Es Sir Formation</td><td rowspan="4">Ajloun Group</td><td>Wadi Es Sir Limestone</td></tr>
<tr><td>Hummar Formation</td><td colspan="2">Shueib Formation</td><td>Shueib Formation</td></tr>
<tr><td>Fuheis Formation</td><td rowspan="2">Nodular limestone Unit</td><td colspan="2">Hummar Formation</td><td>Hummar Formation</td></tr>
<tr><td>Na'ur Formation</td><td colspan="2">Limstones Sandy, Marly Marls, Shales (A1-A2)</td><td colspan="2">Fuheis Formation</td><td>Fuheis Formation</td></tr>
<tr><td>Lower cretaceous</td><td>Baqa Formation</td><td colspan="2">Kurnub Group</td><td>Varigated Sandstone
Massive white Sandstone</td><td>Kurnub Group</td><td>Subihi Fm.
Arda Fm.</td><td colspan="2">Kurnub Sandstone Group</td></tr>
<tr><td>Na'ur Formation</td><td colspan="2">Na'ur Formation</td><td colspan="2">Unit</td><td colspan="2">Na'ur Formation</td><td>Na'ur Formation</td></tr>
<tr><th>Stratigraphy</th><th></th><th colspan="3">Quenell (1951)
Burdon (1959)</th><th>G.G.M. (1961-1966) Bender (1974)</th><th colspan="2">Lloyd (1969)</th><th colspan="2">1:50,000 Geological Mapping Project</th></tr>
<tr><th></th><th></th><th colspan="3"></th><th></th><th colspan="2"></th><th>Group</th><th>Formation</th></tr>
<tr><td rowspan="3">Cambrian</td><td rowspan="3"></td><td rowspan="3">Quweira Series</td><td colspan="2">upper Queira sandstone</td><td>Massive, Brownish Weatherd Sandstone</td><td rowspan="3">Disi Group</td><td>Ishrin</td><td colspan="2">Umm Ishrin</td></tr>
<tr><td colspan="2">Burj Limesone group</td><td>Dolomite Limestone Shale Unit</td><td></td><td colspan="2">Burj Dolomite Shale</td></tr>
<tr><td colspan="2">Lower Queira sandstone</td><td>Bedded Arkose & Sandstone Basal Conglomerate</td><td>Salib</td><td colspan="2">Salib Arkose</td></tr>
<tr><td>Pre-Cambrian</td><td></td><td>Sarmouj Series</td><td>Intrusives</td><td>Sarmouj Conglomerate</td><td colspan="3">Sarmouj Conglomerate</td><td>Qunai Diorite</td><td>Sarmouj Conglomerate</td></tr>
</table>

➢ **Dardour formation (DR)** consists of cream, yellowish, black and dark green marl, shale, dolomitic limestone with cross-bedded sandstone, and dolomitic sandstone. It is outcropping along the eastern shoreline of the Dead Sea between Wadi Abu Khusheiba to the south and Wadi Mukheiris to the north. Its age is Anisian-Carnian and its depositional environment is near coast (Bandel and Khoury 1981).

➢ **Ain Musa formation (AM)** consists of dirty white massive glauconite sandstone intercalated with siltstone, clay beds and marl with some fossiliferous limestone. This formation is outcropping between Wadi Manshala to the south and Wadi Mukheiris to the north. It is of Anisian age (Bandel and Khoury 1981) deposited in a marine depositional environment (Makhlouf et al. 1991).

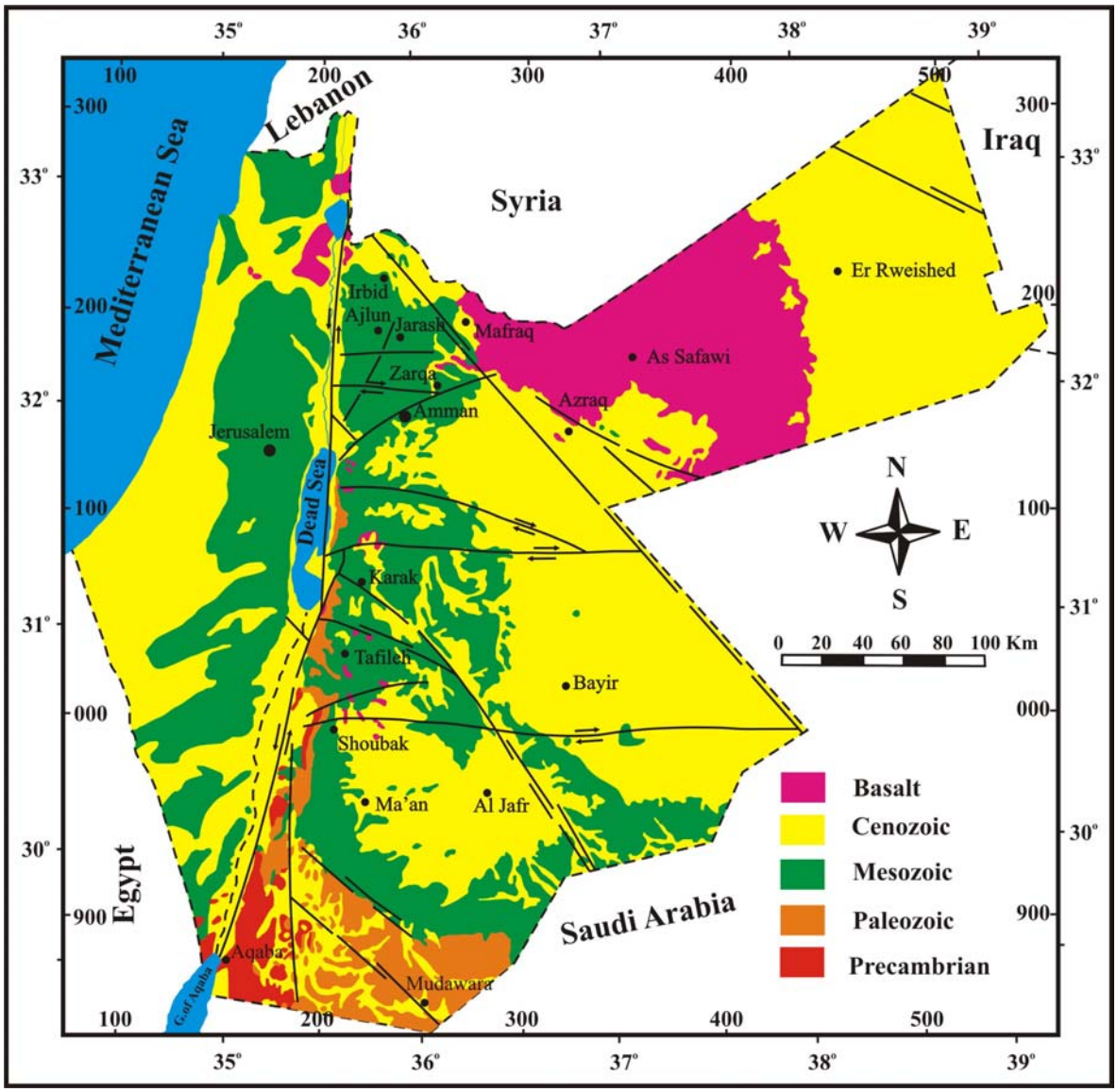

Fig. 3.2: Outcropping map of Jordan (Geology Directorate-NRA 1996).

➢ **Husban Limestone formation (HL)** consists of massive partly dolomitized limestone. The formation was deposited in shallow water environment of Anisian age (Bandel and Khoury 1981).

➢ **Mukheiris formation (MK)** is outcropping directly at the shore of the Dead Sea in the end of Wadi Mukheiris and Wadi Dardur. It consists of calcareous sandstone intercalated with sand and clay with shells of bivalves and cephalopods. Its age is Anisian and it was deposited under intertidal flat depositional environment (Makhlouf et al 1991).

➢ **Umm Tina formation (UT)** is outcropping in the northeastern part of the Dead Sea. It consists of succession of limestones that contain stromatolite and marl that contains oolite and stromatolite. It is of Lladinian age and has near shore depositional environment (Makhlouf et al.1991).

- **Abu Rweis Gypsum formation (AR)** crops out in the vicinity of the Zarqa River. It comprises mainly massive gypsum and thin bituminous silty mudstone. It is of Carnian age and was deposited in a coastal supratidal sabkha with saline pools (Muneizel and Khalil 1993).

3.2.1.4 Jurassic

The Jurassic sediments crops out from Wadi Al Zarka until the Jordan Valley in the west which includes the Arda mountains and also to the west of Mahis. Both the Triassic and the Jurassic are called the Zarka group; the Triassic is called Ma'in Formation (Z1) while the Jurassic is called Azab or Al Honeh Formation (Z2). The Jurassic outcrops along the Zarka River until Al Arda in the Jordan Valley with a thickness of about 40-60 m near Mahis, 290 m near Zaraka River and 400 m near Deir Alla. It represents most of the Jurassic but not the upper part of it, which is the Tithonian-Kimmeredgian because it seems to be eroded and the clue is the presence of the Kurnub unconformity (Bender 1968, 1974, Basha 1981, Bandel 1981).

The Azab Group (AZ) consists of Hihi Clay stone (HI), Nimr Limestone (NR), Silal Sandstone (SL), Dahab Limestone (DH), Ramla Sandstone (RM), Hamam Sandstone (HA), and Mughanniya Limestone (MUG).

3.2.1.5 Cretaceous

The Cretaceous sediments consist of the lower Cretaceous Kurnub formation and the upper Cretaceous Ajloun and Belqa groups:

- **Kurnub Sandstone formation (KS)** was formed during the lower cretaceous. Kurnub Sandstone is locally outcropping along the eastern heights of the Jordan Valley. It is easily distinguished from the overlying Cenomanian (Upper Cretaceous) calcareous sediments. Kurnub sandstone is composed mainly of quartz grains with varying proportion of clay and siltstone horizons. The formation is easily distinguished by its red, violet, purple, and brown coloration with in the upper third, where are the rest of the succession has a white color with shade of light pink or violet (Amiereh 1993). The source of these colors is referred to the presence of iron oxides and the white colors is related to the quartz content of these super mature Sandstone (Amiereh 1991). The upper part of this unit is characterized by the increase in the presence silty shale and marl and characterized by cross bedding. Its thickness in Zarka-Ma'in area is around 330 m (Abed 2000). It is from the Alpian-Aptian (Wetzel and Morton 1959).

The German geological mission (1961-1966) divided the Kurnub in Jordan into two units: the first one is massive white sandstone, which is present in the lower part and contains plant fossils. It is extensively cross-bedded and its thickness is around 180 m (Bender 1974). The second unit is vari-colored sandstone, which is composed of light violet and multi colored sandstone with sandy shale and shale intercalation. Its thickness is around 150 m. It was deposited by rivers with NNW paleocurrent and braided meandering streams

with possible shallow reworking for the bioturbated horizons and its age is Necomanian to early Cenomanian (Moh'd 1988, Shawabkeh 1998).

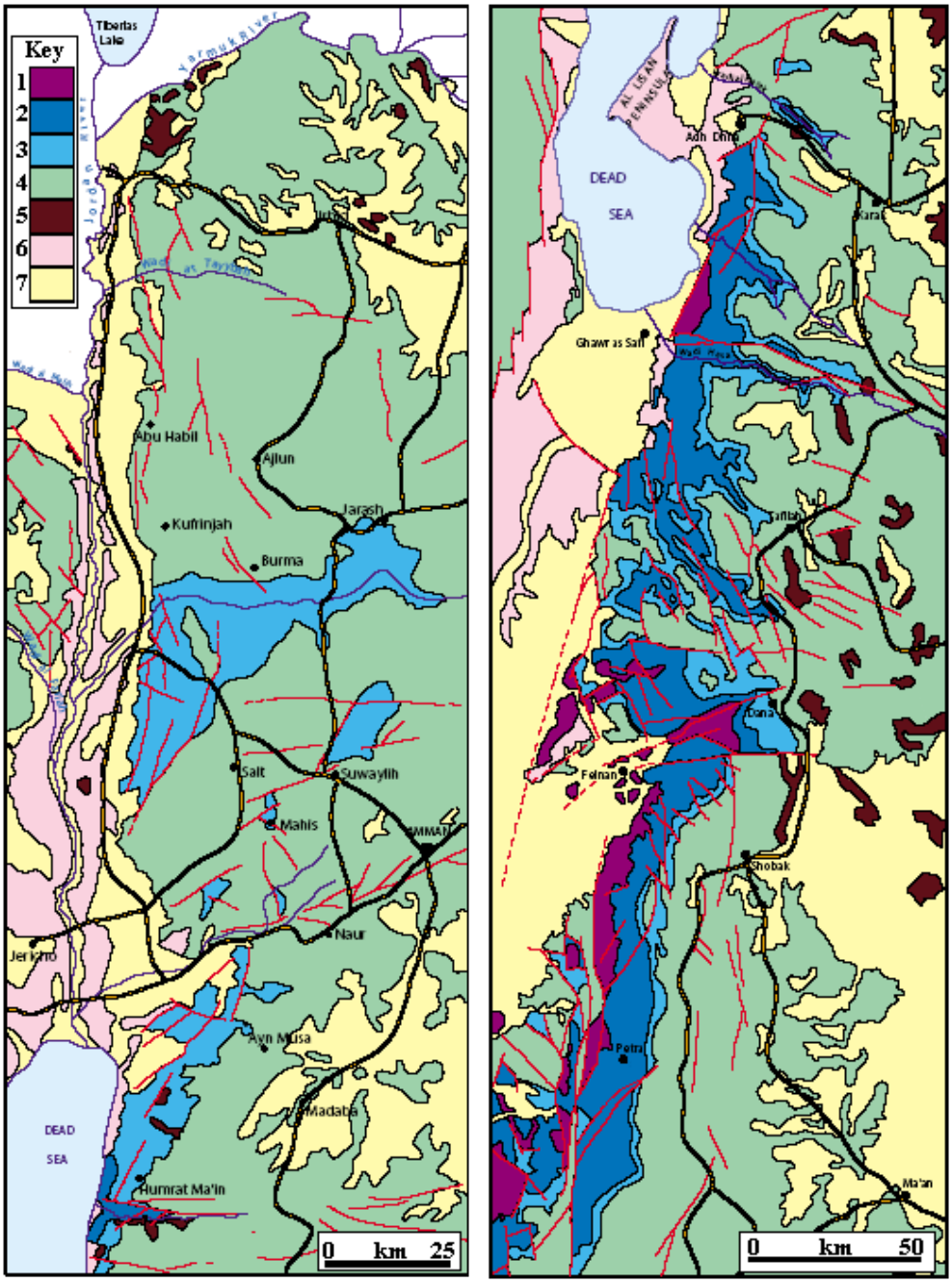

Fig. 3.3: Geological map of the Dead Sea Transform; the Jordan Valley and the Northern part of the Dead Sea to the left and the southern part of the Dead Sea with Wadi Araba to the right, modified after Capaccioni et al. (2003), where the key numbers symbolize the following formations: (1) The crystalline basement of Pre-Cambrian to Early Cambrian age; (2) A sequence which begins with Salib formation, Umm Ishrin and Disi formations of Early Cambrian to Ordovician age; (3) Krnub Sandstone formation of Necomian to Albian age; (4) different carbonatic formation s of Cenomanian to Eocene age; (5) basaltic effusions and cinder cones; (6) Lisan formation (70-17 ka) in age; (7) undifferentiated lacustrine, fluvial and terrestrial Quaternary deposits.

Quennell (1951) divided the upper Creataceous into two groups; Ajloun Group and Belqa Group. The **Ajloun Group** consists of five formations (Na'ur, Fuheis, Hummar, Shueib and Wadi Es-Sir):

- **Na'ur Limestone formation (NL)** represents the bottom of the upper Cretaceous rocks, which is marked by fully marine calcareous facies. The lower contact is recognized by the lithological change from sandstone to carbonate intercalated with shales, marl and thin bedded of glauconitic siltstone and grey mudstone. The upper contact is marked by white limestone beds (Tarawneh 1987). It consists of succession of limestone, dolomite, and Marl. It is from Lower Cenomanian age (Powell1989). Its depositional environment is subtidal (Bender 1974 and Basha 1978).

- **Fuheis formation (F)** is equivalent to A3 of Wolfart (1959) and Macdonald Sir M. and Partners (1965) and the middle part of the nodular limestone of Bender (1974). It consists of yellow grey calcareous siltstone, marl, and marly limestone, nodular limestone and fossiliferous limestone. It is exposed along the deep Wadis north of Wadi Abu Khusheiba and road cuts between Ma'in village and Ma'in hot springs. Its age is Cenomanian developing in a subtidal depositional environment (Wetzel and Morton 1959).

- **Hummar formation (H)** is equivalent to A4 of Wolfart (1959) and to the Echinoidal limestone of Bender (1974). It consist mainly of grey limestone, dolomitic limestone and dolomite, subhorizantal burrows are also common which are interbedded with shelly wakestone. Its age is Cenomanian and it was deposited under intertidal to subtidal marine environment (Powell 1988).

- **Shueib formation (S)** is equivalent to A5 and A6 of Wolfart (1959) and Macdonalds Sir M and Partners (1965). It consists of red green buff calcareous siltstone with gypsum viens, thin limestone beds with orange algal laminated dolomite and mudstone. It outcrops in Wadi Abu Khusheiba. Its age is Cenomanian to early Turonian developed in a shallow subtidal marine deep environment (Powell 1988).

South of Wadi Abu Khusheiba the afore mentioned three formations are difficult to be differentiated and considered to be one formation called **Fuheis, Humar, Shueib undifferentiated (F/H/S)**. It consists generally of greenish grey marl with beds and nodules of micritic mudstone with gypsum (Tarawneh 1987). They range from subtidal to tidal flat conditions and there age is Cenomanian-Turoninan (Powell 1988).

- **Wadi Es Sir Limestone formation (WSL)** comprises the upper most part of Ajloun Group and termed A7 (Macdonaled et, al. 1965, Wolfart 1959). It is equivellant to the massive limestone of Bender (1974). This formation is considered as an index horizon because it is easily distinguished all over Jordan. The formation consists of alternating thick and thin limestones, dolomitic limestones, marly sandstone, thinly chert and some oolitic and rudist layers. The upper part consists of thick-bedded fossiliferous limestone alternating of thin bands of chert. Its thickness is 100 m in Wadi Abu Khusheiba and 85 m north of Wadi Zarqa Ma'in. It is exposed along the deep valleys like Wadi Tayba and

Wadi Al-Arab. The age of this formation is Turonian while its depositional environment is marine subtidal (Powell 1988).

Belqa Group comprises the strata from Coniacian (upper Creatceous) to the upper Eocene. This group is divided stratigraphically into four formations (Ghudran, Amman, Al-Hasa phosphorite and Muwaqar):

- **Wadi Umm Ghudran formation (WG)** is equivalent to B1 of (Mackdonald et, al. 1965). This formation is well exposed above the prominent cliff of Wadi Es Sir formation. Lithologically this formation varies from the north to the south. In the north of Irbid region to Madba, it is massive chalk with Oysters and Qucina, but from Madba until Wadi Al-Hasa it consists of white or buff chalk with broken bivalve fragments. The upper part of this formation consists of beds of chert and chalky limestone with phosphatic sandstone and siltstone. The depositional environment of the chalk of this formation in Amman area is open marine condition (Abed 2000). The age of this formation is Coniacian and possibly Early Santonian (Bender 1974 and Powell 1988). This formation has been recently divided by the Natural Resources Authority (NRA) into three members (Mujib, Tafieleh and Dhiban).

- **Amman Silicified Limestone formation (ASL)** was divided by Wolfart (1959) into two parts B2a for the lower part and B2b for the upper part. It varies laterally from the north to the south. This formation consists of limestone, dolomite and chalk with thin to thick beds of chert. It is from Campanian age (Wetzel and Morton 1959 Burdon 1959, Bender 1974 and Abed 2000). It was formed under shallow marine environment and it becomes a little bit deeper to the south in Wadi Al-Mujib (Krishan 1988, Abed 1989, Abed and Krishan 1991).

- **Al-Hasa Phosphorite formation (AHP)** is a part of Amman formation (Masri 1963) and equivalent to B2b of Wolfart (1959). On the other hand Bender (1974) consider it as one distinctive unit and he named it Phosphorite unit. The Natural Resources Authority (NRA) considered it as a formation named Al-Hasa formation. It crops out in Wadi Al-Rayan with a thickness of about 8 meters. The first 5 meters consist of coarse grained phosphates and ends with bedded phosphates and the upper three meters consist of one bed with out structures phosphatic grains and it is friable; in general this bed consist of calcareous, silicified, argiallaceous phosphorites beds, phosphate, limestone, chert, marl, and Oyster Lumlachella (Coquina) beds in Wadi Al-Hasa in the south. In central Jordan it was divided by El-Hiyari (1985) into three members (Sultani phosphorite, Bahiya Coquina, and Qatrana phosphorite. It is from the upper Campanian to lower Mastrichtian (Quennel 1951, Hamam 1977, Dilley 1985). It is of shallow marine subtidal to intertidal depositional environment (Shawabkeh 1998).

- **Muwaqar Chalk Marl formation (MCM)** is equivalent to the B3 of Wolfart (1959). It consists of soft marl and white yellowish chalk. The formation in middle and north Jordan becomes black because of the presence of organic matters (oil shale). The thickness of this formation is 332 m in Yarmouk area, 240 m in Irbid and 158 m east of

Lisan area. Its age is from upper part of the upper Mastrichtian and the upper part of this formation is from the Paleocene age from the Cenozoic, which means that the borders between the Creatceous and the Tertiary (K/T) or (Mesozoic/Cenozoic) are found in this Formation (Yassini 1979). It was deposited in a shallow open marine environment (Jarrar 1989).

3.2.1.6 Cenozoic

The Cenozoic sediments consist of eight formations: Umm Rijam, Wadi Shallala, Tayyiba, Waqas, Saham, Irkheim, Dana and Usdum.

- **Umm Rijam Chert Limestone formation (URC)** is equivalent to B4 of Wolfart (1959) and it is also equivalent to limestone-chert of Bender (1974). It exists in the study area like in Al-Kharazeh area east of Lisan above the Muwaqar formation. It consists of successions of chalk, chalky limestone, limestone with beds of chert, and some phosphate. Its thickness in Al-Kharazeh area east of Lisan is about 247 m. It is from lower to middle Eocene (Naji 1983). It is depositional environment is the Tethys outer shelf (Abed 2000).

- **Wadi Shallala Chalk formation (WSC)** was introduced by Parker (1970), it is equivalent to the upper Chalky limestone unit (Weismann and Abdullatif 1963) and unit B5 of Wolfart (1959). It consists of wispy chalk, locally bituminous at the base, barite concretion (1-10 cm in diameter) are common. In the Ghor area local chert beds exist. Its age is Eocene and it was deposited in warm shallow marine environment (Moh'd 2000).

- **Tayyiba Limestone formation (TL)** crops out in North Shuna area and the mountains overlooking the Jordan Valley. It consists of two members: lower glauconitic and upper cliffy limestone. It was deposited in the Oligocene in a marginal shallow marine environment (Moh'd 2000).

- **Waqas Conglomerate formation (WC)** is outcropping in the Jordan Valley. The eastern most outcrops occur only in Wadi Zahar and consist of conglomerate, siltstone, limestone and marls. It is from the Miocene. Its depositional environment ranged between alluvial fans, braided rivers, and fresh water lakes (Moh'd 2000).

- **Saham formation (SF)** outcrops in the vicinity between Aqraba and Saham. It is a good evidence of the existence of a lake, which covered parts of the present day Yarmouk river. At its base friable sandstone beds followed by conglomerate and limestone and alternating chalky-marly porecellanite, its age is Miocene-Pliocene (Mor et al. 1997).

- **Irkheim formation (IR)** is exposed in the high lands overlying the Rift. It consists of three members; marly clastic member sandwiched between two massive limestones members. It is of Miocene-Pliocene age and it was deposited under fresh water lacustrine environment (Moh'd 2000).

- **Dana Conglomerate formation (DC)** crops out in Wadi Al-Karak in the south and in Al-Kharazeh east of the Lisan. It consists of Marl, sandy marl, layers and nodules of conglomerate, which is from the Cretaceous and Eocene that is being redeposited and there is half a meter of chert and fine beds of limestone.

- **Usdom formation** is a rock salt but it doesn't out crop anywhere in Jordan. Its rocks are found in the south western of the Dead Sea. This Formation consists of 4000 meters of the rock salt, marl and Carnalite. The age of this Formation is Oligocene-Miocene (Abed 2000).

3.2.1.7 Quaternary

The Jordan Valley is mainly covered by Quaternary sediments. During the Pleistocene successive lakes occupied the Jordan valley; the sediments of these are intercalated with fluviatile deposits coming from the surrounding mountains. This epoch was interrupted by basaltic eruptions (Bender 1974, Horowitz 1979). It consists of the six formations: Shaghur, Ghor Al-Katar, Abu Habil, Kufranjeh, Samra and Lisan.

- **Shaghur Conglomerate formation (SHC)** consists of well-cemented calcareous sandstone, conglomerate (blocks up to 1 m in diameter), limestone, and travertine (Abed 2000). It is exposed in the southern Jordan Valley in Wadi Abu Qaraf, 3 km south east of Al-Kafreen. It overlies Pre Quaternary rock unit. The thickness of this formation reaches 100 m. It is highly dissected with north-south Pleistocene faults (Sahawneh 1991). Its age is from the upper Pliocene to Early Pleistocene (Bender 1974).

- **Ghor Al-Katar Conglomerate formation (GR)** is a domal conglomeretic that outcrops in Ghor Al-Katar, 26.5 km north of the Dead Sea. It consists of steeply dipping layers of alternating conglomerates, sandstone, marls and marly clays. The depostional environment was a lacustrine–fluviatile. Its total thickness is about 350 m and it decreases northwards to reach 75 m 2 km south east of Kuraimeh (Abed 2000). It is of lower middle Pleistocene age (Bender 1974).

- **Abu-Habil Conglomeratic Limestone** consist of hard conglomeratic, partly pisolitic limestone unconformably overlying the Ghor Al-Katar Formation. It is exposed in Abu-Habil area 65 km north of the Dead Sea. It is of Middle Pleistocene age (Horowitz 1979).

- **Kufranjeh Gravels** consists of unconsolidated gravels with red argillaceous matrix and early Paleolithic artifacts. It is from the Middle Pleistocene age (Abed 2000).

- **Samra formation** consists of 35 m of pseudo-oolitic limestone, alternating with white, chalky marls containing nodules of chert and conglomeratic layers (Picard 1943). Its depositional environment is a brackish water lake (Begin 1975) but Abed (1983) considered that these sediments were deposited in a fresh water lake. Its age is of late Pleiostocene (Picard 1943 and Begin 1975).

- **Lisan formation (LM)** is formed due to an extensive lake have occupied the hole Jordan Valley in the upper Pleistocene (65-16 ka B.P), its northern limit was the Tiberias Lake and it extended 40 km south of the present Dead Sea (Horowitz 1979). The Lisan lakes surface reached about 180 m BSL and the out cropping thickness is about 60 mm. It consists of two alternating lithofacies; laminated evaporite, and massive mudstone with occasional sandstone. The evaporite facies is generally thin bedded and varve-like throughout the formation except at the top, where it forms a massive white cliff (Abed and Helmdach 1981, Begin et al. 1974). According to Sir Alexander Gibb and Partners (1984), the Lisan formation can be divided into six parts from the top to the bottom: upper clays, main laminated unit, middle clays, lower laminated unit, lower clays, and basal clay (or basal sand and gravels). This formation is well exposed along the cliffs of the Jordan River and there is a lateral change in Lisan formation; in the north the formation is more fresh than in the south. Laterally it consists of north Al-Qarn area. In central Jordan Valley aragonite dominate, so the salinity of its water was not the same in all parts (Al-Taj 2000).

- **Damya formation** represents the upper most Pleistocene rocks about (13-11 ka BP). This formation consist of 14 m of calcareous siltstone to silty limestone, which is deposited in a fresh water lake of the upper most Lisan formation.

3.2.1.8 Holocene-Recent

It consist of the following:

- **Coarse Clastics of Alluvial fans (Alf):** Lake lisan began to shrink because of the tectonic and climatic conditions (Niemi 1997). During this process in the upper most Pleistocene, many of the shorelines of the retreated lake and terraces were formed in the emerged lake deposits and in the coarse clastics that have been transported into the Jordan Valley (Bender 1974). The transportation from the bordering mountain continued forming a belt of alluvial fans, which is deposited on the rim of the Jordan Valley.

- **Jordan Valley Flood plain sediments (Zor):** During the Holocene about 6-8 m height terrace have been formed. It consists of clayey and loamy constituents.

- **Calcrete (Ct)** covers areas of bedrocks of the high lands. It develops a surface cementation of carbonate material at the area of high rainfall.

- **Travertine (Tr)** is a carbonate rock resulting from the precipitation of limestone from hot water, normally occurs at the lower slopes of the thermal spring courses in the Ma'in area and Wadi Al-Arab and the slopes of Yarmouk river.

- **Alluvium and Wadi sediments (Al)** covers the Wadis like Wadi Husban and along the shores of the Dead Sea.

- **Basalt extrusions (B)** are found at the rim and with in the Jordan Graben. They are of Pleistocene age. Bender (1974) arranged them from the north to the south as follows:

1. Lower Wadi Al-Arab basalts;

2. The basalt that is located 3 km south of Wadi El Malih into River Jordan;

3. The basalt that is found 2-5 km WNW of Ain Khuneizir of the lower Arda road;

4. The Ghor El-Katar basalt 26.5 km north of the northern end of the Dead Sea;

5. The basalt that is located at the eastern side of northern part of the Dead Sea;

6. The Basalt Plug with columnar jointing west of the thermal springs of Zarqa Ma'in;

7. The Wadi El Heidan basalts south of the Lisan Peninsula.

➢ **Soil** is divided into three major and three minor types, which can be distinguished in the study area (Bender1974). The major types are:

1. The Red Mediterranean soils that are formed under subhumid conditions (precipitation >600 mm/year) and semiarid (precipitation between 300 and 600 mm/year). It covers wide areas along the high lands east of the rift (Irbid-Ramtha depression, Suweilih depression, Ajloun-via-Madba-Karak-Tafileh);

2. Yellow Steppe soils that are formed under semi and arid conditions (precipitation between 150 and 300 mm/year). It is found on both sides of the Jordan-Wadi Araba Graben south of River Zarqa;

3. Yellow Mediterranean soil that are a transitional soil type between the two afore mentioned soil types. It is formed under semiarid climate (precipitation between 250 and 350 mm/year). It is found as narrow strips on both sides of the Jordan-Wadi Araba Graben, the eastern sides of the high lands of the Rift and in the southern extension of the high lands between Shoubak and Ras en Naqab.

The three minor types are:

1. Renzins that occurs at the outlet of the Yarmouk Valley and in the mountains of Ajloun;

2. Grumsols that occurs in Amman and Salt areas;

3. Solonchaks that occurs south of Deir Alla and on the north and south shores of the Dead Sea.

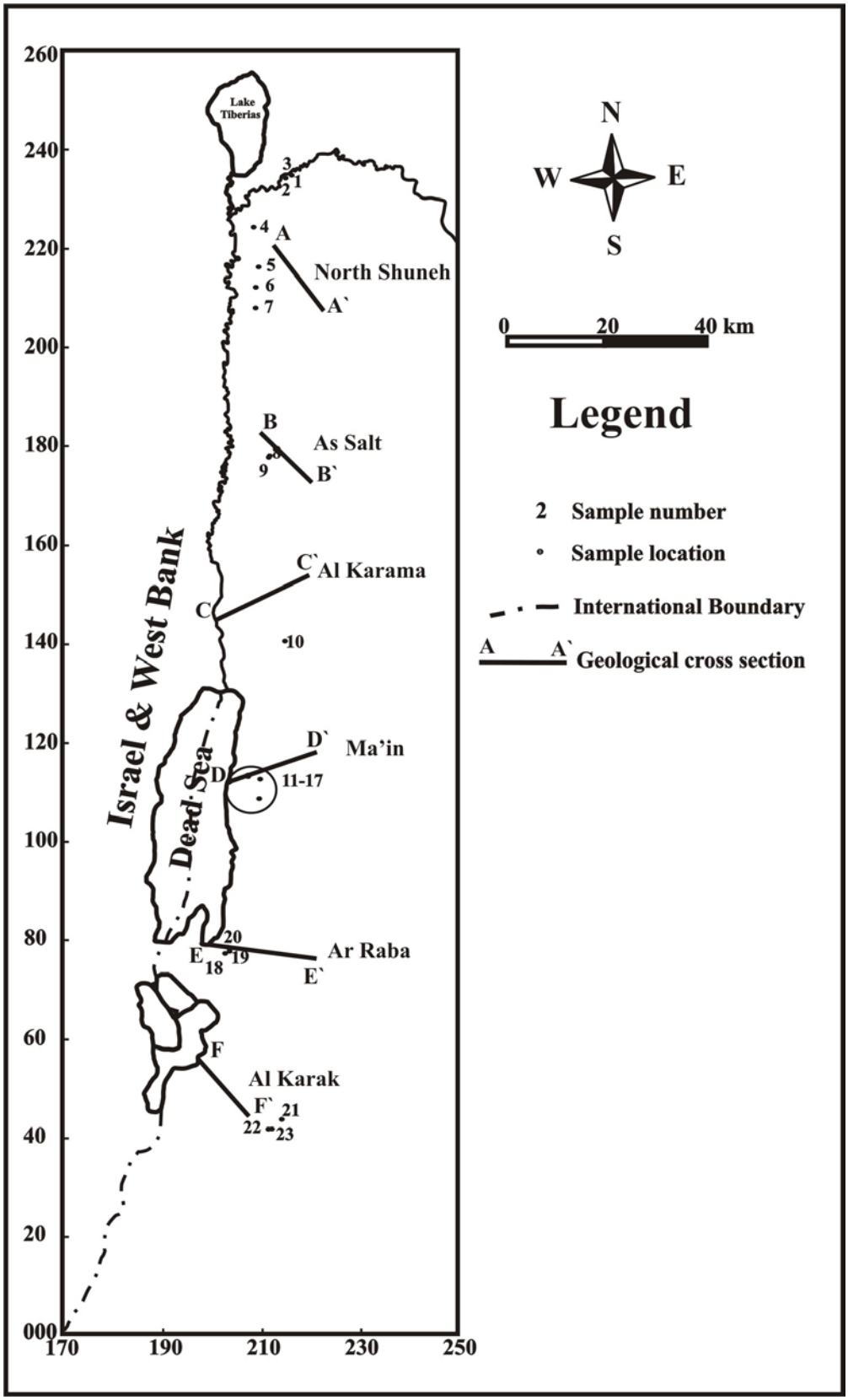

Fig. 3.4: Location map of the geological cross sections along the area of study.

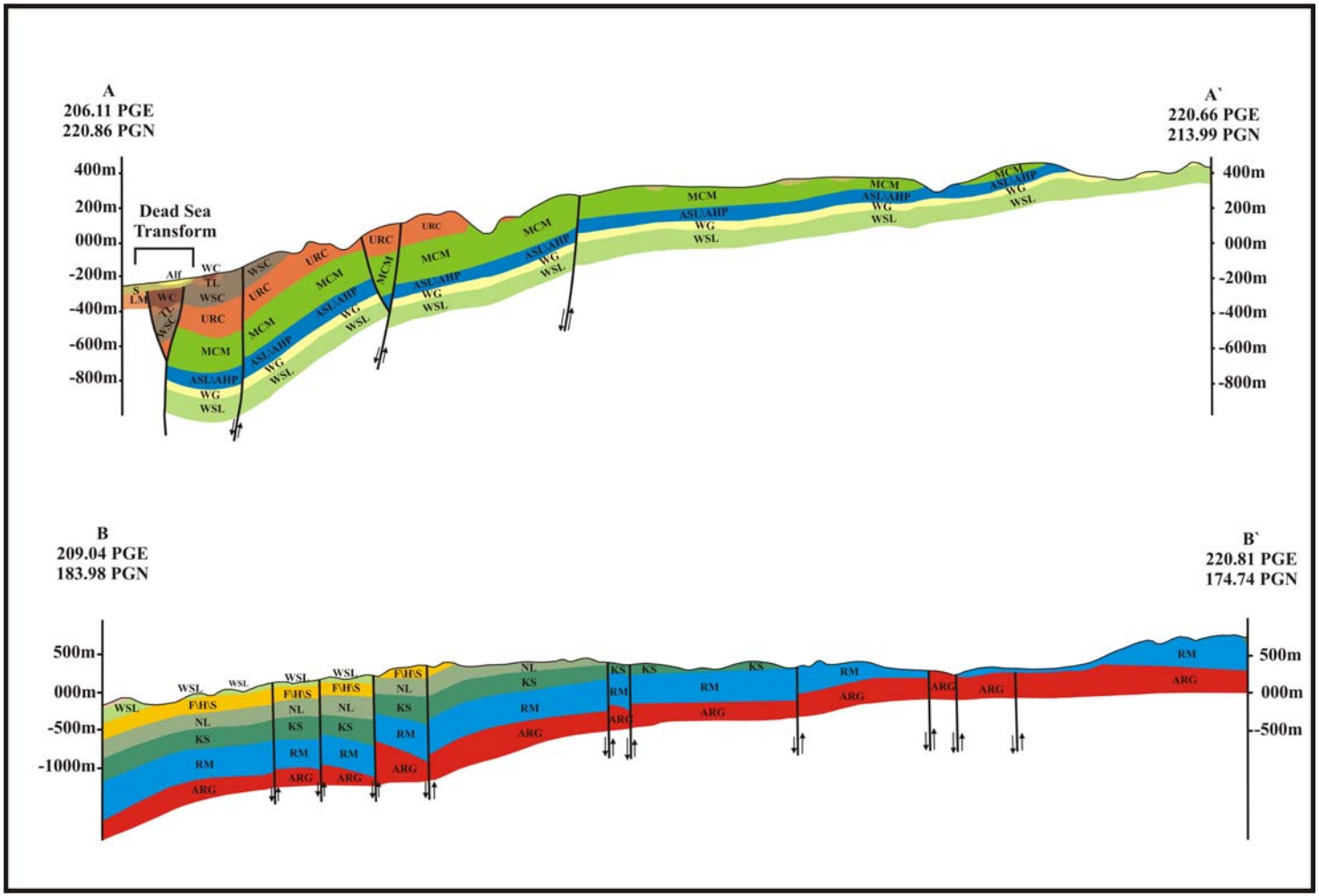

Fig. 3.5: Geological cross-sections A-A` and B-B`(modified after Moh'd 2000 and Muneizel and Khalil 1993).

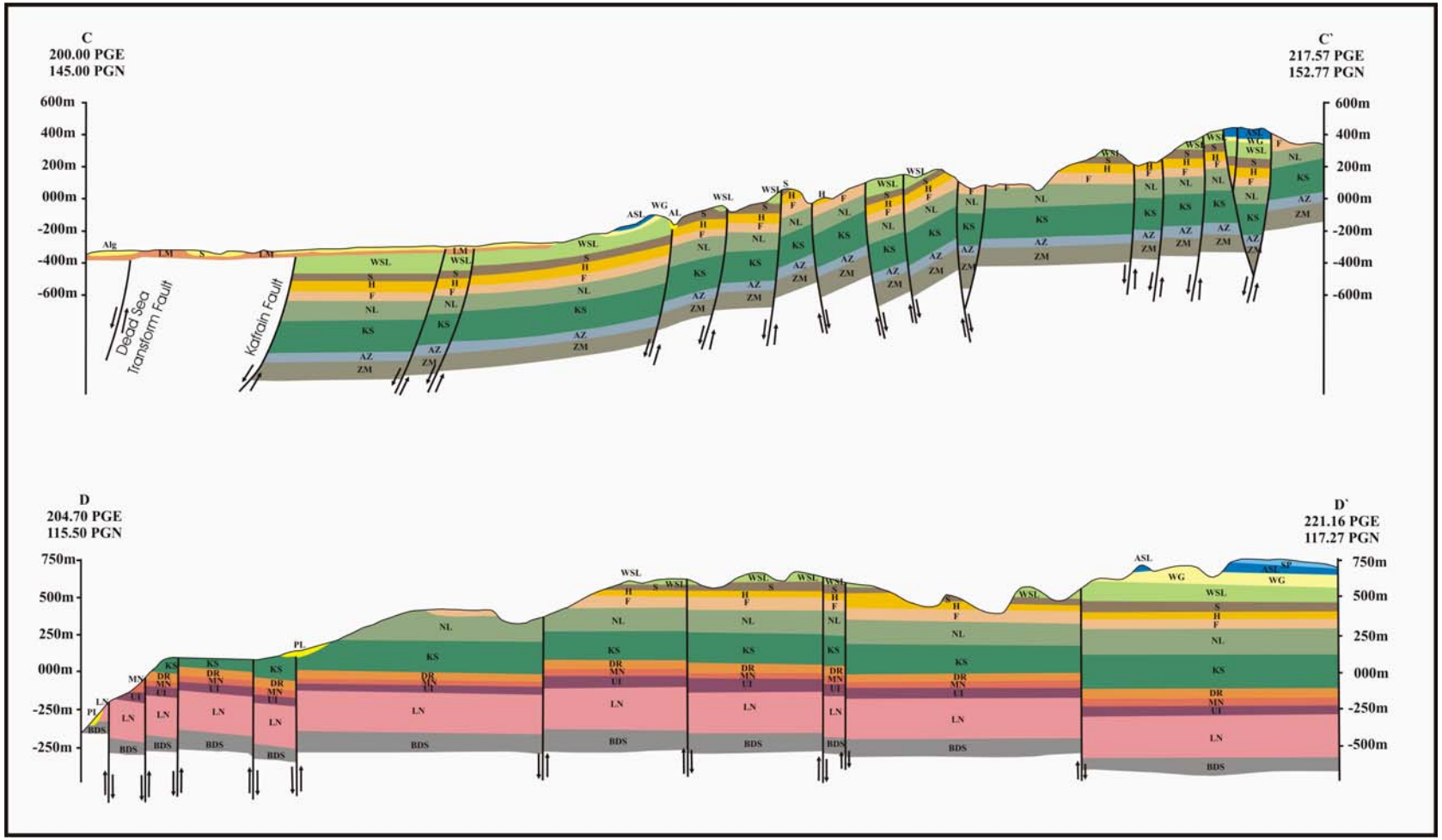

Fig. 3.6: Geological cross-sections C-C` and D-D`(modified after Shawabkeh 2001 and Shawabkeh 1996).

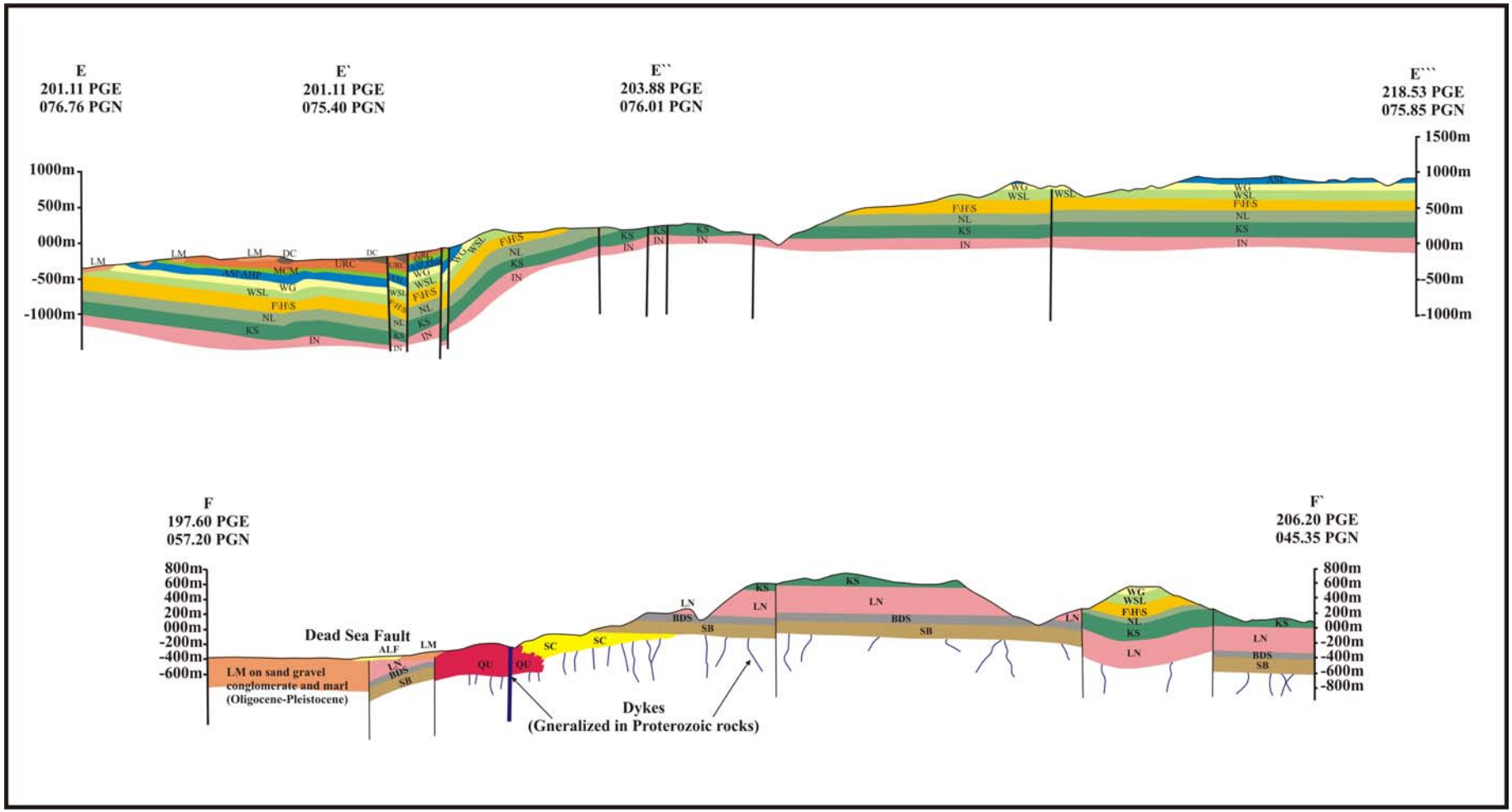

Fig. 3.7: Geological cross-sections E-E`-E``-E``` and F-F`(modified after Moh'd 1988 and Powell 1987).

3.2.2 Tectonics

The area of study is a part of the Dead Sea Transform (DST) or the so-called Dead Sea Rift (DSR), which separates the Arabian Plate from the Sinai-Palestine sub plate. The transform extends from the Sinai triple junction to the Taurus-Zagros collision (Garfunkel 1981). It has a length of about 1100 km (Abed 2000). It is a part of the East African-Turkey system, which extends from east Africa through the Red Sea and the Dead Sea to end in the south of Turkey with a total length of around 6000 km.

The DST is composed of three morphotectonic segments being from the south to the north: Wadi Araba, Dead Sea and Jordan Valley. Together they form a morphological depression that extends from the Gulf of Aqaba to Lake Tiberias. The Wadi Araba segment trends N 15^{o} E with around 174 km. The Dead Sea –Jordan Valley Rift segments trends with N 5^{o} E with about 180 km length.

3.2.2.1 Regional tectonics

The continental crust in the Dead Sea Transform (DST) area was consolidated because of the Pan-African orogeny in the late Proterozoic age. The area was a stable platform during the Phanerozoic. The rifting that happened in the Permian-Early Mesozoic interrupted the stability. This has shaped the eastern Mediterranean (Garfunkel 1997). The continent broke up at the Sinai triple junction. This process occurred by extension along the Red Sea, rifting in the Suez Gulf and transtention on the DST where a left lateral strike slip fault movement was going on (Courtillot et al. 1987). Due to the Red Sea opening; the Arabian plate rotated 5.5^{o} clockwise with respect to the Sinai-Palestine subplate (Garfunkel 1997).

The slip history began in the Late Oligocene-Early Miocene. The total slip was estimated of about 107 km. It happened on two stages: 62 km in the Early Miocene and 45 km in the late Pliocene-Early Pleistocen (Quennel 1958, Freund et al. 1970).

In the late Cretaceous-Miocene, a major tectonic phase has proceeded the DST formation. This stage resulted in forming the Syrian Arc, which is a S-shaped belt (Krenkel 1924) (Fig. 3.8). This arc includes: (1) a bundle of ENE to NE trending folds and (2) a group of EW trending lineaments of aligned faults and folds along which some right-lateral shearing also took place (Garfunkel 1997). According to Attalah (1992) the formation of the Syrian Arc is controlled by NW-SE compression.

According to Horwitz (1979) a third tectonic phase called the “Erythrean Fault Sytem” was active during the Late Miocene-Pliocene period. This system is a faulting phase with NW-SE lineaments parallel to the Red Sea. It had formed as a result of the African plate clockwise rotation in the Miocene. This system was accompanied by E-W strike slip faults. It was responsible of the formation of a series of grabens.

The last tectonic event was the DS. Uplifting and subsidence accompanied this event. En echelon strike slip fault (left step fault or pull apart) formed the morphotectonic

depressions of Aqaba Gulf, Dead Sea, Lake Tiberias, Lake Hula, Beqa', and El-Ghab. According to Bender (1974), the uplifting along normal fault was extensive especially along the areas bordering the transform. They are usually 1-2 km and increase to the south to reach 3-4 km in the area near the Red Sea.

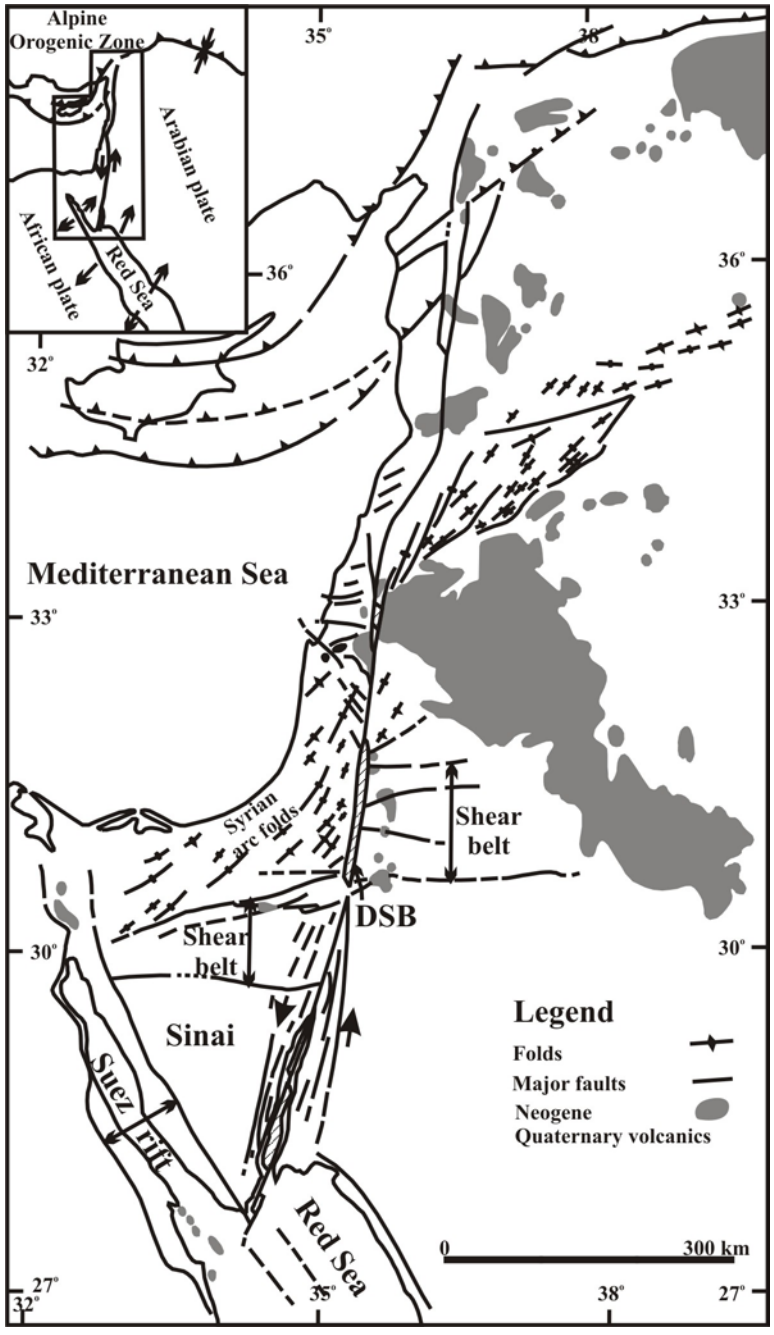

Fig. 3.8: Regional sitting of the Dead Sea Basin (Garfunkel 1997).

3.2.3 Structural pattern in the study area

Fig. 3.9 shows the structural pattern in the area of study. The following discussion is based on the work of Moh'd (1988), Shawabkeh (1998), Muneizel and Khalil (1993), Moh'd (2000), and Shawabkeh (2001).

The northeastern part of the Jordan Valley, which includes the first seven studied thermal waters can be subdivided into three main structural zones:

A. The narrow western N-S trending zone adjacent to the rift, which is dominated by NNW to N-S faults, flexures and some folds;
B. The intensely faulted and gently folded southern parts which include the extension of Ajloun dome;
C. The relatively stable northern and northeastern parts which includes Irbid plaine and Yarmouk river and dominated by north west and northeast lineaments, ENE faults and NW folds;
D. The northern extension of Ajloun dome is the most folding feature in this part of the study area.

The southeastern part of the Jordan Valley is affected by the following main structures

A. Zarqa river Fault strikes E-W. It has not always been recognizable because of the nature of sandstones exposed on both sides of the valley and the landslips in the surroundings of the river;
B. Wadi Shuayb structure is visible to the northeast of the Dead Sea and is around 25 km long and 1-4 km wide folded-faulted belt extending mostly along the eastern flank of the wadi Shuayb in NNE direction and pinches out south Jerash near Zarqa River. This structure also consists of several faulted synclines and anticlines;
C. Amman-Halabat structure: the fault strikes Northeast-Southwest and extended from the northern part of the Dead Sea to Swayma passing to the north of Al Addsiya (Wadi Naur) to Amman. It is 1-5 km wide and consists of many structural elements including faults and folds. It has a downthrow to the northwest with a vertical displacement up to 400m.

The main structural features in the eastern part of both Dead Sea and Wadi Araba are:

A. Siyagha Structure is traceable between Mount Nebu and Siyagha and extends 12 km and disappears southwest of Hisban;
B. Alkafreen fault (NW) lies to the north of the Dead Sea and crossing Ghor AL-Kafreen to the north of the Dead Sea. This fault is very important in the evolution of the Dead Sea Basin;
C. Wadi Zarqa Ma'in fault strikes east west and extends from the Dead Sea to Wadi Sirhan. The thermal springs of Zarqa Ma'in area, which issue from the lower sandstone aquifer lies in the upthrow side. It divides Hammat Ma'in area north and Zara area to the south on the downthrow side;
D. Wadi Atun fault extends more than 30 km from the Dead Sea coast to the Wadi Wala sub parallel to the Zarqa Ma'in fault, it divides the Zara area into two parts northern and southern part;
E. Maslubia fault has a downthrow to the south. It starts at Wadi Kashem Jiwan (in the northwest) and extends about 5 km eastward (north of Ma'in village);
F. Zara fault is parallel to the Dead Sea coast between Wadi Abu Khushiba and Zara;

G. Humrat Ma'in fault is parallel to the Dead Sea coast in the southern part between Wadi Zarqa Ma'in and Wadi Manshala;
H. Wadi Ghabra anticline: its axis strikes and passes through Wadi Ghabra. With an extenssion of 18 km;

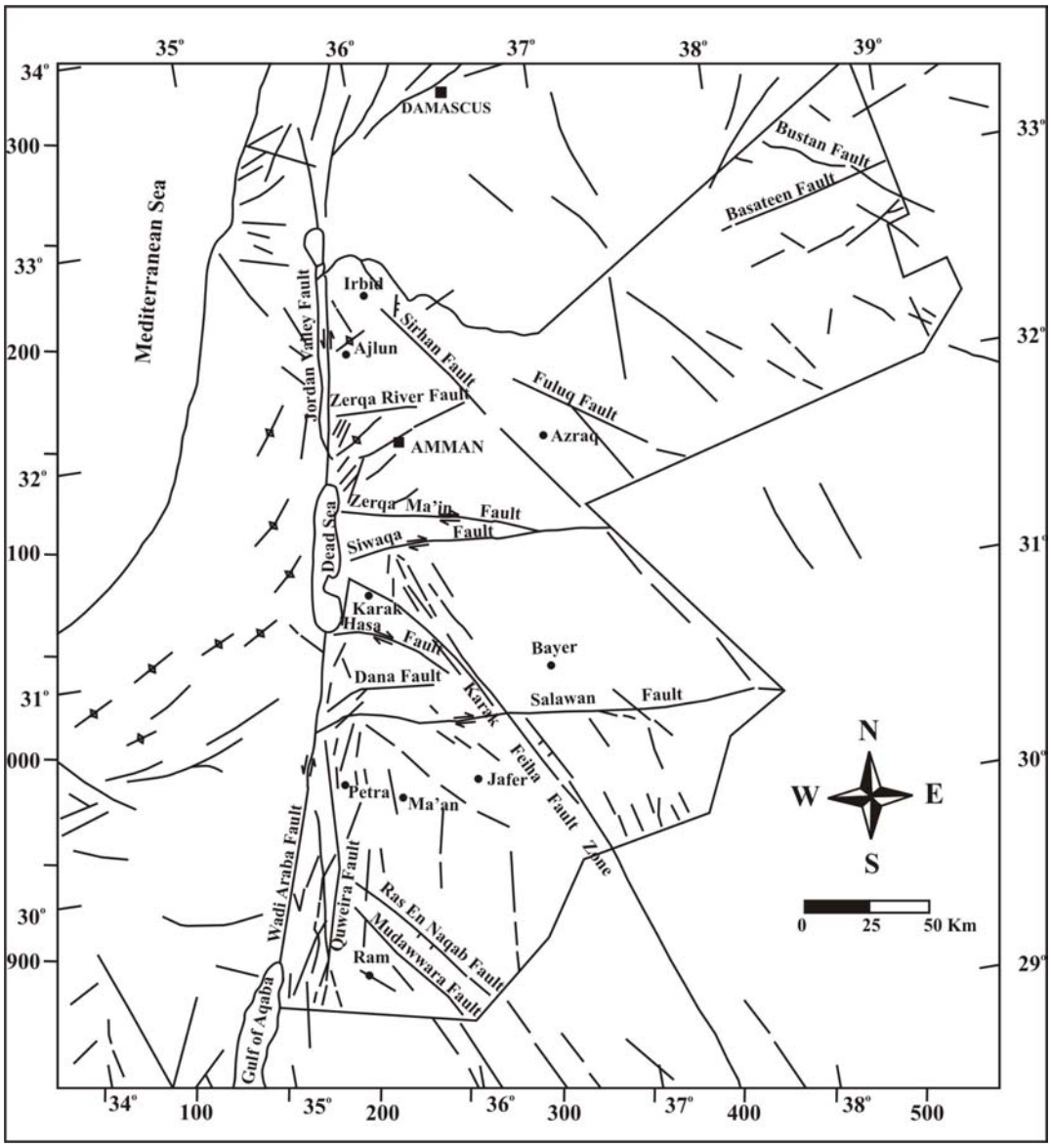

Fig.3.9: Structural map of Jordan (modified after Diabat 2004).

I. Qualat At-Tawil anticline: its axis plunges to the southwest extending 6 km to the Ain El-Dhib;
J. Zara syncline trends east-west from Wadi Dardour in the north to El-Mamalleh in the south;
K. Wadi Zarqa Ma'in monocline extends 2 km and occurs north of the middle part of the east west Zarqa Ma'in fault.
L. Karak Al-Fiha fault zone: trending NW-SE;
M. Main Dead Sea fault: trending NW-SW. The rift margin has a trend of NNE, but it changes its direction towards NNW near Wadi Al-Mujib delta. The Ed-Dhira and

Sirfan fault monoclines are splay parts of the major Dead Sea fault terminated by faulting against the Shihan Siwaga structure;

N. Shihan Siwaga structure is normal fault, which strikes between NNE and ENE. It has a north down throw, while the eastern main fault has a south downthrow. Some folds associate this structure, which might be due to dextral or compressional stress in the south of Shihan Siwaga structure. The faults trends NE-SW while in the northern part they trend NW-SE;

O. Haditha Syncline trends NNE-SSW and plunges NNE.

P. Wadi El-Hisa fault throws Umm Ghudran formation 500 m down against Umm Ishrin formation (Tarawneh 1987).

3.3 Hydrogeology

3.3.1 Groundwater basins

According to the National Water Master Plan of Jordan the country was divided into 12 groundwater basins (Fig. 3.10) solely on the basis of the hydrological factors and these factors includes ground water divides of the most regional aquifer systems, important physiographic features, and the limits of an aquifer (GTZ and NRA 1977). These basins are: Yarmouk basin, Side wadis basin, Jordan Valley floor basin, Amman-Zarqa basin, Dead Sea basin, Azraq basin, Wadi Hammad basin, North Wadi Araba basin, South Wadi Araba (Red Sea) basin, Wadi Sirhan, El-Jafr basin, and Disi-Mudawara basin. Table 3.2 shows the safe yield for both: the renewable and non-renewable resources for 50 years. The total safe yield for the renewable resources is around $275.5 \cdot 10^6$ m^3/year while for the non-renewable resources it is of around $143 \cdot 10^6$ m^3/year.

Table 3.2: Safe yields of the groundwater resources in Jordan (Belbisi 1992).

	Basin/Well field	**Safe yield (10^6 m^3)**
Renewable	Yarmouk	40
	Jordan river side wadis (N. Jordan Valley)	15
	Jordan river valley	21
	Zarqa river basin	87.5
	Dead Sea including Mujib basin	57
	North Wadi Araba	3.5
	South Wadi Araba	5.5
	Azraq	24
	Jafer basin	9
	Sirhan basin	5
	Hammad basin	8
Non Renewable	Disi-Mudawara	125
	Jafer	18

The area of study is located with in five groundwater basins: Yarmouk, North Jordan Valley (Side Wadis), Jordan Valley floor, Dead Sea and North Wadi Araba.

- **Yarmouk basin** is located in the northern part of Jordan (the High land and the Plateau) with 1426 km^2 catchment area (Exact 2004). It is underlain by chalk, chert, limestone, Marl and the sandstone of the Kurnub sandstone formation. In the eastern part of the basin basaltic flows covers the rocks of the Belqa group (Eraifej and Abu-Jaber 1999). In this basin the ground water is recharged at an average volume of about $40 \cdot 10^6$ m^3/yr (by precipitation). The ground water flow is controlled by two major faults which cut across the basin, so part of the flow is directed towards Yarmouk River in the north and the other one is directed towards the Jordan River to the east (Exact 2004, El-Naser 1991). Four principal aquifers are found in this basin: the Basalt system, the Rijam limestone system, Amman-Wadi Es Sir which consist of limestone and chert and the lower sandstone aquifer complex which consist of sandstone.

The most important aquifer in this basin is the Amman-Wadi Es Sir (B2/A7). The ground water in this aquifer is found at a depth of 200 m in the High land. This formation is overlain by geological formations that consist of marly layers and forms aquicludes and dipping with increasing angle towards both the Yarmouk and Jordan rivers and the result is a confining conditions, for example the El-Mokhybeh wells which is located at the slopes of the Yarmouk river tapping the B2/A7 aquifer and discharging artesian wells (Salameh 1996). El-Naser (1991) has calculated the recharge to the B2/A7 and he estimated about $12 \cdot 10^6$ m^3/yr with base spring flows of $100 \cdot 10^6$ m^3/yr.

- **North Jordan Valley (Side Wadis basin)** contains the deeply incised wadis, which flows along the escarpment along the escarpment of the Jordan Valley towards the Jordan Valley (Exact 2004). There are two subdivisions for this basin (1300 km^2 of Ajloun area north of the Zarqa River and the 1200 km^2 in As Salt area which extends from the Zarqa River to the Dead Sea in the south).

This basin is underlain by Belqa and Ajloun groups and Kurnub formation. The main aquifers are Amman-Wadi Es Sir, Hummar and Kurnub. The amount of precipitation is estimated to be at an average of $15 \cdot 10^6$ m^3/yr and the direction of flow of the ground water is to the west towards the Jordan Valley (Exact 2004).

- **Jordan Valley floor basin** is located in the flood plain of the Jordan River to the south of Lake Tiberias. This entire basin is found in the Jordan Valley and pronounced as a geological depression, which range from around 210 m ASL to 417 m BSL. The recharge by precipitation is estimated at an average of $21 \cdot 10^6$ m^3/yr (Exact 2004). 80% of the fresh water in this basin is in the alluvial fans of the side wadis, potential groundwater occurs as lenses of sand and gravel within the marl in the Lisan formation or as sand and gravell in the Alluvial fans, the rest (20%) of the water is found in Kurnub and Zarqa groups. The southern part of this basin has brackish water with a chloride concentration ranging from 700 to about 1850 mg/l.

➢ **Dead Sea basin** is located in the eastern part of the Dead Sea extending 50 km eastwards. It covers an area of about 1525 km^2 between three physiographic divisions: the High land and plateau, the Rift Valley and the Rifts Valley escarpment (Exact 2004).

Groundwater is found in two major aquifer complexes: upper limestone aquifer and lower sandstone aquifer complex. According to Salameh (1996) ground waters in the previous mentioned two aquifers have totally different origin. Waters in the upper limestone aquifer are renewable by precipitation and infiltration through soil and rocks and discharge after a few years of mean residence time. The available ground water amount is about $87 \cdot 10^6$ m^3 /yr, half of this amount discharges as springs like Zarqa Ma'in, Mujib, Wala, Shaqiq, Iben Hammad, etc. On contrary the lower sandstone aquifer doesn't receive much from the recharge because the water originate from other areas. This is due to its outcropping altitude, which is below the sea level and the presence of the graben and the Dead Sea. The Dead Sea serves as ultimate base level for all surface and ground water. The source of water in the sandstone complex comes from different aquifers like leaking from the upper aquifer and underground flows in the Disi area. A very limited amount comes from direct recharge to the outcrops. The total discharge is around $90 \cdot 10^6$ m^3/yr and they are mostly thermal mineralized water (Salmeh and Udluft 1985).

➢ **North Wadi Araba basin** is the fifth basin in the study area**.** Alluvium sediments that are brought from the surrounding mountains in the east and the west build up the Wadi floor with thousands of meters. The flow direction of the groundwater is from the mountains in the east to the west with a north component discharging into the Dead Sea (Salameh 1996). The water discharge from this area to Dead Sea was calculated by Abu Zirr (1989) to be $22 \cdot 10^6$ m^3/yr. According to Salameh (1996) the salinity of the groundwater increases from the areas near the recharge area with the flow direction to the discharge area.

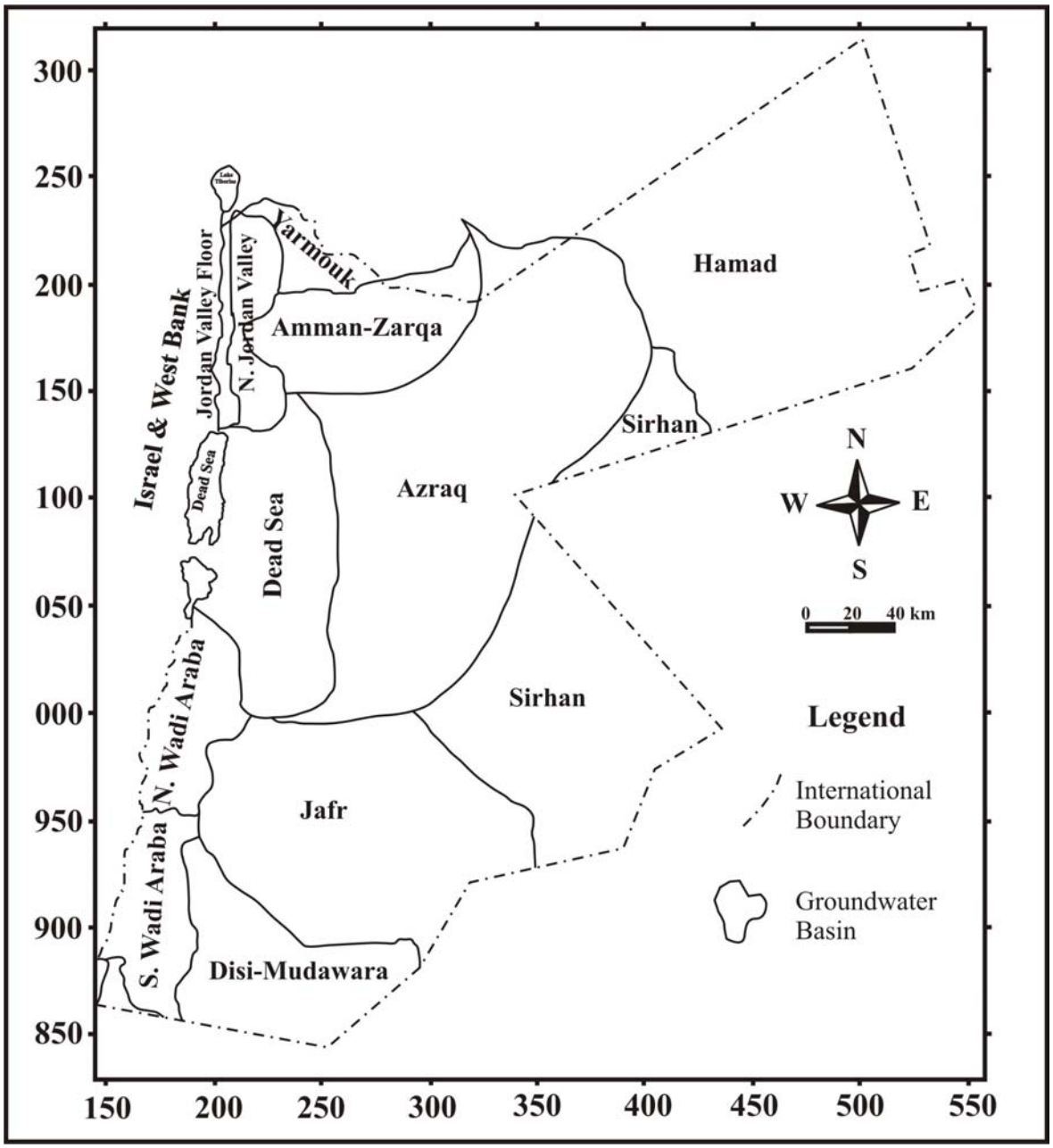

Fig. 3.10: Groundwater basins in Jordan (GTZ and NRA 1977).

3.3.2 Surface water

Low rainfall and high evapotranspiration causes limited surface water in Jordan and the neighboring area. The stream flow characteristics follow the precipitation pattern. The stream flow decrease from west to the east getting farther from the Mediterranean moisture and from north to the south with the increase of both temperature and evaporation (Exact 2004). Fig. 3.11 shows the fifteen surface water basins in Jordan. Table 3.3 shows the area and the total flow of the main surface water basins. Table 3.4 shows the names and total capacity of the dams that are constructed in order to benefit from the surface water before it drains into the Dead Sea.

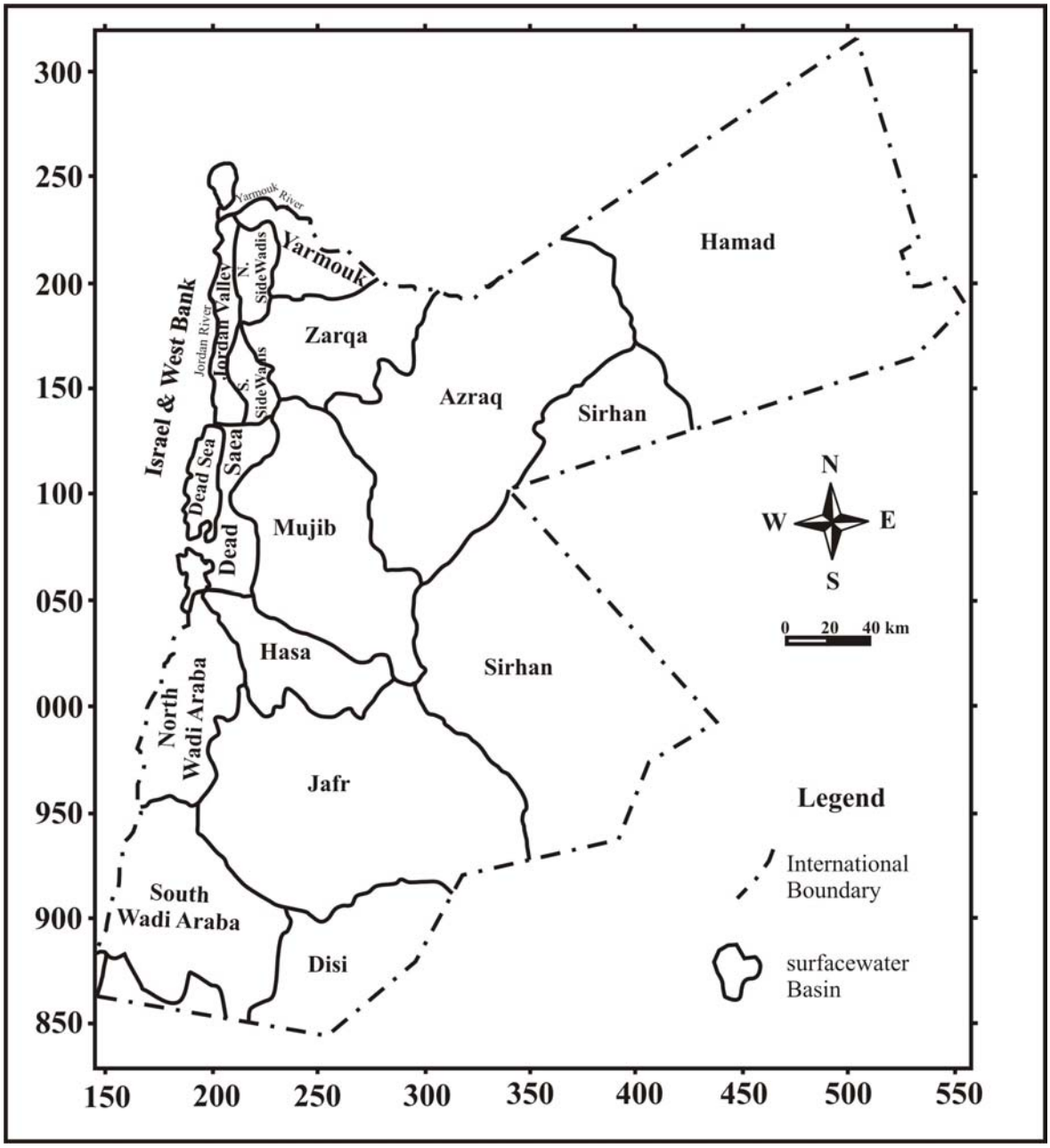

Fig. 3.11: Surface water basins in Jordan (GTZ and NRA 1977).

Table 3.3: The area and total flow of main basins in Jordan (Salameh 1996).

Basin	Area (km^2)	Total flow (10^6 m^3/yr)
Yarmouk	6790	360
Jordan Valley	-	-
North Jordan river Side wadis	267 (W. Al-Arab) 106 (Wadi Ziglab)	28 10
South Jordan river Side wadis	180 (Wadi Shueib) 189 (Wadi Kafrain)	5.71 6.4
Zarka river	4025	64.88
Dead Sea	272 (W. Zarqa Ma'in) 190 (Wadi Karak) 972 (in between Wadis)	30 18 30
Mujib	6596	83
Hasa	2520	34
North Wadi Araba	2938	26
South Wadi Araba	1278	1
Southern desert	4400 (W. El-Yutum)	1.5
Azraq	11600	27
Sirhan	15155	-
Hammad	19270	10
Jafer	12200	15

Table 3.4: The total capacity of dams in Jordan (after Salameh 1996 and Abed 2000).

Dame Name/Location	Total capacity (10^6 m^3)
King Talal/Zarqa river	89
Wadi Al-Arab/ Wadi Al-Arab	20
Ziglab(sharhabeel)/Wadi Ziglab	4.3
Shueib/Wadi Shueib	2.3
Kafreen/Wadi Al-Kafreen	2.5
Al-Waleh/ Wadi Al-Waleh	9.3
Al-Mujib/Wadi Al-Mujib	35
Tanoor/Wadi Al-Hasa	16.8
Al-Karameh/Wadi Al-Mallheh	55

3.3.3 Aquifers

The surface extensions of aquifers are shown in Fig. 3.12. The aquifers of Jordan described by Salameh (1996) are divided into three main complexes (Table 3.5):

3.3.3.1 The Lower Sandstone aquifer complex:

This complex is the oldest part forming one unit in the south of Jordan with gradually thick limestones and marls separating it into two aquifers in the northern parts but still hydraulically connected. It consists of the following aquifers:

- **Disi aquifer** is from the Paleozoic and considered to be the deepest water bearing aquifer in Jordan and underlies the whole area of Jordan. It outcrops in the southern part of Jordan and along the Dead Sea-Wadi Araba Rift Valley. Waters in this aquifer flow mainly towards the northeast, while in the southern parts the groundwater flow is separated by a water divide in the Rum area, following to the south and the west.

- **Zarqa and Kurnub aquifers** (Jurassic to lower cretaceous) consist of sandstones. They overlie the Disi aquifer. They outcrop along the escarpment of the Dead Sea, Wadi Araba and Disi area, also along the lower Zarqa River and its tributaries (Fig. 3.12). The ground water flow is directed towards northeast in the southern part and towards west in the center of Jordan and to the southwest in the north (Salameh and Udluft 1985). The deep sandstone aquifer complex is forming a basal aquifer being connected hydraulically through the Khreim group (Table 3.5).

The average thickness of the lower aquifer system in the northwestern part of Jordan is ranging between 200 m to 300 m in the Jordan Rift and have a transmissivity of about $9.6 \cdot 10^{-4}$ m^2/s in the Jarash and Abu Nasier area with an average saturated thickness of around 32 m (El-Naser 1991). El-Naser (1991) has also estimated the permeability to be $3 \cdot 10^{-5}$ m/s. An average permeability of about $4.84 \cdot 10^{-5}$ m/s was calculated by Salameh and Udluft (1985) for the central part of Jordan. Many other studies have estimated the permeability of this aquifer to be ranging between $6 \cdot 10^{-7}$ to $5 \cdot 10^{-4}$ m/s (NDP/FAO 1970, GTZ and NRA 1977, Humphreys 1978 and Salem 1984).

In the vicinity of the Zarqa river, the Zarqa aquifer is found under artesian pressure and have a higher piezometric pressure than that of the Kurnub. Also it has a higher salinity than that of the Kurnub, which proves the presence of a marly layers which separates the two aquifers hydraulically. The marly layers are ranging between 25 and 55 m in thickness. However, the layers don't separate the two aquifers completely (Jica 1995).

A schematic hydrogeological cross section shown in Fig. 3.13 explains the leakage distribution of the lower aquifer near the Jordan Valley floor. Due to the relief of the potential of the Kurnub aquifer to the Zarqa aquifer, there is not only downward but also upward leakage.

Table 3.5: Lithostratigraphic record of the different geological units in the study area.

Geological time scale			Group	Stage	Symbole		Aquifer
Era	Period	Epoch					
Cenozoic	Quaternary	Holocene	Jordan Valley	Alluvium	Basalt (B)	Qa1	shallow aquifer complex
		Pleistocene		Lisan		JV3	
		Pliocene		Samra		JV1-2	
		Miocene					
	Tertiary	Oligocene		Neogene			
		Eocene	Belqa	Shallala	B5		
		Paleocene		Rijam	B4		upper crtaceous aquifer complex
Mesozoic	Cretaceous	Maastrichtian		Muwaqar	B3		
		Campanian		Amman	B2		
		Santonian		Um Ghudran	B1		
		Turonian	Ajloun	Wadi Es Sir	A7		
		Cenomanian		Shuaib	A5/6		
				Hummar	A4		
				Fuheis	A3		
				Naur	A1/2		
		Albian	Kurnub	Subeihi	K2		Lower sandstone aquifer complex
		Aptian					
		Barremian		Arda	K1		
		Hauterivian					
		Valanginan					
	Jurrasic	Porttandian					
		Kimmeridgian					
		Lusitanain					
		Oxfordian	Zarqa	Huni	Z2		
		Callovian					
		Bathonian					
		Bajocian					
		Liassic					
	Triassic	Keuper		Ma’in	Z1		
		Muschelkalk					
		Bundsandstein					
Paleozoic	Permian			Ram Sandstone			
	Devonian						
	Silurian		Khreim				
	Ordovician						
	Cambrian	Upper	Disi	Quweira series			
		Middle					
		Lower					

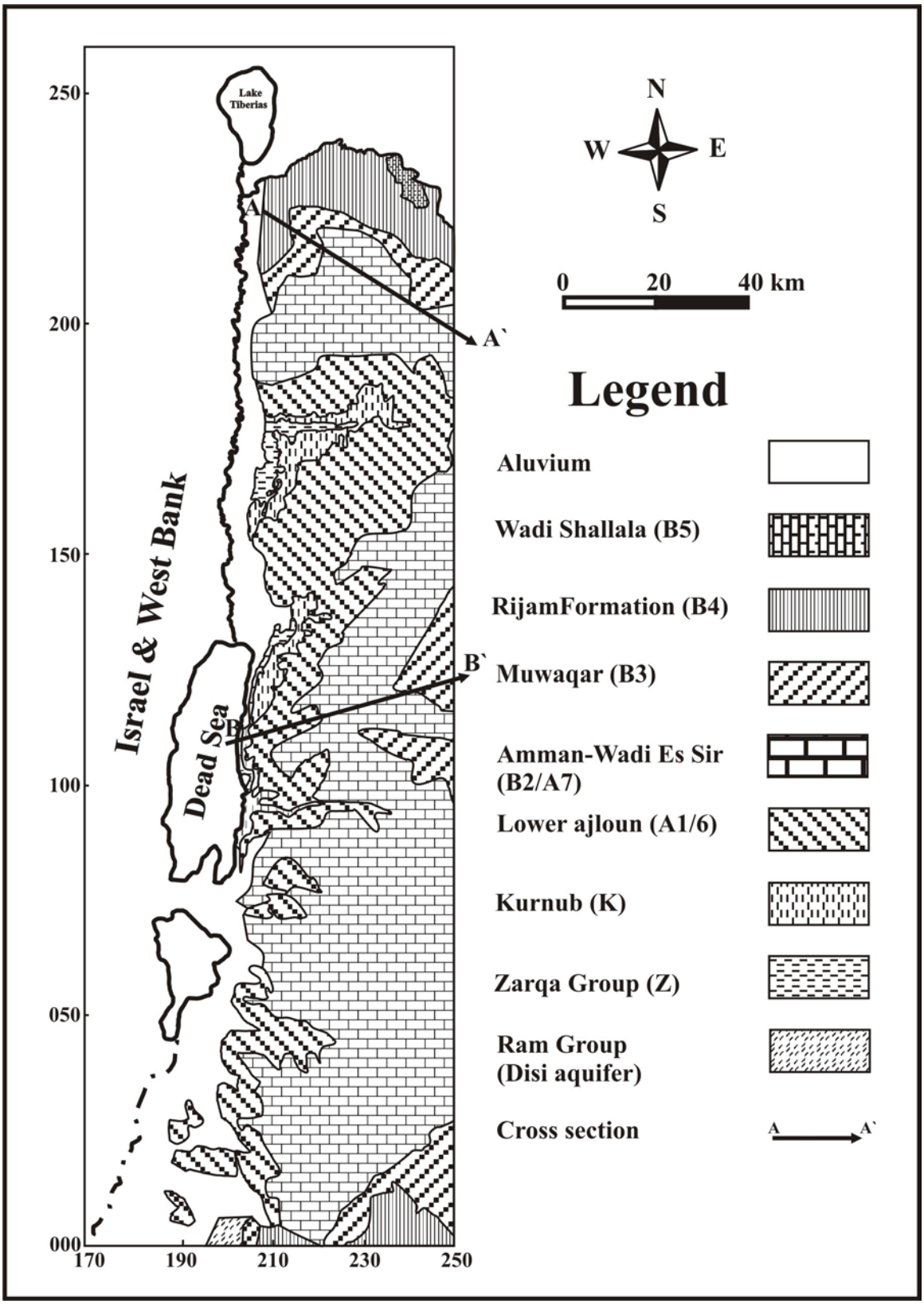

Fig. 3.12: Outcrop of groundwater aquifers in the area of study (GTZ and NRA 1977). For A-A` see Fig. 3.17. For B-B` see Fig. 3.18.

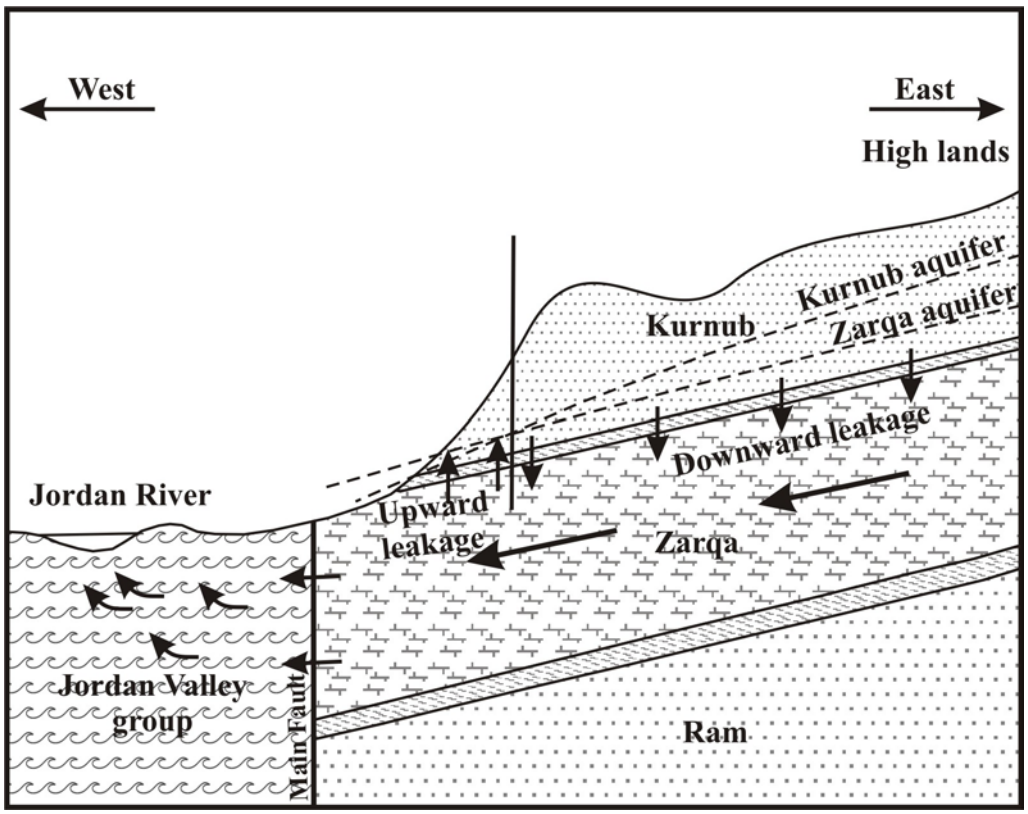

Fig. 3.13: E-W schematic hydrogeological cross section for the lower aquifer in the Zarqa River vicinity (modified after Jica 1995).

The lower aquifer receives only little recharge from the direct infiltration from precipitation because it is covered by thick aquifers and aquitards. Thus direct recharge from its outcrops in the lower part of the Zarqa River is dominant. Bender et al. (1991) have suggested that the lower sandstone aquifer in the central part of Jordan is recharged from the fractured carbonate formations through the A1-6 aquitard. An average value of 0.017 l/km^2.s is being estimated as leakage rate from Naur aquifer (A1-2) to the Kurnub aquifer in the northwestern part of Jordan (El-Naser 1991). The afore mentioned author have proved the occurrence of an upward leakage from the kurnub aquifer (with a potentiometric surface of about 418 m ASL) towards the B2/A7 aquifer with a potentiometric surface of about 35 m ASL in the El-Mokhybeh-Wadi Al Arab area.

In the northwestern part of Jordan the ground water flows from the eastern to northeastern (Syrian) side mainly westward to the Jordan Rift Valley partially converging along the Zarqa river, while in the central part of Jordan, the groundwater flows to the west and discharges along the slopes which borders the Dead Sea as shown in Fig. 3.14.

Fig. 3.14 and 3.15 shows the contour lines of the ground water head in both, the upper cretaceous aquifer system and the lower sandstone aquifer system, which was constructed through the measurements of pizometric head (GTZ and NRA 1977, Salameh and Udluft 1985). This configuration of the groundwater table indicate that the groundwater in the upper cretaceous flows eastwards and partly infiltrates the sand stone aquifer system. In the

sandstone aquifer groundwater flows to the west and discharges along the Dead Sea borders.

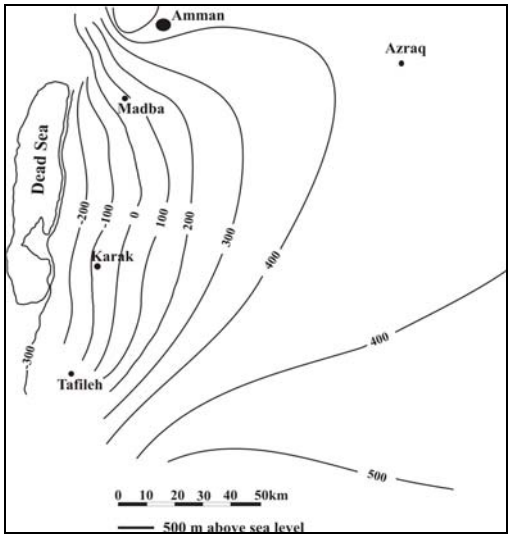

Fig 3.14: Equipotential lines of the groundwater in the lower sandstone aquifer (Salameh and Udluft 1985).

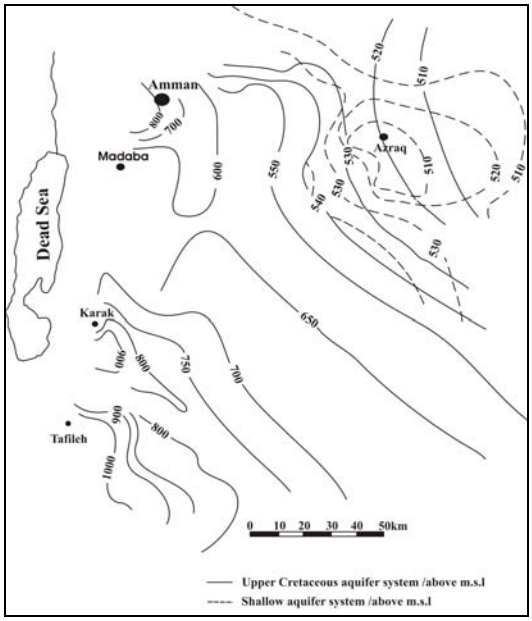

Fig.3.15: The equipotential lines of the ground water in the upper cretaceous and the shallow aquifer system (Salameh and Udluft 1985).

3.3.3.2 Upper Cretaceous Complex

This complex consists of limestones, dolomites, marlstones, and chert beds with a total thickness of about 700 m in central Jordan. This aquifer complex begins in the lower part with the **Naur aquifer (A1/2)** which consist of about 200 m of marls and limestones, Table 3.6 shows the A1/2 properties, this aquifer is overlain with **Fuheis aquitard (A3)** which has a thickness of about 80 m and consist of marls and shales. This aquitard separates the A1/2 from the **Hummar aquifer (A4)** which consist of pure semi crystalline karstic

limestones and outcrops in the high lands and recharged there. Table 3.7 shows the A4 properities. The **Shuaib aquitard (A5/6)** overlie the A4 aquifer in the eastern parts of Jordan and consist of marls and limestones. The A5/6 is considered to be a good aquifer in the El-Mokhybeh area because it contains a secondary transmissivity and storativity (Joudeh 1983).

Table 3.6: Naur Formation (A1/2) properties.

Property	Value	Reference
Specific capacity	0.01 to 12 m^2/hr	El-Naser (1991)
Transmissivity	0.3 to 100 m^2/d	El-Naser (1991)
Hydraulic conductivity	$2.0 \cdot 10^{-8}$ to $3.0 \cdot 10^{-5}$ m/s	Salem (1984)
Yield	30-70 m^3/hr	Salem (1984)

Table 3.7: Hummar Formation (A4) properties.

Property	Value	Reference
Permeability	$8.0 \cdot 10^{-7}$to $7.5 \cdot 10^{-5}$ m/s average: $3.97 \cdot 10^{-4}$ m/s	Salem (1984), Salameh and Udluft (1985)
The specific capacity	0.01 to 73 m^2/hr	Salem (1984)

The previous mentioned A5/6 aquifer is overlain by the **Amman-Wadi Es Sir (B2/A7)**, which is the most important aquifer in the upper cretaceous complex. This aquifer consists of two formations: Wadi Es Sir (A7) and Amman (B1) and they are separated by **Um Ghudran aqiutard (B1)**, which is missing in some places. The B2/A7 consist of limestones, chert limestones, sandy limestones, and marly limestones. The B2/A7 aquifer is recharged in the High lands where it outcrops. Where it is overlain with marly layers the ground water becomes confined. The thickness of this aquifer ranges from 180 m in the east and increase to 400 m in the Jordan Rift Valley (El-Naser 1991).

According to GTZ and NRA (1977), Woshah (1979), Joudeh (1983), and Rimawi (1985), the hydraulic proprieties of this aquifer are highly anistropic. The transmissivity ranges from 7.0 to more than 8000 m^2/d. Such a high values occur in the artesian area of El-Mokhybeh and Wadi Al-Arab, which is referred to deep-seated faults and fractures in addition to the occurrence of cavities. The aquifer has a storage coefficient in the order of 0.01 to 0.04 in the unconfined section (Woshah 1979) and in the order of 0.0003 in the artesian part (Joudeh 1983). Its saturated thickness ranges from 50 to 100 m in the unconfined part and increases to become completely saturated in the Jordan Valley (El-Naser 1991).

This aquifer is recharged directly from precipitation, which ranges between $20\text{-}40 \cdot 10^6$ m^3/yr (NJWRIPS 1989 and El-Naser et al. 1992). Several reasons limit the recharge to this aquifer: the presence of B4 and B5 low permeable stratas that overlain the aquifer, the thick soil (up to 20 m thick) east of Irbid and the low average rainfall in the eastern part of Jordan. The main recharge occurs from subsurface flow, which originates from areas with

increased rainfall (Ajloun and Nuaimeh). The waters flows from there northwest to Wadi Al-Arab area and El-Mokhybeh and northwestwards to Ramtha basin and Mafraq area. The waters, which are recharged from the basalt aquifer in Jabal Al-Arab, converge in Ramtha northwestwards and westwards towards El- Mokhybeh and Wadi Al-Arab and Yarmouk River area (El-Naser 1991) (Fig. 3.16).

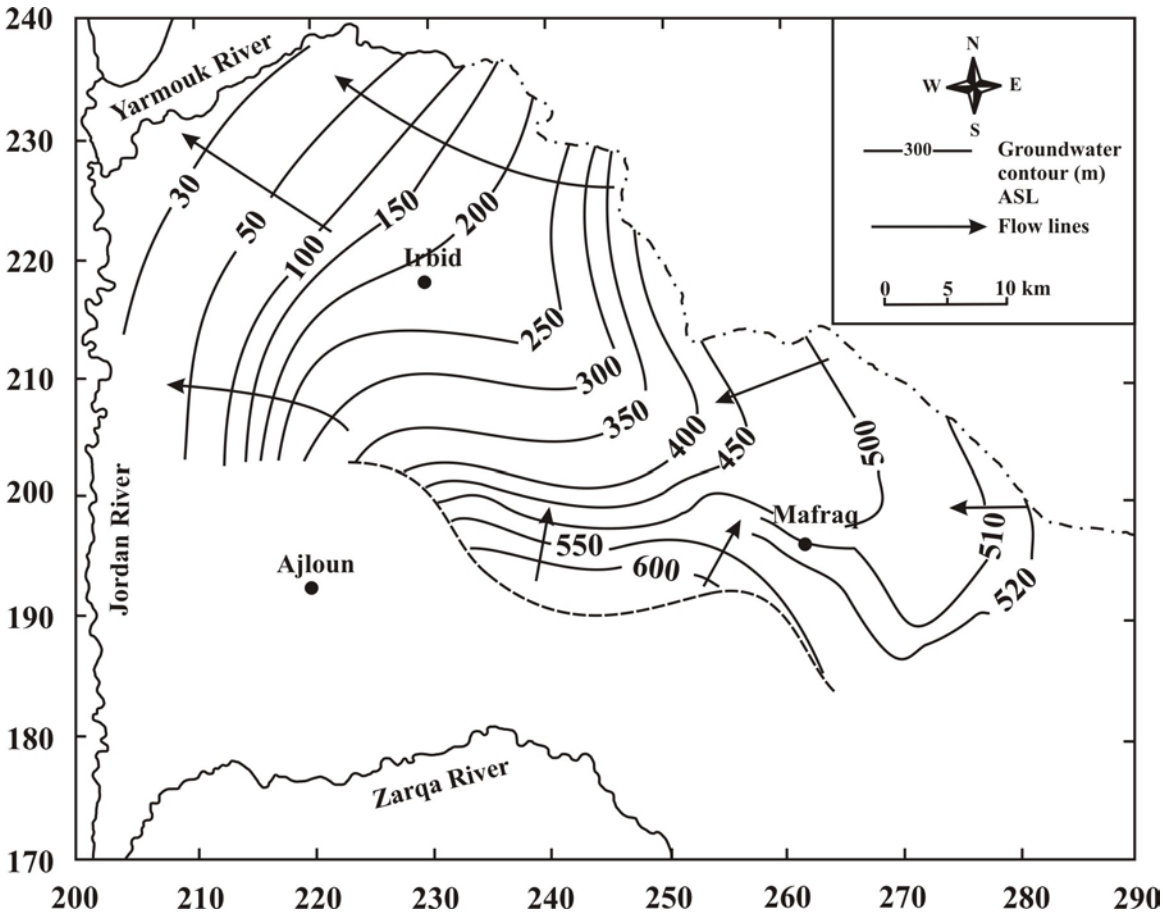

Fig. 3.16: Groundwater flow direction in the B2/A7 aquifer (El-Naser 1991).

Measurable discharge occurs through the base flow with an average of $74.9 \cdot 10^6$ m^3/yr and through springs with an average of $34.5 \cdot 10^6$ m^3/yr along the Jordan valley escarpment, while non-measurable discharge is assumed throughout subsurface flow across deep faults to alluvial aquifer in Jordan Valley (El-Naser 1991).

The afore mentioned complex is being covered with the **Muwaqar aquitard (B3)**, which forms a confining bed and because of that in some locations the wells flows in artesian conditions. This aquitard has a thickness of about 300 to 500 m in the northwestern part of the country in El-Mokhybeh area and the Jordan Rift valley. The afore mentioned aquitard is overlain by **Rijam aquifer (B4)** which consist of limestone, chert and chalk beds being recharged locally in the northern parts of Irbid and Ramtha area with about $4.55 \cdot 10^6$ m^3/yr (NJWRIPS 1989). Table 3.8 shows the properties of this aquifer.

Table 3.8: Rijam aquifer properties.

Property	Value	Reference
Permeability	$1.2 \cdot 10^{-4}$ to $3.3 \cdot 10^{-4}$ m/s	Arsalan (1976)
Transmissivity	5 to 300 m^2/d	Bajjali 1994

3.3.3.3 Shallow aquifer complex

The shallow aquifer complex consists mainly of the following aquifers:

- **The Basalt aquifer** extends from the Jabal Al Arab in Syria in the north to the Azraq and Wadi Dhuleil region in the south. This aquifer is recharged from the precipitation in Jabal Al Arab where the ground water moves radially to all directions.

- **Sedimentary rocks and alluvial deposits** of Tertiary and Quaternary ages form local aquifers overlying partly the previous mentioned complexes or they are separated from them by aquitards. They are mainly occurring in Wadi Araba, Jordan Valley, Yarmouk River area, Jafr basin and the eastern desert. These aquifers are recharged directly or through the underlying basalt aquifer or from the surrounding aquifers like the case of Wadi Araba and Jordan Valley. The waters flowing in the main valley fills depends on the under ground conditions and mainly takes place from the escarpments into the valley deposits.

3.3.4 Hydrodynamic pattern

Fig. 3.17 shows the hydrodynamic pattern in the northern part of the study area presented by El-Naser (1991). It shows that there are two lateral movements: the one that occurs in the upper B2/A7 aquifer, the other one occurs in the lower Kurnub aquifer. In the B2/A7, the water flows laterally from Jabal Al Arab to north and northeast of the Mafraq area. There it converges with the water coming from the southeast and partially from Ajloun area towards the Ramtha area, where it continues from there to the Yarmouk River the Rift Valley. In the Kurnub aquifer, the waters flow from the northern parts eastwards and northeastwards to the Rift Valley. Part of the flow is directed towards the Zarqa River (Fig. 3.16).

In the Rift Valley area, the Kurnub potentiometric surface is higher than that of the B2/A7 (Fig 3.17), therefore the upward leakage happens in this vicinity, otherwise, the Kurnub aquifer gains its water from the downward leakage of the B2/A7. The Kurnub hydraulic gradient is lower than that of the B2/A7. Therefore it is less mobile.

The A1-6 aquitard behaves in a very complex manner. The lateral motion is limited within the areas of high permeability. The upward (to the B2/A7) or downward leakage (to the kurnub) occurs in the faulted sections.

The whole sequence in the vicinity of Wadi Al Arab- Mokhybeh area is a hydraulic active region because this part of the study area is highly faulted, occurance of cavities, and thus high transmissivities.

Fig. 3.18 shows the hydrodynamic pattern of the central part of Jordan presented by Salameh and Udluft (1985). It shows a flow net along across section from the Dead Sea to the Azraq Oasis. It shows that after penetrating the surface aquifers, the waters flows either to the east or to the west, which is governed by the water shed in Madba. The waters which flow to the west of the Madba watershed flows through the upper cretaceous aquifer westwards and discharge as springs on the borders of the Dead Sea, while the waters which flow to the east of the Madba watershed infiltrates through the upper cretaceous to the lower sandstone aquifer and partly discharge in the Azraq Oasis, while the rest continue flowing south westwards to the Sirhan depression. The lower sandstone aquifer water flows to the west where it discharges at elevation below sea level along the slopes on the borders of the Dead Sea. The waters become thermal due to deep percolation.

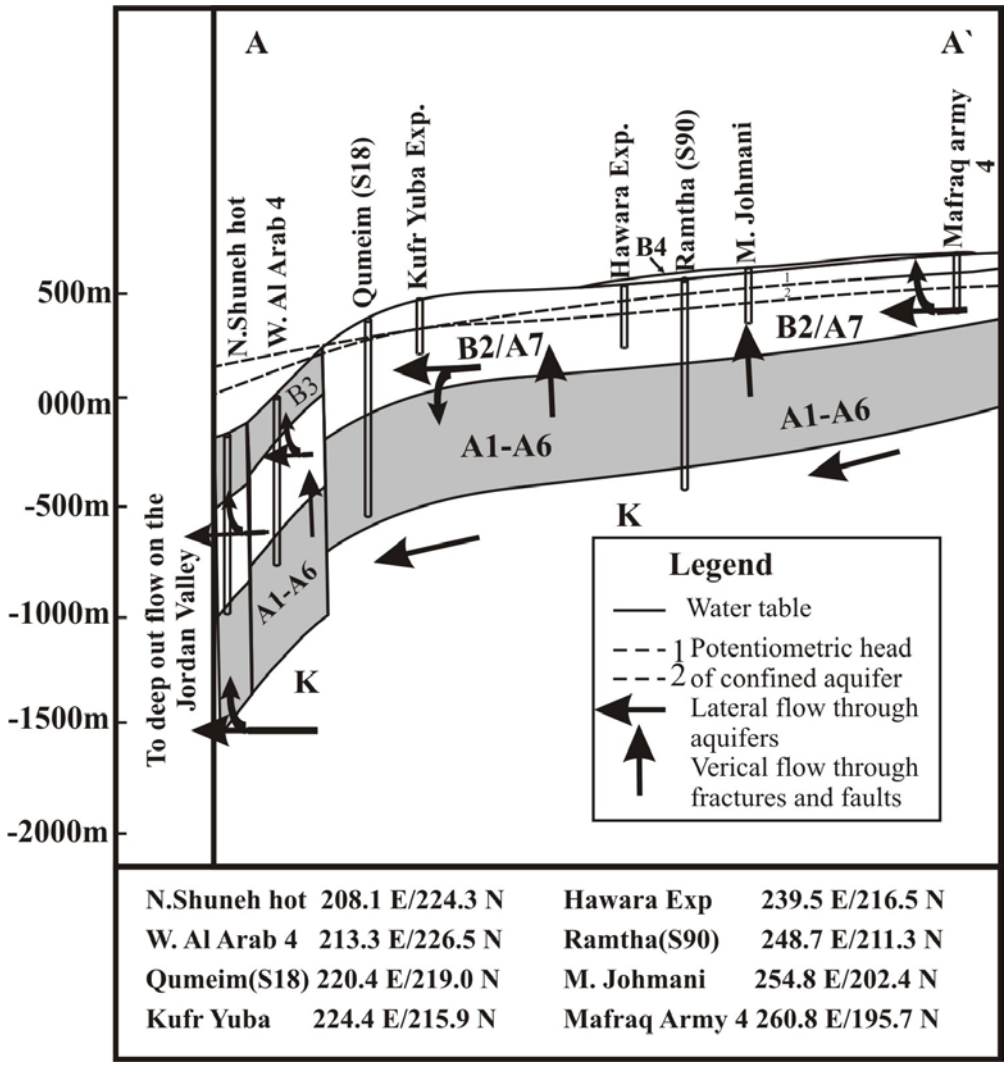

Fig. 3.17: Hydrodynamic pattern of the northern part of the study area (modified after El-Naser 1991).

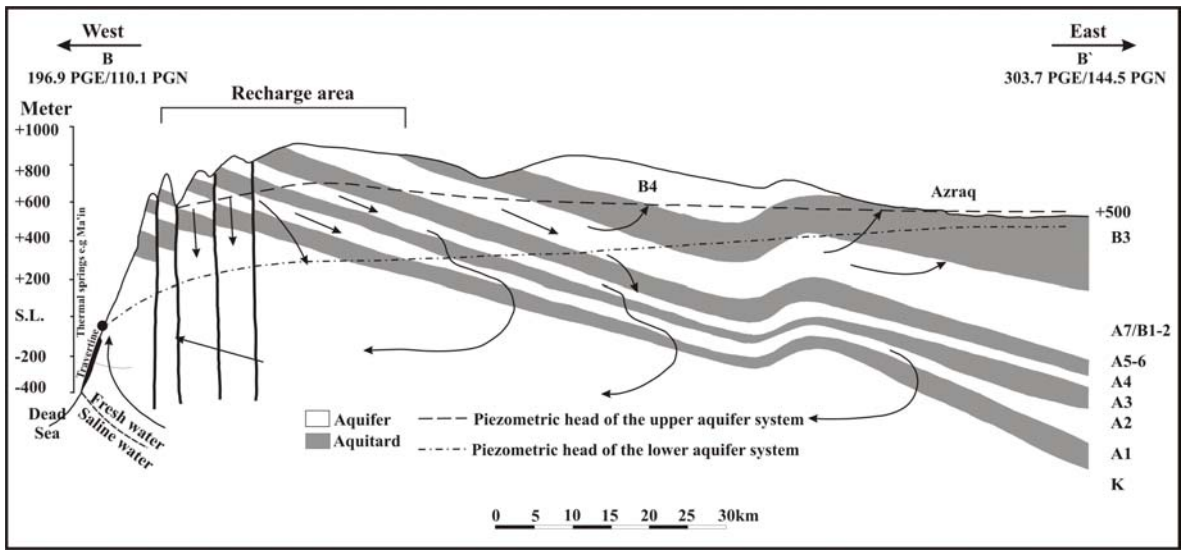

Fig. 3.18: Hydrodynamic pattern of the central part of Jordan (modified after Salameh and Udluft 1985).

3.4 Dead Sea

3.4.1 Physiography

The Dead Sea (DS) is located in the lowest continental topographic spot in the east African-Red Sea-Jordan Valley. It has a total length of 80 km and a maximum width of 17.5 km. It consists of two sub basins: the deep Northern sub basin has a water level of about 417 m below sea level and the maximum depth is about 400 m below that. The southern sub basin was exposed since the middle of the 1980's. The Dead Sea water levels drop due to severe impact on the Jordan river water balance: a) Israel is diverting huge amount of water via the national water carrier from lake Tiberias to Negev area; b) artificial irrigation in Jordan Valley by Israel, Jordan, and Palestine. Jordan and Israel use the southern sub basin nowadays as solar ponds.

The total area of the historical DS is about 1000 km^2, now it is about 700 km^2. The water volume stands currently at 128 km^3, which dropped from around 155 km^3 in the twentieth century (Neev and Emery 1967). The drop of the DS level is estimated to be about 0.8 m/year (Anati and Shasha 1989).

3.4.2 Geological history of the Dead Sea.

In the middle Paleozoic, the western Arabian promentory jutted into the Tethyan seaway. Through the geological history, this area was a site of transgressional-regressional cycles that formed a stratigraphic column of alternating continental fluviatile sediments and shallow marine limestone and marl with some chert and phosphorite deposits (especially in the late Cretaceous and Eocene) (Abu Jaber et al. 1989).

During the middle Eocene, the Red Sea was formed with its northern extension the Jordan Rift Valley. Since that time this area was controlled by continental regime, except in the middle of the rift (Bender 1974).

The rift system in the DS area is a left lateral strike-slip fault system, which forms series rhomb-shaped grabens. The DS is located with in the lowest rhomb (Garfunkel 1981). Manspeizer (1985) estimated the lateral displacement of about 107 km. The rift system that was formed in the Miocene have resulted a thick sediment sequence that range in age between Miocene-Present (Bender 1974). The thickness of the post rift sediments is around 12 km.

Since Pliocene successive lakes have occupied the Jordan valley that had various sizes and different salinities, in which lacustrine sediments have accumulated. According to Abed (1985) and Zak (1967) the most important lakes are:

- **Lake Sedom** formed in the late Miocene-Pleiocene (7-3 Ma). It formed the oldest post-rift sediment (Usdum Formation) that consists of 4 km of salt rocks interbeded with marl and carnalite.

- **Lake Samra** (350-63 ka) is a fluvio-limnic lake, that extended 190 km. It formed 25-35 m thick sediments.

- **Lake Lisan** developed during the Middle Pleistocene. The sediments of this period belong to Lisan formation. Lake Lisan extended from lake Tiberias in the north to about 35 south of southern basin of the DS (Horowitz, 1979). Gradual enrichment of ^{18}O in carbonate deposited on the fringes of the lake indicates the progressive evaporation of waters in lake Lisan (Bani Sakhir, 1996). It is believed that the modern DS evolved from lake Lisan as a result of tectonic subsidence in the north about 18000 BP and because of changing climatic conditions (18-11 ka BP) (Horowitz, 1979).

The modern DS has evolved in the Holocene. The Holocene climate of the region was devided by Horwitz (1979) into three periods: The Versillian (11-7 ka BP), which was interpluvial with relatively dry conditions where halite continued to precipitate in the area. Gat and Margaritz (1980) debated this interpretation and suggested more humid conditions, based on the development of red soils at this stage. The Atlantic stage (7-4.5 ka BP), which had a pluvial period where a divide between Bisan lake (in the central Jordan Valley) and the northern Dead Sea basin caused additional flooding of the northern basin (Neev and Emery 1967). The recent period is dry interpluvial, which began 4.5 ka BP. It is believed that it had some fluctuations in climatic conditions.

3.4.3 Limnology

The DS receives its waters from the Jordan River (~$120 \cdot 10^6$ m^3/year), rivers east of the DS (~$219 \cdot 10^6$ m^3/year), rivers west of the DS (~$163 \cdot 10^6$ m^3/year) (Abu-Jaber 2004) and from intermittent streams south of the DS (~$81 \cdot 10^6$ m^3/year) (Salameh and El-Naser 1999).

Abu-Jaber (1998) and Salameh and El-Naser (2000) estimated the groundwater discharge into the DS to be about 200-300·10^6 m^3/year.

The waters of the DS are stratified; a deep anoxic dense fossil water layer and an upper less dense mix renewable water of about 40 m deep, which kept getting deeper and denser because of the imbalance between the inflow and the evaporation until the last overturn event that happened in the 1979 (Carmi et al. 1984). Anati and Stiller (1991) discussed the physical parameters controlling the relationship between the afore mentioned two layers and the stability of the pycnocline.

3.4.4 The Dead Sea Brines

The Dead Sea contains around 332 g/l dissolved ions. It is a natural brine that consist of water that is characterized by Mg>Na>Ca>K and Cl>Br and traces of of SO_4 (1 wt%). The brine is of Ca-chloride composition with >5 g/l bromine. According to Zak (1997), it is believed that the Dead Sea results from a mixture of three types of brines:

1. **The Arava-Lot Ca-Chloridic diagenetic brine** which is highly saline (320 g/l dissolved solids), deep-seated ground water and Ca-chloridic waters with Ca > HCO_3+SO_4. It has a very low Na/Cl ratio compared to seawater and a K/Cl ratio lower than that of the Dead Sea. It is thermal hot waters with around 42^{o}C. It is considered to be a relict of the evaporated water in the Sedom Gulf. During its residence with in the carbonate rocks and under the high temperatures in the aquifer; the Mg-Chloride-sulfatic marine brine was modified to Ca-Mg-chloridic brine throughout the replacement of Calcium in the carbonates with magnesium of the brine. The sulfate was also removed by Sulfate reducing bacteria.

2. **Meteoric water** that are chloridic-sufatic and bicarbonatic rainwater and surface runoff that issue from springs around the Dead Sea. They marked by close-to-marine composition. They gain salinity from airborne sea salts. In the vadose zone they become more saline and modified the SO_4>Cl ratio by evapotranspiration. Compared to seawater, some springs have higher sulfate concentration, other springs have higher K ratios. Br/Cl is higher while Na/Cl is lower of that of the seawater.

3. **Siddim-Ashlag metamorphic brine** is characterized as Mg-Ca-K-Na-chlorides water >340 g/l dissolved salts. It has lower Br/Cl ratio than the Dead Sea. They issue from valley floor springs near Mount Sedom. They are also found in high artesian wells. The brines are generally saturated with respect to halite, sylvite and carnalite, which evolved through alteration and dissolution of hydrous evaporite minerals by Ca-chloride brines.

Those brines mixture produces different water types that drains into the Dead Sea. They are described by Mazor et al. (1969), Mazor (1997), and Starinsky (1974). Those groups are:

1. **Yesha-Zohar group**, which is a thermal water (up to 42°C) with a salinity of ≤ 175 g/l. It contains radon, radium and H_2S. The Br/Cl ratio is lower but close to that of the Dead Sea while the Ca/Mg ratio and Na/Cl ratio is higher and K/Cl ratio is lower than in the Dead Sea. Mazor et al. (1969) considered that those waters result from recycling of the Dead Sea water and mixing with the Kikar-Noit group and diluted with meteoric water. Starinsky (1974) suggested that those waters have the same origin as the Dead Sea but went through a process of evaporation.

2. **Kikar Noit group** is a thermal water (around 42°C) that has low-medium salinity (5-50% of seawater). It contains H_2S. Mazor et al. (1969) considered them as unevaporated seawater that invaded the rift forming the later lake Lisan and percolated deep. This water is characterized by high sulfate and potassium contents. The waters have higher Ca/Mg and Br/Cl ratios and lower Na/Cl compared to seawater. The high sulfate, Na, and K content was explained as a result of mixing with meteoric waters.

3. **Kaneh-Samar group**, which is a thermal waters with low salinity (500-10000 mg/l) containing H_2S and Radon. They are of two sub-types: sulfatic and Ca-chloridic. The sulfatic sub-type is of low salinity (500-1000 mg/l). High Na/Cl, K/Cl and Mg/Cl ratios and low Br/Cl ratio characterize it. The Ca-chloridic subtype is higher in salinity (up to 10000 mg/l) and has an ionic ratio similar to that of the Dead Sea. Lower Mg/Cl and Br/Cl and higher K/Cl characterize it.

Several models were proposed to describe the evolution of the Dead Sea brines. They will be discussed in the following:

Bentor (1961) stated that the volume of the salts that enters the DS lakes through the Jordan River and the small tributaries cannot account for its high salinity. He attributed the rest of the salinity volume to subsurface brines that leaks into the lake. He also rejected the dissolution of salts from Usdum Formation and post Lisan Halite because of the high Br/Cl ratio found in the waters and that dissolution of poor-Br Halite cannot account for the high Br concentrations in the DS waters.

Starinsky (1974), Vengosh et al. (1991), and Stein et al. (1997) have attributed the salt source to a modified marine origin to explain the discrepancy between the real evaporated sea waters and the unique composition of the DS water which is Ca-Cl_2 waters enriched in K, Mg and Br while SO_4 and HCO_3 are relatively low.

Hardie (1990) and Abu-Jaber (1998) suggested a deep continental origin for the salts, while Abu-Jaber (1998) have suggested that a continuous salt input into the DS is needed in order to account for its recent chemical composition while the modified sea water model suggested a terminal salt source.

3.4.5 Geofluids flow, paleohydrogeology of hydrocarbon maturation and migration

According to Gvirtzman et al. (1997), their are three types of flow driving forces:

1. Gravity driven flow that result from groundwater gradient. It is characterized by a flow of around 10 m/yr.
2. Buoyancy driven flow that is associated with temperature and salinity differences. It creates a flow rate of around 1 m/year.
3. Compact-driven or tectonic driven flow that is associated with abnormal overpressure. It is characterized by a flow rate of around 0.1-0.001 m/yr.

The first two forces are stable on a long period of time while the third one vanishes quickly when stress is released.

Gvirtzman and Stanislavsky (2000a) carried out a numerical simulation for the Dead Sea rift. They used a two dimensional JHU2D-code, which is based on finite element method to solve the transient fluids and heat flow equations. They also used JHH2D-code to simulate the separation of gas phase from petroleum phase. They prepared a detailed cross section, which is 5 km deep and 170 km long. It traverses the Mediterranean, Dead Sea, and Moa'b mountains in Jordan (Fig. 3.19).

They suggested that the seawater that had invaded the rift have partially evaporated and became more saline. This caused unstable conditions because heavier water was overlying lighter groundwater. Thus rapid downward penetrations have happened. This has formed free convection cells throughout faulting blocks. Because of afore mentioned phenomena, a lateral density driven migration of the brines from the rift westwards was initiated. Once the seawater retreated the lake level dropped and a hydraulic gradient between the High Lands and the rift was formed. A local topography driven flow toward the drainage basin was initiated (within the shallower aquifer. Thus the percolating meteoric water at the High Lands flushed the formerly formed brines back to the rift.

Stanislavsky and Gvirtzman (1999) suggested the present coexistence of two basin-scale groundwater flow systems. They are topping each other with opposite flow direction (Fig. 3.20). The first one is topography driven flow, which is a shallow one (down to around 1 km) that is directed from the surrounding High Lands toward the Rift Valley. The second one is a density driven flow, which goes through deeper aquifer (down to 5 km) in the opposite direction from the rift outwards.

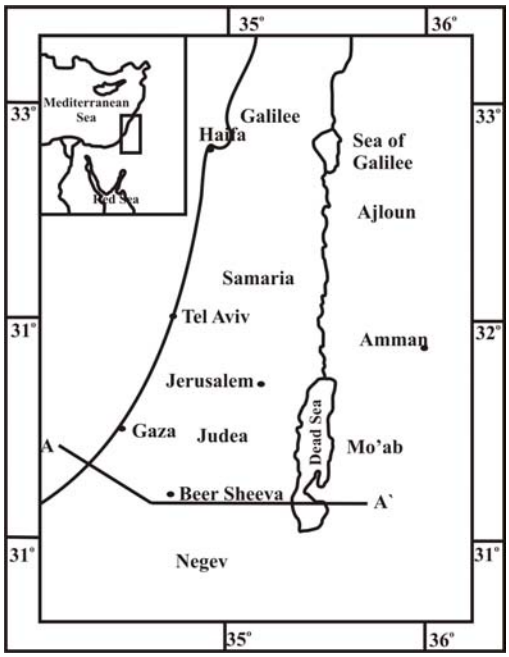

Fig. 3.19: Map showing the location of the Geological cross section A-A`(Gvirtzman and Stanislavsky 2000a).

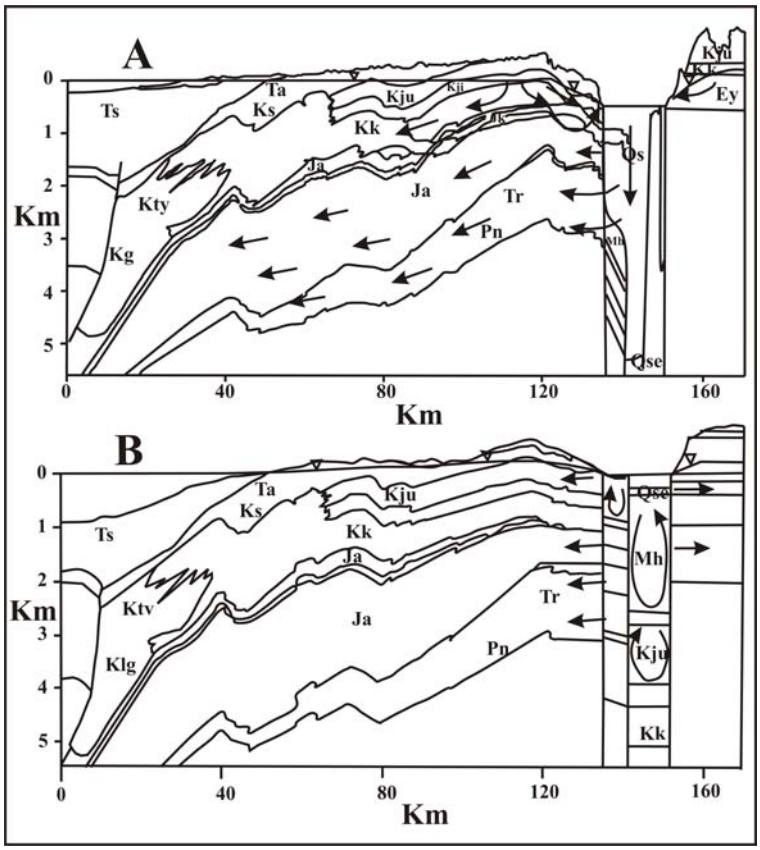

Fig. 3.20: Geologic cross section and more flow direction (A) at present, and (B) at the early Pleiocene, illustrating the evolution of the Dead Sea evolution.(for symbols see Table 3.9) (Stanislavsky and Gvirtzman 1999).

Table 3.9: Hydrostratigraphic units associated with the geological cross section (modified after Gvirtzman and Stanislavsky 2000a).

Symbol	Age	Group/Formation		Lithology
		Israil	Jordan	
Qs	Quaternary	Samra Fm.	Jordan Valley	Marlstone
Qse	Neog.-Quat.	Sedom Fm.		Salt
Mh	Miocene	Hazeva Fm.		Sandstone and conglomerate
Ts	Tertiary	Saqiye Gp.		Marlstone
Ta	Tertiary	Avidat Gp.	Belqa	Chalk and limestone
Ks	Cretaceous	Mt. Scopus Gp.		Chalk
Kju	Cretaceous	Up. JudeaGp.	Ajloun	Dolomite and limestone
Kji	Cretaceous	Low. Judea Gp.		Chalk and marl
Kty	Cretaceous	Talme Yafe Gp.		Marlstone
Kg	Cretaceous	Gevar'am Gp.		Marlstone
Kk	Cretaceous	Kurnub Gp.	Kurnub	Limestone and sand
Jk	Jurassic	Kidod Fm.		Marlstone
Ja	Jurassic	Arad Gp.	Zarqa	Carbonates
Tr	Triassic	Ramon Gp.		Carbonates
Pn	Permian	Negev Gp.		Carbonates
Ey	Cambrian	Yam Suf Gp.	Safi	Sandstone
PE	Precambrian	Basement	Ram	Granite

Gvirtzman and Stanislavsky (2000a and 2000b) indicated that the second driving force affected the migration and petroleum maturation (Fig 3.21). The scenario began when the seawater invaded the rift, then evaporated, and then penetrated downward. The decent of cold water and ascent of thermal water have interrupted the geothermal gradient and the position of the oil window changed (between 2.5-4 km).

Lateral migration is then started. Gas and oil migrated westward together with the brines but with different rates. Because of their high viscosity and lower density, the oil moved at a rate of few centimeters with in the Triassic and Jurassic while gas was entrapped in the accumulated in the rift flank. Later on the meteoric water washed and removed the saturated and aromatic hydrocarbons from the oil forming heavy oil and asphalts.

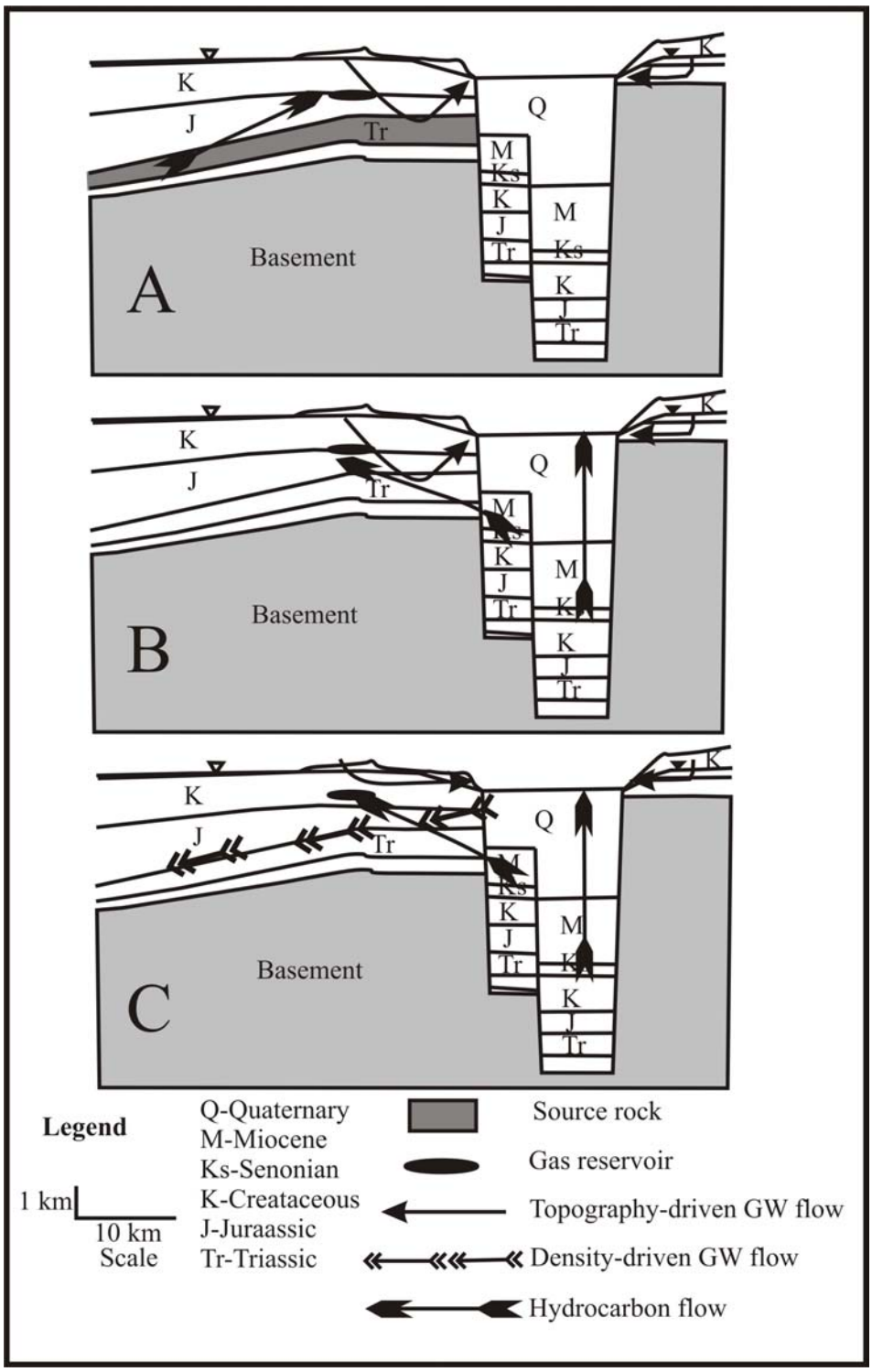

Fig.3.21: Schematic E-W cross-sections illustrating the conceptual models suggested for gas entrapment at the Zohar anticline. (A) Hydrocarbons originated in the Triassic formations and migrated eastward, independently of regional groundwater flow systems. (B) Hydrocarbons originated in the Senonian bituminous marls, buried in the graben, which have migrated westward, against the direction of topography-driven groundwater flow. (C) Hydrocarbons originated in the Senonian bituminous marls buried in the graben, which have migrated westward, with the direction of density-driven groundwater flow (Gvirtzman and E. Stanislavsky 2000b).

4. RESULTS

This chapter includes the results that were obtained in the field, water chemistry labs (major elements and rare earth elements (REE)), and isotope labs (^{3}H, $\delta^{18}O$, δD, $\delta^{34}S_{Sulfate}$ and $\delta^{18}O_{Sulfate}$, δHe, δNe and the isotopes of CH_4, H_2S and CO_2 gasses). It includes also the results derived from statistics, geothermometers and geochemical modelling using PhreeqC (analysis error, species distribution, saturation indices, calculated reaction inverse modelling paths) and SolminEQ88 (saturation index depend on pressure).

4.1 Field data and chemical analysis

23 samples were collected and analyzed twice from the thermal springs and wells in the area of study along the Dead Sea Transform (DST). The physical and chemical parameters were applied for all of the 23 samples as mentioned in chapter 2 (Methodology). The result of the first sampling campaign, the second sampling campaign and the averaged chemical analysis are tabulated in Appendices (1, 2 and 3.) The results of the Rare Earth Elements (REE) are shown in Appendix (4).

4.1.1 Total dissolved solids

Since there was no direct measurement for the total dissolved solids (TDS) in the field, the equation of Freeze and Cherry (1979) was used to estimate the TDS value where all the components of this formula are in mg/l as follows:

$$\mathbf{TDS\ (mg/l)= Ca^{2+}+Mg^{2+}+Na^{+}+K^{+}+SO4^{2-}+Cl^{-}+NO^{3-}+0.5*HCO3^{-}}$$

Appendix 5 presents the calculated TDS from the previous formula and the types of water according to Caroll classification (1962). It can be noticed that the upper aquifer (B2/A7) samples are almost fresh waters because even the waters which are classifid as brackish waters are having values on the fresh-brackish water threshold. In the lower sandstone aquifer waters, it is noticed that the Abu El-Zeeghan wells are having the highest salinity of the thermal waters, and the rest of the waters are ranging from fresh to brackish waters.

4.1.2 Electrical conductivity

The electrical conductivity (EC) measurements, which are conducted for the thermal waters showed that the EC values in the upper aquifer (B2/A7) ranges between 707 µS/cm to 2220 µS/cm where the lowest value is being recorded in Waqas well and the highest is recorded in Abu Zyad well. In the lower sandstone aquifer, the EC value is found to be ranging between 530 µS/cm to 10420 µS/cm where the lowest value is being recorded in the Burbyta spring and the highest is being found in Abu El-Zeeghan/2 well.

Since the EC and TDS are measurement of the total salt content, there must be a certain relation between them. The correlation between these two parameters for the samples was

plotted in Fig. 4.1, TDS in mg/l can be calculated from EC µS/cm according to the formula:

TDS mg/L= 0.581 EC µS/cm.

The relatively small residues between TDS and EC and vice versa are a proof that the chemical composition of all waters is considerably similar.

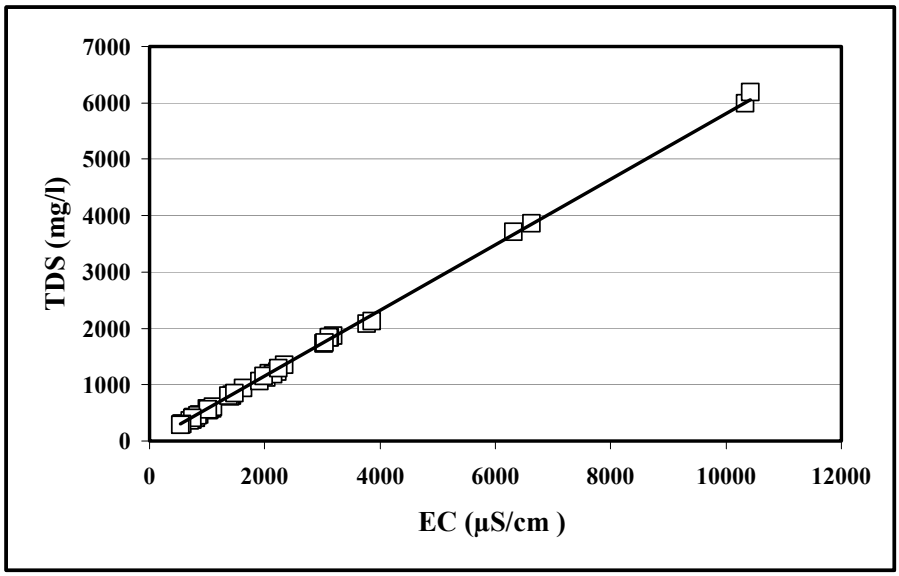

Fig. 4.1: Plot presenting the relationship between the EC and TDS values of the analyzed thermal waters.

4.2 Isotope results

4.2.1 Tritium

Appendix 6 shows the long term tritium measurements from the Jordanian rainfall stations: Amman Airport, Amman-WAJ, Azraq, Deir Alla, Queen Alia Airport, Ar Rabba, Ras Munif, Shoubak and Walla (GNIP and ISOHIS 2002). Since the tritium record of the afore mentioned stations is insufficient; the data of the long tritium record rainfall stations of Isarel (Beer Sheeva, Haar Kna'an and Bet Dagan) were also used to provide a base data for comparison (GNIP and ISOHIS 2002) (Appendix 6 and Appendix 7).

The oldest tritium record in Jordan dates back to 1965. It is found in Amman-Airport station (with an average of 148 TU), Ar Raba station (with an average of 154 TU), and in Shouback station (with an average of 111 TU). The maximum value was recorded in 1966 in Amman-Airport to be 330 TU. On the other side of the rift (Israel), the oldest record dates back to 1961 in Haar Kna'an with an average of 920 TU. The maximum value in Israel was recorded in Beer Sheeva in 1963 to be 6450 TU.

According to the piston flow recharge model assumption and based on the half life of the Tritium which is (4500±8) day (Lucas and Unterweger 2000) and no mixing, the expected

tritium value to remain in the water from the initial concentration in the precipitation when it discharges in year 2003 was calculated (Appendix 6) by using the well known decay equation:

$$a_t = a_o.exp.(-\lambda t)$$

where:
a_t is the Isotopes content after some period of time (t);
a_o is the isotope content at the beginning;
λ is the decay constant, where $\lambda = Ln2 / T_{1/2}$;
t is the time period.

Table 4.1 shows the results of the tritium isotope analysis that was analyzed in the laboratories of the (Angewandte Physik) at TU-Bergakademie Freiberg.

Table 4.1: The tritium concentration of the thermal water samples collected in the period between March 10, 2003 and March 28, 2003.

No.	Name of the Spring/well	Tritium TU/Error	No.	Name of the Spring/well	Tritium TU/Error
1	EL-Mokhybeh	0.3±0.3	13	El-Seel El-Hami	0.0±0.3
2	El-Hmmeh/Maqla	0.4±0.3	14	Tal El-Rojom	0.0±0.3
3	El-Hammeh/Bajeh	0.4±0.3	15	Ma'in/El-Mabkhara	0.0±0.3
4	North Shuneh hot well	0.0±0.3	16	Ma'in/El-Ameer	0.0±0.3
5	Waqas well	0.1±0.3	17	Ma'in/El-Shallal	0.1±0.3
6	Abu-Zyad Well	0.1±0.3	18	TA1	0.0±0.3
7	Abu-Thableh	0.4±0.3	19	TA2	0.0±0.3
8	Abu El-Zeeghan/1	0.0±0.3	20	Iben Hammad	0.2±0.3
9	Abu El-Zeeghan/2	0.0±0.3	21	Burbyta	0.2±0.3
10	Al-Kafreen well	0.0±0.3	22	Afra/Sawna	0.0±0.3
11	Zara/Istraha	0.3±0.3	23	Afra/Maqla	0.4±0.3
12	Zara/Maghara	0.0±0.3			

4.2.2 Helium and Neon Isotopes

Four samples were analysed for Helium and Neon: El-Mokhybeh, Waqas, TA1, and TA2. Appendix 8 shows the results of analysis done by Abteilung Ozeanograpphie-Institute für Umweltphysik Dienstleistungen, Bremen university. And it shows the calculation of the Weise-plot parameters for the analysed samples. ^{3}He range from $1.5 \cdot 10^{-12}$ to $7.5 \cdot 10^{-12}$ Nml/g while ^{4}He range between $5.6 \cdot 10^{-7}$ and $4.7 \cdot 10^{-5}$ Nml/g. ^{20}Ne range from $1.9 \cdot 10^{-7}$ to $2.5 \cdot 10^{-7}$ Nml/g while ^{20}Ne range between $1.8 \cdot 10^{-8}$ and $5.4 \cdot 10^{-8}$ Nml/g.

4.2.3 Water stable isotopes ($\delta^{18}O$ and δD)

The isotopic composition of $\delta^{18}O$ and δD, the excess, and the aquifers are listed in Table 4.2. The excess is ranging from –0.3 $^{o}/_{oo}$ to 19.0 $^{o}/_{oo}$.

4.2.3.1 Deuterium

The δD values for all of the thermal waters were found to be ranging between -26.1°/oo and -50.6 °/oo with a mean of -35.2 °/oo and a standard deviation of 7.32. The deuterium value of the upper aquifer (B2/A7) thermal waters was found to be ranging between -26.1 °/oo and -32 °/oo with a mean of -28.46 and a standard deviation of 1.69. For the lower sandstone aquifer, the values range from -30.5 °/oo and -50.6 °/oo with a mean of -38.81 °/oo and a standard deviation of 6.55.

4.2.3.2 Oxygen-18

The $\delta^{18}O$ values for all of the thermal waters were found to be ranging between -3.77 °/oo and -7.5 °/oo with a mean of -5.82 °/oo and a standard deviation of 1.06. The $\delta^{18}O$ values for the upper aquifer (B2/A7) thermal waters were found to be ranging between -5.5 °/oo and -6.09 °/oo with a mean of -5.79 °/oo and a standard deviation of 0.1. For the lower sandstone aquifer, the values range between -3.77 °/oo and -7.5 °/oo with a mean of -5.83 and a standard deviation of 1.32.

Table 4.2: The δD and $\delta^{18}O$ isotopic composition of the thermal waters and their excess and aquifers.

No.	Spring/Well	$\delta^{18}O$ °/oo	δD °/oo	Excess °/oo	Aquifer
1	EL-Mokhybeh	-5.78	-28.7	17.5	B2/A7
2	El-Hmmeh/Maqla	-6.09	-32.0	16.8	B2/A7
3	El-Hammeh/Bajeh	-5.82	-29.2	17.4	B2/A7
4	North Shuneh hot well	-5.67	-27.8	17.6	B2/A7
5	Waqas well	-5.88	-28.0	19.0	B2/A7
6	Abu-Zyad Well	-5.76	-27.6	18.5	B2/A7
7	Abu-Thableh	-5.85	-28.3	18.5	B2/A7
8	Abu El-Zeeghan/1	-7.01	-42.8	13.2	Zarqa
9	Abu El-Zeeghan/2	-6.21	-35.6	14.0	Zarqa
10	Al-Kafreen well	-5.50	-26.1	18.0	Kurnub
11	Zara/Istraha	-4.58	-35.2	1.5	Kurnub
12	Zara/Maghara	-4.36	-32.9	2.0	Kurnub
13	El-Seel El-Hami	-5.79	-42.3	4.0	Kurnub
14	Tal El-Rojom	-5.85	-42.9	3.9	Kurnub
15	Ma'in/El-Mabkhara	-4.06	-31.2	1.3	Kurnub
16	Ma'in/El-Ameer	-4.10	-31.4	1.4	Kurnub
17	Ma'in/El-Shallal	-3.77	-30.5	-0.3	Kurnub
18	TA1	-7.43	-50.5	9.0	Kurnub
19	TA2	-7.50	-50.6	9.4	Kurnub
20	Iben Hammad	-7.20	-43.4	14.2	Kurnub
21	Burbyta	-6.50	-40.8	11.3	Kurnub
22	Afra/Sawna	-6.58	-36.0	16.7	Kurnub
23	Afra/Maqla	-6.54	-36.0	16.3	Kurnub

4.2.4 Sulfate isotopes ($\delta^{34}S_{Sulfate}$ and $\delta^{18}O_{Sulfate}$)

Table 4.3 shows the sulfate concentrations, $\delta^{34}S_{Sulfate}$ and $\delta^{18}O_{Sulfate}$ of the waters. The sulfate concentrations range from 46.07 to 188.22 mg/l for the upper aquifer (B2/A7) waters and from 40.81 to 1253.17 mg/l for the lower sandstone aquifer samples. The $\delta^{34}S_{Sulfate}$ ranges from -1.5 to 27.8 ‰ for the upper aquifer (B2/A7) samples and from 4.6 to 21.40 ‰ for the lower sandstone aquifer samples. The $\delta^{18}O_{Sulfate}$ range 5.3 to 13.5 ‰ for the upper aquifer (B2/A7) and from 5.10 to 14.10 ‰ for the lower sandstone aquifer.

Table 4.3: The $\delta^{34}S_{Sulfate}$ and $\delta^{18}O_{Sulfate}$ and sulfate results of the thermal waters samples.

No.	Well/Spring	$\delta^{34}S$ Sulfate (‰)	$\delta^{18}O_{Sulfate}$ (‰)	Sulfate (mg/L)
1	EL-Mokhybeh	11.0	5.3	47.78
2	El-Hmmeh/Maqla	27.8	12.9	152.93
3	El-Hammeh/Bajeh	17.5	9.4	86.43
4	North Shuneh hot well	12.4	11.0	115.48
5	Waqas well	12.0	10.3	46.07
6	Abu-Zyad Well	21.5	13.5	188.22
7	Abu-Thableh	9.3	8.4	168.05
8	Abu El-Zeeghan/1	21.4	13.9	910.35
9	Abu El-Zeeghan/2	18.3	14.1	1253.17
10	Al-Kafreen well	-1.5	6.8	79.22
11	Zara/Istraha	16.5	11.7	170.90
12	Zara/Maghara	18.3	12.4	172.71
13	El-Seel El-Hami	16.0	9.5	126.76
14	Tal El-Rojom	14.7	12.2	142.38
15	Ma'in/El-Mabkhara	21.4	11.6	212.31
16	Ma'in/El-Ameer	20.6	12.4	213.41
17	Ma'in/El-Shallal	20.8	13.2	217.97
18	TA1	12.7	7.8	126.03
19	TA2	11.9	9.1	90.99
20	Iben Hammad	10.1	9.0	55.22
21	Burbyta	12.0	6.5	43.93
22	Afra/Sawna	4.8	7.2	43.45
23	Afra/Maqla	4.6	5.1	40.81

4.2.5 CH_4, H_2S and CO_2 gasses

The developed methodology (Gas trapping unit) has been tested in Jordan with the thermal waters. Five thermal wells were chosen to apply the new methodology; springs were not considered due to possible degassing. Those wells are distributed along the study area: El-Mokhybeh, North Shuneh hot, Waqqas, TA1 and TA2. Other wells were found in a technical conditions that doesn't allow the methodology to be applied properly.

The new methodology was found to be successful for both H_2S and CO_2 while no precipitate of CH_4 was formed. The amount of PbS (H_2S precipitate) was very low and the gathered amount was not sufficient for isotope analysis. Five $BaCO_3$ (CO_2 precipitate)

samples were found to be sufficient for the analysis. The $\delta^{13}C$ isotope has been analyzed in the laboratories of the Mineralogy institute of the TU Bergakademie-Freiberg. Table 4.4 shows the results. The standard that has been used is Vienna Pee Dee Belemnite (V-PDB) with an accuracy of $\leq \pm 0.2$ $^{o}/_{oo}$. The $\delta^{13}C_{CO2}$ in the thermal waters have been found to be ranging between -16.9 and -22.9 $^{o}/_{oo}$.

Table 4.4: $\delta^{13}C_{CO2}$ values of the thermal waters along the Dead Sea Transform.

No.	Well	$\delta^{13}C_{CO2}$ ($^{o}/_{oo}$)
1	El-Mokhybeh	-19.3±0.2
4	North Shuneh hot	-22.9±0.2
5	Waqas	-22.9±0.2
18	TA1	-16.9±0.2
19	TA2	-20.6±0.2

4.3 Statistical analysis

Tables 4.5 and 4.6 show the descriptive statistics (minimum, maximum, mean and standard deviation) for both the upper aquifer (B2/A7) and the lower sandstone aquifer. By drawing the frequency histograms and by applying the Kolomogorov-Smirnov test for all of the variables of the studied thermal waters (tempreature, EC, pH, Ca, Mg, Na, K, Cl, SO_4, HCO_3, NO_3, PO_4, NH_4 and SiO_2) in both the 1st and the 2nd sampling campaigns most of the variables were found to be asymmetrical distributed except for temperature, pH, NH_4, and SiO_2. Appendix 9 shows the results of Kolmogorov-Smirnov test for normality where the afore mentioned four variables were having a significant of more than 0.05 indicating a normal distribution.

Table 4.5: Descriptive statistics of the upper (B2/A7) aquifer.

Parameter	N	Minimum	Maximum	Mean	Std. Deviation
Tempreature	16	32.7	52.7	41.262	7.0712
EC(µs/cm)	16	707	2220	1255.94	536.506
TDS(mg/l)	16	459.6	1443.0	816.359	348.7291
PH	16	6.44	7.27	6.8425	0.20622
Ca mg/l	16	62.12	172.34	102.8929	40.02298
Mg mg/l	16	26.741	60.775	40.59010	11.272736
Na mg/l	16	24.829	183.920	89.11930	56.088893
K mg/l	16	2.7370	27.4873	9.083419	7.0047548
Cl mg/l	16	28.36	304.90	148.2763	98.90357
SO_4 mg/l	16	38.88	192.11	110.5214	54.06846
HCO_3 mg/l	16	237.9	604.9	372.420	115.3493
NO_3 mg/l	16	0.000	0.000	0.00000	0.0000
PO_4(mg/l)	16	0.000	0.003	0.00138	.001025
NH_4(mg/l)	16	0.000	0.599	0.24150	0.195525
SiO_2(mg/l)	16	16.7	31.0	21.969	4.0194

Table 4.6: Descriptive statistics of the lower sandstone aquifer.

Parameter	N	Minimum	Maximum	Mean	Std. Deviation
Tempreature	30	37.0	62.0	44.830	6.9913
EC(µs/cm)	30	530	10420	2704.33	2613.031
TDS(mg/l)	30	344.5	6668.8	1746.048	1671.3204
PH	30	6.02	7.98	6.8407	0.46363
Ca mg/l	30	41.082	731.460	178.84364	207.128297
Mg mg/l	30	12.1550	133.2188	45.390822	39.1880601
Na mg/l	30	27.5880	1287.4400	309.578742	308.5650893
K mg/l	30	1.4858	148.8928	37.276637	44.4979924
Cl mg/l	30	67.001	1871.918	556.42349	487.867228
SO4 mg/l	30	38.40	1272.74	254.6937	342.21076
HCO3 mg/l	30	122.016	1561.805	364.96764	385.773052
NO3 mg/l	30	0.0000	7.7004	.570101	1.6490457
PO4(mg/l)	30	0.000	0.008	0.00227	0.001946
NH4(mg/l)	30	0	1	0.26	0.289
Si(mg/l)	30	15.8	32.0	23.377	5.1955

The Pearson correlation requires a normal distribution and interval scaling. The bivariate correlation procedure of SPSS computes the correlation coefficient (r), which requires also a normal distribution and since most of the variables are not normal distributed, the non-parametric Spearman's rank correlation has been used. The correlation matrix between all of the variables is shown in Appendix 10. Table 4.7 shows a summary of the positive ($+_{(0.01)}$) and negative ($-_{(0.01)}$) significant correlation at $\alpha = 0.01$ and the positive ($+_{(0.05)}$) and negative ($-_{(0.05)}$) significant correlation at $\alpha = 0.05$.

The thermal waters were sampled in two campaigns, so it was necessary to check if there is a significant difference in the mean concentration of the different parameters between the two sampling campaigns, and since most of the variables are not normal distributed, the nonparametric Mann-Whitney test was applied. According to the fact that an 5% chance of not being true is being acceptable, a calculated significance level of higher than 0.05 ($\alpha = 0.05$) indicates no significant difference between the means of the two sampling campaign, Appendix 11 shows that there are no significant differences between the mean concentration of all the studied variables and based on this result, an average of the two sampling campaign analysis can be used for further statistical analysis.

The Mann-Whitney test was adopted in order to determine the variables that have a significant difference between the two main aquifers: the upper aquifer (B2/A7) aquifer and the lower sandstone aquifer where it is being found that the variables Na, K, Cl, HCO_3 and NO_3 are the variables that have a significant difference between the two aquifers (Appendix 12).

Table 4.7: Significant correlations at $\alpha = 0.01$ and $\alpha = 0.05$.

	pH	**T**	**EC**	**TDS**	**Ca**	**Mg**	**Na**	**K**	**Cl**	**SO_4**	**HCO_3**	**PO_4**
T												
EC												
TDS			+(0.01)									
pH												
Ca			+(0.01)	+(0.01)								
Mg			+(0.01)	+(0.01)	+(0.01)							
Na			+(0.01)	+(0.01)	+(0.01)	+(0.01)						
K			+(0.01)	+(0.01)	+(0.01)	+(0.01)	+(0.01)					
Cl			+(0.01)	+(0.01)	+(0.01)	+(0.01)	+(0.01)	+(0.01)				
SO_4			+(0.01)	+(0.01)	+(0.01)	+(0.01)	+(0.01)	+(0.01)	+(0.01)			
HCO_3			+(0.01)	+(0.01)	+(0.01)	+(0.01)	+(0.05)	+(0.01)	+(0.05)	+(0.01)		
NO_3			+(0.01)	+(0.01)	+(0.01)	+(0.01)	+(0.01)	+(0.01)	+(0.01)	+(0.05)		
PO_4												
NH_4		+(0.01)	-(0.01)	-(0.01)	-(0.01)		-(0.05)	-(0.01)	-(0.05)	-(0.01)	-(0.05)	+(0.01)
SiO_2	+(0.05)	+(0.01)										

4.3.1 Cluster analysis

In order to group the samples statistically, a cluster analysis was performed and a dendrogram was plotted (Fig. 4.2) under the following conditions: Ward's method, Euclidean distance, transform values were standardized with a range from 0 to 1 and the transformed measures were rescaled to 0-1 range.

The thermal waters shows two groups at low clustering level (level 1): group A and B. At a higher clustering level (level 2) group A is divided into two minor groups, they are A_1 and A_2. At the highest clustering level group A_1 is divided into A_{1a} and A_{1b} while group A_2 could be divided into A_{2a} and A_{2b} and since that the Mann-Whitney test have showed that the group A_{2b} is not significantly different from the other groups (Appendix 13); group A_2 will not be further divided and will considered as one cluster.

Those groups could be interpreted as follows:

Group A_1: It includes the fresh water wells and springs that have the lowest salinity of the studied thermal waters. **Group A_{1b}** includes the thermal waters that tap the upper aquifer (B2/A7), while **group A_{1a}** includes the thermal waters that tap the lower sandstone aquifer (Kurnub aquifer) but their chemical characteristics are similar to the upper aquifer (B2/A7) waters.

Group A_2: It includes the brackish wells and springs that tap the lower sandstone aquifer (Kurnub aquifer). One well (Abu-Zyad) and one spring (Abu-Thableh) are from the upper aquifer (B2/A7) but even so, they are clustering with in this group; this can be easily interpreted by knowing that the Kurnub aquifer water contribute with a high percent of the waters of both of them, where it contribute with 38% of Abu-Zyad well waters and with 34% of the Abu-Thableh spring waters (explained later in section 5.1.3).

Group B: It includes two wells (Abu El-Zeeghan 1 and 2) that tap the lower sandstone aquifer (Zarqa aquifer). They are having the highest salinity of the studied thermal waters.

Appendix 14 shows the descriptive statistics of the 4 groups. The mean of the 4 groups analysis is represented graphically by bar diagrams (Fig.4.3), where it shows that the largest similarity exist between groups A_{1a} and groups A_{1b}.

The nonparametric Kruskal-Wallis and Mann-Whitney tests were used to determine the statistical difference between the 4 groups. The Kruskal-Wallis test have proved that the mean of each group is significantly different from the means of the other groups for most of the variables except the Tempreature, pH, PO_4 and NH_4 (Appendix 15). Since that the Kruskal-Wallis test doesn't distinguish between the mean of any two groups the Mann-Whitney test was used where it shows that group (B) is significantly different from the other groups (Appendix 16).

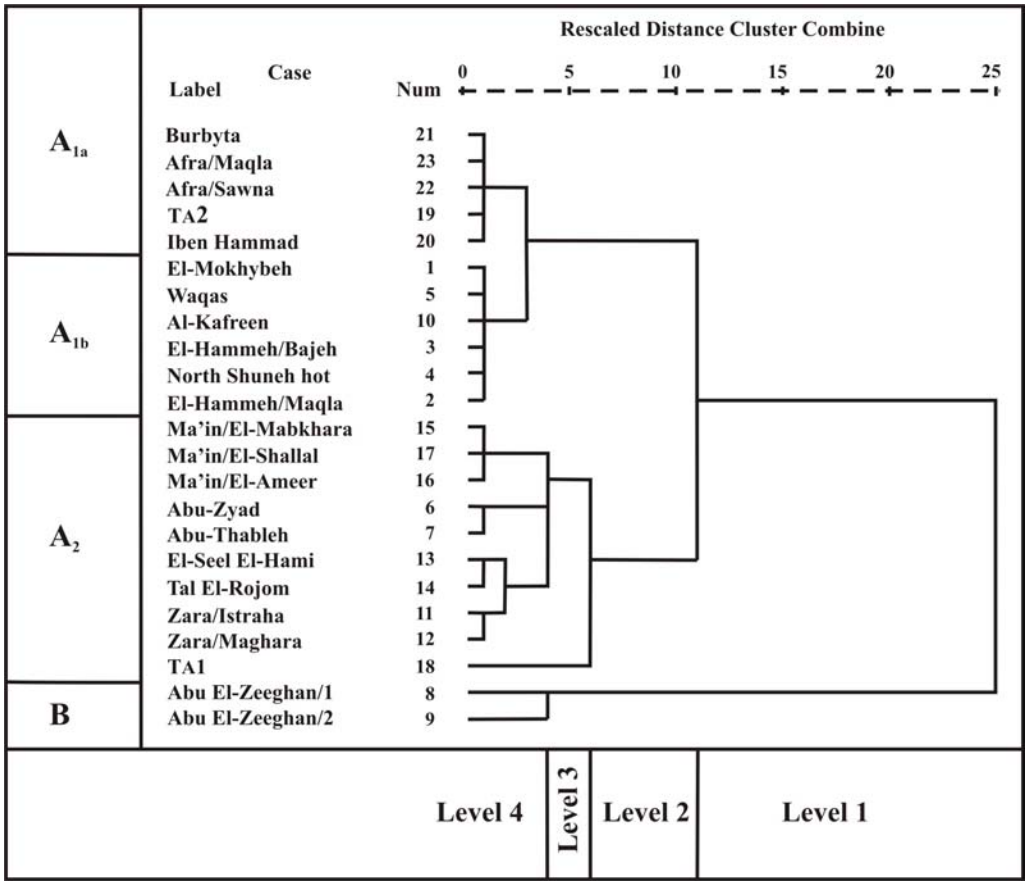

Fig. 4.2: Dendrogram showing the different clustering of the thermal waters.

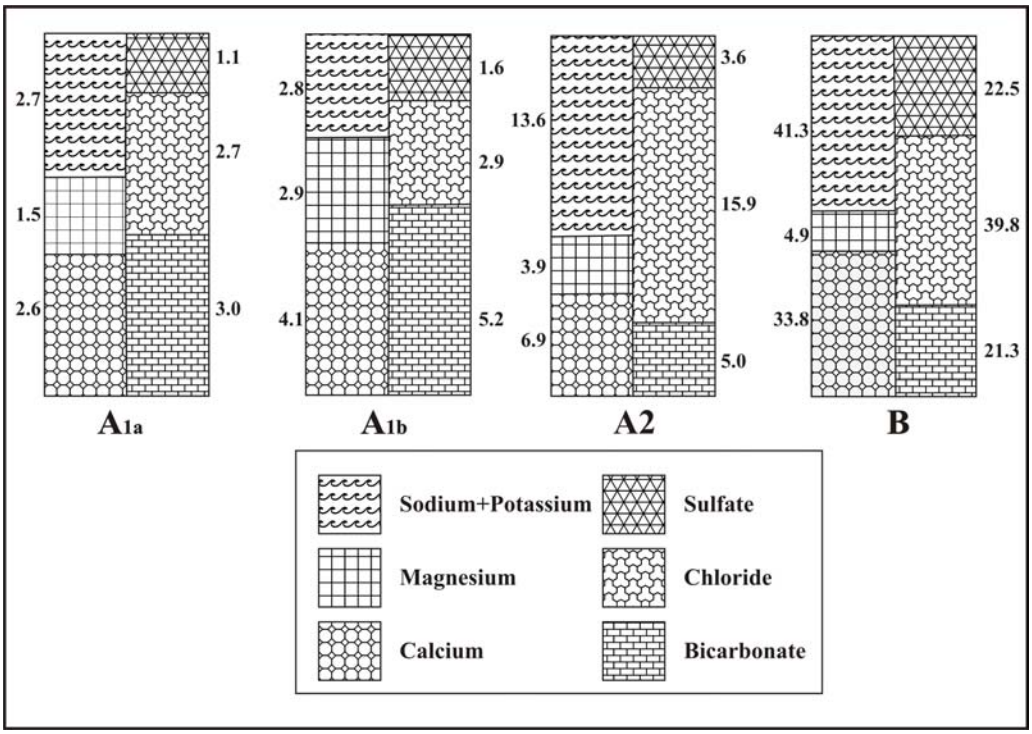

Fig. 4.3: Bar diagram for the major characteristics of the five groups (concentrations in meq/l).

4.4 Geothermometeres

Based on the Giggenbach triangle (illustrated in section 2.5.1) (Fig. 4.4), all of the thermal waters plot in the area of immature waters, therefore solute geothermometry is not likely to yield a meaningful Na/K equilibrium temperatures which are in general giving a high temperatures (Giggenbach 1988).

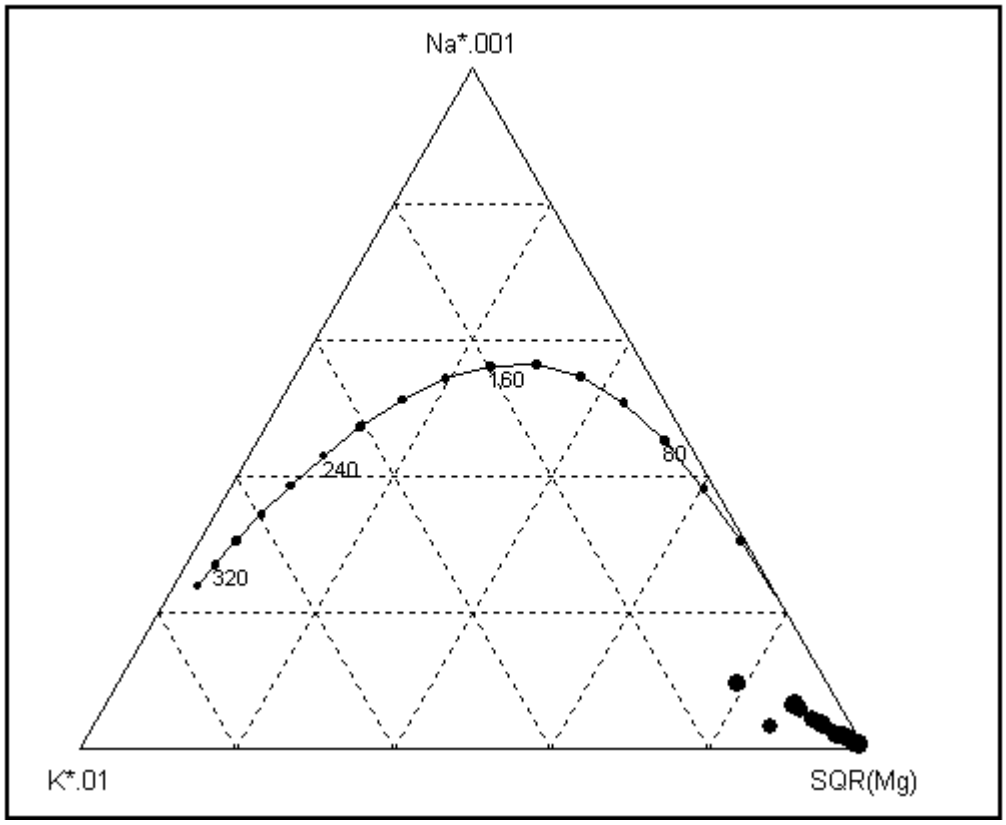

Fig. 4.4: Plot presenting the location of the thermal waters of both the upper aquifer (B2/A7) and the lower sandstone aquifer on the Giggenbach triangle.

The temperatures calculated from sixteen different geothermometers are listed in Appendix (17). The geothermometers of Amorphous silica, Cristobalite Alpha and Cristobalite Beta are giving lower temperatures than those measured on the surface. Table 4.8 shows the temperatures, which are determined from selected geothermometers: Chalcedony, Quartz, Quartz steam loss, K/Mg, Na-K-Ca-Mg corrected and isotope SO_4-H_2 after Kusakabe (1974).

Rimawi and Salameh (1988) have estimated the reservoir temperatures in the geothermal system of Zerqa-Ma'in and Zara area using the SiO_2 geothermometry to be 77.7± 2.6 ^oC, which agree with the calculated temperatures of Truesdell (1979) who suggested that these waters exist at a maximum temperature of 110^oC at depth.

It is noticeable that all of the thermal waters are over saturated with respect to quartz (Appendix 18). Five thermal waters were found to be oversaturated with respect to chalcedony (El-Hammeh/Maqla, Zara/Istraha, Zara/Maghara, Tal El Rojom and Ma'in/El-

Shallal). By assuming that the quartz is the source of silica in these waters, the Quartz geothermometer estimates the upper aquifer (B2/A7) samples (sample 1 to 7 and 10) to be ranging from 57 to 80 ^{o}C and the lower sandstone aquifer samples (sample 8, 9 and 11 to 23) to be ranging from 57 to 82 ^{o}C which agrees with the results of Bajjali (1994), Rimawi and Salameh (1988), and Treusdell (1979).

Table 4.8: (1) Average SiO_2 value in (mg/l), (2) average measured temperature in ^{o}C, (3) Chalcedony geothermometer, (4) Quartz geothermometer, (5) Quartz steam loss geothermometer, (6) K/Mg geothermometer, (7) Na-K-Ca-Mg corrected geothermometer, (8) Kusakabe (1974) Isotope SO_4-H_2O geothermometer where the calculated temperature in (^{o}C)

No	Well/Spring	(1)	(2)	(3)	(4)	(5)	(6)	(7)	(8)
1	EL-Mokhybeh	19.95	36.05	31	63	69	63	36	131
2	El-Hmmeh/Maqla	30.7	39.15	49	80	84	54	45	65
3	El-Hammeh/Bajeh	21.1	35.4	33	65	71	59	36	92
4	North Shuneh hot	24.2	52.55	39	71	75	67	22	81
5	Waqas well	20.9	48.3	33	65	70	67	24	85
6	Abu-Zyad Well	22.2	48.3	35	67	72	51	41	63
7	Abu-Thableh	19.95	35.2	31	63	69	55	43	100
8	Abu El-Zeeghan/1	18.85	37.35	29	61	67	41	91	52
9	Abu El-Zeeghan/2	16.7	37.35	24	57	63	38	100	57
10	Al-Kafreen well	16.75	35.15	25	57	63	59	31	118
11	Zara/Istraha	27.15	41.6	44	75	79	45	46	92
12	Zara/Maghara	26.9	42.75	43	75	79	43	57	81
13	El-Seel El-Hami	31.75	58.85	50	82	85	43	60	92
14	Tal El-Rojom	31.35	43.65	50	81	85	43	65	71
15	Ma'in/El-Mabkhara	25.9	61.5	42	73	78	41	61	89
16	Ma'in/El-Ameer	24.55	49.5	40	71	76	43	47	82
17	Ma'in/ElShallal	29.85	44.5	48	79	83	41	54	79
18	TA1	18.10	44.1	27	60	66	56	27	92
19	TA2	18.05	43.05	27	60	66	47	50	81
20	Iben Hammad	16.85	37.95	25	57	63	51	45	84
21	Burbyta	22.85	39.9	37	68	73	54	48	111
22	Afra/Sawna	20.95	45.35	33	65	70	68	32	104
23	Afra/Maqla	20.9	45.05	33	65	70	65	47	125

Depending on the before mentioned results it is possible to conclude the following notes:

- The Chalcedony geothermometer (Fournier 1977) is giving much lower reservoir temperatures than the ones that are estimated through the Quartz geothermometer and the temperatures that are estimated by the before mentioned authors. This means that this geothermometer is not suitable for these waters.

- The Quartz steam loss geothermometer (Fournier 1977) is giving reservoir temperatures, which are a little bit higher than the Quartz geothermometer, but even so it is in the range, which was agreed about by the before mentioned authors, it doesn't exceed the 110^{o}C (Truesdell 1979).

- In general Na-K-Ca geothermometers are giving high estimated reservoir temperatures, which range between (114 and 232) ^{o}C. Thus the Mg-correction is more suitable in this case because it lowers the estimated values to put it within the accepted range, but even so in many of the samples it is not giving a logical result (Table 4.8 and Appendix 17) which are very low and in some cases they are lower than that measured at the time of sampling.

- The K/Mg geothermometer of Giggenbach (1988) gives to some limits reliable results for the upper aquifer (B2/A7) samples (generally close to the Quartz geothermometer estimated temperatures). It is giving good results for TA1, Iben Hammad, Burbyta, Afra/Sawna and Afra/Maqla, and these results are almost the same as of the Quartz geothermometer, but for the rest of the lower sandstone aquifer samples it is not giving suitable results and in some cases it is lower than the measured temperatures on the surface.

- Concerning the Isotope SO_4-H_2O geothermometers, it is noticeable that the geothermometer after Lloyd (1968) is found to give a very high reservoir temperatures, which are above the ones that are determined through other geothermometers and above what was determined by the before mentioned authors. The Kusakabe (1974) geothermometer is always in the range and can be considered to be a suitable tool. The geothermometer according to Mizutani and Rafter (1969) gives high results for most of the samples.

4.5 Geochemical modeling

4.5.1 Percent error, ionic strength and electrical balance

The percent error was calculated by PhreeqC according to the equation: Percent error =100*(Cat-|An|)/(Cat+|An|). Table 4.9 shows the percent error for the chemical analysis of the first sampling campaign, second sampling campaign and the averaged samples. The error was found to be less than 5% for all of those samples. The accuracy of the analysis is good and can be used for further modeling.

The lowest ionic strength in the upper cretaceous (B2/A7) samples was found in Waqas well with a value of $9.84 \cdot 10^{-3}$ mol/l while the highest value was found in Abu-Zyad water with $2.71 \cdot 10^{-2}$ mol/l. The ionic strength of the Zarqa aquifer samples (8 and 9) was found to be ranging between $7.75 \cdot 10^{-2}$ and $1.17 \cdot 10^{-1}$ mol/l. The lowest ionic strength in the Kurnub samples was found in Burbyta waters with a $7.17 \cdot 10^{-3}$ mol/l while the highest was found in TA1 with $4.88 \cdot 10^{-2}$ mol/l (Table 4.9).

The electrical balance is ranging between $-1.06 \cdot 10^{-4}$ and $7.09 \cdot 10^{-5}$ for the upper Aquifer (B2/A7) samples. For the Zarqa aquifer samples it was found to be ranging between $1.05 \cdot 10^{-4}$ and $1.46 \cdot 10^{-3}$. For the Kurnub aquifer it was found to be ranging between $-1.58 \cdot 10^{-5}$ and $1.27 \cdot 10^{-4}$.

Table 4.9: The ionic strength, electrical conductivity and percent error of the 1st sampling campaign, the 2nd sampling campaign and the averaged samples (Avg).

No	Well/Spring	Electrical balance (Avg)	Ionic strength (Avg)	% Error (1st)	% Error (2nd)	% Error (Avg)
1	EL-Mokhybeh	$4.31 \cdot 10^{-5}$	$1.05 \cdot 10^{-2}$	0.29	0.50	0.07
2	El-Hmmeh/Maqla	$-1.06 \cdot 10^{-4}$	$1.82 \cdot 10^{-2}$	-0.4	-0.15	-0.42
3	El-Hammeh/Bajeh	$3.65 \cdot 10^{-5}$	$1.39 \cdot 10^{-2}$	0.19	-0.44	0.83
4	North Shuneh hot	$-4.50 \cdot 10^{-5}$	$1.42 \cdot 10^{-2}$	-0.22	-0.09	-0.35
5	Waqas well	$-1.87 \cdot 10^{-5}$	$9.84 \cdot 10^{-3}$	-0.14	-0.62	0.37
6	Abu-Zyad Well	$7.09 \cdot 10^{-5}$	$2.71 \cdot 10^{-2}$	0.18	0.12	0.22
7	Abu-Thableh	$-7.56 \cdot 10^{-5}$	$2.49 \cdot 10^{-2}$	-0.21	-0.06	-0.36
8	Abu El-Zeeghan/1	$1.05 \cdot 10^{-4}$	$7.75 \cdot 10^{-2}$	0.09	0.12	0.07
9	Abu El-Zeeghan/2	$1.46 \cdot 10^{-3}$	$1.17 \cdot 10^{-1}$	0.79	1.56	0.04
10	Al-Kafreen well	$1.94 \cdot 10^{-5}$	$1.15 \cdot 10^{-2}$	0.12	-0.06	0.32
11	Zara/Istraha	$-1.58 \cdot 10^{-4}$	$2.43 \cdot 10^{-2}$	-0.41	-0.39	-0.42
12	Zara/Maghara	$-4.62 \cdot 10^{-5}$	$2.72 \cdot 10^{-2}$	-0.11	-0.07	-0.14
13	El-Seel El-Hami	$-2.99 \cdot 10^{-5}$	$1.69 \cdot 10^{-2}$	-0.11	-0.03	-0.19
14	Tal El-Rojom	$1.80 \cdot 10^{-5}$	$1.87 \cdot 10^{-2}$	0.06	0.41	-0.3
15	Ma'in/El-Mabkhara	$7.73 \cdot 10^{-5}$	$3.54 \cdot 10^{-2}$	0.13	0.01	0.26
16	Ma'in/El-Ameer	$1.27 \cdot 10^{-4}$	$3.54 \cdot 10^{-2}$	0.22	0.12	0.31
17	Ma'in/ElShallal	$-8.95 \cdot 10^{-5}$	$3.51 \cdot 10^{-2}$	-0.15	-0.18	-0.12
18	TA1	$-3.93 \cdot 10^{-5}$	$4.88 \cdot 10^{-2}$	-0.05	-0.10	-0.01
19	TA2	$6.33 \cdot 10^{-5}$	$1.26 \cdot 10^{-2}$	0.33	-0.23	0.89
20	Iben Hammad	$-2.08 \cdot 10^{-5}$	$9.65 \cdot 10^{-3}$	-0.14	0.39	-0.69
21	Burbyta	$-4.47 \cdot 10^{-5}$	$7.17 \cdot 10^{-3}$	-0.43	0.29	-1.16
22	Afra/Sawna	$-3.44 \cdot 10^{-5}$	$7.71 \cdot 10^{-3}$	-0.32	-0.17	-0.46
23	Afra/Maqla	$-4.98 \cdot 10^{-5}$	$7.32 \cdot 10^{-3}$	-0.47	-0.85	-0.1

4.5.2 Distribution of species

The Wateq4f.dat database was used to determine the distribution of the major species of the four groups that resulted from the cluster analysis (A_{1a}, A_{1b}, A_2 and B) (section 4.3.1). The species distribution of the four groups are tabulated in Appendix (19). In general the species distribution is the same with in the four groups, but their molality differs according to the chemical composition of each group. The lower molality is found in group A_{1a} and the highest is in group B. Only species that have a minimum of 10^{-8} mol/l were interpreted.

The major species of carbon are: HCO_3^-, CO_2^0, $CaHCO_3^+$, $MgHCO_3^0$, $NaHCO_3^0$, CO_3^{2-}, $CaCO_3^0$, $MgCO_3^0$ and $NaCO_3^-$. The molality of HCO_3^- range between $2.955 \cdot 10^{-3}$ and $1.956 \cdot 10^{-2}$ mol/l to with a mean of $8.08 \cdot 10^{-3}$ mol/l. The CO_2 molality range between $1.01 \cdot 10^{-3}$ to $1.286 \cdot 10^{-2}$ mol/l with a mean of $4.056 \cdot 10^{-3}$ mol/l. $CaCO_3^0$ and $MgCO_3^0$ have a molaity mean of $6.257 \cdot 10^{-6}$ mol/l and $1.427 \cdot 10^{-6}$ mol/l respectively. The major species of Calcium are Ca^{2+}, $CaSO_4^0$, $CaHCO_3^+$ and $CaCO_3^0$. The Ca^{2+} molality mean is $4.813 \cdot 10^{-3}$ mol/l while the rest of the calcium species range between $1.06 \cdot 10^{-6}$ and $2.685 \cdot 10^{-3}$ mol/l. Cl^- is the only species for chloride where it ranges between $2.688 \cdot 10^{-3}$ and $4.002 \cdot 10^{-2}$ mol/l with a mean of $1.536 \cdot 10^{-2}$ mol/l. Potassium has a major species, which is K^+ that

range between $1.353 \cdot 10^{-4}$ and $3.58 \cdot 10^{-3}$ mol/l with a mean of $1.150 \cdot 10^{-3}$ mol/l. The minor species of potassium is KSO_4^-, which range between $3.101 \cdot 10^{-7}$ and $6.693 \cdot 10^{-5}$ mol/l with a mean of $1.785 \cdot 10^{-5}$ mol/l. Magnesium have four species: Mg^{2+}, $MgSO_4^0$, $MgHCO_3^+$ and $MgCO_3$. Mg^{2+} range between $6.882 \cdot 10^{-4}$ and $3.517 \cdot 10^{-3}$ mol/l while the rest of the species range between $3.386 \cdot 10^{-7}$ and $8.872 \cdot 10^{-4}$ mol/l. Sodium has one major species, which is Na^+ and three minor ones: $NaSO_4^-$, $NaHCO_3^0$ and $NaCO_3^-$. Na^+ range between $2.566 \cdot 10^{-3}$ to $3.709 \cdot 10^{-2}$ mol/l with a mean of $3.709 \cdot 10^{-2}$ mol/L. The rest of the sodium species range between $3.597 \cdot 10^{-8}$ and $5.015 \cdot 10^{-4}$ mol/l. Sulfur has five species: SO_4^{2-}, $CaSO_4^0$, $MgSO_4^0$, $NaSO_4^-$ and KSO_4^-. Their molaity range between $3.101 \cdot 10^{-7}$ and $7.184 \cdot 10^{-3}$ mol/l. Silicon has two species: $H_4SiO_4^0$ and $H_3SiO_4^-$. They range between $1.517 \cdot 10^{-7}$ and $4.289 \cdot 10^{-4}$ mol/l.

4.5.3 Saturation indices

Section 2.5.1 explains the theoretical background of the saturation index. Table 4.10 shows the calculated saturation indices of relevant minerals for the four groups: A_{1a}, A_{1b}, A_2 and B. Section 5.2 discuss the saturation indices in more details along hydrogeological cross sections.

With increasing of salinity (going from group A_{1a} to group B); the waters tend to become more saturated with respect to Calcite, Dolomite, and aragonite. The mineral phases Calcite and Dolomite represent the limestone-dolomitic origin in the aquifers. The water of the four groups (A_{1a}, A_{1b}, A_2 and B) were found to be over saturated with respect to Quartz and Chalcedony. The following phases were found to be under saturated: Anhydrite, Gypsum, and Halite.

4.5.4 Inverse modeling

Section 2.5.2 explains the theoretical background of the inverse modeling. The input files for each group (A_{1a}, A_{1b}, A_2 and B) are shown in Appendix (20). As a starting solution the low mineralized precipitation of (Jaradat et al.1999) was used. Only the pH and the major cations and anions (Na, K, Ca, Mg, SO_4 and HCO_3) were used in the modeling. The difference between the low mineralized precipitation in the recharge area and the higher mineralized thermal ground water analysis are supposed to be resulting from the reaction between the water and the minerals which have been selected in the inverse model according to the previous knowledge of the geology of the area and the aquifers. The object of this inverse modeling is to find a set of suitable minerals, which when react in a certain amount will account for the difference in composition between the starting solution (precipitation) and the final solution (thermal waters) (Table 4.11, Fig. 4.5). In the inverse modeling the minor elements, trace elements, reaction kinetics, oxidation or concentration through out evaporation were not taken into consideration.

Significant amount of Gypsum has to dissolve in group B ($1.13 \cdot 10^{-2}$) compared to the $4.47 \cdot 10^{-4}$ mol/l in group A_{1a}. It is also noticeable that the Calcite in group A_{1b} and A_2

Table 4.10: The saturation indices for the relevant minerals of the four groups:A_{1a}, A_{1b}, A_2 and B.

Phase	Saturation Index			
	A1a	**A1b**	**A2**	**B**
Anhydrite	-2.2	-1.9	-1.55	-0.5
Aragonite	-0.86	-0.35	-0.24	0.33
Artinite	-8.82	-7.7	-7.61	-8.16
Brucite	-6.61	-6.1	-6.03	-6.84
Calcite	-0.72	-0.21	-0.09	0.47
Chalcedony	0.07	0.12	0.19	0.04
Chrysotile	-8.48	-6.84	-6.49	-9.23
Clinoenstatite	-4.59	-4.03	-3.89	-4.86
CO2(g)	-1.53	-1.43	-1.49	-0.41
Cristobalite	0.11	0.16	0.22	0.07
Diopside	-6.15	-5.12	-4.75	-6.37
Dolomite	-1.56	-0.44	-0.3	0.52
Dolomite(d)	-2.11	-0.99	-0.85	-0.03
Epsomite	-4.68	-4.28	-4.02	-3.28
Forsterite	-11.33	-10.26	-10.04	-11.82
Gypsum	-1.98	-1.68	-1.33	-0.28
H2(g)	-21.51	-21.77	-21.79	-20.8
H2S(g)	-61.61	-62.77	-62.68	-57.15
Halite	-6.83	-6.8	-5.41	-4.63
Huntite	-7.58	-5.25	-5.06	-3.72
Hydromagnesite	-18.81	-15.87	-15.7	-15.48
Magadiite	-5.91	-5.43	-4.29	-5.42
Magnesite	-1.42	-0.81	-0.79	-0.53
Mirabilite	-7.64	-7.48	-5.95	-4.54
Nahcolite	-4.66	-4.43	-3.8	-2.8
Natron	-10.08	-9.71	-8.41	-7.49
Nesquehonite	-3.83	-3.22	-3.2	-2.94
O2(g)	-40.08	-39.56	-39.52	-41.5
Portlandite	-12.32	-11.91	-11.74	-12.25
Quartz	0.5	0.55	0.62	0.47
Sepiolite	-5.74	-4.57	-4.22	-6.3
Sepiolite(d)	-8.64	-7.47	-7.12	-9.2
Silicagel	-0.46	-0.41	-0.35	-0.5
SiO2(a)	-0.77	-0.72	-0.65	-0.8
Sulfur	-45.94	-46.84	-46.73	-42.19
Talc	-4.63	-2.9	-2.41	-5.45
Thenardite	-8.58	-8.42	-6.88	-5.46
Thermonatrite	-11.51	-11.15	-9.85	-8.92
Tremolite	-12.32	-8.53	-7.29	-13.58
Trona	-15.8	-15.2	-13.27	-11.35

should precipitate while it should dissolve for the A_{1a} and the B. More or less the other phases behave similar in most of the groups.

Table 4.11: Amounts of each phase in mol/l that have to be dissolved (+) or precipitated (-) in order to obtain the 4 groundwater types A_{1a}, A_{1b}, A_2 and B from low mineralized rain water (KX, NaX CaX2 = kation exchanger).

Phase		**A_{1a}**	**A_{1b}**	**A_2**	**B**
Calcite	$CaCO_3$	$2.41 \cdot 10^{-5}$	$-3.16 \cdot 10^{-4}$	$-1.42 \cdot 10^{-3}$	$1.35 \cdot 10^{-3}$
Gypsum	$CaSO_4.2H_2O$	$4.47 \cdot 10^{-4}$	$7.92 \cdot 10^{-4}$	$1.69 \cdot 10^{-3}$	$1.13 \cdot 10^{-2}$
CO2(g)	CO_2	$2.41 \cdot 10^{-3}$	$3.72 \cdot 10^{-3}$	$3.48E \cdot 10^{-3}$	$2.34 \cdot 10^{-2}$
Dolomite	$CaMg(CO_3)_2$	$7.01 \cdot 10^{-4}$	$1.41 \cdot 10^{-3}$	$1.92 \cdot 10^{-3}$	$4.68 \cdot 10^{-3}$
Quartz	SiO_2	$3.32 \cdot 10^{-4}$	$3.71 \cdot 10^{-4}$	$4.30 \cdot 10^{-4}$	$2.98 \cdot 10^{-4}$
Halite	NaCl	$2.55 \cdot 10^{-3}$	$2.72 \cdot 10^{-3}$	$1.58 \cdot 10^{-2}$	$4.01 \cdot 10^{-2}$
KX	KX	$1.16 \cdot 10^{-4}$	$1.30 \cdot 10^{-4}$	$7.13 \cdot 10^{-4}$	$3.64 \cdot 10^{-3}$
NaX	NaX	$-1.17 \cdot 10^{-4}$	$-1.93 \cdot 10^{-4}$	$-2.99 \cdot 10^{-3}$	$-2.58 \cdot 10^{-3}$
CaX_2	CaX_2	$5.61 \cdot 10^{-7}$	$3.11 \cdot 10^{-5}$	$1.14 \cdot 10^{-3}$	$-5.26 \cdot 10^{-4}$

4.5.5 Pressure-saturation index relation

In order to study the effect of pressure on the species and the mineral solubility; SolminEQ88 (Kharaka et al. 1988) have been run to model five scenarios for each group. The scenarios were: at the surface conditions (atmospheric pressure), at 500 m depth (50 bar), at 1000 m depth (100 bar), at 1500 m (150 bar) and at 2000 m depth (200 bar). Tables 4.11 and 4.12 show the calculated saturation indices of relevant minerals for the four groups (A_{1a}, A_{1b}, A_2 and B) in the five suggested depths. The Chalcedony, Cristobalite and Quartz are having positive saturation indices. Those saturation indices decrease with depth increase. The rest of the phases are having negative saturation indices. Their saturation indices are increasing with the increase in depth and pressure (more negative values at higher pressures).

However, the question is, if the differences are significant and meaningful. In case of clear undersaturated or clear oversaturated are propably less important. On the contrary they are more meaningful close to equilibrium. For examples, in the case of Group $A_{1a,}$ the Chalcedony saturation index that is around +0.088 at the surface and +0.046 at 2000 m depth. In case of Group A_2, the Christobalite Alpha saturation index is changing from +0.01 (oversaturated) at the surface to –0.041 (undersaturated) at 2000 m depth.

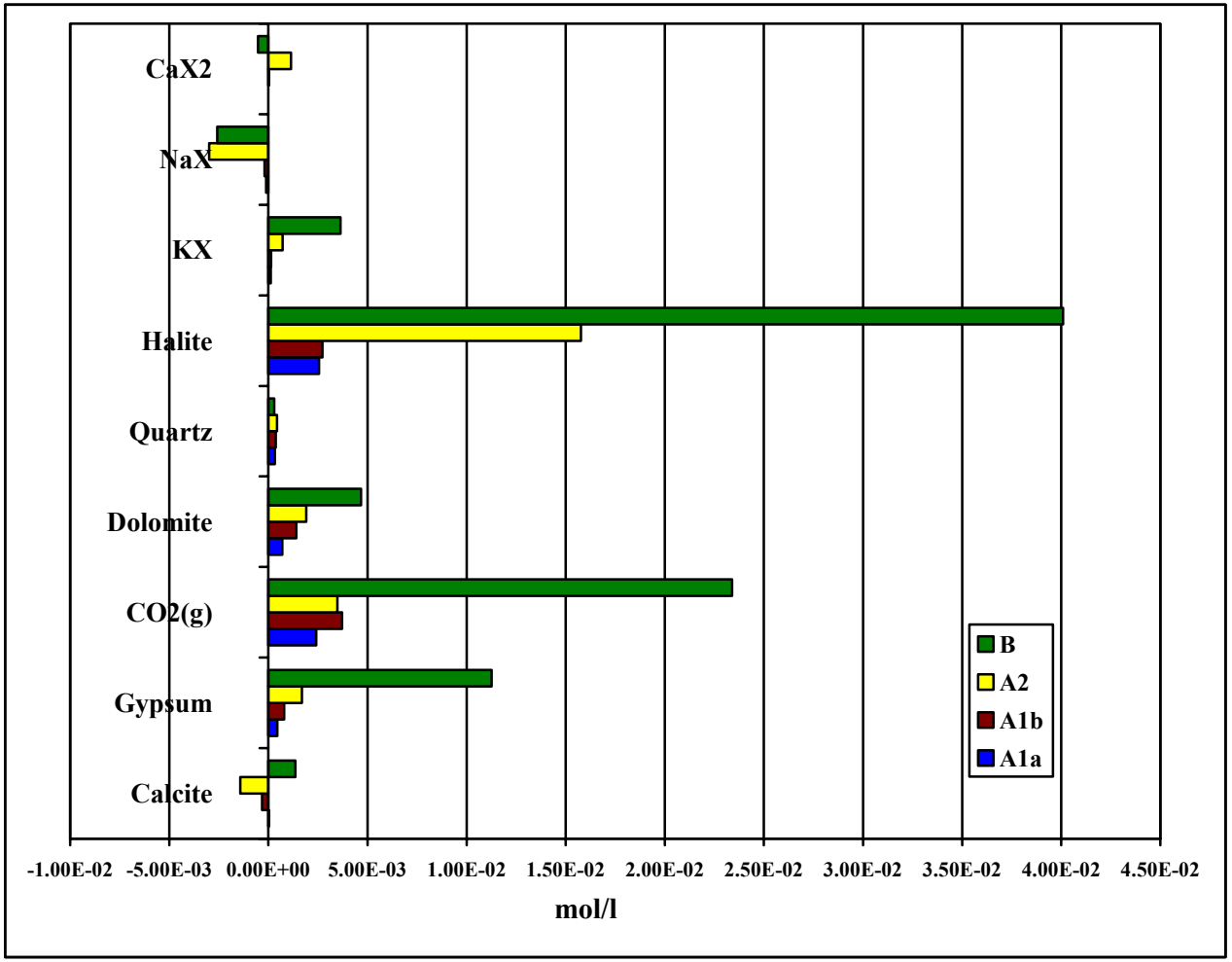

Fig. 4.5: Graphical presentation of the inverse modeling results (x-axis: amounts of each mineral in mol/L that have to be dissolved (+) or precipitated (-) in order to obtain the 4 groundwater samples (A_{1a}, A_{1b}, A_2 and B) from a low mineralized rain water; KX, NaX and CaX_2 are cation exchangers.

Table 4.12: The saturation indices for the relevant minerals of the groups: A_{1a} and A_{2a} at the surface, 500 m, 1000 m, 1500 m, and 2000 m.

	A1a					A1b				
	Surface	**500 m**	**1000 m**	**1500 m**	**2000 m**	**Surface**	**500 m**	**1000 m**	**1500 m**	**2000 m**
Phase										
AKERMANI	-18.403	-18.435	-18.468	-18.502	-18.536	-18.288	-18.318	-18.348	-18.378	-18.409
ANHYDRIT	-2.058	-2.099	-2.14	-2.18	-2.221	-1.768	-1.808	-1.849	-1.889	-1.929
BRUCITE	-5.258	-5.276	-5.295	-5.315	-5.335	-5.197	-5.214	-5.232	-5.25	-5.269
CHALCEDO	0.088	0.078	0.067	0.056	0.046	0.139	0.128	0.117	0.107	0.096
CRYSOTIL	-6.048	-6.112	-6.177	-6.242	-6.307	-5.76	-5.821	-5.882	-5.944	-6.007
C-ENSTAT	-3.671	-3.696	-3.722	-3.748	-3.774	-3.559	-3.584	-3.608	-3.633	-3.658
CRISTOBA	-0.039	-0.052	-0.065	-0.078	-0.09	0.011	-0.002	-0.015	-0.027	-0.04
CRISTOBB	-0.581	-0.596	-0.61	-0.624	-0.639	-0.532	-0.546	-0.56	-0.575	-0.589
DIOPSIDE	-4.516	-4.572	-4.629	-4.685	-4.742	-4.375	-4.429	-4.483	-4.538	-4.593
ENSTATIT	-3.845	-3.87	-3.896	-3.922	-3.948	-3.733	-3.758	-3.783	-3.808	-3.833
FORSTERI	-10.049	-10.093	-10.137	-10.182	-10.226	-9.877	-9.919	-9.961	-10.004	-10.046
GYPSUM	-1.901	-1.932	-1.964	-1.996	-2.028	-1.609	-1.641	-1.672	-1.704	-1.735
HALITE	-6.918	-6.929	-6.94	-6.951	-6.962	-6.833	-6.844	-6.855	-6.866	-6.876
HYPHILIT	-19.366	-19.396	-19.426	-19.456	-19.486	-19.124	-19.154	-19.184	-19.214	-19.243
KENYAITE	-8.344	-8.348	-8.351	-8.355	-8.358	-7.855	-7.858	-7.861	-7.864	-7.867
LARNITE	-19.235	-19.28	-19.326	-19.372	-19.418	-19.233	-19.277	-19.321	-19.365	-19.409
LIME	-47.439	-47.443	-47.447	-47.451	-47.455	-47.16	-47.165	-47.17	-47.175	-47.18
MAGADITE	-5.39	-5.394	-5.398	-5.401	-5.405	-5.096	-5.099	-5.102	-5.105	-5.109
$MgCl_2$	-29.289	-29.313	-29.338	-29.362	-29.386	-28.968	-28.992	-29.016	-29.04	-29.064
MERWINIT	-29.389	-29.484	-29.579	-29.674	-29.77	-29.3	-29.39	-29.482	-29.573	-29.665
MIRABILT	-8.458	-8.46	-8.461	-8.463	-8.464	-8.239	-8.24	-8.241	-8.242	-8.243
MONTICEL	-11.026	-11.074	-11.122	-11.17	-11.218	-10.938	-10.984	-11.03	-11.076	-11.122
PERICLAS	-9.908	-9.937	-9.967	-9.997	-10.026	-9.85	-9.878	-9.906	-9.935	-9.963
PORTLAN	-10.921	-10.944	-10.967	-10.991	-11.015	-10.946	-10.967	-10.99	-11.013	-11.036
POTASSI	-74.621	-74.759	-74.896	-75.034	-75.173	-74.689	-74.826	-74.963	-75.1	-75.237
QUARTZ	0.33	0.319	0.309	0.298	0.287	0.38	0.37	0.359	0.348	0.338
SEPIOLIT	-9.125	-9.168	-9.212	-9.256	-9.301	-8.572	-8.611	-8.651	-8.691	-8.731
SILICAAM	-0.822	-0.833	-0.845	-0.856	-0.868	-0.772	-0.784	-0.795	-0.807	-0.818
SILICGEL	-0.821	-0.821	-0.821	-0.821	-0.821	-0.771	-0.771	-0.771	-0.771	-0.771
Na_2O	-56.075	-56.091	-56.108	-56.124	-56.14	-56.191	-56.207	-56.222	-56.237	-56.253
SYLVITE	-7.637	-7.711	-7.785	-7.859	-7.933	-7.524	-7.598	-7.672	-7.746	-7.82
TALC	-2.527	-2.615	-2.703	-2.792	-2.882	-2.137	-2.222	-2.308	-2.393	-2.48
THENARDI	-8.504	-8.533	-8.563	-8.592	-8.622	-8.289	-8.319	-8.348	-8.377	-8.407
TREMOLIT	-12.033	-12.244	-12.457	-12.67	-12.885	-11.361	-11.566	-11.771	-11.977	-12.184
WOLLASTO	-5.415	-5.445	-5.476	-5.507	-5.537	-5.382	-5.411	-5.441	-5.471	-5.5

Table 4.13: The saturation indices for the relevant minerals of the groups: A_2 and B at the surface, 500 m, 1000 m, 1500 m, and 2000 m.

	A2					B				
	Surface	**500 m**	**1000 m**	**1500 m**	**2000 m**	**Surface**	**500 m**	**1000 m**	**1500 m**	**2000 m**
Phase										
AKERMANI	-17.363	-17.395	-17.427	-17.46	-17.492	-19.34	-19.367	-19.395	-19.422	-19.449
ANHYDRIT	-1.391	-1.431	-1.47	-1.509	-1.549	-0.445	-0.484	-0.523	-0.563	-0.602
BRUCITE	-4.955	-4.972	-4.99	-5.009	-5.028	-5.772	-5.788	-5.805	-5.822	-5.84
CHALCEDO	0.125	0.114	0.104	0.093	0.082	0.102	0.092	0.081	0.07	0.059
CRYSOTIL	-5.218	-5.28	-5.342	-5.405	-5.468	-7.453	-7.51	-7.568	-7.626	-7.684
C-ENSTAT	-3.324	-3.349	-3.374	-3.399	-3.424	-4.174	-4.197	-4.221	-4.244	-4.268
CRISTOBA	0.01	-0.003	-0.016	-0.029	-0.041	-0.036	-0.049	-0.062	-0.075	-0.088
CRISTOBB	-0.511	-0.525	-0.54	-0.554	-0.568	-0.592	-0.607	-0.621	-0.636	-0.65
DIOPSIDE	-3.938	-3.993	-4.048	-4.103	-4.159	-5.137	-5.189	-5.242	-5.295	-5.347
ENSTATIT	-3.495	-3.52	-3.545	-3.57	-3.596	-4.349	-4.373	-4.396	-4.42	-4.443
FORSTERI	-9.346	-9.388	-9.431	-9.474	-9.517	-11.101	-11.141	-11.18	-11.22	-11.26
GYPSUM	-1.279	-1.309	-1.34	-1.371	-1.401	-0.258	-0.288	-0.319	-0.349	-0.379
HALITE	-5.458	-5.469	-5.479	-5.49	-5.5	-4.677	-4.687	-4.697	-4.708	-4.718
HYPHILIT	-17.279	-17.309	-17.338	-17.368	-17.398	-16.487	-16.517	-16.546	-16.576	-16.605
KENYAITE	-6.585	-6.588	-6.591	-6.594	-6.598	-8.055	-8.058	-8.06	-8.063	-8.065
LARNITE	-18.474	-18.518	-18.563	-18.608	-18.653	-19.716	-19.759	-19.803	-19.846	-19.889
LIME	-46.288	-46.293	-46.297	-46.302	-46.306	-46.273	-46.278	-46.284	-46.29	-46.295
MAGADITE	-4.075	-4.078	-4.081	-4.085	-4.088	-4.946	-4.949	-4.951	-4.954	-4.956
$MgCl_2$	-26.988	-27.012	-27.036	-27.06	-27.084	-26.864	-26.887	-26.91	-26.933	-26.956
MERWINIT	-27.961	-28.053	-28.145	-28.238	-28.331	-30.593	-30.682	-30.77	-30.859	-30.947
MIRABILT	-7	-7	-7.001	-7.001	-7.002	-5.224	-5.223	-5.222	-5.221	-5.22
MONTICEL	-10.358	-10.404	-10.451	-10.498	-10.545	-11.747	-11.791	-11.836	-11.88	-11.924
PERICLAS	-9.486	-9.514	-9.542	-9.571	-9.6	-10.503	-10.531	-10.558	-10.585	-10.612
PORTLAN	-10.562	-10.584	-10.607	-10.63	-10.654	-11.168	-11.19	-11.212	-11.234	-11.257
POTASSI	-72.205	-72.337	-72.469	-72.602	-72.734	-73.545	-73.684	-73.824	-73.963	-74.103
QUARTZ	0.373	0.362	0.352	0.341	0.33	0.338	0.327	0.316	0.305	0.295
SEPIOLIT	-7.955	-7.994	-8.035	-8.075	-8.116	-10.924	-10.959	-10.993	-11.028	-11.062
SILICAAM	-0.752	-0.763	-0.774	-0.786	-0.797	-0.833	-0.844	-0.856	-0.867	-0.879
SILICGEL	-0.751	-0.751	-0.751	-0.751	-0.751	-0.83	-0.83	-0.83	-0.83	-0.83
Na_2O	-53.953	-53.968	-53.983	-53.999	-54.014	-55.361	-55.375	-55.389	-55.403	-55.418
SYLVITE	-6.186	-6.257	-6.328	-6.4	-6.471	-5.106	-5.181	-5.257	-5.332	-5.408
TALC	-1.654	-1.739	-1.825	-1.912	-1.998	-3.882	-3.964	-4.045	-4.127	-4.209
THENARDI	-6.782	-6.81	-6.838	-6.867	-6.895	-5.439	-5.466	-5.493	-5.521	-5.548
TREMOLIT	-9.995	-10.201	-10.408	-10.616	-10.824	-14.635	-14.834	-15.032	-15.23	-15.428
WOLLASTO	-5.348	-5.378	-5.408	-5.438	-5.468	-5.423	-5.453	-5.482	-5.511	-5.54

5 DISCUSSION

In this chapter, the hydrochemical characteristics, $\delta^{34}S_{Sulfate}$ and $\delta^{18}O_{Sulfate}$, $\delta^{13}C_{CO2}$, tritium isotopes, Helium and Neon isotopes and the stable water isotopes ($\delta^{18}O$, δD) are being used to shed light on the deep rock water interaction, the water circulation, the sources of the constituent, the residence time, and the thermal waters source along the Dead Sea Transform (DST).

5.1 The chemical characteristics (Hydrochemistry) of the waters

This part of the study provides a geochemical and hydrochemical characteristics, genesis, types of the thermal waters, and the suitability of those waters for both domestic and agricultural purposes. This chapter discusses the possible heat source for the waters and direct thermal water uses in the past, present, and the future.

5.1.1 Water classification using Piper diagram

Fig. 5.1 shows all analyzed samples in both of the sampling campaigns. The waters that tap the upper aquifer (B2/A7) (black circles) are mainly located in two major zones, which are (d) and (e) which means that they are initial earth alkaline water with increased portions of alkalis and according to Langguth (1966) this water type is divided into two zones which are:

1. d: with prevailing Bicarbonates;
2. e: with prevailing Sulfate and Chloride.

Fig. 5.2.A shows the upper aquifer (B2/A7) waters from the 1st sampling campaign. Fig. 5.2.B shows the upper aquifer (B2/A7) waters from the 2nd sampling campaign. Table 5.1 shows the classification of the upper aquifer (B2/A7) waters in both sampling campaigns.

From Fig. 5.2.A, Fig. 5.2.B and Table 5.1, it is noticeable that the chemistry of the El-Hammeh/Bajeh and North Shuneh hot well have changed from zone (d) to zone (e) which is caused by a slight increase of Mg, Cl and SO_4 and the decrease of Ca and HCO_3. The Waqas water have shifted from zone (d) to zone (a) to become normal earth alkaline water with prevailing bicarbonate which is caused mainly by the slight decrease of Na, K, and Cl. The rest of the samples showed the same water type in both the 1st and the 2nd sampling campaigns.

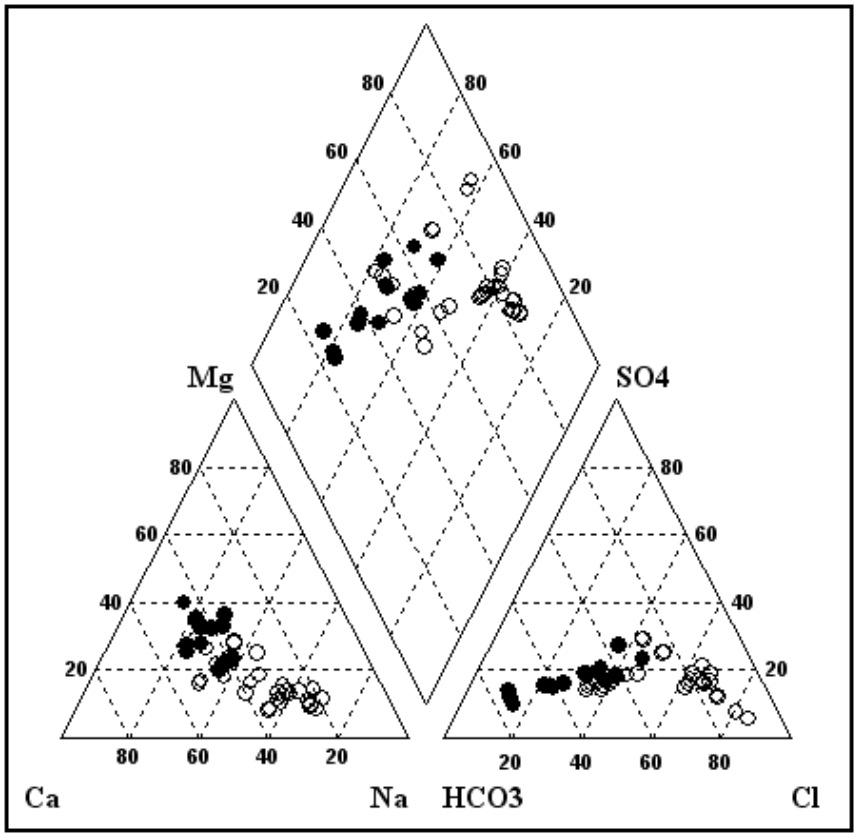

Fig. 5.1: Piper diagram showing the composition of the thermal waters in the two sampling campaigns, the black circles present the upper aquifer (B2/A7) thermal waters while the white circles present the lower sandstone aquifer thermal waters.

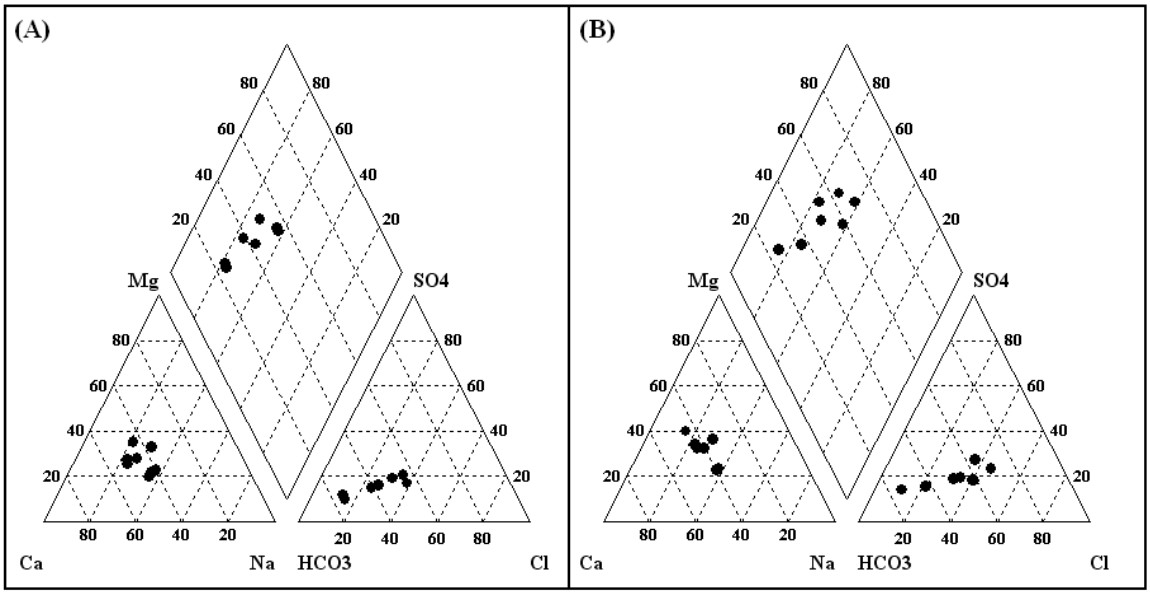

Fig. 5.2: Piper diagram illustrating the results of the upper aquifer (B2/A7) thermal waters. (A) present the results of the first sampling campaign while (B) present the results of the second sampling campaign.

Table 5.1: The upper aquifer (B2/A7) water types in the first and the second sampling campaigns (for symbols explanation see Table 2.3).

Sample No	Well/Spring	Water Type (1st)	Water Type (2nd)
1	EL-Mokhybeh	d	d
2	El-Hmmeh/Maqla	e	e
3	El-Hammeh/Bajeh	d	e
4	North Shuneh hot well	d	e
5	Waqas well	d	a
6	Abu-Zyad Well	e	e
7	Abu-Thableh	e	e
10	Al-Kafreen well	e-d	e-d

Fig. 5.1 shows that lower sandstone aquifer waters (white circles) are located mainly in two major zones and they are (g) and (e) and according to Langguth (1966) they are:

1. e: Earth alkaline water with increased alkalis and prevailing sulfate and chloride.
2. g: Alkaline water with prevailing sulfate-chloride.

Fig. 5.3.A shows the lower sandstone aquifer waters from the 1st sampling campaign. Fig. 5.3.B shows lower sandstone aquifer waters from the 2nd sampling campaign. Table 5.2 shows the classification of the lower sandstone aquifer waters in both of the sampling campaigns. The slight differences between the two sampling campaigns of the deep sandstone thermal waters did not affect the waters type classification.

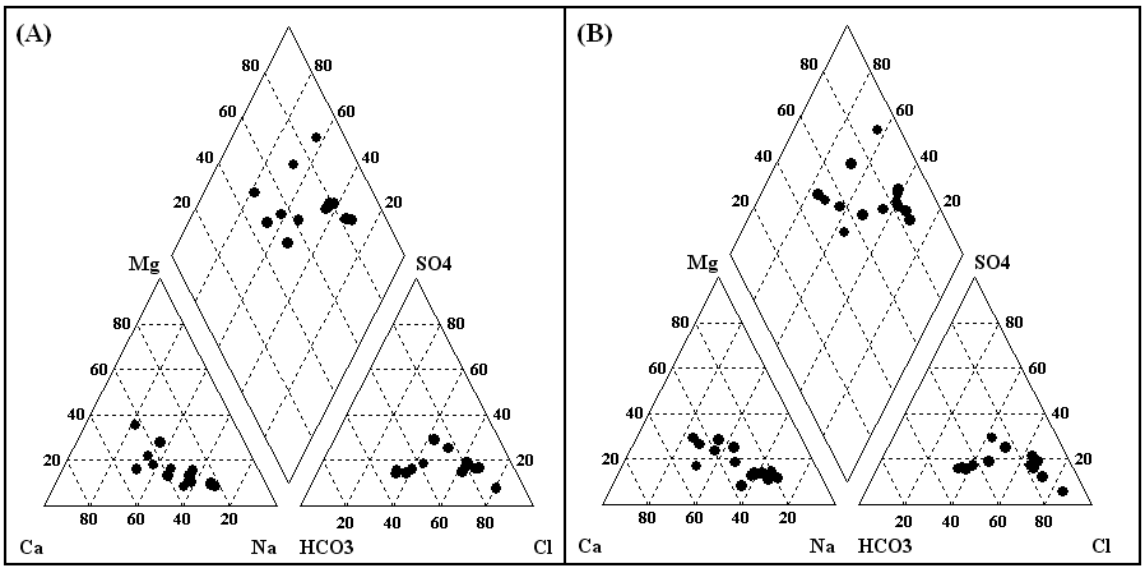

Fig. 5.3: Piper diagram illustrating the results of the lower sandstone aquifer thermal waters. (A) present the results of the first sampling campaign while (B) present the results of the second sampling campaign.

Table 5.2: The lower sandstone aquifer water types in the first and the second sampling campaigns (for symbols explanation see Table 2.3).

Sample No.	Well/Spring	Water type (1^{st})	Water type (2^{nd})
8	Abu El-Zeeghan/1	e	e
9	Abu El-Zeeghan/2	g	g
11	Zara/Istraha	g	g
12	Zara/Maghara	g	g
13	El-Seel El-Hami	g	g
14	Tal El-Rojom	g	g
15	Ma'in/El-Mabkhara	g	g
16	Ma'in/El-Ameer	g	g
17	Ma'in/ElShallal	g	g
18	TA1	e	e
19	TA2	e	e
20	Iben Hammad	e	e
21	Burbyta	e	e
22	Afra/Sawna	e	e
23	Afra/Maqla	e	e

As a result, the thermal waters could be categorized in three groups according to the Langguth (1966) classification:

1. Type I: They are located in zone (d) and they are from the upper aquifer (B2/A7);
2. Type II: They are located in zone (e) and they are they are from both the upper (B2/A7) aquifer and the lower sandstone aquifer;
3. Type III: They are located in zone (g) and they are from the lower sandstone aquifer.

Those groups were checked statistically by means of Kruskal-Wallis test. It has been found that the mean of each group is significantly different at 5% criteria for EC, TDS, Na, K, Cl, SO_4, and SiO_2 but not for T, Ca, Mg and HCO_3 (Table 5.3).

Table 5.3: Kruskal-Wallis results for thermal waters which are classified according to Langguth (1966) on the Piper diagram.

Parameter	**T**	**EC**	**TDS**	**pH**	**Ca**	**Mg**
Asymp.Sig.	0.294	0.025	0.025	0.655	0.158	0.949
Parameter	**Na**	**K**	**Cl**	**SO_4**	**HCO_3**	**SiO_2**
Asymp.Sig.	0.002	0.005	0.004	0.010	0.365	0.036

5.1.2 Water classification using Durov diagram

The data are being presented using Durov diagram, which illustrates some geochemical processes, which might affect the water genesis (Lloyd and Heathcoat 1985).

Samples from both sampling campaigns were plotted on the Durov diagram (Fig. 5.4), the upper aquifer (B2/A7) waters with black circles and the lower sandstone aquifer with white circles.

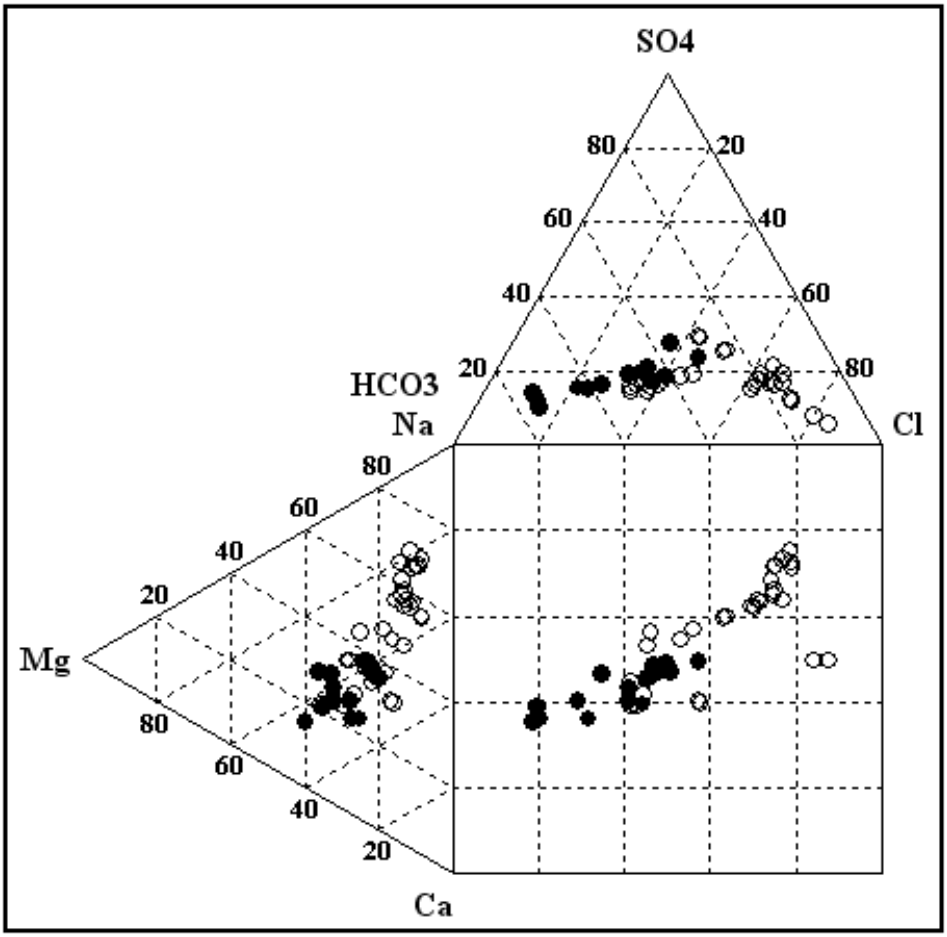

Fig. 5.4: Durov diagram showing the results of the thermal waters in the two sampling campaigns, the black circles present the thermal waters of the upper aquifer (B2/A7) while the white circles present the thermal waters of the lower sandstone aquifer.

Fig. 5.5.A shows the upper aquifer (B2/A7) waters from the 1st sampling campaign. Fig. 5.5.B shows the upper aquifer (B2/A7) waters from the 2nd sampling campaign. Table 5.4 shows the classification of the upper aquifer (B2/A7) from both the 1st and the 2nd sampling campaign.

The samples in the upper aquifer (B2/A7) are mainly located in two zones and they are (2) and (5) and according to (Lloyd and Heathcoat 1985):

1. Zone (2): waters are dominated by Ca and HCO_3 ions with presumed association to dolomite if the Mg is significant, However, an important exchange is presumed if the Na is significant in the sample.
2. Zone (5): water with no dominate anion or cation, which indicates water exhibiting simple dissolution or mixing.

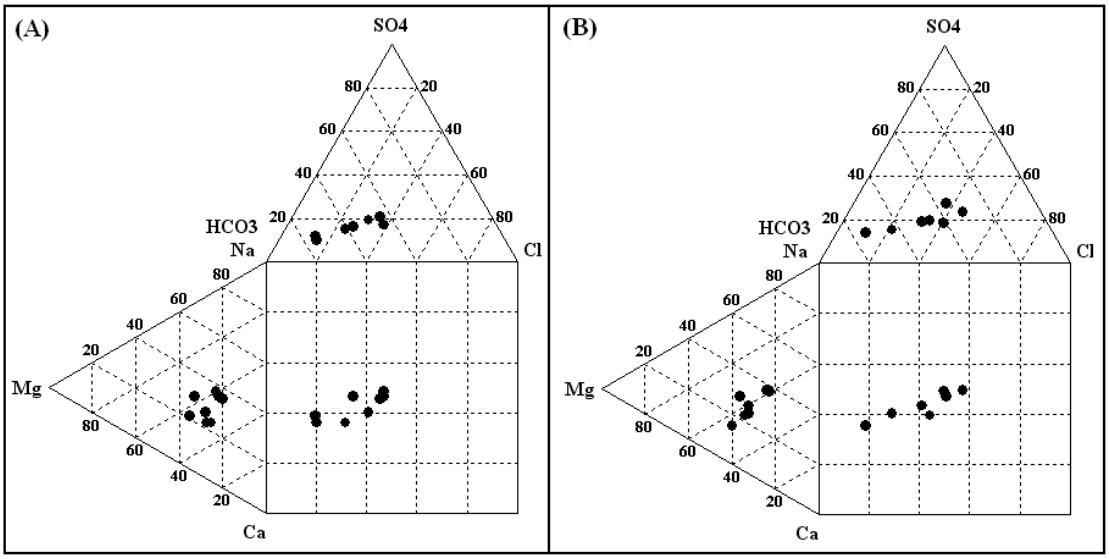

Fig. 5.5: Durov diagram illustrating the pattern of the thermal waters from the upper aquifer (B2/A7). (A) present the results of the first sampling campaign while (B) present the results of the second sampling campaign.

Table 5.4: The upper aquifer (B2/A7) water types in the first and second sampling campaigns (for symbols explanation see Table 2.4).

Sample No.	Well/Spring	Water type (1^{st})	Water type (2^{nd})
1	EL-Mokhybeh	2	2
2	El-Hmmeh/Maqla	5	5
3	El-Hammeh/Bajeh	5	5
4	North Shuneh hot well	5	5
5	Waqas well	2	2
6	Abu-Zyad Well	5	5
7	Abu-Thableh	5	5
10	Al-Kafreen well	5	5

From Fig. 5.5.A, Fig.5.5.B, and Table 5.4, it is clear that the seasonal variation have no affect on the sample location on the Durov diagram, where the samples are located in the same zones in both of the sampling campaigns.

Fig. 5.6.A shows the lower sandstone aquifer waters from the 1^{st} sampling campaign. Fig. 5.6.B shows the lower sandstone aquifer waters from the 2^{nd} sampling campaign. Table 5.5 shows the deep sandstone water classification in both sampling campaigns.

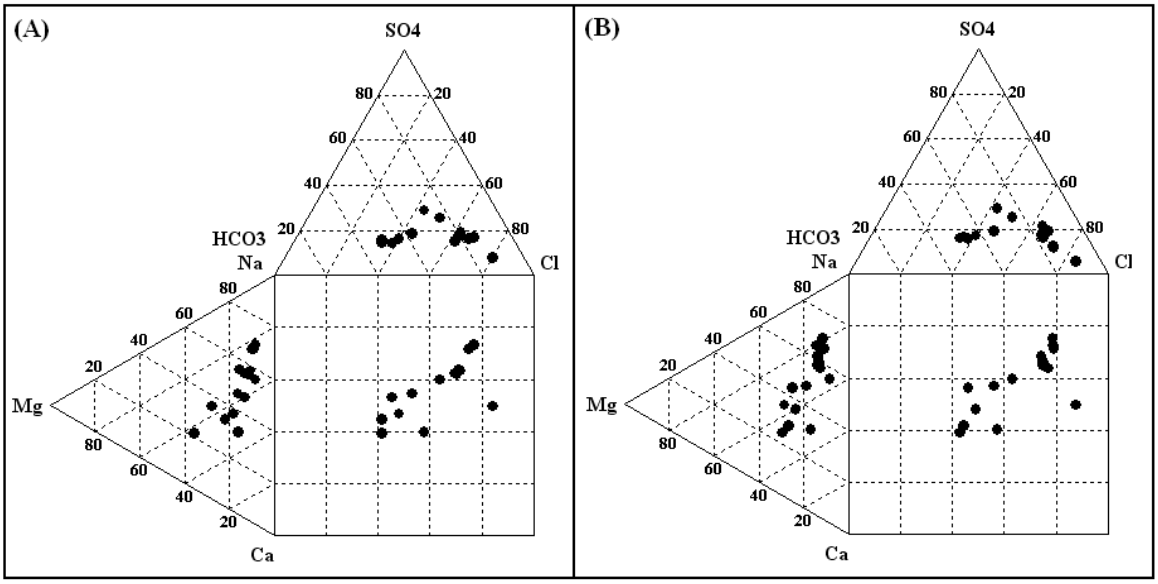

Fig. 5.6: Durov diagram illustrating the pattern of the thermal waters from the lower sandstone aquifer. (A) present the results of the first sampling campaign. (B) present the results of the second sampling campaign.

Table 5.5: The lower sandstone aquifer water types in the first and second sampling campaigns (for symbols explanation see Table 2.4).

Sample No.	Well/Spring	Water Type (1^{st})	Water Type (2^{nd})
8	Abu El-Zeeghan/1	5	5
9	Abu El-Zeeghan/2	5	5
11	Zara/Istraha	8	8
12	Zara/Maghara	8	8
13	El-Seel El-Hami	8	8
14	Tal El-Rojom	8	8
15	Ma'in/El-Mabkhara	8	8
16	Ma'in/El-Ameer	8	8
17	Ma'in/ElShallal	8	8
18	TA1	8	8
19	TA2	5	5
20	Iben Hammad	5	5
21	Burbyta	5	5
22	Afra/Sawna	5	5
23	Afra/Maqla	5	5

The samples in the lower sandstone aquifer are mainly located in two zones and they are (5) and (8) and according to Lloyd and Heathcoat (1985):

1. Zone (5): are water with no dominate anion or cation, which indicates water exhibiting simple dissolution or mixing.

2. Zone (8) are water where Cl is a dominant anion and Na dominant cation which indicates that the ground waters can be related to reverse ion exchange of Na-Cl waters.

From Fig. 5.6.A, Fig. 5.6.B, and Table 5.5, it is clear that the seasonal variation have no effect on the sample locations on the Durov diagram, where the samples are located in the same zones in both of the sampling groups.

As a result the thermal waters could be categorized in three groups according to the Lloyd and Heathcoat (1985) classification:

1. Type I: They are located in Zone (2), which includes almost the non-mixed upper aquifer (B2/A7) samples;
2. Type II: They are located in Zone (5), which includes mixed upper aquifer (B2/A7) waters and the lower sandstone aquifer (Zarqa) samples;
3. Type III: They are located in Zone (8), which includes non-mixed lower sandstone aquifer samples (explained in section 5.10.4).

The only anomaly, which is occurring in the TA2 well, is found in the second group instead of being in the third one. Those groups were checked statistically by means of Kruskal-Wallis test. It was found that the mean of each group is significantly different at 5% criteria for the EC, TDS, Na, K, Cl, and SiO_2 but not for T, pH, Ca, Mg, SO_4 and HCO_3 (Table 5.6).

Table 5.6: Kruskal-Wallis results for thermal waters which are classified according to Lloyd and Heathcoat (1985) on the Durov diagram.

Parameter	**T**	**EC**	**TDS**	**pH**	**Ca**	**Mg**
Asymp.Sig.	0.113	0.030	0.030	0.140	0.188	0.768
Parameter	**Na**	**K**	**Cl**	**SO_4**	**HCO_3**	**SiO_2**
Asymp.Sig.	0.005	0.011	0.004	0.051	0.206	0.018

5.1.3 Mixing model

El-Naser (1991) has proposed that the thermal waters in the Jordan valley is a result of a mixing between two end members, which are the pure B2/A7 waters end member and the Kurnub end member which loses some of its waters through upward leakage throughout the deep seated faults. Mixing is further supported in this study through the presentation of the samples on the Piper and Durov diagrams. It is very clear that the upper aquifer (B2/A7) samples are located between the two end members-proposed by El-Naser 1991- on the Piper diagram (Fig. 5.7), also most of the upper aquifer (B2/A7) waters are located in zone (5) on the Durov diagram (Fig. 5.8) which indicates the presence of mixing.

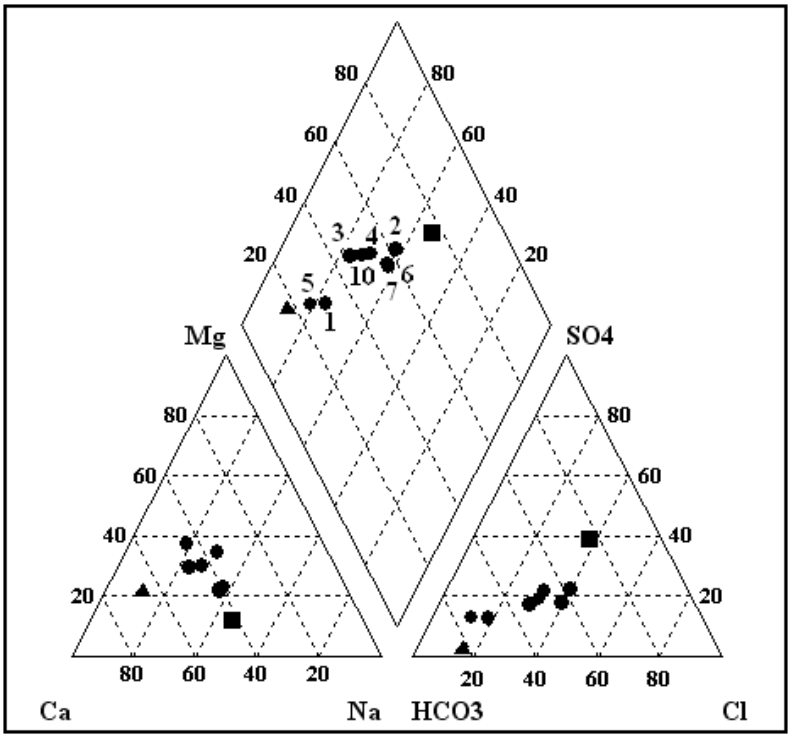

Fig. 5.7: Plot illustrating the location of the thermal waters of the upper aquifer (B2/A7) and the two end members: the pure B2/A7 (black triangle) and the Kurnub waters (black square) on the Piper diagram.

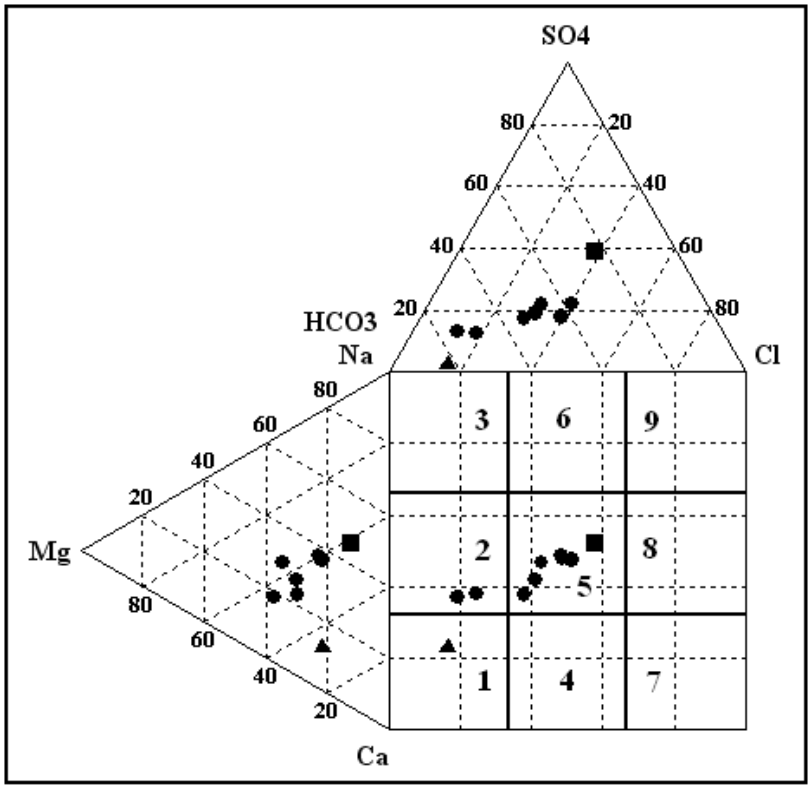

Fig. 5.8: Plot illustrating the location of the thermal waters of the upper aquifer (B2/A7) and the two end members: the pure B2/A7 (black triangle) and the Kurnub waters (black square) on the Durov diagram.

In order to determine the mixing ratio of each end member in the thermal waters a mixing model was run. Mixing of two samples was performed in order to determine the optimal mixing ratio of the two selected samples that most closely matches a third target sample. The two initial samples are being mixed in 2% increment until the Euclidean distance between the calculated mixture and specified resulting sample is minimized. The data is being taken from El-Naser (1991) where the Al-Hamam spring analysis are being used to represent the Kurnub aquifer pure water (Appendix 21) while for the pure upper aquifer (B2/A7) El-Naser (1991) proposed that the average chemical analysis of Rasun spring, Ain Diek, El-Qantarah, Ain Jarash, El Magahsil, Nu'aymeh Mun #1, Yarmouk Uni.#1, Aurjan Foga, Et Teis represents the pure B2/A7 waters (Appendix 22).

The average chemical analysis of the two sampling campaigns was being used for the optimised sample in the mixing model. Table 5.7 shows the ratio of both of the pure B2/A7 water and the Kurnub waters in each of the upper aquifer (B2/A7) thermal waters.

Table 5.7 shows that the most affected thermal waters with the contribution of the Kurnub aquifer through upward leakage is Abu-Zyad well with 38%, then 34% in Abu-Thableh, 26% in El-Hammeh/Maqla, 16% in North shuneh hot well, 12% in El-Hammeh/Bajeh, 10% in Alkafreen well. The least share was found in El-Mokhybh with 6% and Waqas well with 4% that are located in zone (2) in Durov diagram.

Table 5.7: The contribution share of the Kurnub and the pure B2/A7 end members in the upper aquifer (B2/A7) thermal waters.

Sample No.	Well/Spring	Kurnub %	B2/A7 %
1	EL-Mokhybeh	6	94
2	El-Hmmeh/Maqla	26	74
3	El-Hammeh/Bajeh	12	88
4	North Shuneh hot well	16	84
5	Waqas well	4	96
6	Abu-Zyad Well	38	62
7	Abu-Thableh	34	66
10	Al-Kafreen well	10	90

5.2 The Hydrochemical characteristics along cross sections

This section discusses the thermal waters characteristics of the two aquifers along geographical cross sections from the north to the south. The upper aquifer (B2/A7) thermal water characteristics are first discussed, then followed by the lower sandstone aquifer water characteristics, which includes the Zarqa and the Kurnub thermal waters.

5.2.1 The upper aquifer (B2/A7) hydrochemical cross sections

The thermal waters that tap the upper aquifer (B2/A7) are restricted to the Jordan valley.

5.2.1.1 Salinity

The salinity that is expressed by means of EC units is ranging from 725 µs/cm in Waqas well to 2185 µs/cm in Abu-Zyad well with a general increase in the salinity from north to south. This phenomenon was explained by Salameh (2001) as a result of increasing of the contribution from the lower aquifer, and was further checked by comparing the salinity with the calculated percent of the Kurnub aquifer waters (Fig.5.9). It was found that the percent Kurnub water contribution is direct proportional to the salinity of the upper aquifer (B2/A7) waters.

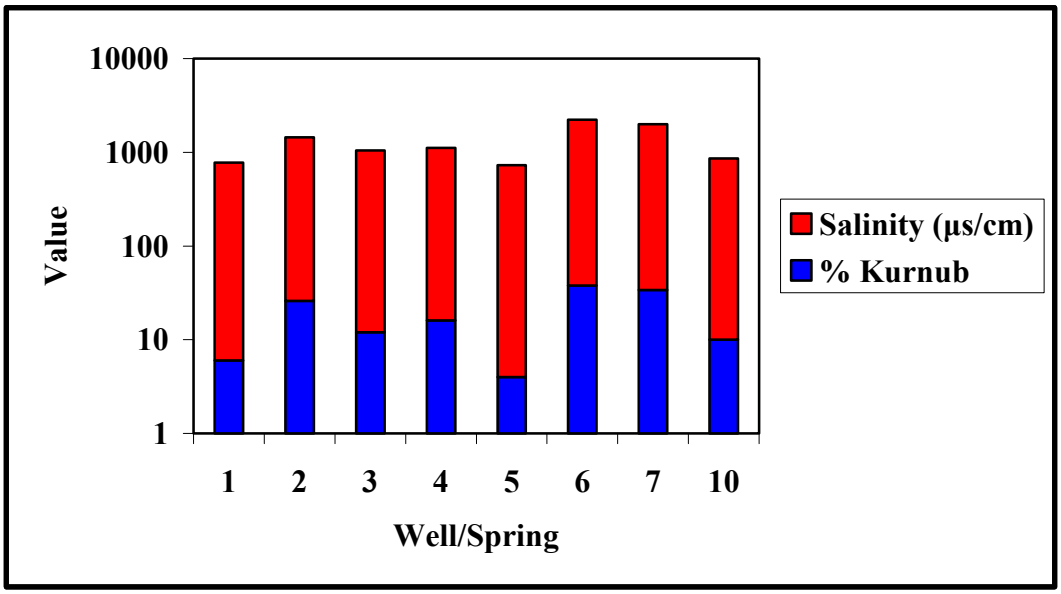

Fig. 5.9: Relationship between the upper aquifer (B2/A7) salinity and the relative share of Kurnub water contribution in the upper aquifer waters.

5.2.1.2 Ratios

The ionic ratios of the samples of the upper aquifer (B2/A7) hydrochemical cross section are shown in Appendix (23) shows. The Halite dissolution process is indicated by the **Na/Cl,** which are being found to be around unity. The **Ca/SO_4** ratios are found to be higher than unity, which indicate a Gypsum dissolution or Plagioclase weathering from the lower sandstone aquifer (Salameh 2001), and since it is higher than unity, this means that the waters are deviated towards calcium enrichment. Generally the **Na/Ca** ratios are increasing with increasing salinity, which can be explained as a faster dissolution of Halite than of Gypsum and of Plagioclase. The **HCO_3/Cl** is more than unity, which indicates faster dissolution of Carbonates relative to Halides.

5.2.1.3 Saturation indices (SI)

Table 5.8 shows the saturation indices of relevant minerals along the upper aquifer (B2/A7) hydrochemical cross section. Those thermal waters are undersaturated with respect to Halite, Gypsum and Anhydrite. With increasing of salinity the Halite saturation

index decrease from -7.65 to -5.94, the Gypsum decreases from -2.04 to -1.26 and the Anhydrite saturation index also decrease from -2.14 to -1.34. Those thermal waters are saturated or slightly supersaturated with respect to Calcite and Dolomite where the Calcite saturation index ranges from -0.47 to 0.21 and the Dolomite saturation ranges from -0.87 to 0.48.

Table 5.8: The saturation indices for the relevant minerals along the upper aquifer (B2/A7) thermal waters hydrochemical cross section.

No	Well/Spring	Halite	Gypsum	Anhydrite	Calcite	Dolomite	Salinity
1	EL-Mokhybeh	-7.3	-1.97	-2.14	0.14	0.32	**772.5**
2	El-Hmmeh/Maqla	-6.27	-1.39	-1.54	0.2	0.37	**1419.5**
3	El-Hammeh/Bajeh	-6.86	-1.66	-1.83	-0.02	-0.01	**1036**
4	North Shuneh hot	-6.71	-1.64	-1.96	0.03	0.33	**1094.5**
5	Waqas	-7.65	-2.04	-2.13	0.08	0.38	**725**
6	Abu-Zyad	-5.94	-1.26	-1.34	0.21	0.48	**2185**
7	Abu-Thableh	-6	-1.3	-1.47	0.14	0.24	**1967**
10	Al-Kafreen	-6.93	-1.77	-1.94	-0.47	-0.87	**848**

5.2.1.4 Water types

In general those thermal waters are earth alkaline water with increased portions of alkalis, where the low salinity waters are with prevailing bicarbonates and the ones, which have higher salinity, are with prevailing sulfate and chloride.

5.2.2 The lower sandstone aquifer hydrochemical cross section

This cross section includes the thermal waters that tap the lower sandstone aquifer mainly from the Kurnub and Zarqa. The samples that tap the Zarqa aquifer are found in the Jordan Valley (JV): Abu El-Zeeghan wells 1 and 2 while the ones that tap the Kurnub are mainly located at the eastern and southeastern parts of the Dead Sea.

5.2.2.1 Salinity

The salinity that is expressed by means of EC is ranging between 6465 to 10375 µs/cm for the thermal waters of the Zarqa aquifer in the Jordan Valley. The high salinity of those wells could be attributed to the high confining pressure and to the nitrate and sulfate reduction where H_2S and CO_2 attack the rock matrix, which causes the high dissolution of carbonate, sulfate, and evaporites (Salameh 2001). Furthermore, this aquifer contains about 30 m of evaporite mainly Gypsum and Anhydrite (Bajjali 1994).

The salinity of the Kurnub thermal waters increase generally from the south going northwards where the Zara–Ma'in thermal waters are located. Only one anomaly occurs where the TA1 well is having the highest salinity of them all with about 3815 µs/cm, which is caused by the high chloride content of this well. This can be explained by local marine impact on the sedimentation.

5.2.2.2 Ratios

Appendix 23 shows the ionic ratios of the samples of the lower sandstone aquifer hydrochemical cross section. The halite dissolution process is indicated by the **Na/Cl** ratios, which are found to be around unity, while there are some waters that are not close to unity like Abu El-Zeeghan/1, TA1, and Afra/Sawna. The **Ca/SO_4** ratios are found to be higher than the unity and deviated towards the Calcium enrichment, which indicate Gypsum dissolution or plagioclase weathering from the aquifer. The **Na/Ca** ratios are increasing with increasing salinity which indicate faster dissolution of Halite than Gypsum and Plagioclase weathering except Abu El-Zeeghan wells (1 and 2) and TA1, which do not go with this rule.

5.2.2.3 Saturation indices (SI)

Table 5.9 shows the saturation indices of relevant minerals along the lower sandstone aquifer hydrochemical cross section. The lower sandstone aquifer (Zarqa and Kurnub) thermal waters are under saturated with respect to Halite, Gypsum and Anhydrite. With increasing of salinity the Halite saturation index decreases from -7.32 to -5.13, Gypsum saturation index from -2.13 to -1.29 and the Anhydrite satuation index also decrease with increasing salinity from -2.26 to -1.73 except for the TA1.

The Zarqa aquifer thermal waters are oversaturated with respect to both Calcite and Dolomite. The Calcite saturation index increase with increasing of salinity from 0.46 to 0.78. The Dolomite also behaves the same where it increases with increasing of salinity from 0.67 to 1.18.

In general the Calcite saturation index increases with increasing salinity for the Kurnub aquifer from -0.84 to 0.94. The Dolomite also behaves the same where it increases from -1.73 to 1.86 (Table 5.9). The waters of the Al-kafreen well is slightly undersaturated with respect to both Calcite and Dolomite, this could be caused by subsequent cooling of the waters. The undersaturation with respect to Calcite and Dolomite could be interpreted by subsequent cooling of the waters. In the case of the springs it might be caused by the decay of organic matter, which produce CO_2 and thus leads the waters to undersaturation with respect to Calcite and Dolomite.

5.2.2.4 Water types

With increasing of the salinity, the water type of the Zarqa thermal waters change from earth alkaline water with increased portions of alkalis with prevailing Sulfate and Chloride to alkaline water with prevailing Sulfate–Chloride.

The Kurnub thermal waters type change going from the south northward from earth alkaline water with increased portions of alkalis with prevailing Sulfate and Chloride to alkaline water with prevailing Sulfate-Chloride. This relationship corresponds also with

increasing salinity but with one anomaly in the TA1, which have a water type typical of the southern samples.

Table 5.9: The Saturation indices for the relevant minerals along the deep sandstone complex thermal waters hydrochemical cross section.

No	Well	Halite	Gypsum	Anhydrite	Calcite	Dolomite	Salinity
8	Abu El-Zeeghan/1	-5.09	-0.36	-0.51	0.46	0.67	6465
9	Abu El-Zeeghan/2	-4.39	-0.27	-0.42	0.78	1.18	10375
11	Zara/Istraha	-5.85	-1.43	-1.56	0.13	0.26	2027
12	Zara/Maghara	-5.49	-1.63	-1.49	0.25	0.43	2285
13	El-Seel El-Hami	-5.49	-1.56	-1.55	-0.63	-1.35	1400
14	Tal El-Rojom	-5.81	-1.49	-1.61	0.42	0.7	1550.5
15	Maain/El-Mabkhara	-5.19	-1.29	-1.25	-0.34	-0.75	3100
16	Maain/El-Ameer	-5.17	-1.33	-1.4	-0.1	-0.17	3075
17	Maain/El-Shallal	-5.13	-1.34	-1.45	0.94	1.86	3070
18	TA1	-5.18	-1.39	-1.5	0.25	0.69	3815
19	TA2	-5.39	-1.73	-1.85	-0.41	-0.85	1006
20	Iben Hammad	-6.71	-2	-2.16	-0.37	-0.76	753
21	Burbyta	-7.06	-2.12	-2.26	-0.84	-1.73	539
22	Afra/Sawna	-7.32	-2.11	-2.21	-0.39	-0.63	360
23	Afra/Maqla	-7.2	-2.13	-2.23	-0.48	-0.93	544

5.3 Hydrochemical reationships

The four groups: A_{1a}, A_{1b}, A_2 and B have been compared in this section chemically with each other and with the average chemical composition of the Dead Sea. The relationships are being drawn between Cl and each of Na, Ca, K, Mg, SO_4 and HCO_3 for the thermal waters and the Dead Sea i.e. if the Dead Sea is an end member for the thermal waters that are located along the Dead Sea Transform (DST).

From the fingerprint diagrams (Schöller diagrams) (Figs. 5.10, 5.11, 5.12, 5.13), all the groups were found to have a different fingerprints from that of the Dead Sea. From the composition diagrams (Figs. 5.14, 5.15, 5.16, 5.17), it seems that the Dead Sea is not an end member for the thermal waters because the constituents of the thermal waters are not found to be locating on the trend line of the constituents of the Dead Sea. It should be noted here that this is a critical methodology due to possible precipitation of Halite and other minerals, which could change the whole situation.

Group A_{1a} consists of TA2, Iben Hammad, Burbyta, Afra/Sawna and Afra/Maqla and they are from the lower sandstone aquifer (Kurnub aquifer). Both the TA2 and Iben Hammad are characterized by Na>Ca>Mg>K and Cl>HCO_3>SO_4 while the Burbyt, Afra/Sawna and Afra/Maqla are characterized by Ca>Na>Mg>K and HCO_3>Cl>SO_4 (Fig. 5.14).

Group A_{1b} consists of El-Mokhybeh, El-Hammeh/Maqla, El-Hammeh/Bajeh, North Shuneh hot, Waqas and Al-Kafreen and they are from the upper aquifer (B2/A7). This

group is mostly characterized by Ca>Na>Mg>K and HCO_3>Cl>SO_4 except Waqas well which is having Ca>Mg>Na>K and HCO_3>SO_4>Cl (Fig. 5.15).

Group A_2 consist of Abu-Zyad and Abu Thableh from the upper aquifer (B2/A7) and Ma'in/El-Mabkhara, Ma'in/El-Ameer, Ma'in/El-Shallal Zara/Istraha, Zara/Maghara, El-Seel El-Hami, Tal El-Rojom, and TA1 from the lower sandstone aquifer (Kurnub Aquifer). The upper aquifer (B2/A7) thermal waters (Abu-Zyad and Abu-Thableh) are characterized by Na>Ca>Mg>K and HCO_3>Cl>SO_4 while the lower sanstone aquifer thermal waters are characterized by Na>Ca>Mg>K and Cl>HCO_3>SO_4 (Fig. 5.16).

Group B consists of two wells that tap the lower sandstone aquifer (Zarqa aquifer), which are Abu El-Zeeghan 1 and 2. The Abu El-Zeeghan/1 is characterized by Ca>Na>Mg>K and HCO_3>Cl>SO_4 while Abu El-Zeeghan/2 is characterized by Na>Ca>Mg>K and Cl>HCO_3>SO_4 (Fig. 5.17).

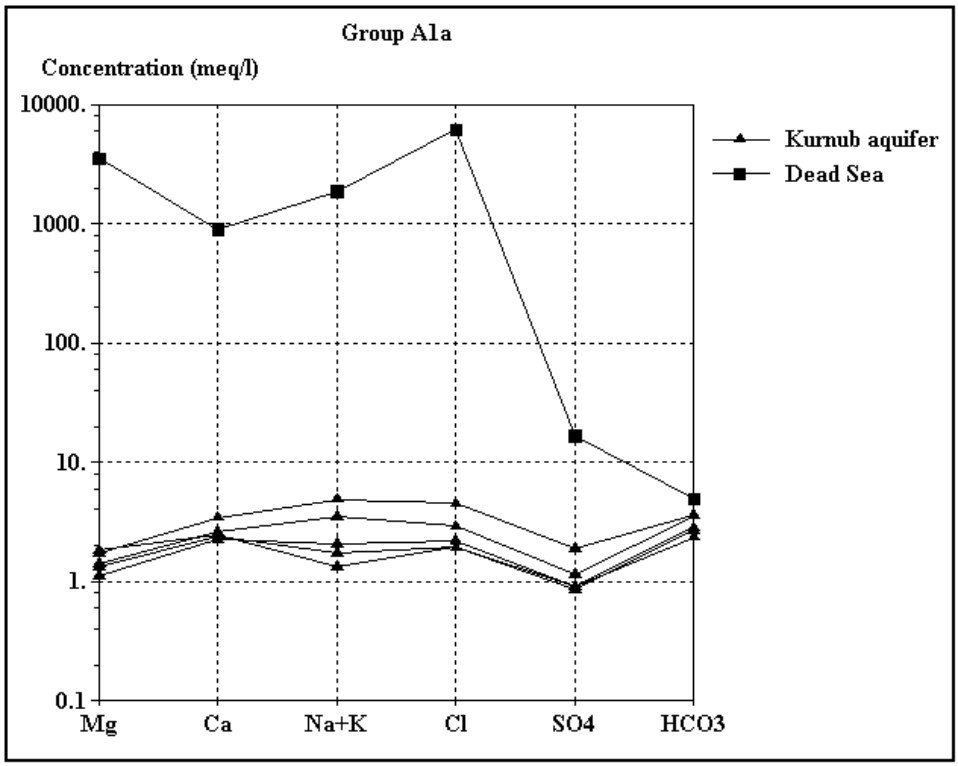

Fig. 5.10: Fingerprints diagram of Group A_{1a} thermal waters compared with the Dead Sea fingerprint.

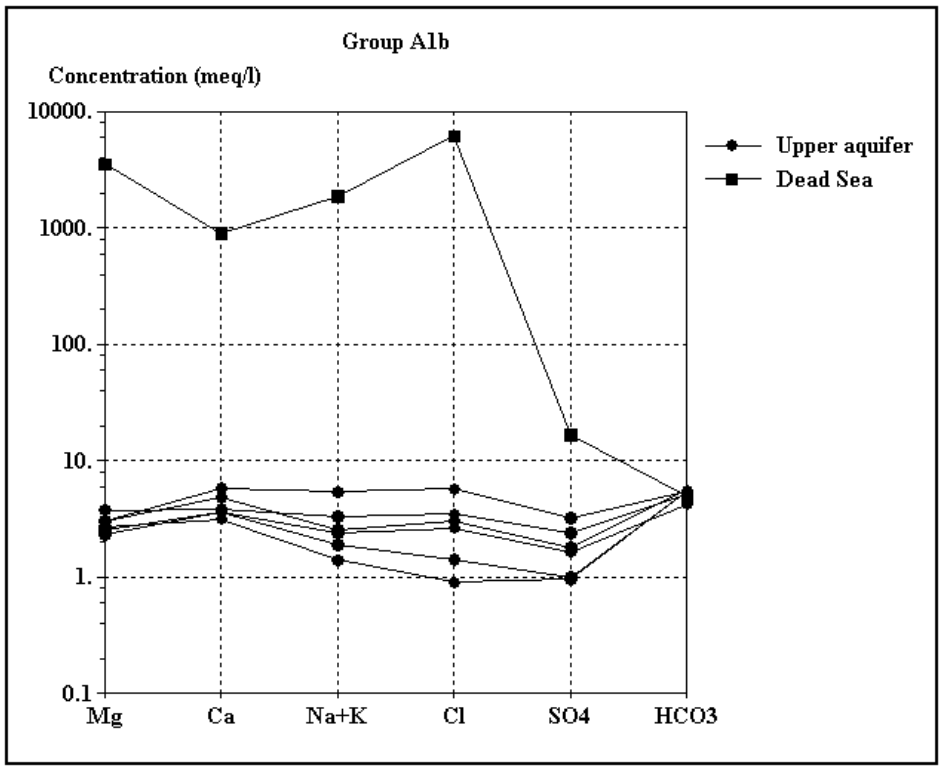

Fig. 5.11: Fingerprints diagram of Group A_{1b} thermal waters compared with the Dead Sea fingerprint.

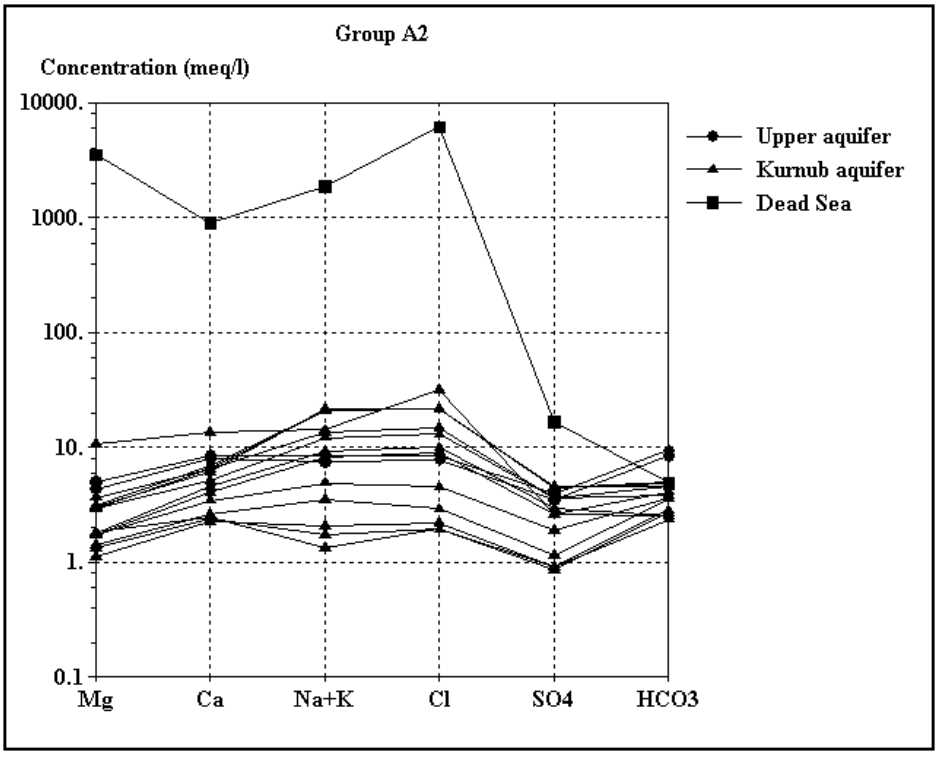

Fig. 5.12: Fingerprints diagram of Group A_2 thermal waters compared with the Dead Sea fingerprint.

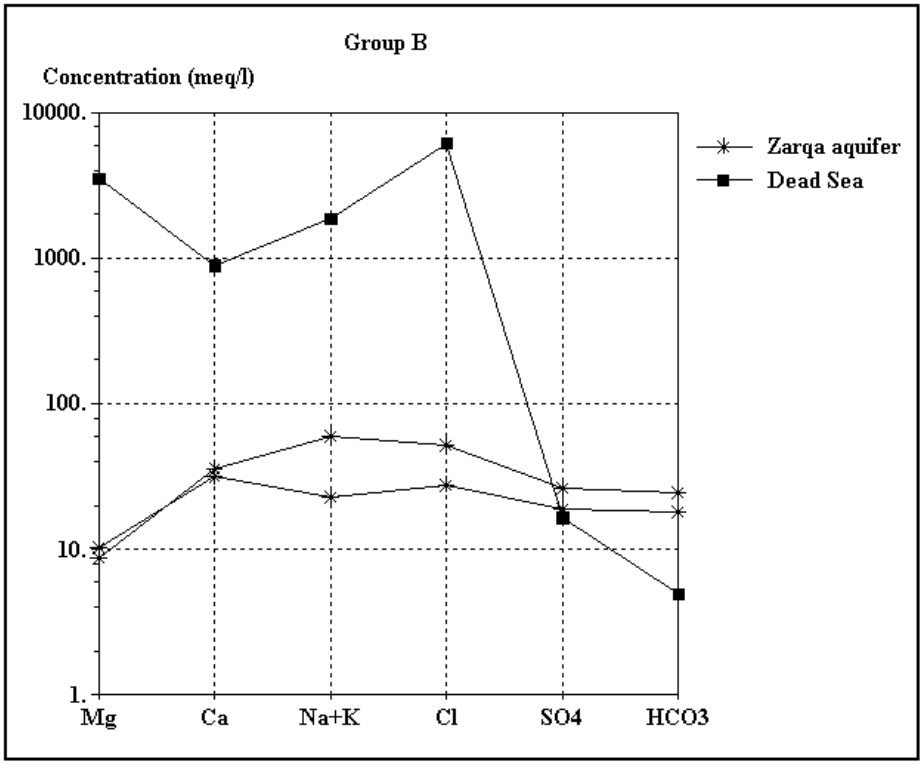

Fig. 5.13: Fingerprints diagram of Group B thermal waters compared with the Dead Sea fingerprint.

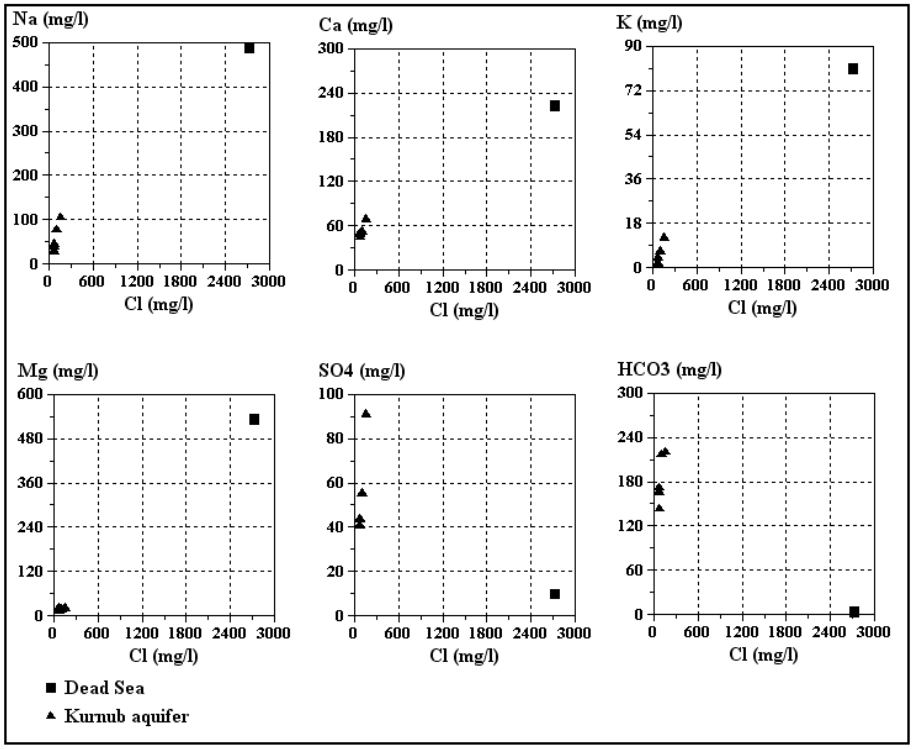

Fig. 5.14: Composition diagrams suspecting that the Dead Sea is not an end member of Group A_{1a} thermal waters (Dead Sea constituents divided by 80 to fit into the graph).

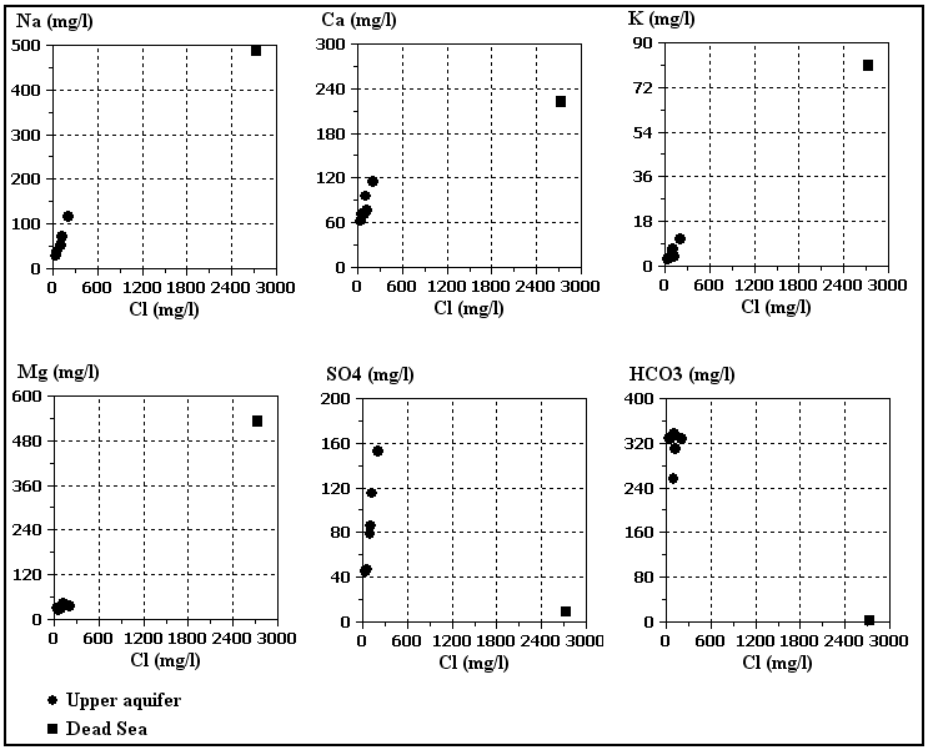

Fig. 5.15: Composition diagrams suspecting that the Dead Sea is not an end member of Group A_{1b} thermal waters (Dead Sea constituents divided by 80 to fit into the graph).

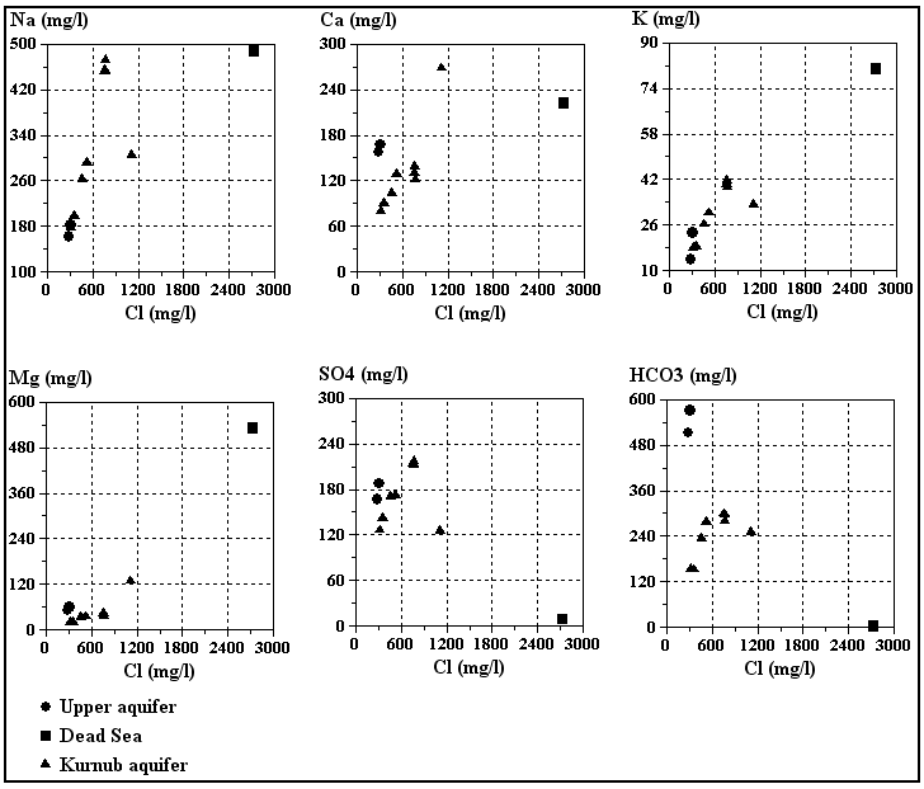

Fig. 5.16: Composition diagrams suspecting that the Dead Sea is not an end member of Group A_2 thermal waters (Dead Sea constituents divided by 80 to fit into the graph).

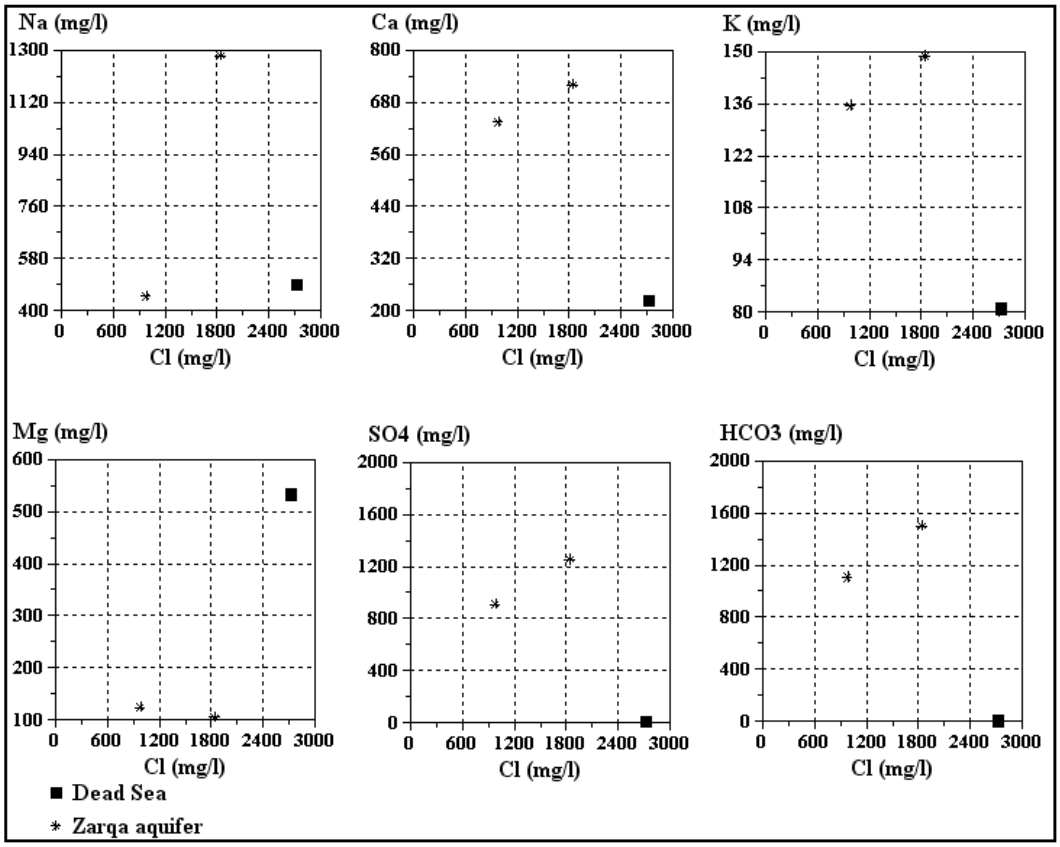

Fig. 5.17: Composition diagrams suspecting that the Dead Sea is not an end member of Group B thermal waters (Dead Sea constituents divided by 80 to fit into the graph).

Bromide and δD as tracer elements has been used to compare the thermal waters with the Dead Sea waters. Fig. 5.18 shows that also the Dead Sea is not an endmember for bromide; because the Br of the thermal waters are not found to be locating on the trend line of that of the Dead Sea.

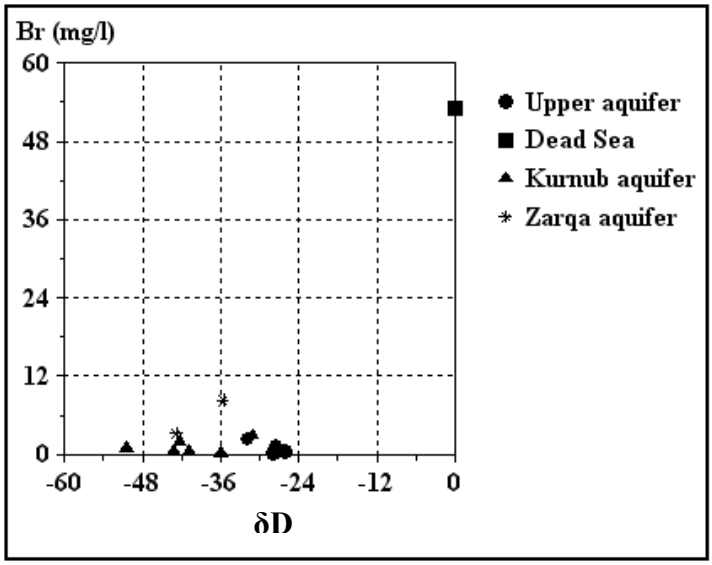

Fig. 5.18: Composition diagrams suspecting that the Dead Sea is not an end member of Br in the thermal waters (Dead Sea constituents divided by 100 to fit into the graph).

5.3.1 The chemical signatures of the Dead Sea

Further more the chemical signatures of the Dead Sea (DS) were compared with the chemical signatures of the thermal springs in order to check the relation ship between the thermal springs and the Dead Sea. Table 5.10 shows the Dead Sea water composition after Abed et al. (1990). Table 5.11 shows the calculation of these signatures. The following signatures have been excluded in order to be compared with the chemical signatures of the thermal waters. They are:

1. The Mg/Ca weight ratio of the DS water which is greater than 2.
2. The HCO_3 weight ratio of the DS water which is about $1.4 \cdot 10^{-3}$.
3. The Na/Cl weight ratio of the DS water which is about 0.18.

Table 5.10: Chemical composition of the Dead Sea (Abed et al. 1990).

Water Depth	Mg (g/l)	Na (g/l)	Ca (g/l)	K (g/l)	Cl (g/l)	SO4 (g/l)	HCO3 (g/l)	TDS (g/l)
0	38.49	37.34	17.86	6.5	202.2	0.75	0.29	310
10	39.51	38.2	18.05	6.61	207.1	0.79	0.30	317
20	40.71	38.75	18.06	6.74	212.1	0.78	0.35	324
25	42.00	39.00	17.50	7.00	217.5	0.69	0.30	330
40	41.68	39.10	17.93	6.34	216.7	0.82	0.29	329
43	41.00	40.00	18.55	7.00	218.0	0.75	0.29	331
70	42.60	39.00	18.75	6.05	218.5	0.9	0.29	332
100	43.48	39.11	17.23	6.10	219.3	0.83	0.30	333
150	43.25	38.00	17.40	6.10	219.4	0.68	0.30	326
200	45.9	39.10	17.60	6.55	222.7	0.88	0.29	336
300	46.35	40.12	17.45	6.55	227.8	0.78	0.30	345
390	46.90	41.25	17.65	6.10	227.9	0.80	0.29	352

Table 5.11: The chemical signatures of the Dead Sea.

Water depth	Mg/Ca	HCO_3/Cl	Na/Cl
0	2.15	0.0014	0.18
10	2.13	0.0014	0.18
20	2.25	0.0016	0.18
25	2.40	0.0014	0.18
40	2.32	0.0013	0.18
43	2.21	0.0013	0.18
70	2.27	0.0013	0.18
100	2.52	0.0014	0.18
150	2.48	0.0014	0.17
200	2.61	0.0013	0.17
300	2.66	0.0013	0.18
390	2.66	0.0013	0.18

By comparing these signatures with that of the thermal waters shown in Appendix (24); it was found that the thermal waters are not identical to the chemical signatures of the Dead

Sea (DS); thus from a chemical point of view this result exclude the Dead Sea as a source or a partner of the chemical composition of the waters of the thermal waters along the Dead Sea Transform (DST). This result contradict the work of Rimawi (1980) in which he supposed the Dead Sea waters an end member for the chemical composition of the thermal waters along the Dead Sea Transform (DST).

5.4 Determining the circulation depth

Williams et al. (1990) and Bajjali (1994) have estimated the geothermal gradient in the Jordan valley to be normal with about 3 ^{o}C/100m while Rimawi and Salameh (1988) have estimated a geothermal gradient of 3.85 ^{o}C/100m in the Ma'in and Zara area.

By considering that the average annual temperature (in winter) in the recharge area to be 11 ^{o}C. This is being subtracted from the quartz calculated geothermometer temperature and depending on the geothermal gradient in the area the circulation depth of waters is being calculated in Table 5.12. The upper aquifer (B2/A7) circulation depth was found to be ranging between 1533.33 m to 2300 m. The Zarqa aquifer circulation depth in was found to be ranging between 1533.33 m to 1666.67 m. The Kurnub circulation depth was found to be ranging between 1533.33 m to 1900 m.

Table 5.12: The estimated circulation depth of the thermal waters.

No	Well/Spring	Circulation depth (m)	No	Well/Spring	Circulation depth (m)
1	EL-Mokhybeh	1733.33	13	El-Seel El-Hami	1844.16
2	El-Hmmeh/Maqla	2300.00	14	Tal El-Rojom	1818.18
3	El-Hammeh/Bajeh	1800.00	15	Ma'in/El-Mabkhara	1610.39
4	North Shuneh hot	2000.00	16	Ma'in/El-Ameer	1558.44
5	Waqas well	1800.00	17	Ma'in/ElShallal	1766.23
6	Abu-Zyad Well	1866.67	18	TA1	1633.33
7	Abu-Thableh	1733.33	19	TA2	1633.33
8	Abu El-Zeeghan/1	1666.67	20	Iben Hammad	1533.33
9	Abu El-Zeeghan/2	1533.33	21	Burbyta	1900.00
10	Al-Kafreen well	1533.33	22	Afra/Sawna	1800.00
11	Zara/Istraha	1662.34	23	Afra/Maqla	1800.00
12	Zara/Maghara	1662.34			

5.5 Heat Source

There is still a debate about the source of heat of the thermal waters in the Dead Sea Transform (DST). Many hypothesis have been proposed to solve the problem of heat source:

1. Cooling of young magma bodies (the presence of hot bodies or hot plutons close to surface which are still hot);
2. Friction that associate the lateral movement along faults of the Dead Sea Transform;
3. Deep circulation under more or less normal geothermal gradient;
4. The presence of heat stowing layers at the upper parts of the lower aquifer.

The first hypothesis, which depends on cooling of young volcanic bodies is supported by the presence of late Cenozoic basaltic flows with a total volume of less than 1 km^3 nearby the Ma'in area, these extrusions have an age ranging between 0.6 to 3.4 Myr (Sawarieh and Massrweh 1996). Other authors argue that those bodies are too small and old to provide sufficient heat, besides thermal waters produced from several shallow wells near Queen Alia airport where the waters originate from the lower aquifer and passes through faults and fractures and mix with the upper aquifer (Sawarieh and Massarweh 1993). Also the thermal waters are found in some places where no volcanic activities are found like Al-Kafreen and the North Shuneh hot well. Thus it is unlikely that the volcanisem is the source of heat for those thermal waters.

The second hypothesis refers the high temperature thermal waters to the high intensity of shearing of faults along the DST especially in Ma'in-Zara area (Hakki and Teimeh 1981). This is more supported by the high heat flow in Ma'in Zara area (up to 472 mW/m^2), which is associated with the Zarqa-Ma'in fault zone rather than the local basaltic eruption (Galanis et al. 1986 and Sawarieh 2005).

The deep circulation under more or less normal geothermal gradient is supported by the lake of volcanisem near some of the thermal waters like the North Shuneh and Al-Kafreen, also lack of volcanism near the eastern end of Wadi Zarqa Ma'in fault and infrequent small eruption near Zarqa Ma'in and Zara area (Truesdell 1979). This hypothesis is more supported by the presence of high heat flow associated with the fault (Sawarieh and Massarweh 1996).

Also the presence of heat stowing layers, which is the non saturated upper portion of the lower sandstone aquifer and the overlying marls and clays may play a role. This layer are of upper cretaceous age, having a heat conductivity of about the half of those of the saturated sandstone. So, those layers works as a stowing or insulating layers, where the measured geothermal gradient in dry sandstone is 7.6 ^oC/100 m and for the shale is about 8 ^oC/100 m (calculated from the NRA wells record in the Zara area (Table 5.13)). The elevated temperature can be a result of bad conductance of the stowing layers overlying the saturated sandstone (Rimawi and Salameh 1988, Sawarieh and Massarweh 1993).

Table 5.13: calculated geothermal gradients in the Zara area (Salameh and Rimawi 1988).

Well No.	**Depth**	**Temperature difference (^oC)**	**Gradient (^oC/100m)**
B.H.4	200	13	6.5
B.H.5	200	11	5.5
B.H.6	170	14	8.2
B.H.7	160	14	6.8
B.H.8	200	18	9.0
B.H.9	180	17	9.4
Average			**7.6±1.5**

5.6 Sulfate isotopes

Fig. 5.19 shows the relationship between the $\delta^{34}S_{Sulfate}$ and the $\delta^{18}O_{Sulfate}$. The regression equation can be expressed as:

$$\delta^{34}S_{SO4}=1.92\ \delta^{18}O_{SO4}-4.97 \qquad \text{with } R^2=0.56$$

Fig. 20 shows the relationship of the $\delta^{18}O_{water}$ and the $\delta^{18}O_{Sulfate}$. The $\delta^{18}O_{Sulfate}$ value was found to have a much wider range than the $\delta^{18}O_{water}$ values. This can be interpreted as either variation in the sulfate source or that the oxygen isotope equilibrium between the water and the sulfate doesn't occur; otherwise it should have shown a much closer relationship (Fontes and Zuppi 1976). The $\delta^{34}S_{Sulfate,}$ $\delta^{18}O_{Sulfate}$ values, and sulfate concentration are found to be having a positive relationship to each other as shown in Fig. 5.21.

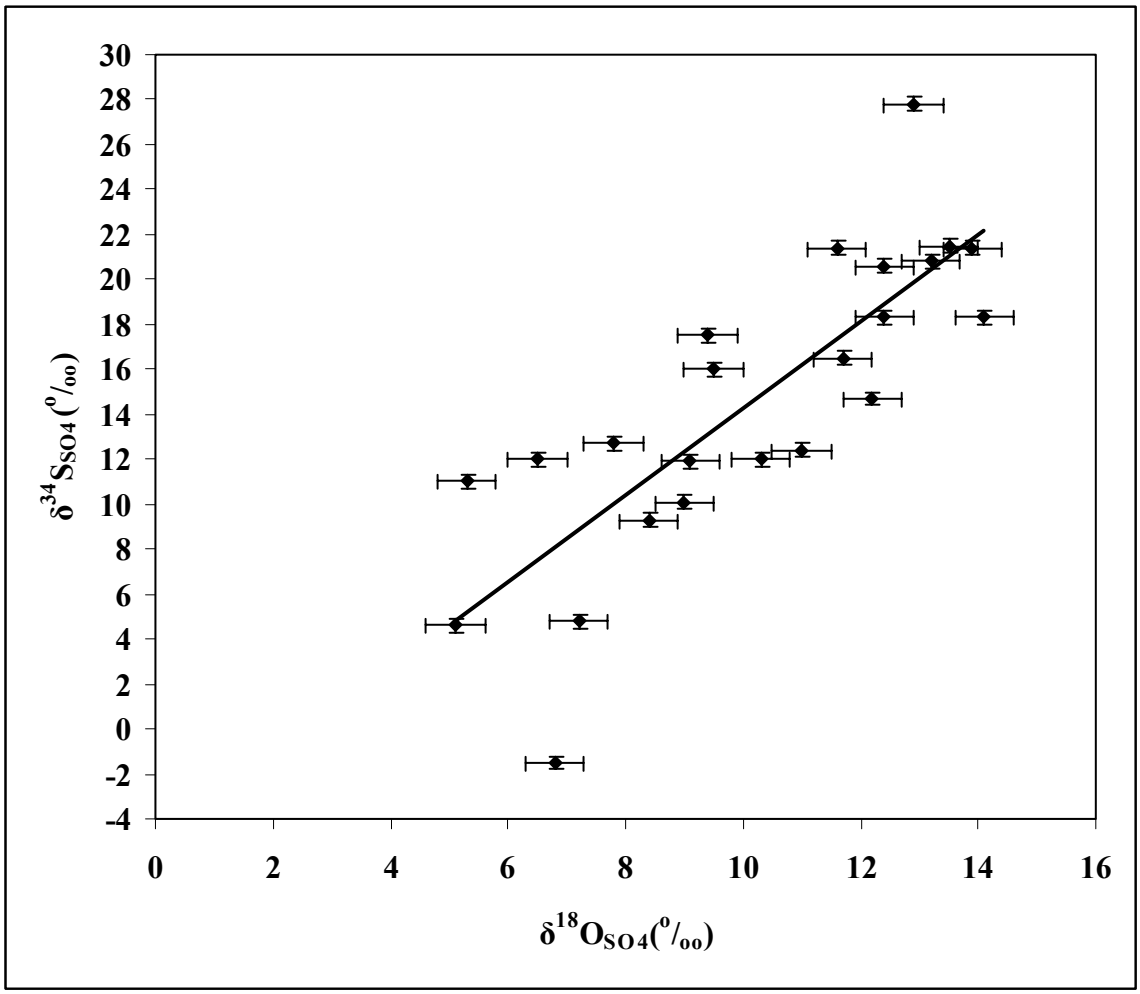

Fig. 5.19: The relation ship between $\delta^{34}S_{Sulfate}$ and the $\delta^{18}O_{Sulfate}$ values.

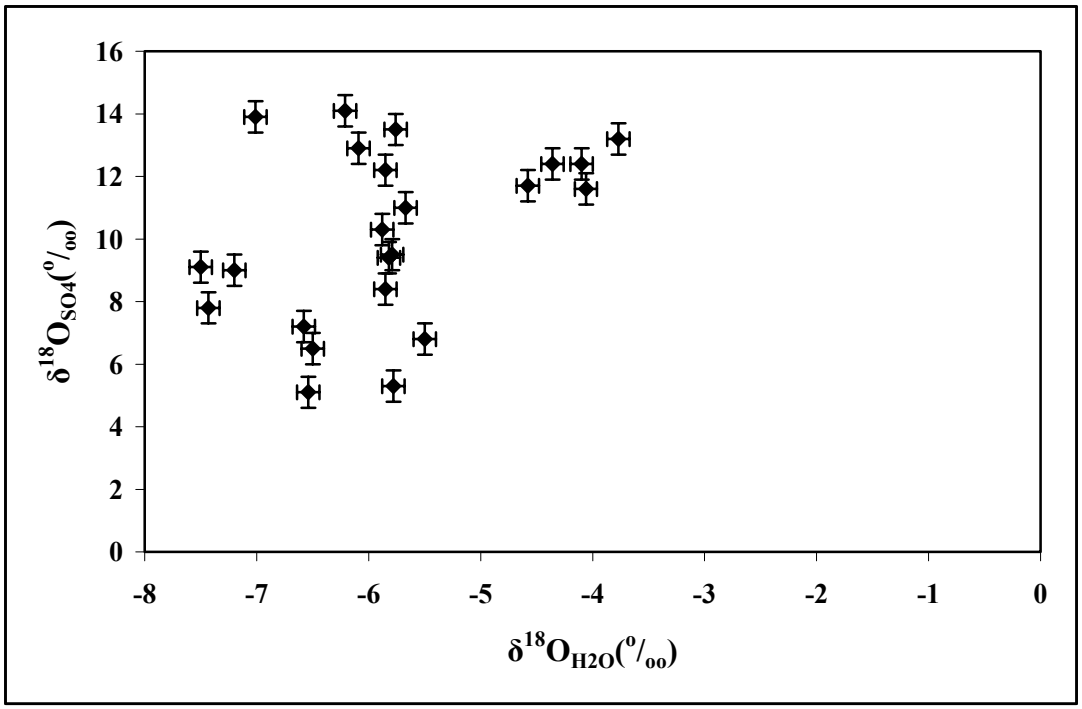

Fig. 5.20: The not significant (not exisiting) relationship between the $\delta^{18}O_{Sulfate}$ and the $\delta^{18}O_{water}$ values.

According to Krouse and Mayer (2000) the $\delta^{34}S_{Sulfate}$ values ranges from 0 to +6 $^{o}/_{oo}$ for both the atmospheric and the soil sulfates, from +7 to +35 $^{o}/_{oo}$ for evaporites and from –34 to +7 $^{o}/_{oo}$ for sulfates from oxidation of sulphides. The $\delta^{18}O_{Sulfate}$ values range between +7 to +18 $^{o}/_{oo}$ for the atmospheric deposition, from 0 to +6 $^{o}/_{oo}$ for the soil sulfates, from +6 to +20 $^{o}/_{oo}$ for evaporites and from –5 to +4 $^{o}/_{oo}$ for sulfates from oxidation of sulphides. By combining both the $\delta^{34}S_{Sulfate}$ values and the $\delta^{18}O_{Sulfate}$ values in Fig. (5.22), it seems that the samples are located on a mixing line between two end members. Furthermore they are the evaporites and the oxidation products of sulphides members, where most of the sulfate is caused by the dissolution of the evaporites from the rock matrix while the samples that are not located with in the first end member region like 10 (Al-Kafreen well), 22 (Afra/Sawna) and 23 (Afra/Maqla) are showing other sources which might be a mixture between atmospheric and soil sulfate sources. But it is most probably that those samples are more affected by the second end member of the mixing line, which is the oxidation of sulphides.

By plotting the sulfate concentration versus the $\delta^{34}S_{Sulfate}$ for the upper aquifer (B2/A7) samples no obvious relationship was noticed. However, the Bajjeh spring seems to be a mixture between El-Mokhybeh wells and Maqla Spring as stated in the work of Bajjali et al. (1997) (he named it Balsam spring). On the $\delta^{34}S_{Sulfate}$-SO_4 diagram, the Bajjeh spring plot between the former two mentioned waters (Fig.5.23). This proof could be more convincing than that of Bajjali et al. (1997) who plotted the three springs on the δD_{water}-$\delta^{18}O_{water}$ diagram; where the Bajeh spring also plot between El-Mokhybeh well and Maqla Spring but within the analytical error (Fig. 5.24).

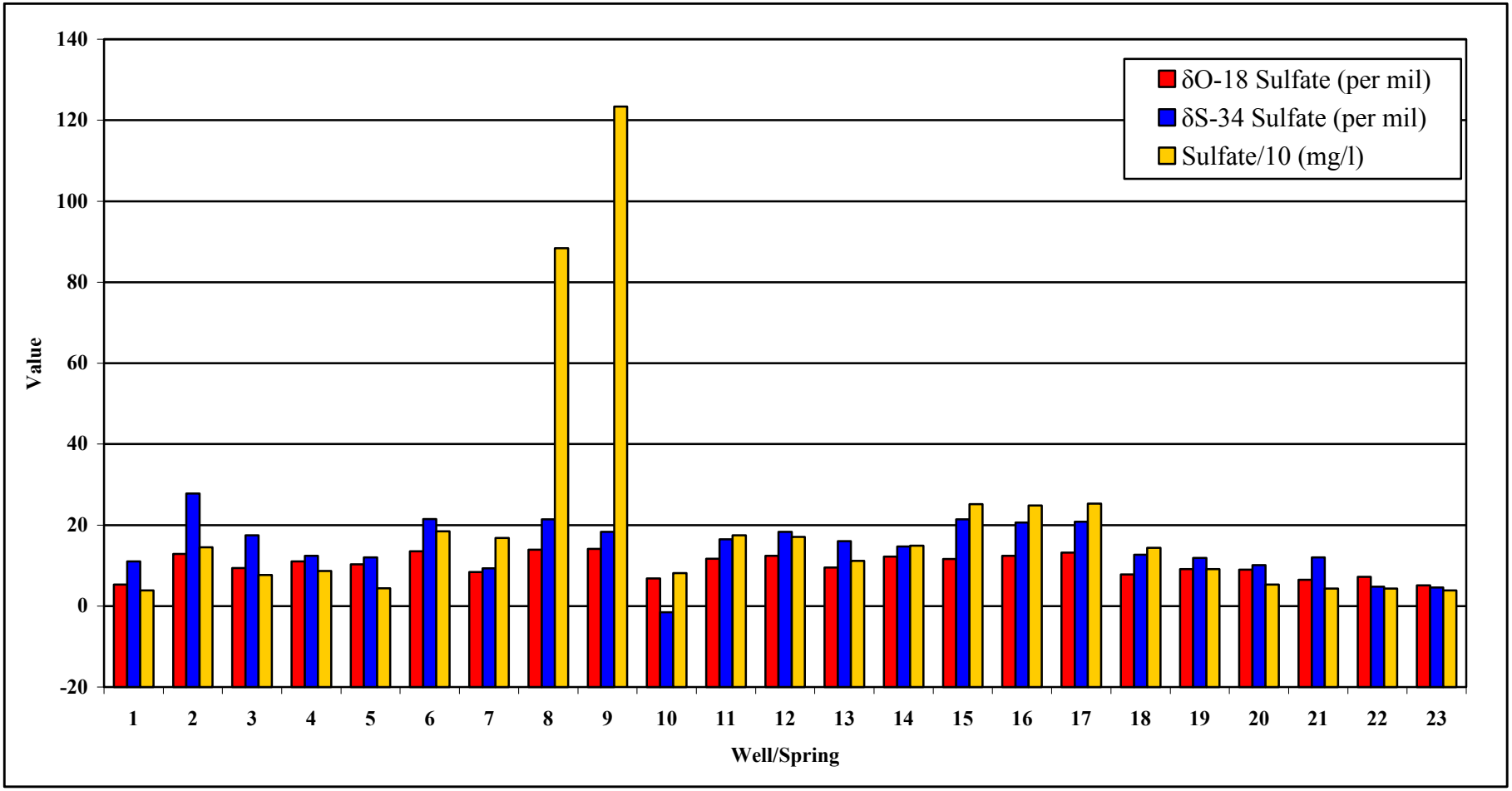

Fig. 5.21: The $\delta^{34}S_{Sulfate}$ ($^{o}/_{oo}$), $\delta^{18}O_{Sulfate}$ ($^{o}/_{oo}$) and sulfate concentration (mg/l) relationship (the sulfate concentrations*10^{-1} (mg/l)).

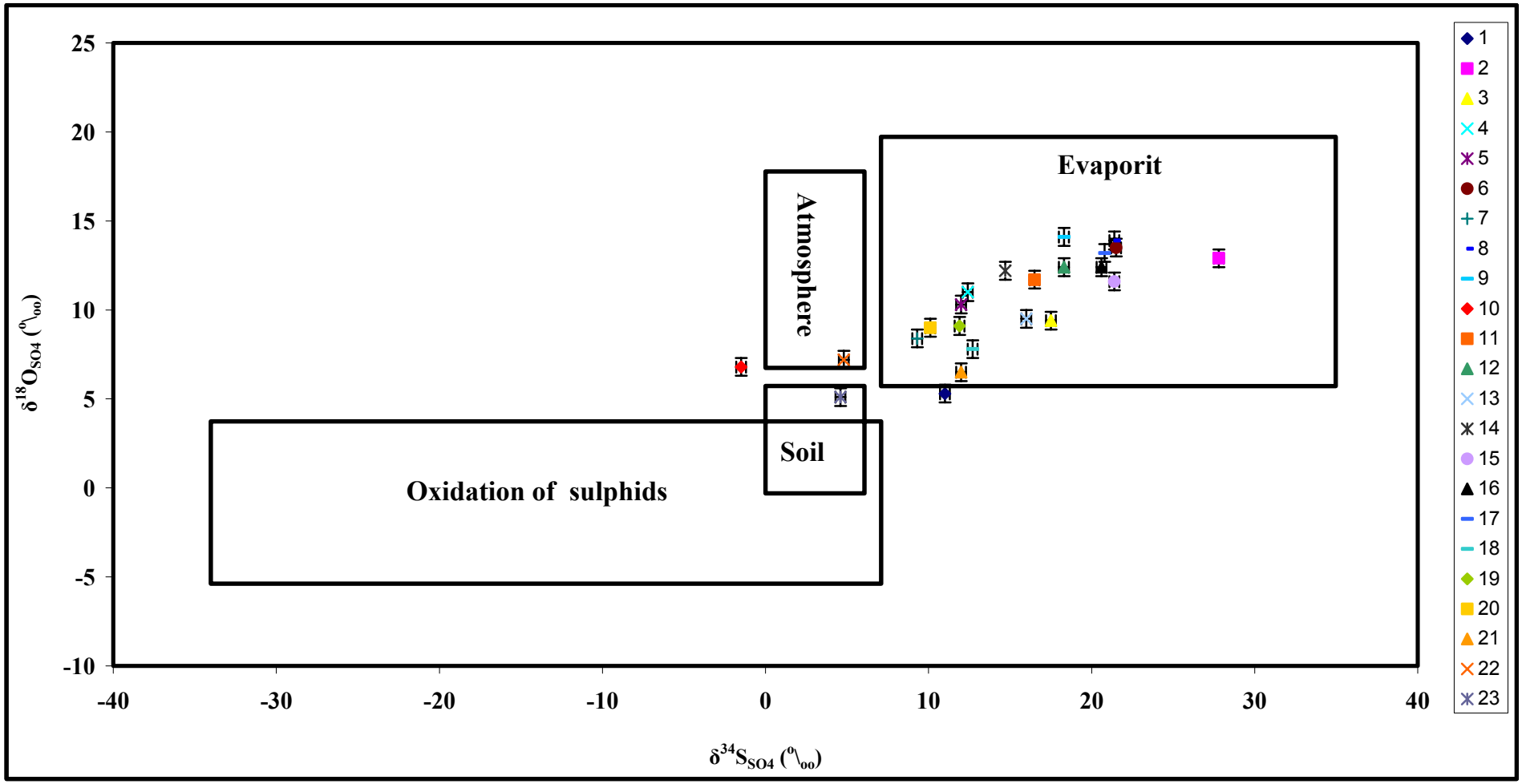

Fig. 5.22: Distribution of thermal waters on the $\delta^{34}S_{sulfate}$-$\delta^{18}O_{sulfate}$ diagram (Krouse and Mayer 2000).

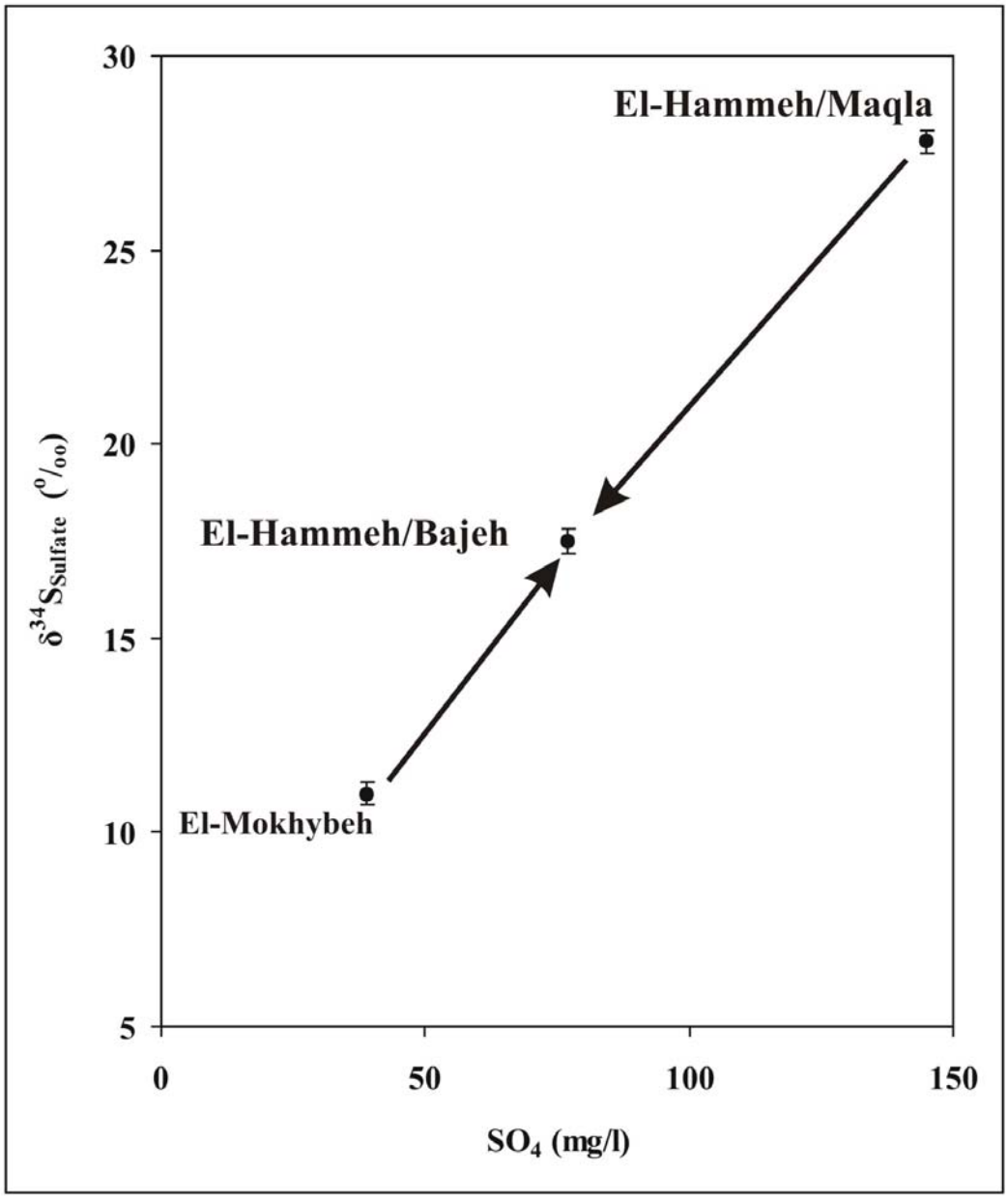

Fig. 5.23: $\delta^{34}S_{Sulfate}$ values and sulfate concentration for the three thermal waters: El-Mokhybeh well, El-Hammeh/Maqla and El-Hammeh/Bajeh.

The EL-Mokhybeh water was theoritically mixed with El-Hmmeh/Maqla and they were optimized to reach the concentration values of the El-Hammeh/Bajeh. The mixing calculation of two samples was performed in order to determine the optimal mixing ratio of the two selected samples that most closely matches a third target sample. The two initial samples are being mixed in 2% increment until the Euclidean distance between the calculated mixture and specified resulting sample is minimized. The results are shown in Table (5.14). The mixing of the chemical constituents, $\delta^{34}S_{sulfate}$, $\delta^{18}O_{sulfate}$, $\delta^{18}O_{water}$ and δD_{water} shows that the EL-Mokhybeh well contribute with 64% while the El-Hmmeh/Maqla spring contribute with 36% from its water to give the waters of the El-Hammeh/Bajeh spring.

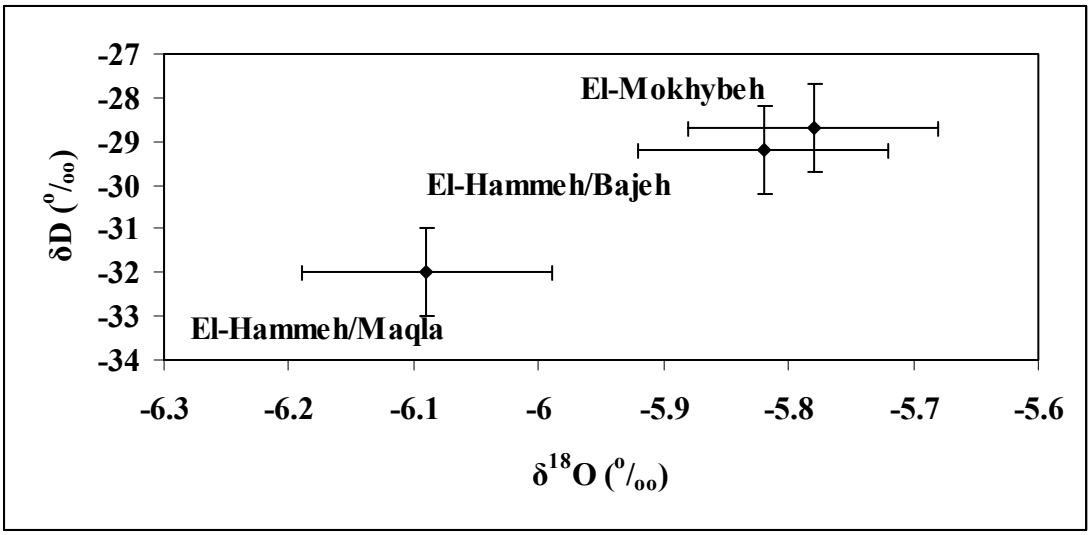

Fig. 5.24: δD values and $\delta^{18}O$ values for the three thermal waters: El-Mokhybeh well, El-Hammeh/Maqla, and El-Hammeh/Bajeh.

Table 5.14: The optimized mixing values for the El-Hammeh/Bajeh from the El-Mokhybeh well and the El-Hammeh/Maqla.

Constituent	El-Mokhybeh	El-Hammeh/Maqla	EL-Hameh/Bajeh	Optimized
Na (mg/l)	41.38	117.25	54.03	68.693
Ca (mg/l)	72.54	115.23	96.29	87.908
Mg (mg/l)	28.08	37.07	37.01	31.316
Cl (mg/l)	49.63	201.90	106.36	104.447
SO_4(mg/l)	47.78	152.93	86.43	85.634
HCO_3(mg/l)	328.80	328.21	338.28	328.588
SiO_2(mg/l)	19.95	30.70	21.10	23.82
$\delta^{34}S_{sulfate}$(°/oo)	11.00	27.80	17.50	17.048
$\delta^{18}O_{sulfate}$(°/oo)	5.30	12.90	9.40	8.036
δD_{water}(°/oo)	-28.7	-32	-29.2	-29.888
$\delta^{18}O_{water}$(°/oo)	-5.78	-6.09	-5.82	-5.892

Fig. 5.25 shows $\delta^{34}S_{Sulphate}$-sulfate concentration relationship, which shows that the sulfate concentration and $\delta^{34}S_{Sulphate}$ of the lower sandstone aquifer samples are increasing from the south to the north. This phenomenon can be explained by plotting the $\delta^{34}S_{sulfate}$ values against the $\delta^{18}O_{sulfate}$ values (Fig. 5.26) where it is obvious that the lower sandstone aquifer waters are plotting on a mixing line between the two end members the evaporites and the oxidation of sulphides. However, the southern samples are closer to the second end member. They are more affected by oxidation of sulphides and sulfate concentrations in the southern waters are decreasing.

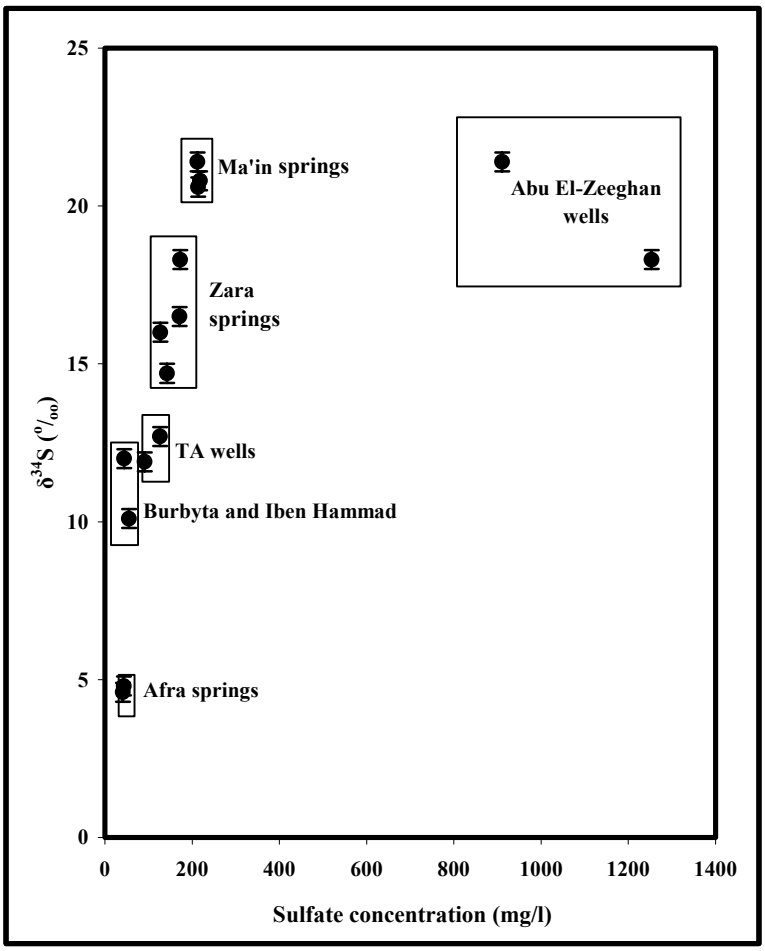

Fig. 5.25: $\delta^{34}S_{Sulphate}$ values-sulfate concentration relation for the lower sandstone aquifer waters.

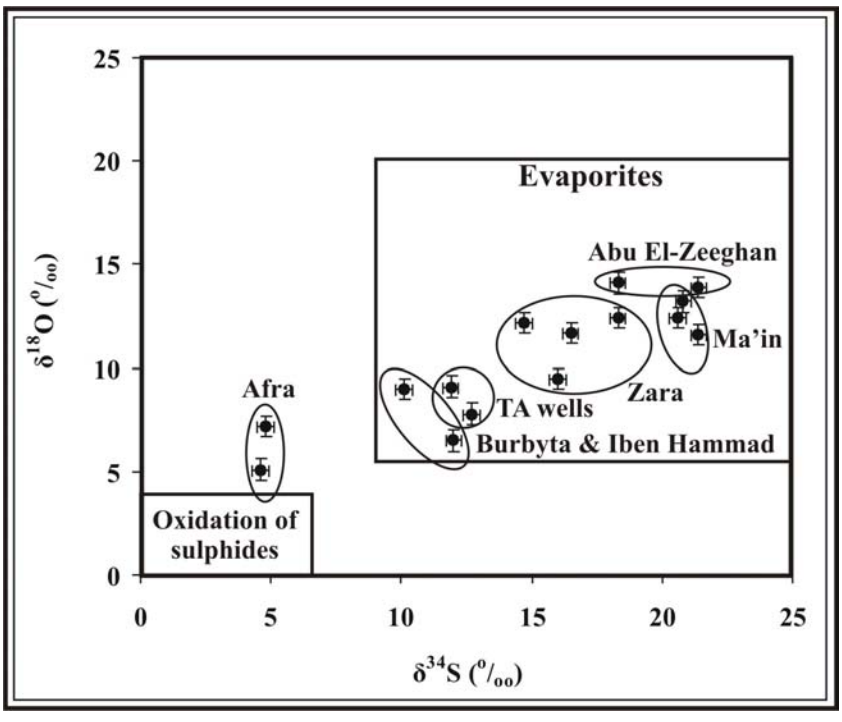

Fig. 5.26: $\delta^{34}S_{sulfate}$- $\delta^{18}O_{sulfate}$ relationship for the lower sandstone aquifer waters.

5.7 The source of CH_4, H_2S and CO_2 gasses

By comparing the $\delta^{13}C_{CO2}$ values with the $\delta^{13}C_{HCO3}$ values (Table 5.15), it is noticeable that system is not in equilibrium. This could be interpreted as the presence of an additional source of the carbon in the CO_2. According to Clark and Fritz (1997) the $\delta^{13}C$ value of the aquifer derived organic carbon is about -25 ± 2-3 $^{o}/_{oo}$ (Fig. 5.27) and since the $\delta^{13}C_{CO2}$ values are almost with in this range, the most probable source for such results should come from an organic material which are usually having depleted $\delta^{13}C$ values. Further more this can be affirmed by the explanation of Bender (1974) and Salameh and Rimawi (1997) that the CO_2 results of oxidation–reduction process of organic matter, which is present in the rock matrix.

Table 5.15: $\delta^{13}C_{CO2}$, $\delta^{13}C_{HCO3}$, values of the thermal springs along the Dead Sea Transform.

No.	Well	$\delta^{13}C_{CO2}$ ($^{o}/_{oo}$)	$\delta^{13}C_{HCO3}$($^{o}/_{oo}$)	References for $\delta^{13}C_{HCO3}$
1	El-Mokhybeh	-19.3±0.2	-12.01	Bajjali et al. (1997)
4	North Shuneh hot	-22.9±0.2	-10.18	Bajjali et al. (1997)
5	Waqas	-22.9±0.2	?	
18	TA1	-16.9±0.2	-4.10	EL-Naser & Subah (2000)
19	TA2	-20.6±0.2	-4.10	EL-Naser & Subah (2000)

According to Felipe et al. (2005) carbon isotope exchange between acetic acid and HCO_3^- and $CO_{2(g)}$ is favoured reaction. This would change the isotopic pattern of HCO_3 and CO_2. However, the data presented would indicate a favoured reaction with CO_2 only. Depending on the afore mentioned, this might indicate the presence of oil in the past which might have migrated leaving acetic acids behind which have affected the $\delta^{13}C_{CO2}$ isotopic signatures alone.

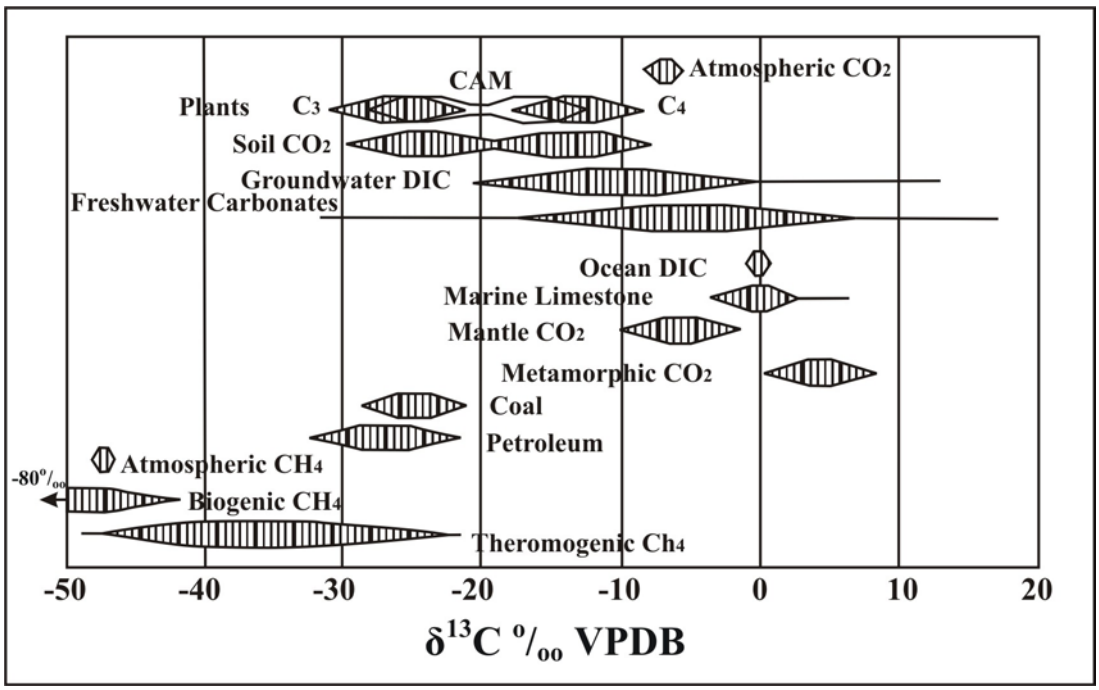

Fig. 5.27: Ranges for $\delta^{13}C$ values in selected natural compounds (Clark and Fritz 1997).

5.8 Water Quality Evaluation

Some thermal waters in Jordan are being used for touristic and therapeutic purposes. In their study, Salameh and Rimawi (1997) have characterized the therapeutic uses for those springs. Beside this, thermal water in Jordan is being used by local people for drinking, household, and irrigation purposes. The purpose of this section is to characterize the waters for both domestic as well as irrigation purposes.

5.8.1 Evaluation of the thermal waters for domestic purposes

According to Sawyer and MacCarty (1967) classification (Table 5.16); the water samples were found to range from hard to very hard (Appendix 25). However, this can be good for the agricultural or irrigation purposes because the presence of the calcium enhance the quality of the soils. The total hardness is being calculated using the following equation:

TH=2.5 Ca (mg/l)+4.1 Mg (mg/l) (Todd 1980)

Table 5.16: Classification of water based on the total hardness (Sawyer and McCarty 1967).

Hardness (mg/l)	Water class
0-75	Soft
75-150	Moderately hard
150-300	Hard
Over 300	Very hard

Some waters suffer from the presence of some constituents that affect the aesthetic characteristics, which affect the taste of the water and might cause household problem. By comparing the results of the Rare Earth Elements (REE) (Appendix 4) with the Jordanian standards (JISM 2001) (Appendix 26) and the world health organization guidelines guidelines (WHO 1996) (Appendix 27), it was found that the water constituents which affects significantly on the health are below the allowed ranges in both of the standards.

5.8.2 Evaluation of thermal waters for agricultural purposes:

The suitability of groundwater for irrigation purposes is contingent on the effects on the mineral constituents of the water on both the plants and the soil.

The following criterias have been used to evaluate the suitability of the thermal waters for agricultural purposes:

1. Salinity (EC);
2. Soluble sodium percentage (SSP);
3. Sodium adsorption ratio (SAR);
4. Residual sodium carbonate (RSC);

5. Toxicities.

Furthermore an evaluation for the suitability of groundwater for irrigation purposes need also to consider as well the soil of the site where irrigation will take place, irrigation method, and type the crops and plants.

5.8.2.1 Salinity (EC)

Salts may harm plant growth physically by limiting the uptake of water through modification of the osmotic processes, or chemically by metabolic reactions such as those caused by toxic-constituents (Todd 1980). Based on the salinity represented by the EC values, water can be classified into four categories (College of Agricultural Sciences 2004) as shown in Table (5.17).

Appendix 28 shows the classification of thermal waters based on the afore mentioned salinity (EC) classification where it shows that most of the thermal waters range between C3 and C4. Only four samples were found to have C2 class and they are Waqas well, Burbyta spring and Afra springs (Maqla and Sawna).

Table 5.17: Classification of the irrigation water based on Salinity (EC) values (College of Agricultural Sciences 2004).

Level	EC (µS/cm)	Hazard
C1	<250	Low hazard; no detrimental effects on plants, and no soil buildup expected.
C2	250-750	Sensitive plants may show stress; moderate leaching prevents salt accumulation in soil.
C3	750-2250	Salinity will adversely affect most plants; requires selection of salt-tolerant plants, careful irrigation, good drainage, and leaching.
C4	>2250	Generally unacceptable for irrigation, except for very salt-tolerant plants, excellent drainage, frequent leaching, and intensive management

5.8.2.2 Soluble sodium percentage (SSP)

The sodium concentration is important in classifying irrigation water because Sodium reacts with soil and reduces its permeability. Soils containing a large proportion of Sodium with Carbonates as a predominant anion are saline soils, ordinarily; either type of Sodium enriched-soil will support a little or no plant growth.

The thermal waters have been classified according the Soluble Sodium Percent (SSP) which is defined as the proportion of Sodium ions in solution in relation to the total cation concentration, defined as follows:

$$\mathbf{SSP=[(Na+K)/(Ca+Mg+Na+K)]*100}$$ (Todd 1980)

where the concentrations of the constituents are expressed in milliequivalent per liter.

Table 5.18 shows the water classification based on the SSP of Todd (1980). Appendix 29 shows the thermal waters classification based on SSP classes. Only one sample showed an excellent SSP-water class, which is Waqas well while the rest of the samples were ranging between (good-doubtful) SSP-water classes.

Table 5.18: Classification of the irrigation water based on the soluble sodium percent (SSP) (Todd 1980).

Water class	SSP	EC (µs/cm)
Excellent	< 20	<250
Good	20-40	250-750
Permissible	40-60	750-2000
Doubtful	60-80	2000-3000
Unsuitable	>80	>3000

It is noticeable that the upper aquifer (B2/A7) thermal waters are mainly having a good SSP-class while the lower sandstone aquifer samples are ranging between permissible to doubtful SSP-water class except Iben Hammad spring, Burbyta spring and Afra springs (Maqla and Sawna) that have a good SSP-class. The Abu El-Zeeghan /1 and TA1 wells show a good SSP-water class but they have a high salinity which exceed 3000 µs/cm so they might be classified as unsuitable according to the EC.

5.8.2.3 Sodium adsorption ratio (SAR)

Because of its direct relation to the adsorption of sodium by soil; the sodium adsorption ratio (SAR) is also used here. It is defined by the following equation (Todd 1980):

$$\mathbf{SAR=Na/[(Ca+Mg)/2]^{0.5}}$$

where the concentration of the constituents is expressed in milliequivelant per liter.

The continuous use of waters that have a high SAR leads to a breakdown in the physical structure of the soil, where the sodium replaces calcium and magnesium sorbed on clay minerals and causes dispersion of soil particles. The dispersion causes breakdown of soil aggregates and causes a cementation of the soil under drying conditions and prevent infiltration of rainwater.

Table 5.19 shows the classification of ground water based on SAR (College of Agriculture sciences 2004). Appendix 30 shows the thermal waters classification based on the SAR classification. All the samples were found to have S1-class except Abu El-Zeeghan/2, which have an S2-class.

With the help of GWW software (United Nations 1995) the samples are being presented on a Wilcox diagram (Wilcox 1955). Fig. 5.28 shows both the EC and the SAR thermal water types. The samples 8 and 9, which are Abu El-Zeeghan wells 1 and 2 are not showed on the Wilcox diagram because they are out of range. Appendix 31 shows the SAR and the water classes based on the Wilcox diagram classification.

Table 5.19: Classification of the irrigation water based on the sodium adsorption ratio (SAR) (College of Agriculture Sciences 2004).

Level	SAR	Hazard
S1	<10	No harmful effects from sodium.
S2	10-18	Appreciable sodium hazard in fine-textured soils of high CEC, but could be used on sandy soils with good permeability.
S3	18-26	Harmful effects could be anticipated in most soils and ammendments such as gypsum would be necessary to exchange sodium ions.
S4	>26	Generally unsatisfactory for irrigation

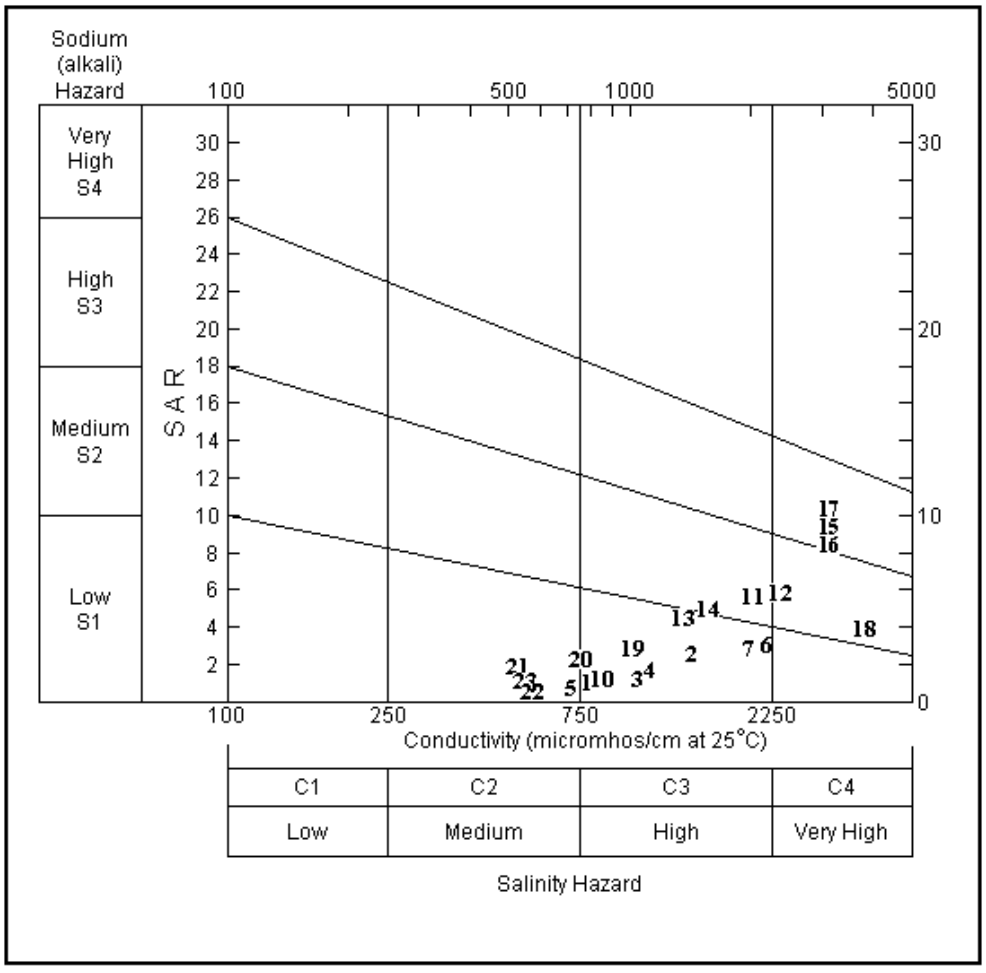

Fig. 5.28: Wilcox diagram presenting the thermal waters collected from both the upper aquifer (B2/A7) and the lower sandstone aquifer.

5.8.2.4 Residual Sodium carbonate (RSC)

The residual sodium carbonate (RSC) equals the sum of the bicarbonate and carbonate concentration minus the sum of Calcium and Magnesium ion concentration, where the ions are expressed in milliequivelant per liter. When the RSC increases, a lot of Calcium and some Magnesium are precipitating from the solution when the waters are applied to the soil; so the increasing of the sodium percentage and hence the rate of sorption of Sodium on the soil particles will increase the potential for Sodium hazard. Table 5.20 shows the degree of Sodium hazard (College of Agricultural Sciences 2004).

All of the samples were found to be having a negative RSC value which means that the sodium buildup is unlikely to happen since sufficient calcium and magnesium are in excess of what can be precipitated as carbonates when the waters are applied to the soils.

Table 5.20: Classification of irrigation water based on the residual sodium carbonate (RSC) (College of Agricultural Sciences 2004).

RSC	Hazard
<0	None.
0-1.25	Low, with some removal of calcium and Magnesium from irrigation water.
1.25-2.50	Medium, with appreciable removal of Calcium and Magnesium from irrigation water.
>2.50	High, with most Calcium and Magnesium removed leaving sodium to accumulate.

As a conclusion, it is being found that the waters of Abu El-Zeeghan wells 1 and 2, Zara/Maghara spring, Ma'in springs (El-Mabkhara, El-shallal and El-Ameer) and TA1 well are showing a very high salinity which is generally unacceptable for irrigation except for salt tolerant plants with excellent drainage, frequent leaching, and intensive management, at the same time those waters are showing medium to high sodium (alkali) hazard especially in fine textured soils. The Ma'in springs and the Zara/Istraha waters show a high SSP, which reduces soil permeability when they are applied for a long period of time. On the other hand, the other thermal waters are ranging between medium to high salinity hazard, which require a salt-tolerant plants agriculture, so the waters can be usable for irrigation if it is going to be applied directly to the soils with out any further treatment such as mixing with low salinity waters.

5.8.2.5 Trace elements and their toxicity

Usually, irrigation water supplies do not need to be checked for trace elements unless there is some reason to suspect toxicity. Not all trace elements are toxic. Many of them are considered to be essential like: Fe, Mn, Mo, and Zn (in small quantities). However high quantities will cause undesirable accumulation of the elements in the plant tissues, which cause growth reduction (Ayers and Westcot 1994). By comparing the Rare Earth Element

(REE) analysis of thermal waters (Appendix 4) with the recommended maximum concentration of trace elements in irrigation water (Appendix 32), it was found most of the elements are with in the accepted range except for the Manganese (Mn) of the El-Seel El-Hami, Ma'in/El-Mabkhara, and TA2 , which are having Mo values higher than 0.2 mg/l.

5.8.3 Scale forming and Corrosivity

Corrosion is a dissolving and wearing away of metal caused by a series of chemical reactions, usually between water and pipes. It is an oxidation/reduction reaction that returns refined or processed metals to their more stable ore state. In a water system the corrosion might cause a structural failure, leaks, loss of capacity, and deterioration of chemical and microbiological water quality.

The corrosion occurs in soft water because of the lack of dissolved cation such as Calcium and Magnesium, while in the hard waters a calcium and magnesium carbonate coat develop inside the pipes, which act as a protector for the pipes because it acts as a barrier, but it can clog the pipes with time and the continuous precipitation of Calcium and Magnesium. There are a lot of parameters which might accelerate the corrosion and they are:

1. Water that have low pH or high pH;
2. High water temperature;
3. High flow rate within the pipes;
4. High levels of dissolved Oxygen and CO_2;
5. High dissolved solids such as sulphates and salts;
6. The presence of suspended solids, sediments and corrosion by-products and rust.

Corrosion may impact the human health, aesthetic quality of the water, damage the household, might cause premature failure of hot water heaters, imparting a bitter taste of the drinking water and cause the formation of red water or greenish blue stains on drains and consumption of the water with elevated levels of toxic metals such as cupper and lead which might cause acute and chronic health problems.

Both the Langlier saturation index and the calcite saturation index have been used to classify the water, and to determine if the water has the tendency to be corrosive or scale forming.

The Langlier saturation index (ΔpH) is an estimate of solutions tendency to dissolve or deposit calcium carbonate, which was often used as an indicator of the water corrosivity. The ΔpH is defined as the difference between the actual pH and the calculated pHs. The pHs represent the point at which water is saturated with calcium carbonates (Calcite) and its formula is as follows:

ΔpH =pH-pHs (Hach company 1993)

The pHs was calculated with the use of PhreeqC software. Appendix 33 shows average measured pH, average calculated pH, ΔpH value and the water classification based on ΔpH. Since no certain limitations for such classification in the Jordanian standards; the German standards where taken into account where the range of -0.2 and 0.2 of the ΔpH is the permissible level and considered to be balanced, while the waters that have ΔpH < -0.2 is considered to be corrosive or aggressive and the ones that have ΔpH > +0.2 is considered to be scale forming (Merkel and Planer-Friedrich 2005).

Appendix 33 shows that the upper aquifer (B2/A7) waters are mainly balanced with in the permissible limit except Al-Kafreen well, which shows a little bit aggressivity. The lower sandstone aquifer thermal waters show a wide variety of water aggressivity, it is noticeable that the south Jordan thermal waters are mainly aggressive.

Table 5.21 shows the water classification based on the calcite saturation index with general recommendations (Wilkes University 2004). Appendix 34 shows the thermal waters classification based on the afore mentioned classification. The thermal waters of both aquifers: the upper aquifer (B2/A7) and the lower sandstone aquifer are found to be ranging between mild scale coating and mild corrosion. It is noticeable that the upper aquifer (B2/A7) thermal waters are mainly near balanced except Al-Kafreen well, which is showing a non-mild corrosion. Only three samples showed that treatment may be needed and they are Abu El-Zeeghan/2 well, Ma'in/El-shallal spring and Burbyta spring.

Table 5.21: The Saturation index (SI) and recommended treatment (Wilkes University 2004).

Saturation Index	Description	General Recommendation
- 5	Severe corrosion	Treatment recommended
- 4	Severe corrosion	Treatment recommended
- 3	Moderate corrosion	Treatment recommended
- 2	Moderate corrosion	Treatment may be needed
-1	Slow corrosion	Treatment may be needed
-0.5	None- mild corrosion	Probably no treatment
0	Near balanced	No treatment
0.5	Some faint coating	Probably no treatment
1	Slow scale coating	Treatment may be needed
2	Slow to moderate coatings	Treatment may be needed
3	Moderate scale forming	Treatment advisable
4	Severe scale forming	Treatment advisable

5.9 Direct use of the geothermal resources

The direct or the so-called non-electrical utilization of the geothermal energy could be defined as: the use of heat energy directly rather than converging it into other forms like electrical energy. Direct use includes: Swimming, bathing, balneology (therapeutic use), space heating, agricultural (like green house heating and animal farming), industrial processes and heat pumps. Generally, lower geothermal water temperatures are needed for

the direct use than the ones that required for electrical generation. For direct use, the required temperatures range between 50°-150 °C. So the main factor determining the potential use of particular geothermal resource is the reservoir temperature (summarized in Lindal diagram (Fig. 5.29)).

The agricultural uses require a temperatures ranging between 25°-90 °C, but since the amount of dissolved gasses may affect the plants and animals; the use of heat exchanger is always recommended. Space heating requires temperatures in the range between 40°-100 °C. The industrial processing requires more than 100 °C (Lund 2004). Since that the thermal waters temperature along the DST range between 30 and 61 °C; thus it is not possible to use them directly in the industrial processing.

5.9.1 Present and past use

The past and present direct use of the geothermal resources was and still focused on swimming, bathing, and balneology. Table 5.22 shows the utilization of geothermal energy for direct heat in the 1999. Salameh and Rimawi (1997) studied the therapeutic uses of the different thermal waters along the DST. They found that the use of these waters gives successful results in various degrees. They proved that they could be used for treating blood pressure, rheumatism, skin diseases, nervous system diseases, ulcers, and recuperation after surgery.

Table 5.22: Use of geothermal energy (modified after Sawarieh 2000).

Location	Flow rate	Tempreature (oC)		Capacity MWT	Energy (TJ/yr)
		Inlet	Outlet		
N. Shuneh	194	57	30	22	197.7
Hammeh	833	40	25	52.3	274.8
Ma'in	500	58	30	58.6	739
Zara	167	42	30	8.40	79
Burbyta	87.5	39	25	5.12	111
Afra	104	43	28	6.54	138.5
Total	**1844**			**153.3**	**1540**

5.9.2 Future use

The geothermal energy along the DST is very promising and could be used directly in the following:

1. Space conditioning, like building heating from individual wells;
2. District heating, which originate from central location and supply the hot water through pipe-network to individual blocks and buildings;
3. Agriculture and aquaculture applications, which include green house heating and aquaculture, animal husbandry, soil warming, irrigation, and bio-gas generation. Several vegetables could be grown by the use of these waters like: cucumber, tomatoes and flowers. This can reduce the operating cost of about 35% of the product cost (Lund 2004). It could be used for raising catfish, shrimp, tilapia and tropical fish. Fig. 5.30

shows the effect of temperature on animal and fish growth. Livestock growth can be increased by controlling the heating and cooling, which could lower the mortality of the newborn. The most important factor is the water quality and diseases.

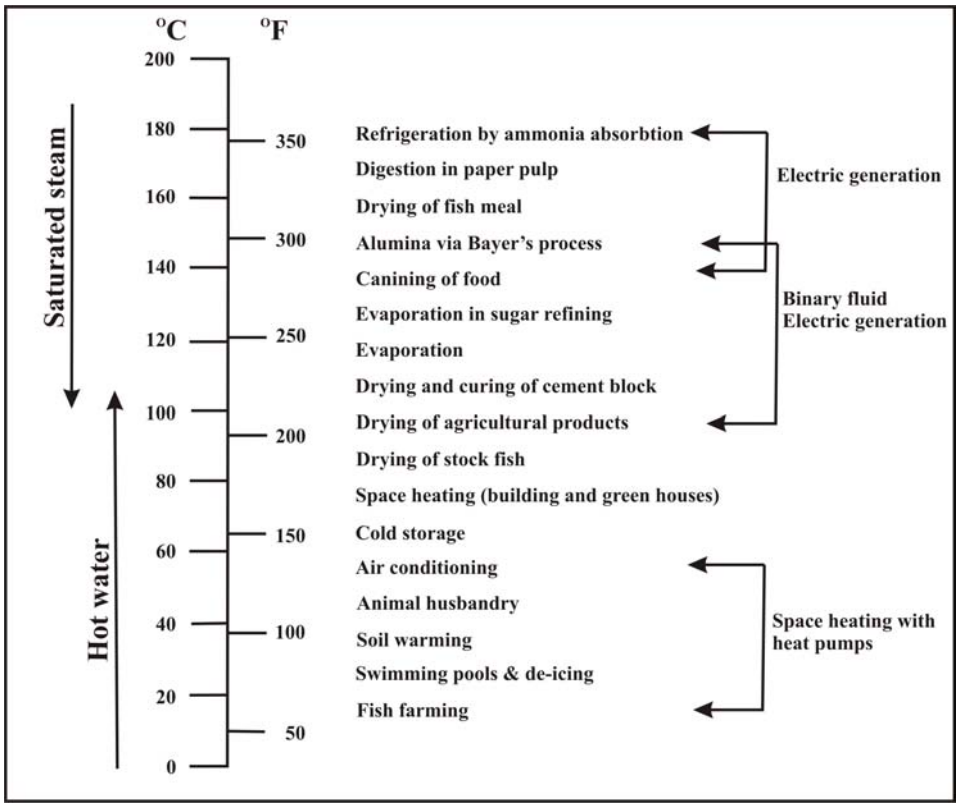

Fig. 5.29: Lindal diagram for the hot water and saturated steam (Gudmundsson et al. 1985).

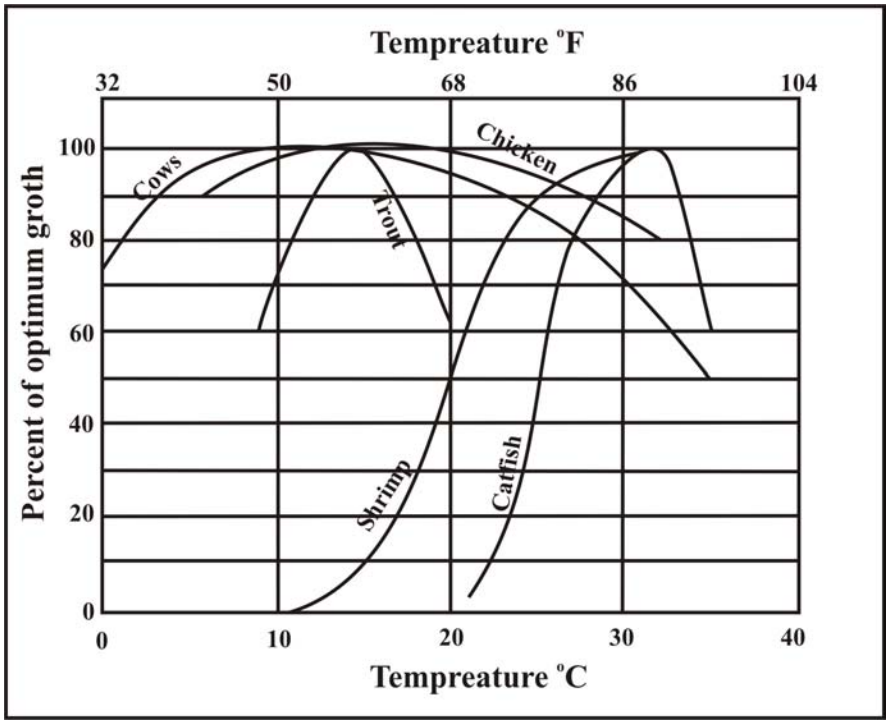

Fig. 5.30: Temperature effect on animals and fish growth (Lund 2004)

5.10 Residence time and source of water

In order to determine the residence time and source of the thermal waters along the Dead Sea transform (DST) the following isotope signatures have been used:
1. Tritium isotopes;
2. Helium isotopes;
3. Stable water isotopes of ($\delta^{18}O$, δD);

5.10.1 Tritium

Kaufman and Libby (1954) measured the pre-bomb tritium in the vintage wines and found it to be ranging between 3.4 and 6.6 TU, which means that if this water discharges in the 2003, the tritium value should be ranging between 0.2 and 0.4 TU. All of the samples have no tritium or a concentration less than 1 TU, which indicates that those waters are tritium free and have been recharged before 1952 (prior the era of thermo nuclear bomb testing) or the share of the younger water (recharged after 1952) is very small. This can be more supported by comparing the measured tritium values (Table 4.1, section 4.2.1) with the calculated tritium values in the proposed discharge of the older than 1950 precipitation (Appendix 6).

5.10.2 Tritium/Helium-3 ($^3H/^3He$) method

The equation $\tau = T_{1/2}/\ln 2 \cdot \ln(1+[^3He]_t/[^3H]_t)$ have been used in order to determine the mean residence time of the water of the four samples TA1, TA2, Waqas and El-Mokhybeh wells (Table 5.23). The mean residence time has been found to be ranging between ≥ 120 to ≥ 160 year taking into account the uncertainty of the analytical determination of the tritium.

Table 5.23: Calculation of mean residence time for the thermal wells sampled based on the ($^3H/^3He$) method.

No.	Well Name	Tritium	^3He	^3He	τ
		T.U.	Nml/g	T.U.	a
1	EL-Mokhybeh	0.3±0.3	$1.5 .10^{-12}$ $1.6 .10^{-12}$	625	≥ 120
5	Waqas	0.1±0.3	$3.1 .10^{-12}$	1250	≥ 140
18	TA1	0.0±0.3	$7.4 .10^{-12}$ $7.3 .10^{-12}$	2950	≥ 160
19	TA2	0.0±0.3	$7.5 .10^{-12}$ $7.5 .10^{-12}$	3015	≥ 160

Table 5.24 shows inverse calculation of the tritium concentrations depending on the final analyzed tritium value and its half-life. It can be noticed; that in 1960 the tritium concentration should have been around 2950 TU. Such a high tritium value must be related to the 1960-1963 period because it must be bomb-derived. If then the calculated 120 to 160 years are added; this will reach the years 2080 to 2120. However, it could be deduced that

some additional Helium-3 (^{3}He) must have invaded the system. This makes the Tritium-Helium age calculation impractical since not all of the measured Helium is resulting from the Tritium decay and it is difficult to speculate how much extra Helium has invaded the system.

Table 5.24: Inverse calculation of the tritium concentrations depending on the tritium half-life.

Half life	Time [a]	Year	T.U.	^{3}He [TU]
0	0	1960	2950	0
1	12.43	1972.43	1475	1475
2	24.86	1984.86	737.5	2212.5
3	37.29	1997.29	368.8	2581.3
4	49.72	2009.72	184.4	2765.6
5	62.15	2022.15	92.2	2857.8
6	74.58	2034.58	46.1	2903.9
7	87.01	2047.01	23.0	2927
8	99.44	2059.44	11.5	2938.5
9	111.87	2071.87	5.8	2944.2
10	124.3	2084.3	2.9	2947.1
11	136.73	2096.73	1.4	2948.6
12	149.16	2109.16	0.7	2949.3
13	161.59	2121.59	0.4	2949.6

5.10.3 Helium source

Fig. 5.31 shows the relationship between the $^3He_{total}$-$^3He_{air}$/$^4He_{totoal}$-$^4He_{air}$ and $^4He_{solubility}$/^4He-$^4He_{air}$, (Weise plot) (calculation in Appendix 8). From the Weise plot and the calculation done in Table (5.24); it could be deduced that additional ^{3}He must have invaded the system. TA1 and TA2 wells are plotting close to the crustal Helium value, which is $2 \cdot 10^{-8}$. The other measured samples are higher than that. Still if the Helium is only gained from the production of the earths crust that would invade the system; then the ^{3}He/^{4}He ratio should be much lower (following the production line). However, since the samples are plotting above the production line, this means that the samples comprise mantle Helium caused by mantle exhalation bounded on more or less open deep faults.

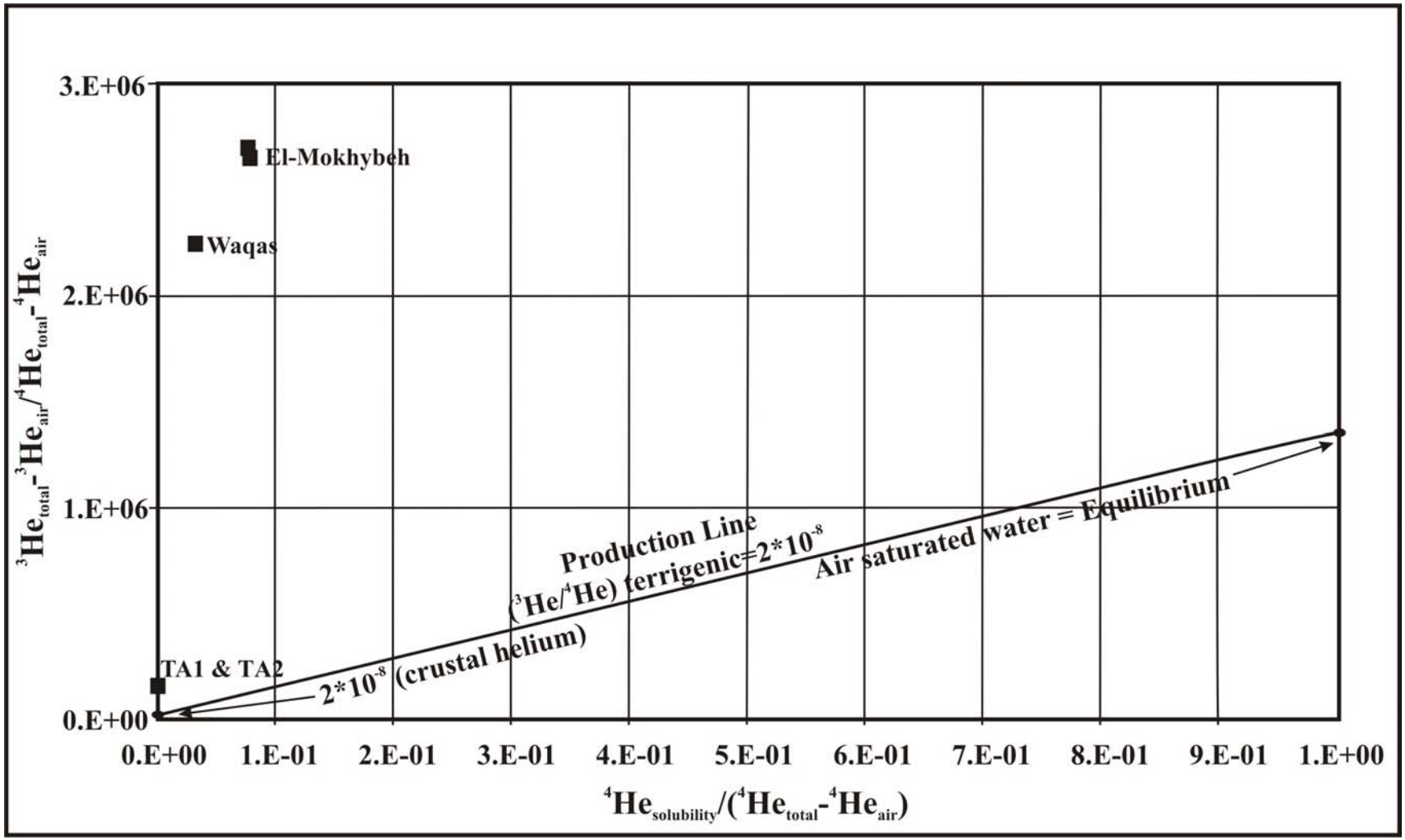

Fig. 5.31:Weise Plot showing that the samples are plotting above the production line.

5.10.4 Stable water isotopes ($\delta^{18}O$ and δD)

The stable isotope pattern ($\delta^{18}O$ and δD) (Fig. 5.32) shows that the thermal waters can be subdivided into four groups:

1. Waters plotting close to the Mediterranean Meteoric Water Line (MMWL);
2. Waters plotting between the Mediterranean Meteoric Water Line (MMWL) and the Global Meteoric Water Line (GMWL). They are isotopically depleted with respect to the first group;
3. Waters plotting close to the Global Meteoric Water Line (GMWL);
4. Waters plotting below the Global Meteoric Water Line (GMWL). They are isotopically more enriched than the third group.

The first group includes the upper aquifer (B2/A7) thermal waters: EL-Mokhybeh, El-Hmmeh/Maqla, El-Hammeh/Bajeh, North Shuneh hot well, Waqas well, Abu-Zyad Well, Abu-Thableh and Al-Kafreen well. They are characterized by a d-excess ranging between 17.5 and 9 mainly signifying recharge that occurred under climatic conditions similar to those, which dominates Jordan and the surrounding areas these days.

The second group includes Abu El-Zeeghan/1, Abu El-Zeeghan/2, Iben Hammad, Burbyta, Afra/Sawna, Afra/Maqla. They are from the lower sandstone aquifer and they are characterized by a d-excess ranging between 11.3 and 14.2.

The third group includes TA1 and TA2. They are from the lower sandstone aquifer and they are characterized by a d-excess of 9 and 9.4.

The fourth group includes Zara/Istraha, Zara/Maghara, El-Seel El-Hami, Tal El-Rojom, Ma'in/El-Mabkhara, Ma'in/El-Ameer, Ma'in/El-Shallal and they are having a d-excess ranging between -0.3 and 4.

The values of the third and fourth group were found to be comparable with the Dead Sea (DS) isotopic signatures. According to Gat and Gonfiatiny (1981) the Dead Sea`s $\delta^{18}O$ range between 4.14 $^{o}/_{oo}$ and 0 $^{o}/_{oo}$ and according to Salameh and Rimawi (1984) the Dead Sea`s δD is 0 $^{o}/_{oo}$. Fig. 5.33 shows that those samples plot on a mixing line with the Dead Sea (DS) water, where TA1 and TA1 are representing minimum mixing with the Dead Sea (DS) water because they are associated with the Global Meteoric Water Line (GMWL) and that the south Zara samples (El-Seel El-Hami and Tal El-Rojom) springs are having around 20% of the Dead Sea (DS) waters, while the Zara-Ma'in springs (Zara/Istraha, Zara/Maghara, Ma'in/El-Mabkhara, Ma'in/El-Ameer and Ma'in/El-Shallal) are having between 30% to 40% of the Dead Sea (DS) waters.

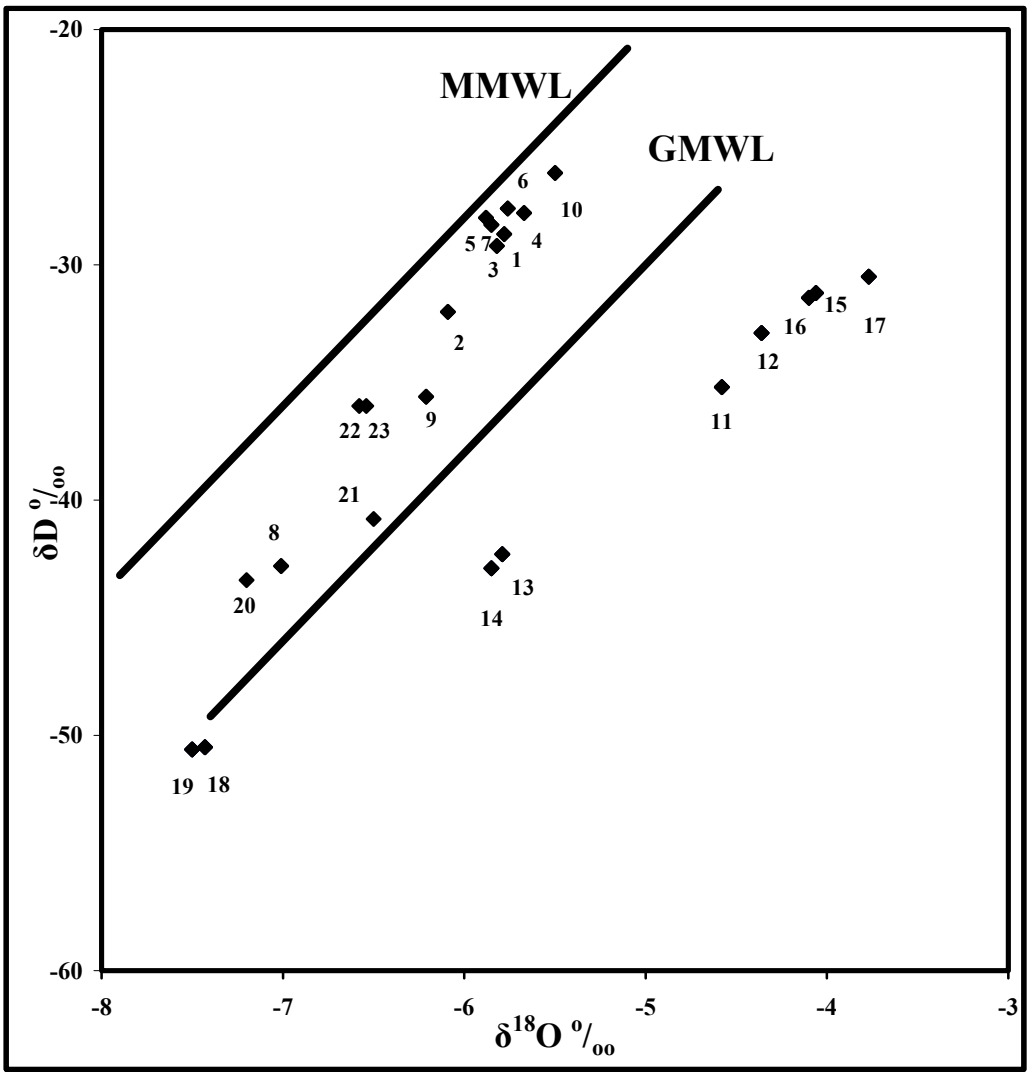

Fig. 5.32: The relationship between $\delta^{18}O$ and δD of the thermal waters along the Dead Sea Transform (DST).

This hypothesis will be discussed in the following; by comparing both the chemistry and the mean residence time of those thermal springs with that of the Dead Sea. Table 5.25 shows the ^{14}C and $\delta^{13}C$ values and the reference for each of EL-Mokhybeh, North Shuneh hot well, El-Hammeh/Maqla spring, TA1 well, TA2 well and Ma'in thermal waters.

Table 5.25: ^{14}C and $\delta^{13}C$ isotope data.

Well/Spring	^{14}C (pmc)	$\delta^{13}C$ ($^{o}/_{oo}$)	Reference
EL-Mokhybeh	16.6 ± 0.9	-12.01	Bajjali et al. (1997)
North Shuneh hot	8.0 ± 1.0	-10.18	Bajjali et al. (1997)
El-Hammeh/Maqla	16.58 ± 0.9	-9.60	Bajjali et al. (1997)
TA1	0.55	-4.10	EL-Naser & Subah (2000)
TA2	0.74	-4.10	EL-Naser & Subah (2000)
Ma'in	2.1 ± 0.7	?	Parker (1970)

Using the ^{14}C measurements, Bajjali et al. (1997) calculated the mean residence time of El-Mokhybeh well, North Shuneh hot well and El-Hammeh/Maqla spring to be 3600, 4500, and 300 years respectively. El-Naser and Subah (2000) calculated the mean residence time of both of TA1 and TA2 wells to be around 31000 years. The residence time of Ma'in thermal waters was calculated to be around 27000 years by using the ^{14}C value of Parker (1970) and by using the dilution factor that was calculated by Bajjali & Abu-jaber (2001) to be 0.53 which is being corrected to eliminate the effect of the dissolution of carbonate by rock-water interaction which lowers the activity of the ^{14}C of ground water by addition of carbon.

By a close look at the mean residence time of the thermal waters and especially the ones that are in the third group and fourth group, it is obvious that partly they coincide with the existence of Lake Lisan, which existed ~70 to 18 Ka. [Kaufman (1971), Kaufman et al.(1992), Stein et al.(1992), Schramm et al. (1995)].

The ages of TA1, TA2 and Ma'in waters are older than the age of the Dead Sea Lake. Also the bromide shows that the Dead Sea is not an endmember for the thermal waters as sown in Fig. (5.18), which indicate that such interpretation is far away from the reality

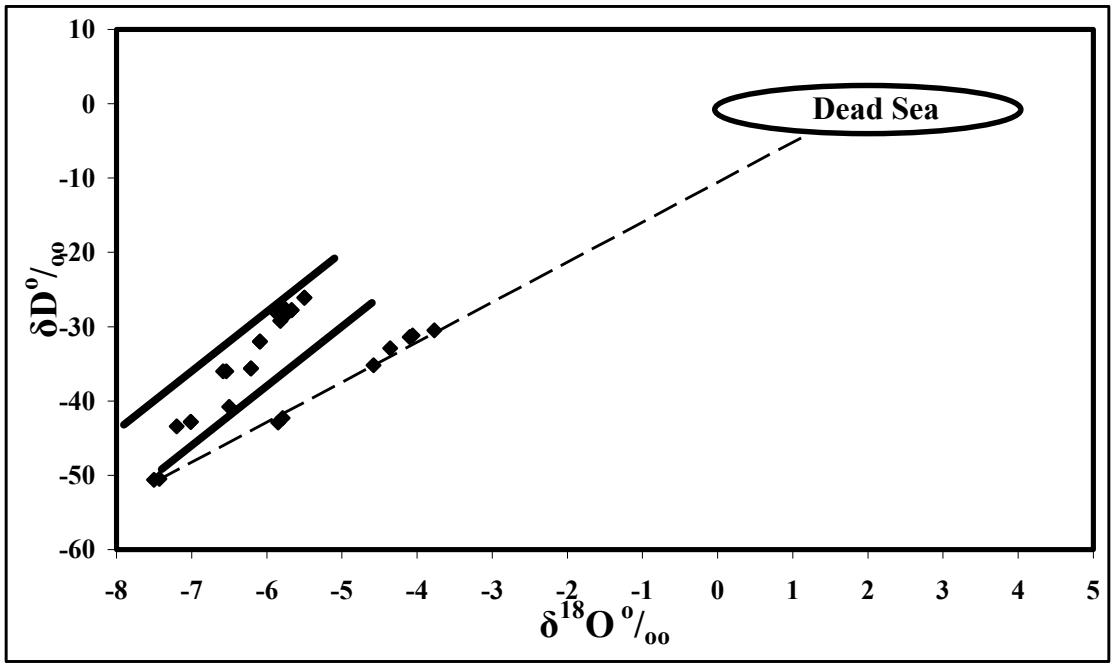

Fig.5.33: The supposed Dead Sea waters mixing line with the thermal waters (TA wells, Ma'in springs, and Zara springs)

Another hypothesis was proposed by Capaccioni et al. (2003), that Ma'in thermal springs waters are a result of meteoric water contaminated with saline waters and those saline waters could represent residual reservoirs of groundwater in equilibrium with those that filled the Dead Sea rift before retreating of Lake Lisan. This hypothesis consider that the water that pertained to Lake Lisan from the intrusion of the Mediterranean sea water as supposed by Kafri and Arad (1979) or remnant of residual ground water pockets that is in

equilibrium with those filling the Dead Sea during the Pliocene-Pleistocene and theyshould have acquired a composition, which is similar to present sea water. The hypothesis proposed that those waters were not significantly evaporated but also isotopically modified (^{18}O enriched) because of the water rock interaction.

This hypothesis seems to be unreasonable for the following reasons:

1. The supposition that there is so called modified sea water is unreasonable because there is no evidence for it or that it could be stored in the aquifers for thousands of years;

2. The salinity of Lake Lisan was 3 to 4 times above recent oceans water especially in the middle part of the lake were the Dead Sea nowadays is located because gypsum was precipitated in this part of the lake (Abed 2000);

3. Bentor (1961) have examined the possible formation of the salts of the Dead Sea by partial evaporation of sea water which was proposed to be entrapped in the Dead Sea rift and concluded that it could be only responsible for one third of the observed salts, and he suggested that the Dead Sea is originating from the Jordan River and two third from the discharge of highly saline springs. Also Abu-Jaber (1998) explained the chemical composition of the Dead Sea by mixing of surface water input with around $50*10^6$ m^3/yr of brines similar to those discharging from the Zohar hot spring (at the western part of the rift), which debate the formation of the salts by invading of the Mediterranean to the Dead Sea rift area;

It is assumed that the data of the third and fourth group plot on an evaporation line (Fig. 5.34) with a regression equation:

$$\mathbf{\delta D=5.65\ \delta^{18}O-8.8\ (r^2=0,99)}$$

This can be further supported by the $\delta^{18}O$-Cl and the δD-Cl relationships (Fig. 5.35 and Fig. 5.36). By plotting $\delta^{18}O$ and δD against Cl it was found that the samples which shows the evaporation effect are located on a line where the Chloride content increase with increasing of the $\delta^{18}O$ and δD values. One anomaly has been noticed: the TA1 well is not located on the $\delta^{18}O$-Cl and δD-Cl trend lines; the high chloride content of this well can be explained by local marine impact on the sedimentation which is reflected on the high chloride content of the TA1 well.

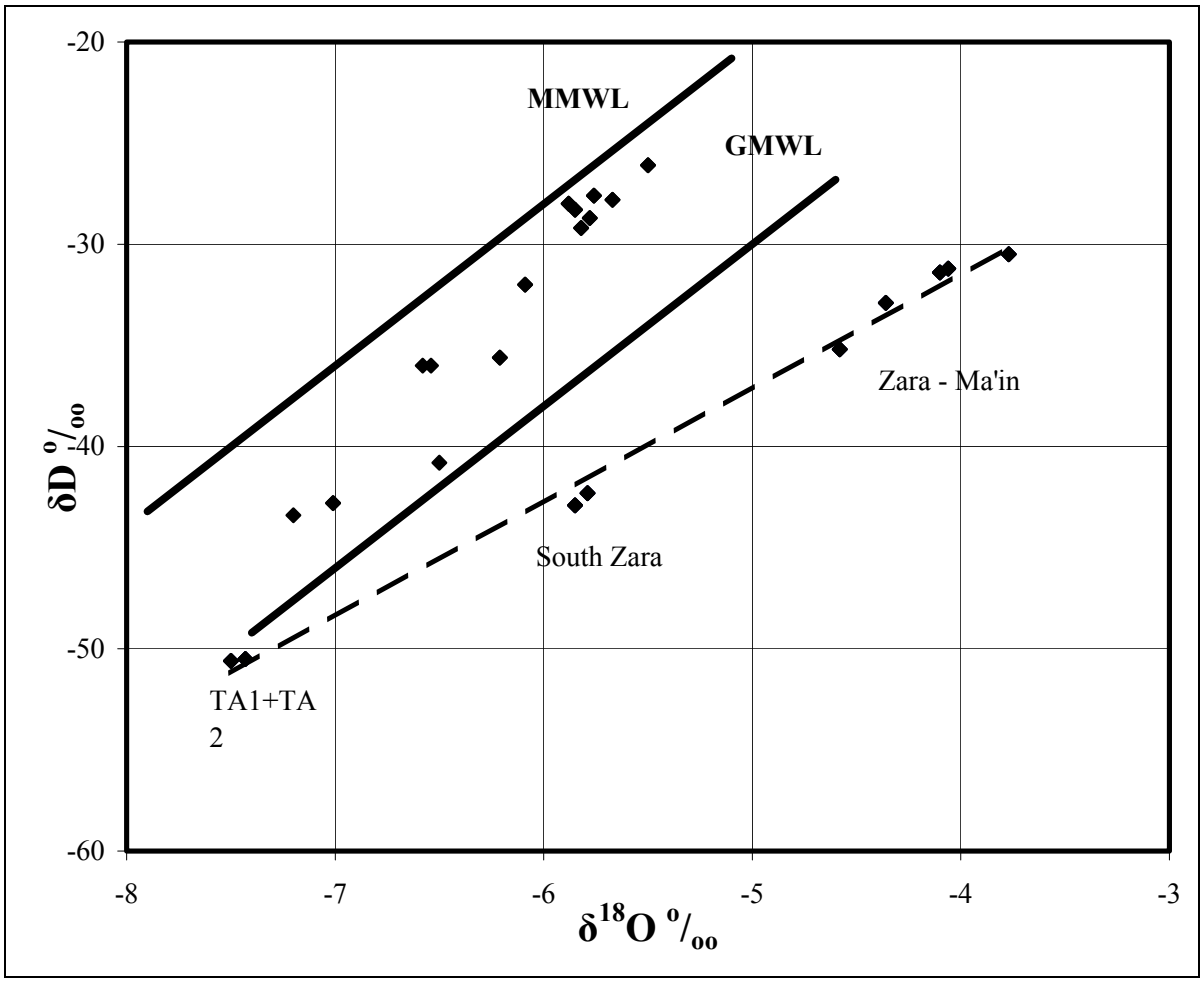

Fig. 5.34: The relationship between the $\delta^{18}O$ and δD for the third and the fourth group producing an evaporation line.

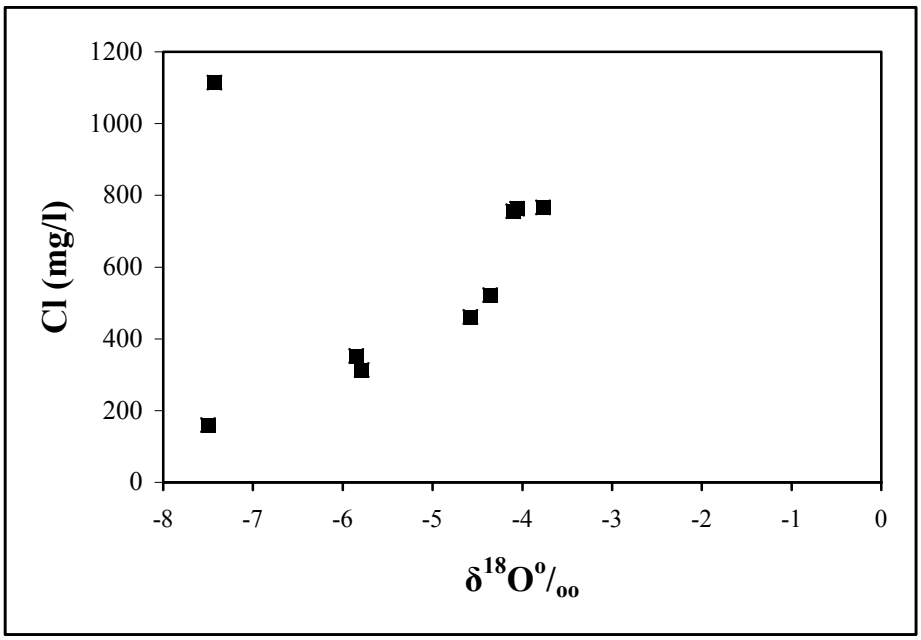

Fig. 5.35: $\delta^{18}O$-Cl relationship with TA1 well far off the trend.

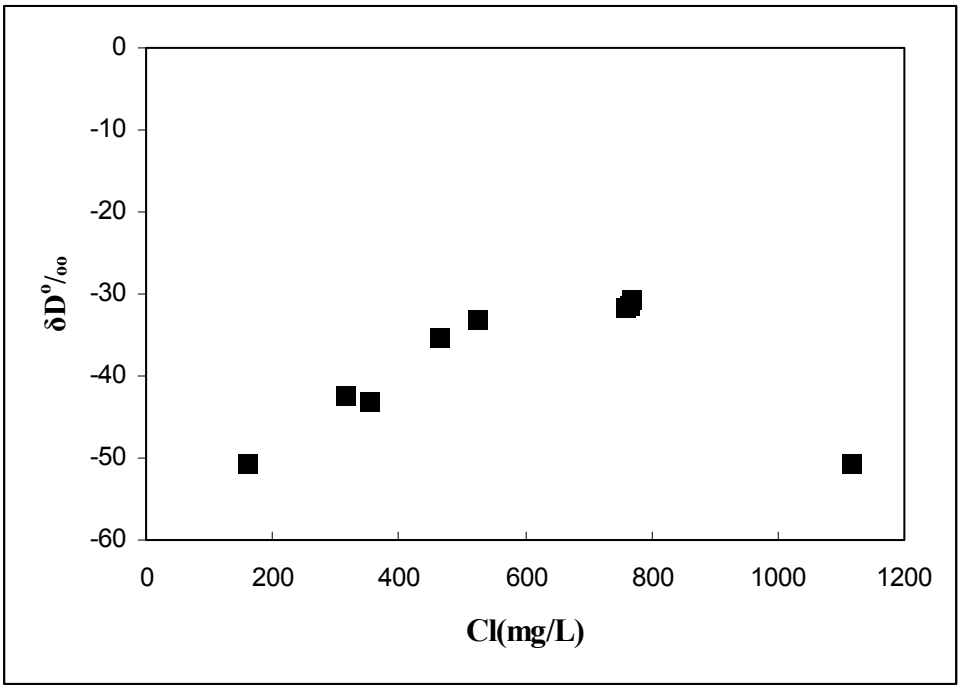

Fig. 5.36: δD-Cl relationship again with the TA1 well being off the trend.

By combining the data which are derived from both Durov classification (Section 5.2.2) and the water stable isotopes ($\delta^{18}O$ and δD) it is clear that the waters of TA wells (TA1 and TA2), south Zara springs (El-Seel El-Hami and Tal El-Rojom) and Zara-Ma'in springs (Zara/Istraha, Zara/Maghara, Ma'in/El-Mabkhara, Ma'in/El-Ameer, Ma'in/El-Shallal) represent the pure lower sandstone aquifer thermal waters which have not suffered mixing effect but they have suffered evaporation effect, though it is possible to use those samples as a comparison tool to detect mixing in other thermal waters especially the ones which are coming from the lower sandstone aquifer (group 2) because those waters (pure lower sandstone aquifer waters) are located in zone (8) on the Durov diagram, which is no mixing zone. If the evaporation effect was removed all of those samples will associate with the GMWL and they will go back to be situated on it (almost on the same location of the TA wells).

Accordingly the lower sandstone aquifer waters, which are located between the (GMWL) and the (MMWL) seems to be resulting from mixing with the (B2/A7) in a different mixing ratios. Fig. 5.32 shows that the isotopic composition of Iben Hammad water is the closest to the composition of the pure lower sandstone aquifer waters, this is being more satisfied because Iben Hammads geographic location is the closest to the TA wells (the pure lower sandstone aquifer waters that was not affected by evaporation).

The effect of mixing with other waters increases in Abu El-Zeeghan/1, Burbyta, Afra springs and the most affected are Abu El-Zeeghan/2. This mixing was proved by a chemical mixing model, using Aquachem (Version 3.7.42) to detect the mixing proportion of the lower sandstone aquifer samples that are located between the GMWL and the MMWL where the pure (B2/A7) water of EL-Naser (1991) (Appendix 22) where used to

mix with the TA2 waters, which is considered to be the more pure lower sandstone aquifer because of its location on the GMWL and its chemistry. The results where found to be encouraging, where it is being found that the lower sandstone aquifer contributes with 60% of the Iben Hammd's water, 38% of the Burbyta's water and between (30-32)% of Afra springs waters, which coincide with the trend in Fig. (5.32). However, the Abu El Zeeghan wells mixing results does not fit to the expected model due to the high salinity of the wells water, which is more than the salinity of the pure B2/A7 waters and the pure lower sandstone aquifer waters which might be interpreted easily because those wells are tapping the Zarqa aquifer which is deeper than the Kurnub and have a higher salinity.

It could be concluded that the thermal waters can be divided into four main groups by using stable isotope data:

1. The thermal waters, which are plotting close to the Mediterranean Meteoric Waters Line (MMWL) and they are mainly from the upper aquifer (B2/A7) signifying recharge, that occurred under climatic conditions similar to those which dominates Jordan and the surrounding areas these days. They are having $\delta^{18}O$ value ranging from -5.5 to -6.09 $^{o}/_{oo}$, δD value ranging between -26.1 and -32 $^{o}/_{oo}$ with d-excess ranging between 16.8 and 19.
2. The thermal waters that are plotting close to the Global Meteoric Water Line (GMWL), which represent the pure lower sandstone aquifer thermal waters that are not being affected by the evaporation effect. They are having $\delta^{18}O$ value ranging between -7.43 and -7.5 $^{o}/_{oo}$, δD value ranging between -50.5 and -50.6 $^{o}/_{oo}$ with d-excess ranging between 9 and 90.4.
3. The thermal waters that are plotting below the Global Meteoric Water Line which represent the lower sandstone aquifer waters that were affected with evaporation effect during precipitation. They are having $\delta^{18}O$ value ranging between -3.77 and -5.85 $^{o}/_{oo}$, δD value ranging between -30.5 and -42.9 $^{o}/_{oo}$ with d-excess ranging between -0.3 and 4.
4. The thermal waters that are located between the Global Meteoric Water Line (GMWL) and the Mediterranean Meteoric Water Line (MMWL) which represent the lower sandstone aquifer thermal waters that are mixed in different ratios with other water sources. They are having $\delta^{18}O$ value ranging between -6.21 and -7.20 $^{o}/_{oo}$, δD value ranging between -35.6 and -43.4 $^{o}/_{oo}$ with d-excess ranging between 11.3 and 16.7.

Those groups were checked statistically by means of Kruskal-Wallis test. The clustering was found to be significant at 0.1 % for both of the variables the $\delta^{18}O$ and δD.

6 SUMMARY AND RECOMMENDATIONS

6.1 Summary

This study attempts to determine origin and mean residence time of the thermal waters along the Dead Sea Transform (DST), the depth and nature of fluid circulation, thermal waters temperature at depths, possible source for the chemical and gaseous constituents, the suitability of the thermal waters for domestic and agricultural purposes, and possible direct uses of the thermal waters. This research tests the quality of different geothermometers for the geological and hydrogeological conditions. It also applies and evaluates new techniques as well as developing of new sampling methodology (gas trapping unit). The conclusions and results are based on the chemical and isotopic composition of the thermal waters and the gases that associate them.

In order to trap the gases, which associate the thermal waters (H_2S, CO_2 and CH_4); a new sampling methodology (gas trapping unit) has been developed and tested in the field. The $PbNO_3$ solution was used to trap the H_2S after adjusting its pH to around 3. The $BaCO_3$ solution was used to trap the CO_2. The $BaCO_3$ solution was also used to trap the CH_4 after being combusted on a Ce_2-ZrO_2-Y_2O_3 mixed oxides catalyst. The catalyst performs 80% efficiency at about 480^oC.

The thermal waters in Jordan taps two aquifers. They are: the upper cretaceous limestone aquifer (B2/A7) and the lower sandstone aquifer (Zarqa and Kurnub), which don't have the same history.

The upper aquifer (B2/A7) waters average temperatures ranges between 32.7 to 52.7 ^oC, while the lower sandstone aquifer have an average temperatures ranging between 37 to 62^oC.

Most of the B2/A7 thermal waters are fresh waters except Abu-Zyad well and Abu-Thableh spring which are Brackish waters, while the waters of the lower sandstone aquifer range between fresh to brackish water type with a high salinity content in Abu El-Zeeghan wells, which tap the high salinity Zarqa aquifer.

The formula [TDS mg/l=0.581 EC µS/cm] represents the relationship between the EC and the TDS for the thermal waters of both the upper aquifer (B2/A7) and the lower sandstone aquifer.

Chemically, the B2/A7 waters are classified as earth alkaline water with increased portions of alkalis, the low salinity waters are with prevailing bicarbonates and the ones that have higher salinity are with prevailing Sulfate and Chloride. The waters type of the Zarqa aquifer (Part of the lower sandstone aquifer) thermal waters change with increasing salinity from earth alkaline water with increased portions of alkalis with prevailing Sulfate and Chloride to alkaline water with prevailing Sulfate–Chloride. The Kurnub aquifer (the upper part of the lower sandstone aquifer) thermal waters type change going from the south

northward from earth alkaline water with increased portions of alkalis with prevailing Sulfate and chloride to alkaline water with prevailing Sulfate-Chloride, this relationship corresponds also with increasing salinity but with one anomaly in the TA1, which have a water type typical of the southern samples.

The lower sandstone aquifer waters contribute in the upper B2/A7 waters in different ratios. It contributes of about 38% in Abu-Zyad well, 34% in Abu-Thableh spring, 26% in El-Hammeh/Maqla spring, 16% in North Shuneh hot well, 12% in El-Hammeh/Bajeh spring, 10% in Al-Kafreen well, 6% in El-Mokhybeh well and the least contribution is found in Waqas well with 4%.

The B2/A7 thermal waters are restricted to the Jordan Valley, their salinity increases with the increase of the lower sandstone aquifer waters contribution. The Zarqa aquifer thermal waters are restricted to the Jordan Valley, their high salinity results from the high confining pressure, Nitrate and Sulfate reduction and the presence of thick layers of Gypsum and Anhydrite. The Kurnub aquifer thermal waters are restricted to the eastern and southeastern parts of the Dead Sea. Its salinity increase generally from the south going northwards.

The thermal waters are mostly nitrate free and release H_2S and CO_2 as a result of oxidation-reduction processes. The Na/Cl ratios (for most of the samples) were found to be around unity, which indicates the halite dissolution. The Ca/SO_4 ratios where found to be higher than the unity. This indicates Gypsum dissolution or Plagioclase weathering. It indicates also deviation towards calcium enrichment. The Na/Ca ratios were found to be increasing with the increasing of the salinity. This indicates a faster dissolution of halite than the Gypsum and the Plagioclase. For the upper aquifer (B2/A7) it was found that the HCO3/Cl is higher than unity, which indicates stronger dissolution of carbonates than Chloride

The thermal waters are undersaturated with respect to Halite, Gypsum and Anhydrite. The B2/A7 waters are slightly over saturated with respect to Calcite and Dolomite. The lower aquifer thermal waters are over saturated with respect to Calcite and Dolomite, which increase with the increasing of the salinity.

The thermal waters clustered statistically into two main groups: A and B. group A consist of two subgroups: A_1 and A_2. Group A_1 includes the fresh water wells and springs that have the lowest salinity of the studied thermal waters and consist of two subgroups: A_{1a}, which represent the thermal waters that tap the lower sandstone aquifer (Kurnub aquifer) but their chemical characteristics are similar to the upper aquifer (B2/A7) waters; group A_{1b} which includes the thermal waters that tap the upper aquifer (B2/A7). Group A_2 includes the brackish wells and springs that tap the lower sandstone aquifer (Kurnub aquifer) and the upper aquifer (B2/A7). It includes the Ma'in and Zara springs plus two thermal waters from the upper aquifer (B2/A7): Abu-Zyad and Abu-Thableh, which have a high percent of Kurnub water contribution. Group B includes the thermal waters that tap

the lower sandstone aquifer (Zarqa aquifer) and have the highest salinity of the studied thermal waters.

All the statistically clustered groups have different fingerprints from that of the Dead Sea. It seems that the Dead Sea is not an end member of those groups. Group A_{1a} is characterized by Na>Ca>Mg>K and Cl>HCO_3>SO_4 for the TA2 and Iben Hammad and Ca>Na>Mg>K and HCO_3>Cl>SO_4 for Burbyta, Afra/Sawnaand Afra/Maqla. Group A_{1b} is characterized by Ca>Na>Mg>K and HCO_3>Cl>SO_4 except Waqas that is characterized by Ca>Mg>Na>K and HCO_3>SO_4>Cl. Group A_2 is characterized by Na>Ca>Mg>K and HCO_3>Cl>SO_4 for the upper aquifer part of this group and by Na>Ca>Mg>K and Cl>HCO_3>SO_4 for the upper aquifer part of this group. Group is characterized by Ca>Na>Mg>K and HCO_3>Cl>SO_4 for Abu El-Zeeghan/1 and Na>Ca>Mg>K and Cl>HCO_3>SO_4 for El-Zeeghan/2.

The Na/K geothermometers don't yield a meaningful equilibrium temperature because all the thermal waters found to be immature on the Giggenbach diagram. The Na-K-Ca geothermometer gave high reservoir temperatures but the Mg correction of this geothermometer lowers the results but still in some cases, it gives a very low reservoir temperature. The K/Mg geothermometer was found to be suitable for the upper aquifer (B2/A7) but not for the lower sandstone aquifer because it gives a very low reservoir temperature. The Chalcedony geothermometer was found also to give low reservoir temperatures, which is not acceptable in this case. The Quartz, Quartz steam loss and the Isotope SO_4-H_2 geothermometer (after Kuskabe (1974)) were found to be suitable for calculating the reservoir temperatures. The other SO_4-H_2 Isotope geothermometers gave higher estimated reservoir temperatures.

The upper aquifer (B2/A7) circulation depth was found to be ranging between 1533.33 m to 2300 m. The Zarqa aquifer circulation depth in was found to be ranging between 1533.33 m to 1666.67 m. The Kurnub circulation depth was found to be ranging between 1533.33 m to 1900 m.

On the $\delta^{34}S_{Sulfate,}$ $\delta^{18}O_{Sulfate}$ diagram, the thermal waters plot on a mixing line between two end members and they are: the evaporites and the oxidation of sulphides members, where most of the samples Sulfate is caused by the dissolution of the evaporites from the rock matrix while the samples that are not located with in the first end member region like 10 (Al-Kafreen well), 22 (Afra/Sawna) and 23 (Afra/Maqla) are showing other sources which might be a mixture between atmospheric and soil Sulfate sources, but most probably that those samples are more affected by the second end member of the mixing line, which is the oxidation of sulphides.

The Bajeh spring is a mixture between El-Mokhybeh wells and Maqla Spring because it is located in the middle between both of the afore mentioned thermal waters on the δD-$\delta^{18}O$ diagram and the $\delta^{34}S_{Sulfate}$-Sulfate concentration diagram. The El-Mokhybeh well contributes with around 64% of the Bajeh waters while the Maqla spring contribute with the rest (36%).

The Sulfate concentration and the $\delta^{34}S_{Sulphate}$ of the lower sandstone aquifer increase from the south to the north. This phenomenon is explained by plotting the samples on the $\delta^{34}S_{sulfate}$-$\delta^{18}O_{sulfate}$. The samples were found to be plotting on a mixing line between two end members, which are evaporite and oxidation of sulphides. However the southern samples are close to the second end member and they are affected by the oxidation of sulphides.Because of that; the sulfate concentration in the south is decreasing.

The $\delta^{13}C_{CO2}$ of the thermal waters were found to be ranging between -16.9 and -22.9 $^{o}/_{oo}$. By comparing those values with the $\delta^{13}C_{HCO3}$ that range between –4.10 and -12.01, the system was found to be not in equilibrium, which means that the CO_2 have other sources. Most probably that the CO_2 is derived from oxidation-reduction processes of the organic matter present in the rock matrix or favoured reaction with the acetic acid left after oil migration.

The thermal waters analysis show that the constituents that affect the health significant are with in the acceptable limits of the Jordanian standards and the WHO guidelines, while most of the thermal waters suffer from hardness and the presence of some constituents that affect the aesthetic characteristics and the taste of these waters.

The suitability of the thermal waters for irrigation purposes was also studied. Most of the thermal waters range based on the salinity between C3 and C4 water class. The C3 water class means that the salinity will adversely affect most plants which requires a salt tolerant plants while C4 means that generally those waters are not acceptable for irrigation purposes except only for very salt tolerant plants and both types requires a good to excellent drainage and careful irrigation. The Waqas, Burbyta, Afra springs (Maqla and Sawna) thermal waters were found to have C2 water class, which requires a moderately leaching to prevent salt accumulation in the soil that cause sensitive plants to show stress.

The upper aquifer (B2/A7) thermal waters have good soluble sodium Percent (SSP). The lower sandstone aquifer thermal waters range between permissible to doubtful except Burbyta and Afra springs, which show a good SSP-class. TA1 and Abu El-Zeeghan/1 are having also a good class but they have high salinity (>3000 mg/l), which is not suitable according to the EC classification.

Most of the thermal waters are showing a low sodium (alkali) hazard (S1) except Abu El-Zeeghan/1 well, which has a medium hazard (S2).

The thermal waters show a negative residual sodium carbonate (RSC), which means that the sodium build up is unlikely to happen since sufficient calcium and magnesium are in excess of what can be precipitated as carbonates when the waters are applied to the soils.

The upper aquifer (B2/A7) thermal waters are balanced in comparison to Langlier saturation index except in Al-Kafreen well, which shows aggressive behaviour. The lower sandstone aquifer waters show a wide range from scale forming to aggressive.

The thermal waters range between mild scale coating to mild scale corrosion. Mainly the upper aquifer (B2/A7) thermal waters are near balanced except Al-Kafreen, which is showing a non-mild corrosion. The Abu El-Zeeghan/2, Ma'in/El-Shallal and Burbyta are the only thermal waters that need treatment.

The thermal waters are used directly now a days for swimming, bathing and balneology. The thermal waters could be used in the future for space conditioning, district heating and agriculture and aquaculture applications.

The thermal waters are Tritum free, which indicates, that all those water components are old and the recharge have occurred before 1952 (prior the era of thermonuclear bomb testing) or the share of younger water (recharged after 1952) is very small

The $^{3}H/^{3}He$ age determination method was found to be not suitable to give a mean residence time estimation. The calculated mean residence time was estimated to be between ≥ 120 to ≥ 160 a. but if the calculation were done in a reversal way (calculation of the tritium concentration depending on the tritium half life); the Tritium concentration would be around 2950 TU. Such tritium concentration existed only in the period between 1960 and 1963. By adding 120 to the 160 and to the 1960; that will end in the year 2080 to 2020. The $^{3}H/^{3}He$ equation has failed in providing the right mean residence time because additional Helium (not a Tritium decay product) has invaded the system.

The TA1 and TA2 wells are having helium isotopic signatures, which are close to the crustal Helium values. The other measured samples were found to have more value than that. Still if the Helium is gained only from the crust, then the samples helium istopic signatures should be much lower following the Helium production line. The extra helium is assumed to be coming from the mantle exhalation bounded more or less to the deep faults in the Dead Sea Transform.

The B2/A7 thermal waters are associated with the Mediterranean meteoric water line (MMWL). This gives a good proof that those waters occurred under climatic conditions that are dominating Jordan and the surrounding areas those days. The thermal waters of the lower sandstone aquifer are distributed in three groups on the δD-$\delta^{18}O$ diagram: the first group is associated with the Global meteoric water line (GMWL), which indicate the pure lower sandstone aquifer thermal waters that are not being affected by the evaporation effect; the second group are located below the GMWL, which indicate the lower aquifer waters that were affected with evaporation effect during precipitatation; the third group is located between the Global meteoric water line and the Mediterranean meteoric water line which represent the lower aquifer thermal waters that are mixed in different ratios with other water sources.

6.2 Recommendations

The following procedures are recommended to enhance the suitability of the thermal waters for both domestic and agricultural purposes as well as to enhance the suitability of theses thermal springs for further research approaches:

- Use of water softener in order to reduce the water hardness in some of the thermal waters.

- Mixing of the thermal waters that have a high EC values with other fresh water resources in order to be used for drinking purposes in order to be dilute the constituents that affect the taste of the waters.

- Rehabilitation of the springs and the flowing wells by constructing orifices for further scientific applications like sampling by the use of helium copper tubes which requires a small orifice springs or wells.

- Rehabilitation of the thermal waters pools for therapeutic and touristic purposes and construction of storage facilities to protect the waters against contamination activities.

- Establishing projects to benefit directly from the thermal energy like buildings and districts heating, animal farming, soil warming, irrigation, bio-gas generation and fish farms

6.2.1 Recommended studies

The following are recommended studies:

- Drilling deep exploration wells. Building a flow and transport model of the deep aquifers for a better understanding of the relationship between the aquifers.

- Compilation of a long-term rain isotopic database for stable water isotopes.

- Determining the local meteoric water line based on the stable isotopes analysis of δD and $\delta^{18}O$ of the precipitation for further future comparisons and studies.

- Analysis of ^{14}C and $\delta^{13}C$ for the thermal waters for a better view of the study of the thermal waters.

- Determining the amount of thermal water flow to the Dead Sea by the means of radon isotopes and arial thermal photography, EC depth profiling, and Radon investigations.

- Construction of a database and long term monitoring of the thermal waters in order to determine the chemistry fluctuation.

- Further development of the gas-trapping unit (established in this study) to be able to quantify the amount of gasses and to determine the efficiency of this unit in gas precipitating.

7 REFERENCES

ABED, A. AND HELMDACH, F. (1981): Biostratigraphy and Mineralogy of the Lisan series (Pleistocene) in the Jordan Valley. Berliner geowissen. Abh. Verlag von Dietrich Reimer, Berlin, 32: 123-133.

ABED, A. M. (1983): Paleoclimates of the uppermost Pleistocene in the Jordan rift. Studies in the History and Archaeology of Jordan, II, Editted by A. Hadadin. Amman, Dept. of Antiquities, 81-93.

ABED, A. M. (1985): Geology of the Damya Formation, Dirasat, Vol.12, No.2: 99-108.

ABED, A. M. (1989): On the genesis of the phoshorite-chert association in the Amman Formation in Tel es Sur area, Ruseifa, Jordan. Science Geologie Bulletin, Strasbourg, 42: 141-153.

ABED, A. M. (2000): The Geology of Jordan, 2nd edition, publication of Jordanian Geologists Association. The new printing and binding company, Jordan, 571 p.

ABED, A. M. AND KRAISHAN, G. M. (1991): Evidence for shallow marine origin of a (Monterey Formation type) chert-phosphorite-dolomite association: Amman formation, Late Cretaceous, central Jordan. Facies, 24: 25-38.

ABED, A., Al-Sbaeay, I. And Khbeis, S. (1990): The Dead Sea: A recent survey of its waters. Proc. Third Jordanian Geol. Conf., 446-472.

ABTEILUNG OZEANOGRAPHY (2000): Edelgas-Isotopenanalyse. Institut für Umweltphysik, Universität Bremen.
http://www.noblegas.uni-bremen.de/edelgas.html (7/9/2003)

ABU AJAMIEH, M. (1980): The geothermal resources of Zarqa Ma'in and Zara. Report of phase-1 of the geothermal energy project in Jordan, Natural Resources Authority, Amman, 82 p.

ABU-JABER, N. (1998): A new look at the chemical and hydrological evolution of the Dead Sea. Geochim. Cosmochim. Acta., 62:1471-1479.

ABU-JABER, N., KIMBERLEY M. AND CAVAROC, V. (1989): Mesozoic-Paleoogene basin development within the eastern Mediterraneanborder land. J. Petrol. Geol., 12: 419-436.

ABU-JABER, N.S. AND WAFA, N.A. (1996): Hydrochemistry of aquifers in the southern Dead Sea area, Jordan. Env. Geol., 28: 213-222.

ABU-ZIR, M. (1989): Hydrochemistry and hydrology of the central part of Wadi Araba. Unpub. M.Sc. Thesis, University of Jordan, Amman.

AL-TAJ, M. (2000): Active faulting along the Jordan valley segment of the Jordan-Dead Sea Transform. Unpub. PhD. Dissertation, Jordan University, Amman, 233p.

AMERICAN PUBLIC HEALTH ASSOCIATION (1995): Standard method for the examination of water and wastewater. 16th edition, Washington, DC, USA.

AMIEREH, B. (1991): Mineral composition of the Cambrian-Cretaceous Nubian Series of Jordan: provenance, tectonic setting and climatology implications. Sedimentary Geology, 71:99-119.

AMIEREH, B. (1993): New occurrence of the Disi Sandstone Formation (Early ordovician) in central Jordan, Dirasat, 20B (3):21-44.

AMIEREH, B., SCHNEIDER, W. AND ABED, A. (1994): Diagenesis and burial history of the Cambrian-Cretaceous sandstone series in Jordan, N. Jb. Geol. Palaont. Abh., 192(2):151-181.

ANATI, D. AND SHASHA, S. (1989): Dead Sea surface-Level changes. Isr. J. Earth Sci., 38: 29-32.

ANATI, D. AND STILLER M. (1991): The post-1979 thermohaline of the Dead Sea and the role of double-diffusive mixing. Limnol. Oceanogr. 36: 342-354.

ARAD, A. AND BEEIN, A (1986): Saline versus fresh water contribution to the thermal waters of the northern Jordan rift valley. J. Hydrol., 83:49-66.

ARSALAN, F. A. (1976): Geologie und Hydrogeologie der Azraq Depression (Ost-Jordanien). Dissertation, Teshniche Hochschule Aachen, Aachen. 185 p.

ATTALAH, M. (1992): On the structural pattern of the Dead Sea Transform and its related structures in Jordan, Abhath Al-Yarmouk, Jordan , 1: 127-143.

AYALON, A., BAR-MATHEWS, M. AND SASS, E. (1998) Rainfall-recharge relationships within a Karstic terrain in the Eastern Mediterranean semi-arid region, Israel: $\delta^{18}O$ and δD characteristics. J. Hydrol., 207: 18-31.

AYERS, R. S. AND WESTCOT, D. W. (1994): Water quality for agriculture. FAO irrigation and drainage paper. FAO, Rom.
http://www.fao.org/DOCREP/003/T0234E/T0234E00.htm#TOC (30.10.2005)

BAJJALI, W. AND ABU-JABER, N. (2001) Climatological signals of the paleogroundwater in Jordan. J. Hydrol. 243: 133-147.

BAJJALI, W. T. (1994): Recharge and regional circulation of thermal groundwater in Northern Jordan using isotope geochemistry. Unpub. Ph.D. Thesis, University of Ottawa, Canada, 257 p.

BAJJALI, W., CLARK, I. D. AND FRITZ, P. (1997): The artesian thermal ground waters of northern Jordan: insight into their recharge history and age. J. Hydrol. 192: 355-382.

BANDEL, K AND KHOURY, H. (1981): Lithostratigraphy of Triassic in Jordan. Facies, 4: 1-26.

BANDEL, K. (1981): New stratigraphic and structural evidence for lateral dislocation in the Jordan rift valley connected with the description of the Jurassic rock column in Jordan. N. Jb. Geol. Palaont. Abh., Stutgart,161: 271-308.

BANI SAKHIR, Z. (1996): Lithofacies, Paleoenvironment and Paleoclimatic changes of the Quaternary sediments (Lisan Formation) east of the southern basin of the Dead Sea. Unpub. M.Sc. Thesis, Yarmouk University. Irbid, Jordan.

BASHA, S. (1978): Foraminifera from the Ajloun Group of the east Jordan. J. Geol. Soc. Iraq, 11: 67-91.

BASHA, S. (1981): Distribution of Triassic rocks in Jordan and the Levant, Dirasat, 9: 49-67.

BEGIN, Z. (1975): The Geology of Jericho Sheet (1:50,000). Bull. Geol. Surv. Israel, 67: 1-35.

BEGIN, Z., EHRILCH, A. AND NATHAN, Y. (1974): Lake Lisan: The Pleistocene precursor of the Dead Sea. Geol. Surv. Isr. Bull., 63:1-30.

BELBEISI, M. (1992): Jordan's water resources and the expected domestic demand by the years 200 and 2010, detailed according to area. In: Jordan water resources and their

future potential, Symposium Proceedings, 27-28 Oct. 1991. Friederich Elbert Stiftung, Amman, Jordan.

BENDER, F. (1968): Geologie von Jordanien,Borntraeger, Berlin, 230 p.

BENDER, F. (1974): Geology of Jordan, , Borntraeger, Berlin, 196 p.

BENDER; F., HOBLER, M. AND RASHDAN, J. (1991): New aspects of the groundwater system of Jordan, Geology of Jordan. Goeteh-Institute, Bundesanstalt für Geowissenschaften und Rohstoffe, Hannover, Amman-Jordan.

BENTOR, K. B. (1961): Some geochemical aspects of the Dead Sea and the question of its age. Geoch. Cosmochim. Acta, 25: 239-260.

BURDON, D. J. (1959): Handbook of the geology of Jordan. Benham and company limited, Colchester.

CAPACCIONI, B., VASELI, O., MORETTI, E., TASSI, F. AND FRANCHI, R. (2003): The origin of thermal waters from the eastern flank of the Dead Sea rift (western Jordan). Terra Nova, 15(3): 145-154.

CARMI, I,, GAT, G. AND STILLER, M. (1984): Tritium in the Dead Se. Earth Planet. Sci. Lett., 71: 377-389.

CARMODY, R. W., PLUMMER, N. L., BUSENBERG, E. AND COPLEN, T. B. (1998): Methods for collection of dissolved sulfate and sulfide and analysis of their sulfur isotopic composition. Open-File Report 97-234. U.S.Geological Survey (USGS).Reston, Virgina. 91 p.

CAROLL, D. (1962): Rain water as a chemical agent of geologic processes- A review. US Geological Survey, Water supply paper, 1535-G, 18 p.

CENTER FOR ISOTOPE GEOCHEMISTRY (2004): Noble gas isotope geochemistry, Lawrence Berkeley National Laboratory.
http://www-esd.lbl.gov/CIG/noblegas/georesources.html (8/9/2004)

CLARK, I. AND FRITZ, P. (1997): Environmental isotopes in hydrogeology, Lewis publisher, Boca Raton, 328 p.

COLLEGE OF AGRICULTURAL SCIENCES (2002): Irrigation water quality. The Pennsylvania State University, USA.
http://www.cas.psu.edu/docs/casdept/Turf/Education/Turgeon/CaseStudy/OldRanch/IrrWatQual.html (6.6.2004).

COURTILLOT, V., ARMIJO, R. AND TAPPONIER, D. (1987): The Sinai triple junction revisited. In Ben Avraham, Z. (ed.): Sedimentary basin within the Dead Sea and other rift zones. Tectonophysics. 141: 181-190.

COX, L. R. (1932): Further notes on Transjordan Trias. Annals and Magazine of Natural History, London, 10: 93-113.**CRAIG, H. (1961):** Isotopic variations in meteoric waters. Science, 133: 1702-1703.

D'AMORE, F. AND ARNORSSON, S. (2000): Geothermometry. 152-200, In Arnorsson, S. (eds): Isotopic and Geochemical techniques in geothermal exploration development and use. International Atomic Energy Agency (IAEA), Vienna, 351 p.

DANSGAARD, W. (1964): Stable isotopes in precipitation. Tellus 16, 436 p.

DIABAT, A. (2004): Structural map of Jordan. Unpublished report, Natural Resources Authority, Amman, Jordan.

DILLEY, F.C. (1985): Cretaceous correlation in the Hamza wells 1-5. Natural Resources Authority, Paleontological report 6.

EL-HIYARI, M. A. (1985): The Geology of Jabal Al Muttaramil. Bull. 1, Geological Mapping Division., Geology Directorate., Natural Resources Authority, Amman, Jordan.

EL-NASER, H. AND SUBAH, A. (2000): Using hydrochemistry and environmental isotopes to define the groundwater system of the Ain Maghara spring, Jordan. Quarterly J. of Eng. Geol. and Hydrogeol. The geological society of London, 33: 87-96.

EL-NASER, H. AYED, R. AND AL-MOMANI, M.(1992): Effect of 1991/1992 rainfall on the groundwater recharge of Yarmouk and Wadi Al Arab basins, Internal report, WAJ, Amman-Jordan, 28 p.

EL-NASER, H.(1991): Groundwater resources of the deep aquifer system in NW Jordan-hydrogeological and hydrochemicl quasi three-dimensional modelling. Heft 3 von Hydrogeologie und Umwelt, Würzburg, Germany.

ERAIFEJ, N. AND ABU-JABER, N. (1999): Geochemistry and pollution of shallow aquifers in the Mafraq area, North Jordan. Env.l Geol., 37(½): 163-170.

EXACT-EXECUTIVE ACTION TEAM (2004): Multilateral working group on water resources, water data bank project.
http://exact-me.org/overview (10/8/2004)

FELIPE, M. A., KUBICKI, J. D. AND FREEMAN, K. H. (2005): A mechanism for carbon isotope exchange between aqueous acetic acid and CO2/HCO3-: An ab initio study. Organic Geochemistry, 36(6): 835.

FERRONSKY, I. V. AND POLYAKOC (1982): Environmental isotopes in the Hydrosphere, New York, Wiley and Sons.

FLANIGAN, V. J. AND EL KAYSI, Q. (1984): Preliminary interpretation of audio-Magnetotelluric (ATM) sounding in the Zara-Zarqa Ma'in geothermal areas. Kingdom of Jordan, Preliminary report, USGS.

FONTES, J. (1980): Environmental isotopes in ground water hydrology. In Fritz and Fontes (eds): handbook of environmental isotope geochemistry. Vol.1, Elsevierscientific publishing company.

FONTES, J. CH. AND GARNIER, J. M. (1979): Determination of initial ^{14}C activity of the total dissolved carbon: A review of the existing models and a new approach, Water Res., 15 (2): 399-413.

FONTES, J. CH. AND ZUPPI, G. M (1976): Isotopes and water chemistry in sulphide-bearing springs of central Italy. In: International of environmental isotope and hydrochemical data in groundwater hydrology. IAEA,Vienna, 143-158.

FOURNIER, R. O. (1973): Silica in thermal waters: Laboratory and field investigation. Proc. Int. Symp. Hydrogeochemistry and Biogeochemistry, Tokyo, 122-139.

FOURNIER, R. O. (1977): Chemical geothermometers and mixing models for geothermal systems. Geothermics, 5: 41-50.

FOURNIER, R. O. (1979): A revised equation for the Na/K geothermometer. Geotherm. Res. Counc. Trans. 5: 1-16.

FOURNIER, R. O. AND POTTER, R. W. (1979): Magnesium correction to the Na-K-Ca chemical geothermometer. Geochim. Cosmochim. Acta, 43: 1543-1550.

FRAGA, M.A., APPEL, L.G., SOARES DE SOUZA, E.(2002): Combustion of methane over catalyst supported on CeO_2-ZrO_2 and CeO_2-ZrO_2-Y_2O_3 mixed oxides. In: American Chemical Society National Meeting, Orlando, 223 p.

FREEZE, R.A. and CHERRY, J.A. (1979): Ground water. Hall Inc., New Jersey.

FREUND, R., GARFUNKEL, Z., ZAK, I., GOLDBERG, M., WEISBROD, T. AND DERIN, B. (1970): The shear along the Dead Sea rift. Phil.Trans. Roy. Soc. London, 267: 107-130.

FRICKE, H.C. AND O'NEIL, J.R. (1999): The correlation between $^{18}O/^{16}O$ ratios of meteoric water and surface temperature: its use in investigating terrestrial climate change over geologic time. Earth Planet. Sci. Lett. 170: 81-196.

FRIEDMANN, A. (1913): Beiträge zur chemischen und physikalishen untersuchung der Thermen Palästinas.Ges.F. Palästina-Forschung 4, Berlin.

FURTAK, H. AND LANGGUTH, H. R. (1967): Zur hydro-chemischen Kennzeichnung von Grundwässern und Grundwassertypen mittels Kennzahlen.-Mem. IAH-Congress, 1965, Hannover, VII: 86-96.

GALANIS, S. P., SASS, J.H., MUNROE, R.J. AND ABU AJAMIEH (1986): Heat flow at Zarqa Ma'in and Zara geothermal reconnaissance of Jordan. USGS.

GARFUNKEL, Z. (1981): Internal structure of the Dead Sea leaky transform (rift) in relation to plate kinematics, Tectonophysics, 80: 81-108.

GARFUNKEL, Z. (1997): The history of the Dead Sea Basin. 36-56, In Niemi, T., Ben-Avraham, Z. and Gat, J. R. (eds.): The Dead Sea-The lake and its setting. Oxford monograms on geology and geophysics no. 36. Oxford University press.

GARRELS, R. M. AND MACKENZIE, F.T. (1967): Origin of the chemical composition of some springs and lakes. In Gould, R. F. (ed.): Equilibrium concepts in Natural waters, Advances in chemistry Ser., Washington DC, American chemical Society, 67: 222-242.

GAT, J. (1980): The isotopes of hydrogen and oxygen in precipitation. In Fritz and Fontes, J. Ch.(eds.): Hand book of Environmental isotope Geochemistry. Elsevier, Amesterdam, 1: 21-47.

GAT, J. (1996): Oxygen and Hydrogen isotopes in the hydrogeologic cycle. Annu. Rev. Earth Planet. Sci. 24: 225-262.

GAT, J. AND CARMI, I. (1970): Evolution of the isotopic composition of atmospheric waters in Mediterranean Sea area. J. Geophys. Res., 75: 3039-3078.

GAT, J. AND MARGARITZ, M. (1980): Climatic variation in the eastern Mediterranean Sea area. Naturwissenschaften 67:80-87.

GAT, J. R. AND GNFIANTINY (EDS.) (1981): Stable istope hydrology, deuterium and oxygen-18 in the water cycle. Tech. Rep. Series No. 210.

GERMAN GEOLOGICAL MISSION (1961-1966): Final Report F. N. R. A. Unpub1. Amman and Geol-Surv of Fed. Repub. Germany, Hannover.

GEYH, M. A. AND SCHLEICHER, H. (1990): Absolute age determination- Physical and chemical dating methods and their application. Springer Verlag, Berlin, Heidelberg, 501 p.

GIGGENBACH, W. F. (1988): Geothermal solute equilibria. derivation of Na-K-Mg-Ca geoindicator. Geochim. Cosmochim. Acta, 52: 2749-2765.

GNIP AND ISOHIS-GLOBAL NETWORK OF ISOTOPES IN PRECIPITATION AND ISOTOPE HYDROLOGY INFORMATION SYSTEM (2002): Isotope hydrology projects, IAEA.
http://isohis.iaea.org/projects.asp (7/9/2004)

GTZ AND NRA (1977): National master plan of Jordan. Agrar and Hydrotechnik GMBH (AHT) and Fed. Inst. for Geosc. and Nat. Res. (BGR), Vol. I-IV. Hannover, Frankfurt, Amman.

GUDMUNDSSON, J. S., FREESTONE, D. H. AND LINEAU, P. J. (1985): The Lindal diagram. Geothermal Resources Council Transaction. 9(1): 15-19.

GVIRTZMAN, H. AND STANISLAVSKY, E. (2000a): Large-scale flow of geofluids at the Dead Sea Rift. J. Geoch. Expl., 69-70: 207-211.

GVIRTZMAN, H. AND STANISLAVSKY, E. (2000b): Palaeohydrology of hydrocarbon maturation, migration and accumulation in the Dead Sea Rift. J. Geoch. Expl. 69–70: 207–211.

GVIRTZMAN, H., GARVEN, G. AND GVIRTZMAN, G. (1997): Thermal anomalies associated with forced and free ground-water convection in the Dead Sea rift valley. GSA Bulletin.109(9): 1167-1176.

HACH COMPANY (1993) Calculating the langlier Saturation index, Lit. No. 5431 Part No. 25987-87, USA.
http://ecommerce.hach.com/stores/hach/pdfs/literature/L5431.pdf (6/7/2003)

HAKKI, W. AND TEIMEH, M. (1981): The geology of Zarqa Ma'in and Zara area. Naural Resources Authority. Amman, Jordan.

HAMMAM, K. (1977): Foraminifera from the Mastrichtian-bearing strata of El-Hasa, Jordan. Journal of Froaminiferal Research 7: 177-186.

HARDIE, L. (1990): The roles of rifting and hydrothermal CaCl2 brines in the origin of potash evaporates: An hypothesis. Amer. J. Sci 290: 43-106.

HOROWITZ, A. (1979): The Quaternary of Israel: Academic Press, New York, 394 p.

HUMPHREYS, H. AND SONS(1978): Water use strategy, North Jordan. 2 Vol., London, Amman.

JACOBY, A. (1905): Das Geographische Mosaik von Madba. Die älteste Karte des Heiligen landes Studien über christliche Denkmäler, neue Folge 3, Leipzig (Dietrischer Verlag).

JARADAT, Q. M., MOMANI, K. A., JIRIES, A. G., EL-ALI, A. BATARSEH, M, I., SABRI, T. G. AND AL-MOMANI, I. F. (1999): Chemical composition of urban deposition in Amman, Jordan. Water, Air and soil pollution, Kulwer Academic Publishers. Netherland. 112: 55-65.

JARRAR, G. H. (1991): Petrology and geochemistry of Triassic subvolcanic suit from central Jordan, East of the Dead Sea, Mutah, 6:183-196.

JARRAR, M. (1989): Organic geochemistry of Wadi Shallala area, Unpub. M.Sc. Thesis, Yarmouk University.

JICA-JAPAN INTERNATIONAL COOPERATION AGENCY (1995): The study on brackish groundwater desalination in Jordan. - Yachiyo Engeneering CO., Ltd, and Mitsui Mineral Development. Engineering CO., Ltd., (main & support interim report), Tokyo, Japan. 318 p.

JISM-JORDAN INSTITUTION FOR STANDARDS AND METROLOGY (2001): Jordanian standards for drinking water, JS 286, 4th Ed. Jordan.13 p.

JOUDEH, O. (1983): Evaluation of groundwater resourced in the deep aquifer in northwest Jordan. Open file, J.V.A, Hydrology and Groundwater Directorate, Amman, 67 p.

KAFRI, U. AND ARAD, A.(1979): Current subsurface intrusion of Mediterranean seawater- A possible source of groundwater salinity in the rift valley system. Israel. J. Hydrol., 44: 267-287.

KAUFMAN, A. (1971) U-Series dating of the Dead Sea carbonates. Geochim. Cosmochim. Acta, 35: 1269-1281.

KAUFMAN, A., YECHIELI, Y. AND GARDOSH, M. (1992) Reevaluation of Lake-sediment chronology in the Dead Sea basin, Israel, based on new ^{230}Th/U dates. Quaternary Res. 38: 292-304.

KAUFMAN, S. AND LIBBY, W (1954): Natural distribution of tritium. Phys. Rev. 93: 337-1344.

KHARAKA, Y.K., GUNTER, W.D., AGGARWALL, P.K., PERKINS, E.H. AND DEBRAAL, J.D.(1988): Solminq88-a computer program code for geochemical modelling of water–rock interactions. US Geological Survey Water Investigations, Report 88.

KRENKEL, E. (1924): Der Syrische Bogen. Centralnl. Mineral., 9: 274-281.

KROUSE, H. R. AND MAYER, B. (2000): Sulphur and oxygen isotopes in sulphate. In Cook, P.G. and Hercezeg, A.L. (eds.): Environmental tracersin subsurface hydrology., 195-231, Kulwer Academic Press, Boston.

KUSKABE, M. (1974): Sulphur isotope variations in nature; 10, Oxygen and sulphur isotope study of Wairakei geothermal well discharges, New Zeeland. J. Sci. 17(2): 183-191.

LACHMANN, S. (1933): Die Mineralquellen Palästinas. Palästina, Z.F. den Aufbau Palästinas 16 (7-9): 222-235, Landeck; schl.

LANGGUTH, H.R. (1966): Die Grundwasserverhältnisse im Bereich des Velberter Sattels, Rheinisches Schiefergebirge. Der Minister für Ernährung, Landwirtschaft und Forsten, NRW, Düsseldorf, (unpublished).

LARTET, L. M. H. (1876): Exploration géologique de la Mer Morte, de la Palastina et de Ildumee. Paris (A Bertrand).

LLOYD, J. W. (1980): Aspects of environmental isotope chemistry in ground waters in eastern Jordan In: Arid Zone Hydrology: Invistigation with isotope Techniques. Proceeding AG-158. International Atomic Eneregy Agency. Vienna.

LLOYD, J. W. AND HEATHCOAT, J. A. (1985): Natural inorganic chemistry in relation to groundwater, Clarendon Pres, Oxford.

LLOYD, R.M (1968): Oxygen isotope behaviour in the sulphate-water system. J. Geoph. Res., 73: 6099-6110.

LUCAS, L. L. AND UNTERWEGER, M. P. (2000): Comprehensive Review and Critical Evaluation of the Half-Life of Tritium. Journal of Research of the National Institute of Standards and Technology., 105: 541-549.

LUND, J. W. (2004): Direct heat utilization of geothermal resources, Geoheat utilization of geothermal resources. Geoheat Center Bulletin. Vol. 17, No. 3.
http://geoheat.oit.edu/bulletin/bull17-3/art20.htm (17.9.2005)

MABEY, R. D. (1980): Recommended program for the Zarqa Ma'in and Zara area.U.S. Geol. Survey.

MACDONALD, SIR M. AND PARTNERS (1965): East bank water resources.Hydrogeologicalsurvey of the Madba-Ma'in area. Volumes 1-3. Central Water Authority, Hashemite Kingdom of Jordan.

MAKHLOUF, I. M., TURNER, B. R. AND ABED, A. M. (1991): Depositional facies and environments in the Permian Umm Irna Formation, Dead Sea area, Jordan. Sedimentary Geology, 73: 117-139.

MANSPEIZER, W. (1985): The Dead Sea rift :Impact of climate and tectonisem on Pleistocene and Holocene sedimentation. In Biddle, K. Christie Black, N. (eds.): Strike-slip Deformation, Basin Formation and sedimentation, SEPM Spec. Pub., 37: 143-158.

MARINI, L. (2000): Geochemical techniques for the exploration and exploitation of geothermal energy, geochimical and geophysical methodologies in geothermal exploration. Divulgación electronica de las ciencias. Vol. 11. Genova. Italy. http://cabierta.uchile.cl/revista/11/revisiones/1_1/a_manzella.htm (20/10/2004)

MASRI, M. (1963): Reports on the geology of the Amman-Zarqa area, Unpub. Report. Central Water Authority, Amman, Jordan, 74 p.

MAZOR, E. (1997): Groundwaters along the western Dead Sea shore. Pp 265-276. In Niemi, T., Ben-Avraham, Z. and Gat, J. R. (eds.): The Dead Sea-The lake and its setting. Oxford monograms on geology and geophysics no. 36. Oxford University press (1997).

MAZOR, E., NADLER, A. AND HARPAZ, Y. (1973): Notes on the geochemical tracing of the Kane-Samar spring complex, Dead Sea basin, Israel. J. Earth Scie., 22: 255-262.

MAZOR, E., ROSENTHAL, E. AND ECKSTEIN, J. (1969): Geochemical tracing of mineral water sources in the southwestern Dead Sea basin, Israel. J. Hydrol., 7: 246-275.

MCEWEN, R. AND HOLOCOMBE, H. (1982): Interpretation of resistivity data in Zarqa Ma'in and Zara hot springs, Exploration Geothermics. Santiago, California, USA.

MERKEL, B.J. AND PLANER-FRIEDRICH, B. (2005) Groundwater Geochemistry: A Practical Guide to Modeling of Natural and Contaminated Aquatic Systems, edited by D.K. Nordstrom; Springer (ISBN 3-540-24195-7).

MERLIVAT, L. AND JOUZEL, J. (1979): Global climatic interpretation of the deuterium–Oxygen 18 relationship for precipitation. J. Geophys. Res. 84: 5029-5033.

MIZUTANI, Y. AND RAFTER, T. A. (1969): Oxygen isotope composition of sulphates. Oxygen isotope fractionation in the bisulphate ion-water system, New Zeeland J. Sci., 12: 54-59.

MOH'D, B. K. (1988): Geological map of Ar Rabba, Map sheet No.3152 IV, 1:50,000.Geological Mapping Division, National Mapping Project. Natural Resources Authority. Amman, Jordan.

MOH'D, B. K. (2000): The geology of Irbid and Ash Shuna Ash Shamaliyya (Waqqas), Bulletin 46. Geology Directorate, Geological Mapping Division, Natural Resources Authority. Amman, Jordan.

MORE, D., MICHEBON, H. DRUCKMANN, Y., MMRA, Y., HEIMANN, A., GOLDBERG, M. AND SNEH, A. (1997): Notes on the Geology of the Golan Heights. Report GSI/15/97, Jerusalem.

MUNEIZEL, S. AND KHALIL, B. (1993): Geological map of As Salt, Map sheet No.3154 III, 1:50,000. Geological Mapping Division, National Mapping Project. Natural Resources Authority, Amman, Jordan.

MWI-MINISTRY OF WATER AND IRRIGATION (1996): Water information system. Hydrological, Geological and hydrogeological data ban, Water resources and planning directorate, Amman, Jordan.

NAJI, F. (1983): Kalkliges nanno plankton aus der ober Kriedi und dem Alt Tertiar Nord Jordanien (Mittel Santonian bis Mittle Eocene). Geol. Jb. 5: 53-185.

NEEV, D. AND EMERY, D. O. (1967): The Dead Sea depositional processes and environments of evaporates. Ministry of Development, Geol. Survey of Israel, 41, Jerusalem. 147 p.

NIEMI, T. (1997): Fluctuation of late Pleistocene Lake Lisan in the Dead Sea rif. In Niemi, T. Garfunke, Z. and Gat, J. (eds): The Dead Sea: The lake and its sitting. Oxford university press, New York, 286 p.

NIR, A. (1964): On the interpretation of tritium 'age' measurements of ground water, J. Geoph. Res., 69: 2589-2595.

NIR, A. (1967): Development of isotope methods applied to the ground water hydrology- In: Isotope techniques in the hydrologic cycle. Amer. Geophys. Unior, Geophysical Monograph Series 11: 109-118.

NJWRIPS-NORTH JORDAN WATER RESOURCES PROJECT STAFF (1989): Yarmouk basin, Water resources study, Water Authority of Jordan (WAJ), Amman-Jordan, 222 p.

NOETLING, F. (1887): Der Jura am Hermon .Stuttgart.

PARKER, D. H. (1970): Investigation of the sandstone aquifer system of east jordan, the hydrogeology of the Mesozoic- Cainozoic aquifer of the western highlands and plateau of east Jordan. UNDP, FAO. AG2:SF/JOR9. Technical Report, 2, Rome, 424 p.

PARKHURST, D. L. AND APPELO, A. A. J. (1999): User's guide to PhreeqC (version 2)- A computer program for speciation, batch-reaction, one dimensional transport, and inverse geochemical modeling U.S. Geol. Survey, water-resource invest., 99-4259.

PICARD, L. (1943): Structure and evolution of Palestine with comparative notes on neighbouring countries. Hebrew Univ., Jerusalem, Geol. Dept. Bull., V.4, Nos. 2,3,4, 187 p.

PIPER, A. (1942): A graphic procedure in the geochemical interpretation of water analysis. AGU tranceation, 25: 914-923.

POWELL, J. H (1987): Geological map of Al Karak Map sheet No.3152 III, 1:50,000.Geological Mapping Division, National Mapping Project. Natural Resources Authority. Amman, Jordan.

POWELL, J. H. (1988): the Geology of the Karak area, Map sheet no.3152III, Geology Directorate, Natural Resources Authority, Amman, Jordan, Bulletin 8, 171 p.

POWELL, J. H.(1989): Stratigraphy and sedimentation of the Phanerozoic rocks in Central and South Jordan: Part B-Kurnub, Ajlun and Belqa Groups. Bull. 11, Geolgical. Mapping Division, Geology Directorate, Natural Resources Authority, Jordan.

QUENNELL, A. M. (1951): The geology and mineral resources of the (former) Transjordan. Colonial Geology and Mineral resources, London, 2: 85-115.

RIMAWI, O. (1980): Geohydrochemistry and isotope hydrology of the Thermal Springs along the eastern side of the Jordan- Dead Sea – Wadi Araba Rift Valley. Unpubl. M.Sc. Thesis, Jordan University, Amman.

RIMAWI, O. (1985): Hydrochemistry and isotope hydrology of the ground and surface water in the Northeast of Mafraq, Duhleil Halabat, Azraq basin, Dissertation, Tech. Universität München, 240 p.

RIMAWI, O. AND SALAMEH, E. (1988): Hydrochemistry and groundwater system of the Zerka Ma'in-Zara thermal Field, Jordan. J. Hydrol. 98: 147-163.

RJGC-ROYAL JORDANIAN GEOGRAPHIC CENTER (2004): Topographic map of Jordan.
www.rjgc.gov.jo (30/6/2004).

ROFE AND RAFFETY CONSULT. ENG. (1963): Jerusalem and District Water Supply, Geological and Hydrological Report. Univeröff. Ber. für die Jordan. Regierung, Central Water Authority; London.

SAHAWNEH, J. (1991): Geology and structural interpretation of the area NE of the Dead Sea . Unpub. M.Sc. Thesis, Yarmouk university.163 p.

SALAMEH, E. (1996): Water quality degradation in Jordan (impact on environmental economy and future generating resources base), Friedrich- Ebert-Stififtungand Royal Society for the conservation of Nature, Higher Council of Science and Technology. The National Library, Deposit No. 1134/8/1996. Amman. 179 p.

SALAMEH, E. (2001) Source of water salinities in the Jordan Valley area/Jordan. Acta hydrochim. hydrobiol. 6-7: 329-362.

SALAMEH, E. AND El-NASER, H. (2000): Changes in the Dead Sea level and their impact on the surrounding groundwater bodies. Acta Hydrochim. Hydrobiol. 28: 24-33.

SALAMEH, E. AND UDLUF, P. (1985): The hydrodynamic pattern of the central part of Jordan, Geoloisches Jahresbuch, Heft 38,Reihe C, 39-53, Hannover.

SALAMEH, E., AND RIMAWI, O. (1997): Curative Water in Jordan. Ministry of Tourism and Antiquities, Amman, Jordan, 62 p.

SALAMEH, E., AND RIMAWI, O.(1984): Isotopic analysis and hydrochemistry of the thermal springs along the eastern side of the Jordan-Dead Sea- Wadi Araba Rift Valle. Journal of Hydrology, 73:129-145.

SALEM, H. S. (1984): Hydrology and Hydrogeology of the area north of Zaqa River/ Jordan. Unpub. M.Sc. Thesis, University of Jordan, Amman, 162 p.

SALMEH, E. AND EL_NASER, H. (1999): Does the actual drop in the Dead Sea level reflect the development of water sources with in its drainage basin. Acta hydrochim. Hydrobiol., 27: 5-11.

SALMEH, E. AND EL_NASER, H. (2000): Changes in the Dead Sea level and their impacts on the surrounding groundwater bodies. Acta hydrochim. hydrobiol., 28: 24-33.

SAWARIEH, A. (1990): Hydrogeology of the Wadi Wala Sub-basin and Zarqa Ma'in hot springs. Unpub. M.Sc. Thesis, University of London, U.K.

SAWARIEH, A. (2000): Geothermal energy resources in Jordan. Country update report, proceeding World Geothermal Congress, Kyushu-Tohoku, Japan.

SAWARIEH, A. (2005): Heat source of groundwater in the Zara-Zarqa Ma'in-Jiza area, central Jordan. PhD Thesis, university of Karlsruhe, Germany. 165 p.

SAWARIEH, A. AND MASSARWEH, R. (1993): Thermal springs in Wadi Iben Hammad, Karak Governate. NRA. Amman, Jordan, 30 p.

SAWARIEH, A. AND MASSARWEH, R. (1996): Geothermal water in Zara and Zarqa Ma'in area. Geothermal Eneregy Project, Internal report No. 8. Natural Resources Authority, Amman, Jordan, 36 p.

SAWARIEH, A. AND MASSARWEH, R. (1997): Geothermal Water in Mukhiebeh and North Shuna areas**,** Geothermal Eneregy Project, Internal report No. 9, Natural Resources Authority, Amman, Jordan. 25 p.

SAWYER, C.N. AND MCCARTY, P.L. (1967): Chemistry for sanitary engineers, 2nd Ed. McGraw-Hall, New York.

SCHOELLER, H. (1962): Les Eaux sutterraines, Masson et cie, 67 Paris.

SCHRAMM, A., STEIN, M. AND GOLDSTEIN, S. L. (1995): Constancy of $^{234}U/^{238}U$ ratios in late Pleistocene aragonite sediments-lake Lisan. Paleo-Dead Sea. Terra Nova 7, 325.

SCHRÖTTER, H. (1924): Das Tote Meer.Wien, Leipzig (M.Perles).

SCHUMACHER (1886): Beschreibung des Dscholan. Z.deutsch.Palästina Ver., Leipzig.

SHAWABKEH, K. F. (1996): Geological map of Ma'in, Map sheet No.3153 III, 1:50,000.Geological Mapping Division, National Mapping Project. Natural Resources Authority. Amman, Jordan.

SHAWABKEH, K. F. (1998): The geology of Ma'in area. Bulletin 40. Geology Directorate, Geological Mapping Division, Natural Resources Authority. Amman, Jordan.

SHAWABKEH, K. F. (2001): Geological map of Al Karama, Map sheet No.3153 IV, 1:50,000.Geological Mapping Division, National Mapping Project. Natural Resources Authority. Amman, Jordan.

STANISLAVSKY, E. AND GVIRTZMAN, H.(1999): Basin-scale migration of continental-rift brine: Paleohydrogeologic modelling of the Dead Sea basin. Geology, 27: 791-794.

STARINSKY, A. (1974): Relation between calcium chloride brine and sedimentary rocks in Israel. Unpub. Ph.D. Thesis, Hebrew Uniersity.

STEIN, M., GOLDSTEIN, S.L., RON, H. AND MARCO, S. (1992): Precise TIMS 230Th-234U ages and magnetostratigraphy of Lake Lisan sediments (paleo-Dead Sea) EOS Trans. AGU 73 (Spring Meet Suppl. 154).

STEIN, M., STARINSKY, A., KATZ, A.GOLDSTEIN, S. MACHLUS, M. AND SCHRAMM, A. (1997): Strontium isotopic, chemical and sedimentological evidence for evolution of lake lisan and the Dead Sea. Geochim. Cosmochim Acta, 61: 3975-3992.

SULTENFUSS, J. AND MASSMAN, G. (2004): Datierung mit der ^{3}He-Tritium Methode am Beispiel der Uferfilterationim Oderbruch. Grundwasser-zeitschrift der Fachsektion Hydrogeologie 4:221-234.

TARAWNH, B. (1987): Geological map of At Tafila, Map sheet No.3151 IV, 1:50,000.Geological Mapping Division, National Mapping Project. Natural Resources Authority, Amman, Jordan.

TODD D. (1980): Ground water Hydrology, second edition, John Wiley and Sons Inc. N.Y. 535 p.

TORGERSEN, T., CLARKE, W. B. AND JENKINS, W. T. (1979): The tritium/helium-3 method in hydrology, Isotope Hydrology 1978, IAEA Symposium 228, June 1978, Neuherberg, Germany, 2:917-930.

Treusdell, A. H. (1979): Final report on the chemistry and geothermal energy possibilities of Zarka Ma'in-Zara hot springs, Jordan**,** U.S. geol. Surv., Unpub. Rep. Submitted to Naturla Resource Authroity, Jordan,12pp.

TRUESDELL, A.H. (1976): Geochimical techniques in exploration. In: 2 Symposium on development and Use of Geothermal Resources, San Francisco 1, Liii-Ixiii, Summary of Section III.

UNDP/FAO (1970): Investigation of the sandstone aquifer of East Jordan**.** U.N. Devp. Program/Food and Agric.Org., AGL,SF/Jor. 9, Rome, 286 pp.

UNITED NATIONS (1995): Groundwater software for windows (GWW), New York.

WAGNER, W. AND GEYH, M. A. (1999): Application of environmental isotope methods for groundwater studies in ESCWA region. Economic and Social Commission for Western Asia. Geologisches Jahrbuch. Reihe C. Heft 67. Hannover.129 p.

WEISMANN, G. AND ABDULLATIF, A. (1963): Geology of the Yarmouk area, North Jordan, GGM report, 81 p.

WETZEL, R. AND MORTON, D. M. (1959): Contribution a la geologie de la Transjordanie. Notes et Memoirs sur le moyen-Orient. Publiees sous la dirction de M.L. DuBertret. Contribution a la Geologie de la Peninsule Arabique, 7:95-188, Museum Nat.d'hist.Nature, Paris.

WHO-WORLD HEALTH ORGANIZATION (1996): Guidelines for drinking water quality. 2nd Ed. Health criteria and other supporting information. Geneva, 2: 940-949.

WILCOX, L.V.(1955): Classification and use of irrigation waters. US Dept. Agric. Circ. 969. Washington, D.C., USA,19 p.

WILKES UNIVERSITY- CENTER OF ENVIRONMENTAL QUALITY, GEO-ENVIRONMENTAL SCIENCE AND ENGENEERING DEPARTMENT (2004): Corrosion, Saturation index, balanced water in drinking water systems-source and cause of corrosion.
http://wilkes.edu/~eqc/corrosion.htm (6/7/2003)

WILLIAMS, H. H., SABBAH, A. FARAJ, B., RAMINI, H. (1990): The regional petroleum geochemistry of Jordan, Petro-Canada and NRA, Amman-Jordan.

WOLFART, R. (1959): Geology and hydrogeology of Irbid District (Hashemite Kingdom of Jordan). Bundesanstalt für Bodenforshung, Hannover.

WOSHAH, A. (1979): An assessment of groundwater resources in Mughayer area Jaber-Mughayer Sirhan-Um Essurab area. Open-file report, Natural Resources Authority, Water Resources Development Directorate, Amman, 69 p.

ZAK, I. (1967): The geology of Mount Sedom. Ph.D Thesis, The Hebrew University, Jerusalem. 208 p (in Hebrew, summary in English).

ZAK, I. (1997): Evolution of the Dead Sea. Pp 133-144 in: Niemi, T., Ben-Avraham, Z. and Gat, J. R. (eds.) The Dead Sea-The lake and its setting. Oxford monograms on geology and geophysics no. 36. Oxford University press (1997).

ZHU, C. AND ANDERSON, G. (2002): Environmental Applications of Geochemical Modeling, Cambridge university press, UK, 284 p.

8 APPENDICES

Appendix 1: Physical and chemical parameters of the thermal waters from the first sampling campaign.

No.	Spring/Well	T	EC	PH	Ca	Mg	Na	K	Cl	SO_4	HCO_3	NO_3	PO_4	NH_4
		°C	µs/cm		mg/l	mg/l	mg/l	mg/l	mg/l	mg/l	mg/l	mg/l	mg/l	mg/l
1	EL-Mokhybeh	37.20	798	6.96	80.16	26.74	41.38	3.71	42.54	38.88	366.60	0.000	0.001	0.065
2	El-Hmmeh/Maqla	38.40	1433	6.94	124.25	34.03	114.95	14.39	177.25	144.96	389.82	0.000	0.002	0.289
3	El-Hammeh/Bajeh	35.50	1048	6.94	104.21	31.60	55.18	7.90	88.63	76.80	389.82	0.000	0.000	0.074
4	North Shuneh hot	52.70	1094	6.93	80.16	43.76	74.95	3.48	102.81	86.40	382.49	0.000	0.002	0.427
5	Waqas well	48.30	743	6.95	64.13	31.60	35.63	3.48	35.45	44.11	342.16	0.000	0.003	0.599
6	Abu-Zyad Well	48.80	2220	6.44	172.34	60.78	183.92	27.49	301.33	184.32	604.89	0.000	0.002	0.496
7	Abu-Thableh	32.70	2030	6.63	168.34	53.48	163.76	15.09	276.51	168.00	551.12	0.000	0.002	0.194
8	Abu El-Zeeghan/1	37.50	6310	6.38	625.25	117.90	439.57	134.00	967.79	884.16	1074.14	0.124	0.001	0.000
9	Abu El-Zeeghan/2	37.50	10330	6.33	709.42	104.53	1273.65	148.89	1807.95	1233.60	1438.29	7.700	0.005	0.000
10	Al-Kafreen well	35.30	866	6.59	78.16	29.17	51.96	6.45	95.72	81.60	264.56	0.000	0.000	0.000
11	Zara/Istraha	40.90	2070	7.08	113.23	38.29	257.03	29.99	460.85	174.67	260.29	0.000	0.000	0.000
12	Zara/Maghara	42.00	2340	6.87	138.28	36.47	287.38	37.42	514.03	171.07	325.05	0.000	0.000	0.000
13	El-Seel El-Hami	58.00	1436	6.44	88.18	19.45	178.86	20.06	315.51	111.36	188.19	0.000	0.001	1.030
14	Tal El-Rojom	43.60	1625	7.25	98.20	20.66	209.74	20.06	354.50	148.85	183.30	0.683	0.002	0.177
15	Maain/El-Mabkhara	61.00	3180	6.49	142.28	35.25	467.41	54.74	751.54	251.71	322.61	0.000	0.002	0.082
16	Maain/El-Ameer	49.00	3130	6.80	140.28	36.47	459.80	52.28	737.36	248.64	322.61	0.000	0.002	0.358
17	Maain/ElShallal	44.00	3110	7.89	132.26	31.60	473.59	49.81	755.09	252.96	281.67	0.000	0.001	0.000
18	TA1	43.90	3770	6.96	264.53	125.20	301.17	39.88	1067.05	144.00	275.56	4.782	0.003	0.246
19	TA2	42.70	1002	6.75	72.14	19.45	103.57	13.88	155.98	91.20	232.18	0.000	0.001	0.000
20	Iben Hammad	37.00	761	6.90	60.12	12.16	80.24	6.73	102.81	52.80	219.96	0.000	0.004	0.435
21	Burbyta	37.70	548	6.74	48.10	12.16	47.34	3.71	77.99	43.20	147.86	0.000	0.004	0.530
22	Afra/Sawna	45.60	561	6.85	48.10	24.31	27.59	1.76	67.36	43.20	174.75	0.000	0.008	0.341
23	Afra/Maqla	44.70	548	6.83	48.10	14.59	41.98	1.49	67.00	38.40	174.75	0.000	0.003	0.444

Appendix 2: Physical and chemical parameters of the thermal waters from the second sampling campaign.

No.	Spring/Well	T	EC	PH	Ca	Mg	Na	K	Cl	SO_4	HCO_3	NO_3	PO_4	NH_4
		^oC	µs/cm		mg/l	mg/l	mg/l	mg/l	mg/l	mg/l	mg/l	mg/l	mg/l	mg/l
1	EL-Mokhybeh	34.9	747	7.27	64.93	29.42	41.38	3.91	56.72	56.67	291.01	0.000	0.001	0.070
2	El-Hmmeh/Maqla	39.9	1406	7.10	106.21	40.11	119.55	7.82	226.54	160.89	266.60	0.000	0.001	0.240
3	El-Hammeh/Bajeh	35.3	1024	6.80	88.38	42.42	52.88	6.26	124.09	96.06	286.74	0.000	0.000	0.060
4	North Shuneh hot	52.4	1095	6.77	74.35	47.65	71.50	4.69	142.52	144.56	237.93	0.000	0.002	0.300
5	Waqas well	48.3	707	6.96	62.12	34.03	24.83	2.74	28.36	48.03	317.24	0.000	0.003	0.500
6	Abu-Zyad Well	47.8	2150	6.71	164.53	59.80	181.62	19.55	304.90	192.11	539.31	0.000	0.001	0.400
7	Abu-Thableh	37.7	1904	6.81	147.90	52.39	160.93	12.90	276.89	168.10	478.30	0.000	0.002	0.150
8	Abu El-Zeeghan/1	37.2	6620	6.26	643.28	130.06	459.34	136.85	996.23	936.55	1134.75	0.093	0.001	0.000
9	Abu El-Zeeghan/2	37.2	10420	6.72	731.46	105.75	1287.44	148.58	1871.92	1272.74	1561.81	1.550	0.003	0.000
10	Al-Kafreen well	35	830	6.68	66.13	32.45	51.50	5.47	92.18	76.84	250.13	0.000	0.000	0.000
11	Zara/Istraha	42.3	1984	7.19	94.59	32.45	270.59	22.68	460.89	167.14	208.65	0.000	0.000	0.000
12	Zara/Maghara	43.5	2230	7.32	119.24	34.88	296.34	23.46	529.67	174.34	231.83	0.000	0.000	0.000
13	El-Seel El-Hami	59.7	1364	6.37	73.95	22.49	177.48	16.03	310.57	142.16	122.02	0.000	0.001	0.900
14	Tal El-Rojom	43.7	1476	7.98	84.17	22.37	187.60	17.20	350.63	135.92	122.02	0.310	0.002	0.130
15	Maain/El-Mabkhara	62	3020	6.02	135.67	39.87	443.71	28.93	774.29	172.90	274.54	0.000	0.002	0.820
16	Maain/El-Ameer	50	3020	6.51	119.24	52.39	443.71	28.54	774.29	178.18	278.20	0.000	0.001	0.340
17	Maain/ElShallal	45	3030	7.80	111.02	42.42	471.30	29.33	777.84	182.99	280.64	0.000	0.001	0.000
18	TA1	44.3	3860	6.80	272.94	133.22	310.37	26.59	1162.15	108.06	226.34	1.860	0.004	0.300
19	TA2	43.4	1010	6.64	65.73	22.49	107.59	10.56	163.08	90.77	208.65	0.000	0.001	0.000
20	Iben Hammad	38.9	745	6.88	45.29	22.49	73.80	6.65	102.46	57.63	213.53	0.000	0.003	0.400
21	Burbyta	42.1	530	6.47	41.08	14.95	42.99	4.30	76.93	44.67	139.10	0.000	0.003	0.500
22	Afra/Sawna	45.1	560	6.90	51.10	19.93	31.04	1.96	69.49	43.71	168.99	0.000	0.007	0.320
23	Afra/Maqla	45.4	540	6.80	48.10	17.50	35.17	1.96	69.49	43.23	156.79	0.000	0.002	0.330

Appendix 3: Average physical and chemical parameters of the thermal waters.

No.	Spring/Well	T	EC	PH	Ca	Mg	Na	K	Cl	SO_4	HCO_3	NO_3	PO_4	NH_4
		^oC	µs/cm		mg/l	mg/l	mg/l	mg/l	mg/l	mg/l	mg/l	mg/l	mg/l	mg/l
1	EL-Mokhybeh	36.05	772.5	7.12	72.54	28.08	41.38	3.81	49.63	47.78	328.80	0.000	0.001	0.068
2	El-Hmmeh/Maqla	39.15	1419.5	7.02	115.23	37.07	117.25	11.10	201.90	152.93	328.21	0.000	0.002	0.265
3	El-Hammeh/Bajeh	35.40	1036.0	6.87	96.29	37.01	54.03	7.08	106.36	86.43	338.28	0.000	0.000	0.067
4	North Shuneh hot	52.55	1094.5	6.85	77.25	45.70	73.22	4.09	122.66	115.48	310.21	0.000	0.002	0.364
5	Waqas well	48.30	725.0	6.96	63.13	32.82	30.23	3.11	31.91	46.07	329.70	0.000	0.003	0.550
6	Abu-Zyad Well	48.30	2185.0	6.58	168.44	60.29	182.77	23.52	303.11	188.22	572.10	0.000	0.002	0.448
7	Abu-Thableh	35.20	1967.0	6.72	158.12	52.94	162.34	14.00	276.70	168.05	514.71	0.000	0.002	0.172
8	Abu El-Zeeghan/1	37.35	6465.0	6.32	634.27	123.98	449.45	135.42	982.01	910.35	1104.44	0.109	0.001	0.000
9	Abu El-Zeeghan/2	37.35	10375.0	6.53	720.44	105.14	1280.54	148.74	1839.93	1253.17	1500.05	4.625	0.004	0.000
10	Al-Kafreen well	35.15	848.0	6.64	72.14	30.81	51.73	5.96	93.95	79.22	257.35	0.000	0.000	0.000
11	Zara/Istraha	41.60	2027.0	7.14	103.91	35.37	263.81	26.33	460.87	170.90	234.47	0.000	0.000	0.000
12	Zara/Maghara	42.75	2285.0	7.10	128.76	35.67	291.86	30.44	521.85	172.71	278.44	0.000	0.000	0.000
13	El-Seel El-Hami	58.85	1400.0	6.41	81.06	20.97	178.17	18.04	313.04	126.76	155.10	0.000	0.001	0.965
14	Tal El-Rojom	43.65	1550.5	7.62	91.18	21.51	198.67	18.63	352.57	142.38	152.66	0.497	0.002	0.154
15	Maain/El-Mabkhara	61.50	3100.0	6.26	138.98	37.56	455.56	41.84	762.92	212.31	298.57	0.000	0.002	0.451
16	Maain/El-Ameer	49.50	3075.0	6.66	129.76	44.43	451.75	40.41	755.83	213.41	300.40	0.000	0.002	0.349
17	Maain/ElShallal	44.50	3070.0	7.85	121.64	37.01	472.44	39.57	766.46	217.97	281.15	0.000	0.001	0.000
18	TA1	44.10	3815.0	6.88	268.74	129.21	305.77	33.24	1114.60	126.03	250.95	3.321	0.004	0.273
19	TA2	43.05	1006.0	6.70	68.94	20.97	105.58	12.22	159.53	90.99	220.41	0.000	0.001	0.000
20	Iben Hammad	37.95	753.0	6.89	52.71	17.32	77.02	6.69	102.63	55.22	216.74	0.000	0.004	0.418
21	Burbyta	39.90	539.0	6.61	44.59	13.55	45.16	4.01	77.46	43.93	143.48	0.000	0.004	0.515
22	Afra/Sawna	45.35	560.5	6.88	49.60	22.12	29.31	1.86	68.42	43.45	171.87	0.000	0.008	0.331
23	Afra/Maqla	45.05	544.0	6.82	48.10	16.04	38.58	1.72	68.24	40.81	165.77	0.000	0.003	0.387

Appendix 4: The measured rare earth elements (REE) of the selected thermal waters along the Dead Sea Transform (concentrations in µgm/l).

No.	Name	Li	Be	Na	Mg	Al	Si	K	Ca	Sc	Ti	V
2	El-Hmmeh/Maqla	67.36	-0.10	93300	32500	55.12	14700	13700	111000	5.40	5.52	1.22
4	North Shuneh hot we	13.79	-0.10	65800	39600	3.12	11100	4090	72000	3.98	2.21	0.88
5	Waqas well	7.50	-0.10	26200	31000	5.58	9820	2850	61500	3.74	1.98	0.70
6	Abu-Zyad Well	166.76	-0.20	171600	52800	10.02	11520	23000	147000	3.95	2.19	2.14
8	Abu El-Zeeghan/1	452.44	-0.50	660000	96500	-10.00	10400	107500	461500	-5.00	2.27	3.78
9	Abu El-Zeeghan/2	1050.08	0.97	1290000	125000	17.73	11050	130000	635000	-5.00	3.81	6.09
10	Al-Kafreen well	18.22	-0.10	44300	22500	-2.00	6970	4540	64600	2.89	1.49	0.49
11	Zara/Istraha	107.14	-0.20	193400	19880	14.57	13220	29000	101800	5.06	2.92	1.26
13	El-Seel El-Hami	77.31	0.31	129000	14800	8.12	13500	19500	78500	5.17	2.93	0.59
15	Maain/El-Mabkhara	209.40	0.59	342000	30600	10.75	13440	44000	131400	4.39	2.52	1.35
19	TA2	62.74	0.14	76400	17500	-2.00	8240	10100	59600	3.30	1.74	0.48
20	Iben Hammad	47.88	0.11	57400	17800	4.30	8790	6870	47500	3.71	2.19	0.29
21	Burbyta	33.88	0.27	30500	12100	7.01	11000	4630	41700	4.72	2.59	0.25
23	Afra/Maqla	14.63	0.26	28500	16100	3.51	9930	2000	40500	4.28	2.23	0.14

No.	Name	Cr	Mn	Fe	Co	Ni	Cu	Zn	Ga	Ge	As	Se
2	El-Hmmeh/Maqla	2.40	4.81	74.02	-0.01	3.71	0.83	4.48	0.02	0.70	0.23	-0.20
4	North Shuneh hot we	2.83	7.13	222.52	-0.01	3.39	0.46	-0.50	0.04	0.20	0.07	-0.20
5	Waqas well	2.11	71.92	1420.00	-0.01	4.66	0.98	-0.50	0.02	0.18	0.09	-0.20
6	Abu-Zyad Well	6.18	9.17	326.25	-0.01	24.74	5.92	-1.00	0.02	0.60	0.13	-0.40
8	Abu El-Zeeghan/1	11.51	4.27	210.66	-0.03	55.12	5.86	-2.50	-0.05	1.73	-0.15	-1.00
9	Abu El-Zeeghan/2	18.06	97.51	4513.56	-0.03	127.15	56.43	39.58	-0.05	3.87	1.29	-1.00
10	Al-Kafreen well	1.54	60.01	4620.00	-0.01	0.70	0.91	1.08	0.07	0.20	0.13	-0.20
11	Zara/Istraha	3.43	77.92	92.72	-0.01	3.32	4.67	7.81	0.05	1.20	-0.06	-0.40
13	El-Seel El-Hami	1.63	884.62	83.58	-0.01	4.00	1.66	1.10	0.14	0.99	-0.03	-0.20
15	Maain/El-Mabkhara	3.67	529.00	105.08	-0.01	16.91	5.63	8.35	0.04	2.38	-0.06	-0.40
19	TA2	1.48	237.96	1970.00	-0.01	4.38	1.81	16.24	0.09	0.38	-0.03	-0.20
20	Iben Hammad	0.76	4.88	28.72	-0.01	0.34	2.01	0.88	0.01	0.30	0.19	-0.20
21	Burbyta	0.69	141.90	196.95	-0.01	0.60	2.75	7.35	0.05	0.08	1.17	0.22
23	Afra/Maqla	-0.50	39.81	515.71	0.53	0.43	1.50	3.39	0.11	0.06	0.75	-0.20

No.	Name	Br	Rb	Sr	Y	Zr	Nb	Mo	Ru	Pd	Ag	Cd
2	El-Hmmeh/Maqla	2440.00	15.97	2880.00	0.04	0.13	0.01	0.57	-0.01	-0.01	-0.20	0.03
4	North Shuneh hot we	612.51	4.80	1050.00	0.01	0.02	-0.01	-0.10	-0.01	0.10	-0.20	0.01
5	Waqas well	178.25	3.32	820.04	0.02	0.05	-0.01	-0.10	-0.01	-0.01	-0.20	0.02
6	Abu-Zyad Well	1424.23	39.04	3300.00	0.01	-0.02	-0.01	-0.20	-0.02	0.05	-0.40	0.03
8	Abu El-Zeeghan/1	3196.89	163.82	9200.00	0.02	-0.05	-0.03	-0.50	-0.05	-0.05	-1.00	-0.05
9	Abu El-Zeeghan/2	8250.00	248.58	12700.00	0.12	0.31	-0.03	-0.50	0.06	0.33	-1.00	0.08
10	Al-Kafreen well	464.45	11.30	597.36	0.02	0.02	0.02	0.96	-0.01	-0.01	-0.20	0.03
11	Zara/Istraha	2380.00	64.31	3140.00	0.03	-0.02	-0.01	-0.20	-0.02	0.06	-0.40	0.04
13	El-Seel El-Hami	2030.00	46.59	2770.00	0.03	0.01	-0.01	-0.10	-0.01	0.06	-0.20	0.02
15	Maain/El-Mabkhara	2920.00	100.59	3800.00	0.17	-0.02	-0.01	-0.20	-0.02	0.06	-0.40	0.15
19	TA2	1080.00	22.86	1200.00	0.01	0.01	-0.01	0.17	-0.01	-0.01	-0.20	0.76
20	Iben Hammad	479.47	14.75	698.87	0.01	0.01	-0.01	0.25	-0.01	0.10	-0.20	0.04
21	Burbyta	490.30	7.79	473.92	0.01	0.01	-0.01	2.50	-0.01	0.08	-0.20	0.10
23	Afra/Maqla	192.13	2.97	354.74	0.02	-0.01	-0.01	2.03	-0.01	0.07	0.22	0.04

No.	Name	In	Sn	Sb	Te	I	Cs	Ba	La	Ce	Pr	Nd
2	El-Hmmeh/Maqla	0.00	-0.10	0.01	-0.10	37.01	1.29	93.61	0.04	0.06	0.01	0.03
4	North Shuneh hot we	0.00	-0.10	-0.01	-0.10	42.13	0.17	173.38	0.00	0.00	0.00	0.00
5	Waqas well	0.00	-0.10	0.01	-0.10	32.53	0.06	314.30	0.01	0.02	0.00	0.01
6	Abu-Zyad Well	0.00	-0.20	-0.02	-0.20	43.90	2.92	70.69	0.00	0.01	0.00	0.00
8	Abu El-Zeeghan/1	-0.01	-0.50	-0.05	-0.50	89.33	7.57	17.03	-0.01	-0.01	-0.01	-0.01
9	Abu El-Zeeghan/2	-0.01	-0.50	0.07	-0.50	168.41	13.18	30.08	0.03	0.05	0.01	0.03
10	Al-Kafreen well	0.04	-0.10	-0.01	-0.10	54.10	0.71	52.02	0.00	0.00	0.00	0.00
11	Zara/Istraha	0.03	-0.20	0.02	-0.20	54.58	4.13	53.72	0.01	0.02	0.00	0.01
13	El-Seel El-Hami	0.03	-0.10	0.01	-0.10	34.04	3.02	97.67	0.01	0.01	0.00	0.01
15	Maain/El-Mabkhara	0.02	-0.20	-0.02	-0.20	52.48	7.98	70.73	0.01	0.03	0.01	0.04
19	TA2	0.03	-0.10	-0.01	-0.10	30.02	2.66	85.08	0.01	0.01	0.00	0.01
20	Iben Hammad	0.00	-0.10	0.01	-0.10	40.51	1.41	50.79	0.01	0.02	0.00	0.00
21	Burbyta	0.00	-0.10	0.04	-0.10	35.45	0.51	94.97	0.01	0.01	0.00	0.01
23	Afra/Maqla	0.00	-0.10	0.03	-0.10	28.63	0.21	85.95	0.01	0.01	0.00	0.00

No.	Name	Ta	W	Au	Os	Pt	Hg	Tl	Pb	Bi	Th	U
2	El-Hmmeh/Maqla	0.00	0.03	0.00	0.00	-0.30	-0.20	0.00	0.13	-0.30	0.00	0.40
4	North Shuneh hot	0.00	0.55	0.00	0.00	-0.30	-0.20	0.00	0.03	-0.30	0.00	0.01
5	Waqas well	0.00	-0.02	0.00	0.00	-0.30	-0.20	0.00	0.06	-0.30	0.00	0.01
6	Abu-Zyad Well	0.00	-0.04	0.00	0.00	-0.60	0.45	0.00	0.20	-0.60	0.00	0.03
8	Abu El-Zeeghan/1	-0.01	-0.10	-0.01	-0.01	-1.50	-1.00	0.02	-0.05	-1.50	-0.01	0.05
9	Abu El-Zeeghan/2	-0.01	-0.10	-0.01	-0.01	-1.50	-1.00	0.02	1.42	-1.50	0.02	0.19
10	Al-Kafreen well	0.00	-0.02	0.00	0.00	-0.30	1.56	0.08	0.14	-0.30	0.00	0.09
11	Zara/Istraha	0.00	-0.04	0.00	0.00	-0.60	1.09	0.02	0.72	-0.60	0.00	0.10
13	El-Seel El-Hami	0.00	-0.02	0.00	0.00	-0.30	0.35	0.09	0.10	-0.30	0.00	0.02
15	Maain/El-Mabkhar	0.00	-0.04	0.00	0.00	-0.60	0.41	0.04	1.61	-0.60	0.00	0.06
19	TA2	0.00	-0.02	0.00	0.00	-0.30	0.25	0.02	0.13	-0.30	0.00	0.01
20	Iben Hammad	0.00	-0.02	0.00	0.00	-0.30	-0.20	0.01	0.06	-0.30	0.00	0.01
21	Burbyta	0.00	-0.02	0.00	0.00	-0.30	0.21	0.06	0.17	-0.30	0.00	0.01
23	Afra/Maqla	0.00	-0.02	0.00	0.00	-0.30	0.26	0.55	0.05	-0.30	0.00	0.01

No.	Name	Sm	Eu	Gd	Tb	Dy	Ho	Er	Tm	Yb	Lu	Hf
2	El-Hmmeh/Maqla	0.00	0.01	0.01	0.00	0.00	0.00	0.00	0.00	0.00	0.00	0.00
4	North Shuneh hot	0.00	0.01	0.00	0.00	0.00	0.00	0.00	0.00	0.00	0.00	0.00
5	Waqas well	0.00	0.02	0.00	0.00	0.00	0.00	0.00	0.00	0.00	0.00	0.00
6	Abu-Zyad Well	0.00	0.00	0.00	0.00	0.00	0.00	0.00	0.00	0.00	0.00	0.00
8	Abu El-Zeeghan/1	-0.01	-0.01	-0.01	-0.01	-0.01	-0.01	-0.01	-0.01	-0.01	-0.01	-0.01
9	Abu El-Zeeghan/2	0.01	-0.01	0.01	-0.01	0.01	-0.01	0.01	-0.01	-0.01	-0.01	0.01
10	Al-Kafreen well	0.00	0.00	0.00	0.00	0.00	0.00	0.00	0.00	0.00	0.00	0.00
11	Zara/Istraha	0.00	0.00	0.00	0.00	0.00	0.00	0.00	0.00	0.00	0.00	0.00
13	El-Seel El-Hami	0.00	0.01	0.00	0.00	0.00	0.00	0.00	0.00	0.00	0.00	0.00
15	Maain/El-Mabkhar	0.01	0.01	0.03	0.00	0.02	0.00	0.01	0.00	0.01	0.00	0.00
19	TA2	0.00	0.00	0.00	0.00	0.00	0.00	0.00	0.00	0.00	0.00	0.00
20	Iben Hammad	0.00	0.00	0.00	0.00	0.00	0.00	0.00	0.00	0.00	0.00	0.00
21	Burbyta	0.00	0.01	0.00	0.00	0.00	0.00	0.00	0.00	0.00	0.00	0.00
23	Afra/Maqla	0.00	0.01	0.00	0.00	0.00	0.00	0.00	0.00	0.00	0.00	0.00

Appendix 5: The thermal waters classification according to Caroll (1962).

No.	Well/Spring	1st TDS (mg/l)	2nd TDS (mg/l)	Average TDS	Classification
1	EL-Mokhybeh	416.72	398.54	407.63	Fresh
2	El-Hmmeh/Maqla	804.74	794.43	799.59	Fresh
3	El-Hammeh/Bajeh	559.22	553.44	556.33	Fresh
4	North Shuneh hot	582.79	604.24	593.52	Fresh
5	Waqas well	385.49	358.74	372.11	Fresh
6	Abu-Zyad Well	1232.62	1192.17	1212.39	Brackish
7	Abu-Thableh	1120.74	1058.25	1089.50	Brackish
8	Abu El-Zeeghan/1	3705.73	3869.68	3787.71	Brackish
9	Abu El-Zeeghan/2	5997.18	6198.79	6097.99	Brackish
10	Al-Kafreen well	475.33	449.65	462.49	Fresh
11	Zara/Istraha	1204.20	1152.66	1178.43	Brackish
12	Zara/Maghara	1347.16	1293.85	1320.50	Brackish
13	El-Seel El-Hami	827.50	803.69	815.60	Fresh
14	Tal El-Rojom	943.65	858.89	901.27	Fresh
15	Ma'in/El-Mabkhara	1864.24	1732.64	1798.44	Brackish
16	Ma'in/El-Ameer	1836.13	1735.45	1785.79	Brackish
17	Ma'in/ElShallal	1836.15	1755.21	1795.68	Brackish
18	TA1	2079.60	2126.50	2103.05	Brackish
19	TA2	572.31	564.55	568.43	Fresh
20	Iben Hammad	424.82	415.08	419.95	Fresh
21	Burbyta	306.42	294.47	300.45	Fresh
22	Afra/Sawna	299.68	301.72	300.70	Fresh
23	Afra/Maqla	298.92	293.84	296.38	Fresh

Appendix 6: The tritium concentration in the precipitation of Jordan and Israel (white square) and the expected remaining concentration when the water discharge at 2003 (black square) (data taken from GNIP and ISOHIS (2002)).

1. Amman airport (Jordan)

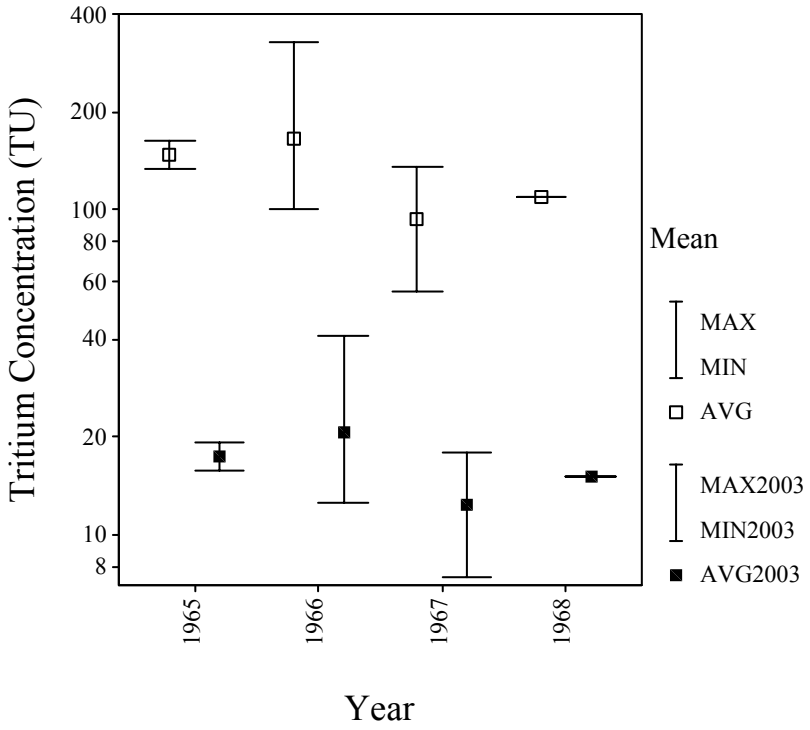

2. Amman-WAJ (Jordan)

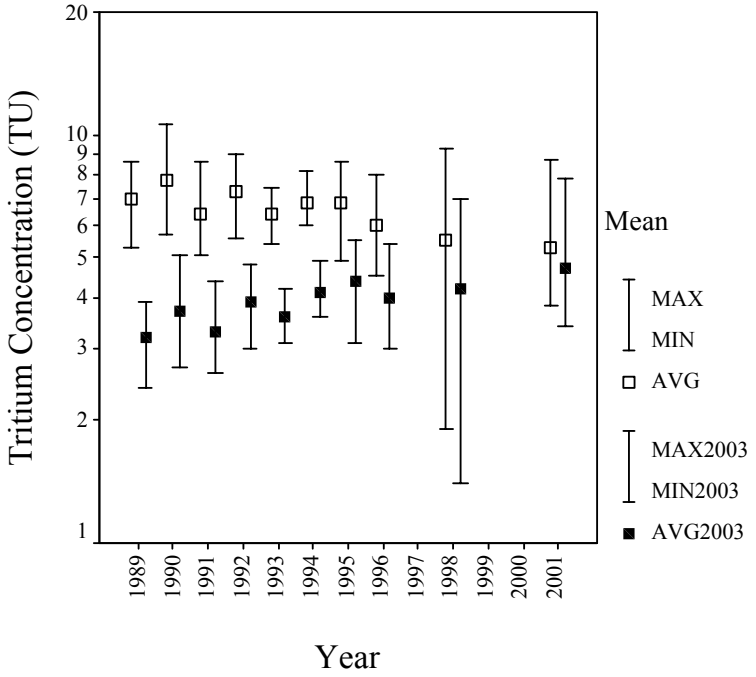

3. Azraq (Jordan)

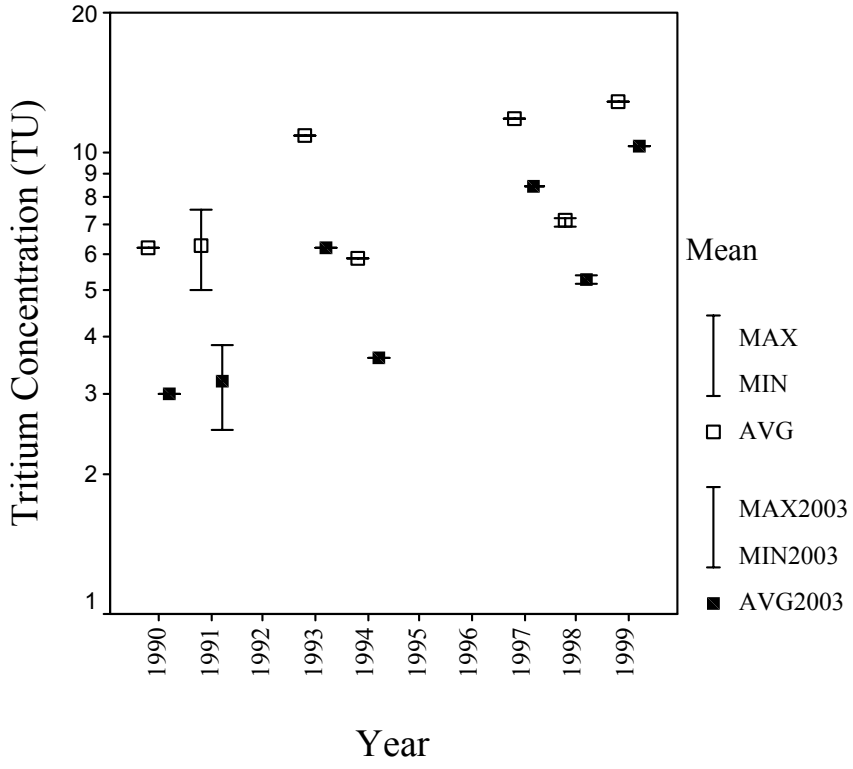

4. Deir Alla (Jordan)

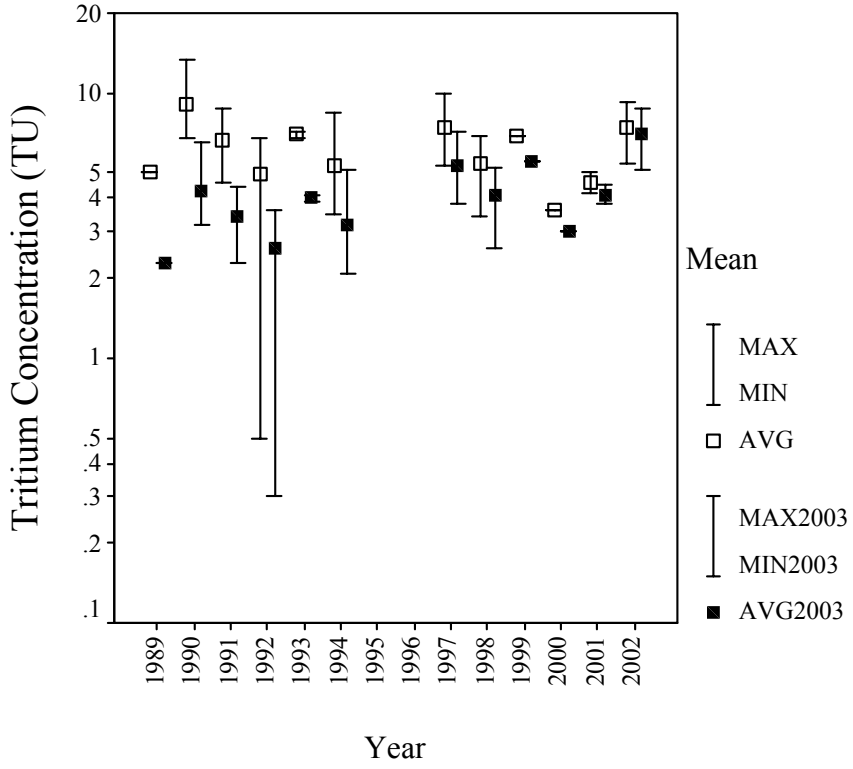

5.Queen Alia (Jordan)

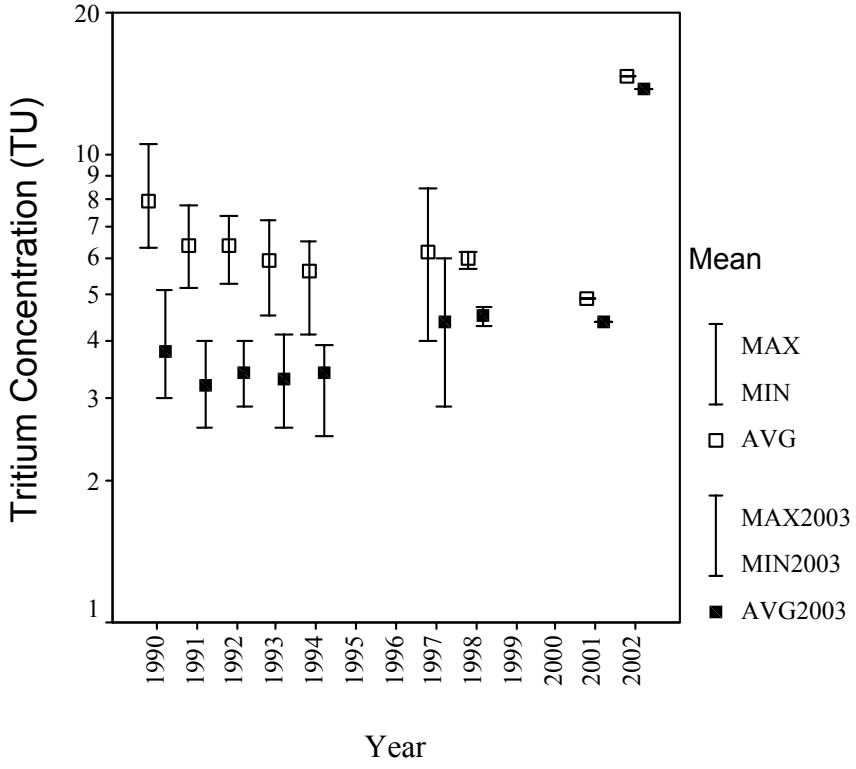

6.Ar Rabba (Jordan)

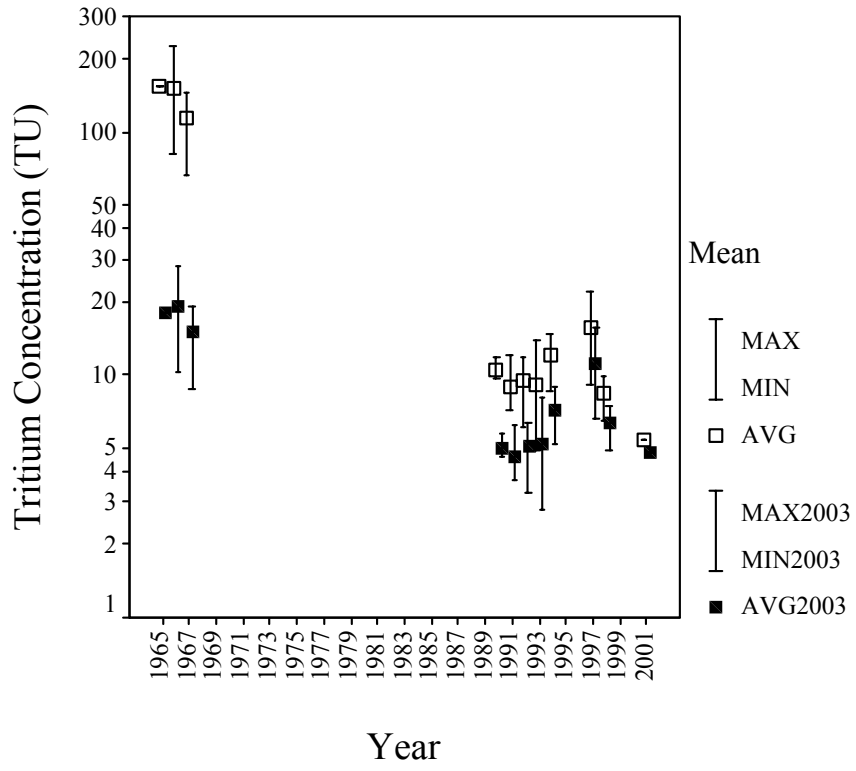

7.Ras Munif (Jordan)

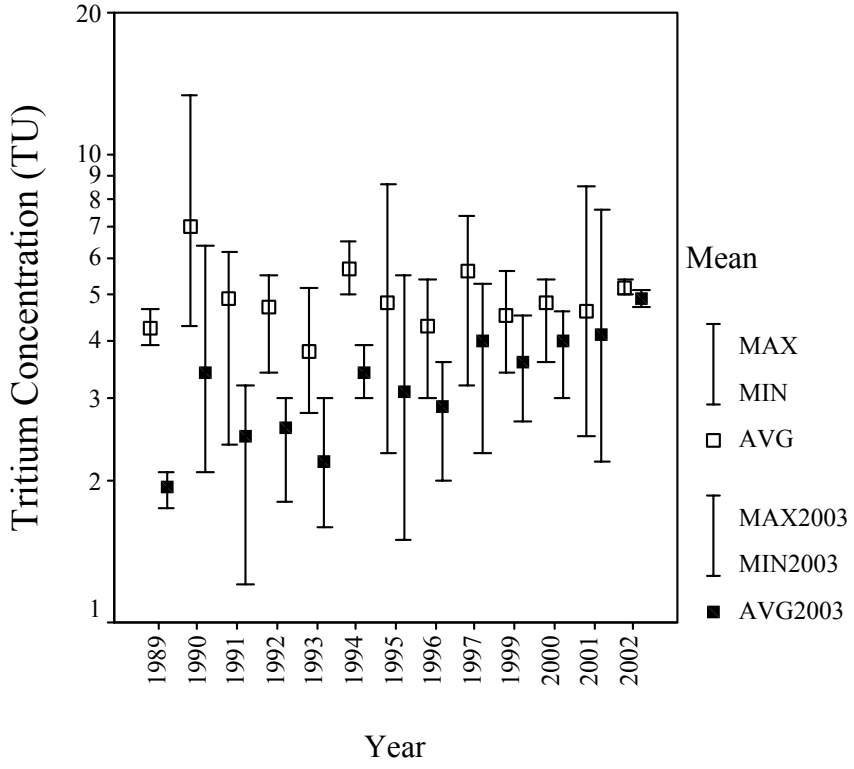

8. Shoubak (Jordan)

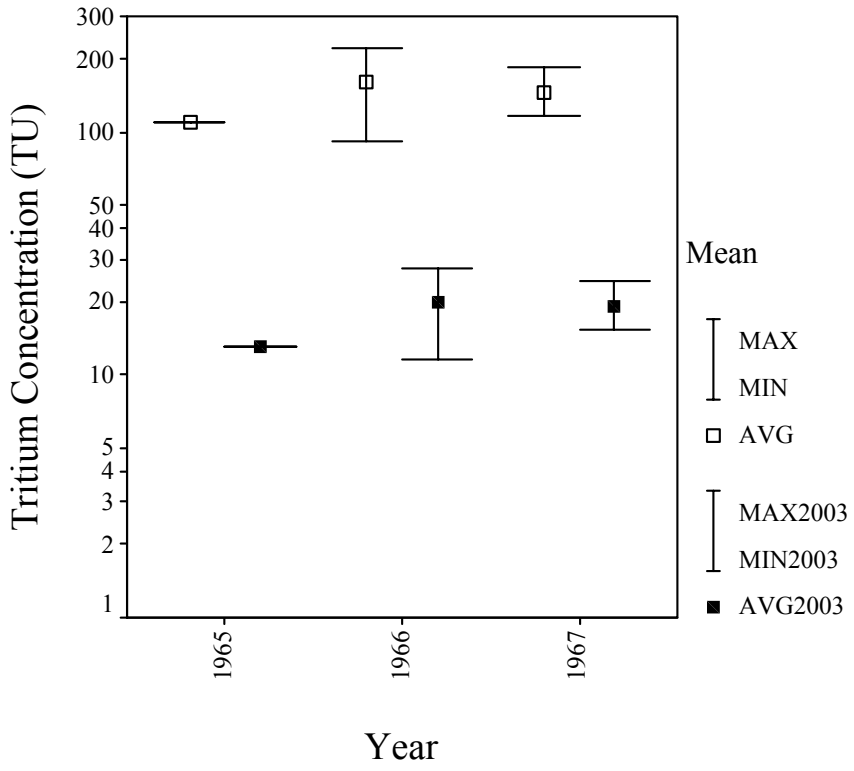

9.Walla (Jordan)

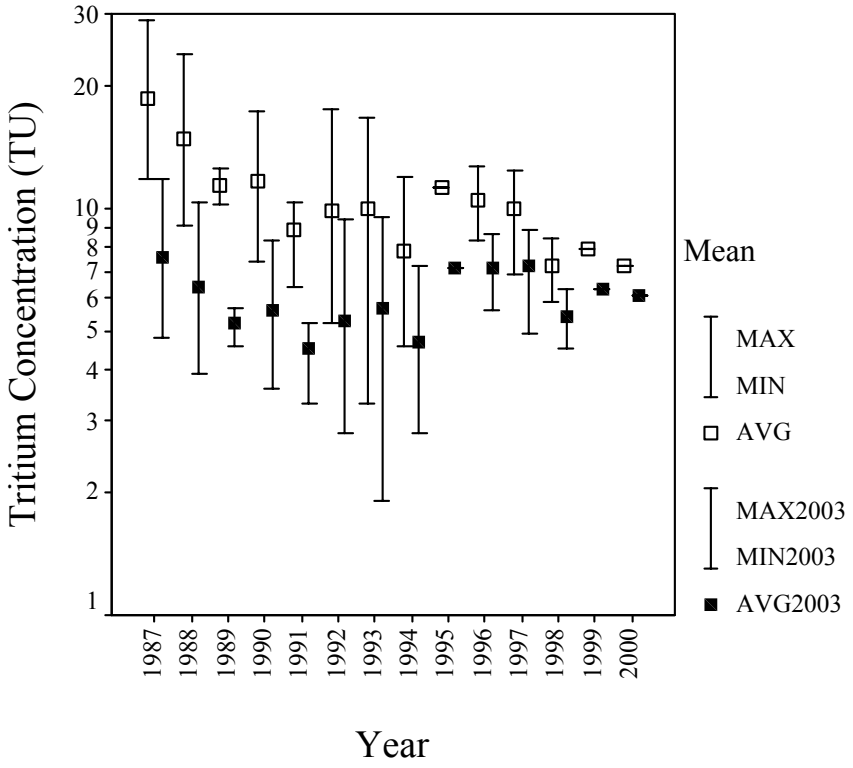

10. Beer Sheeva (Israel)

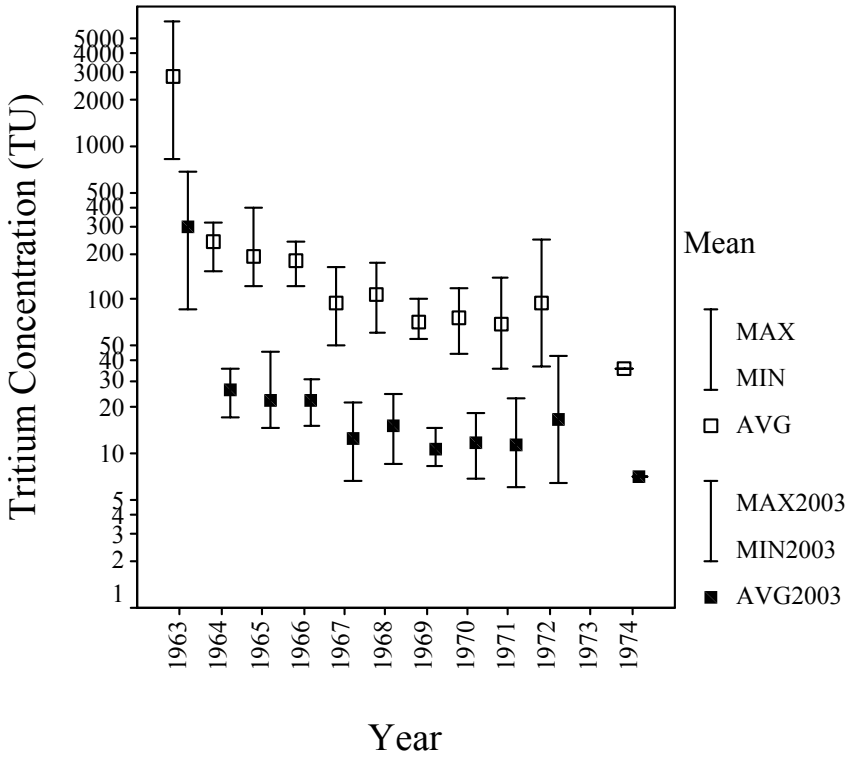

11.Haar Kn'an (Israel)

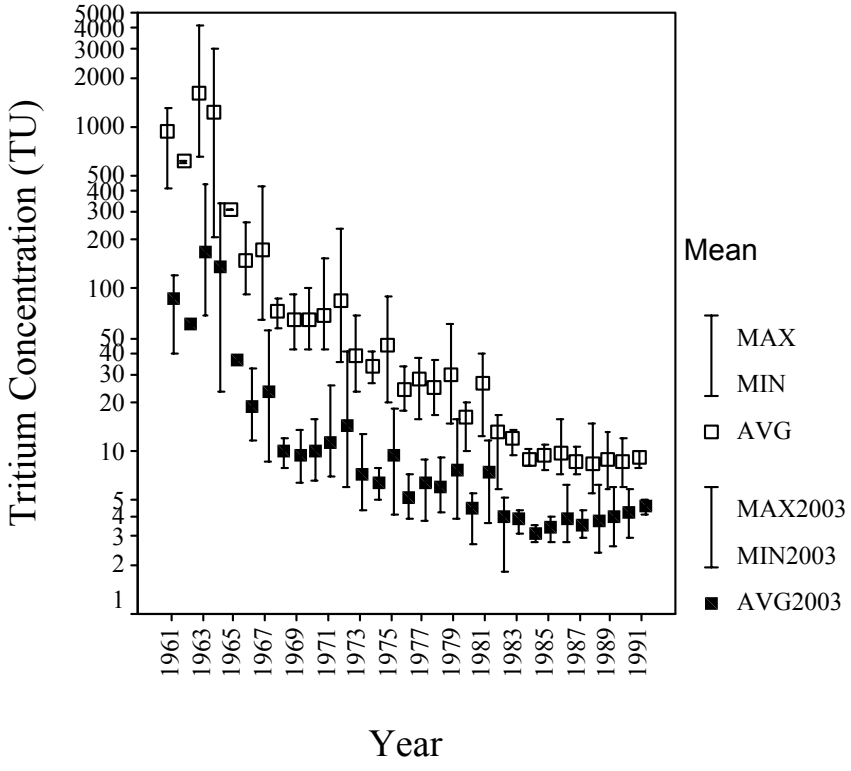

12.Bet Dagan (Israel)

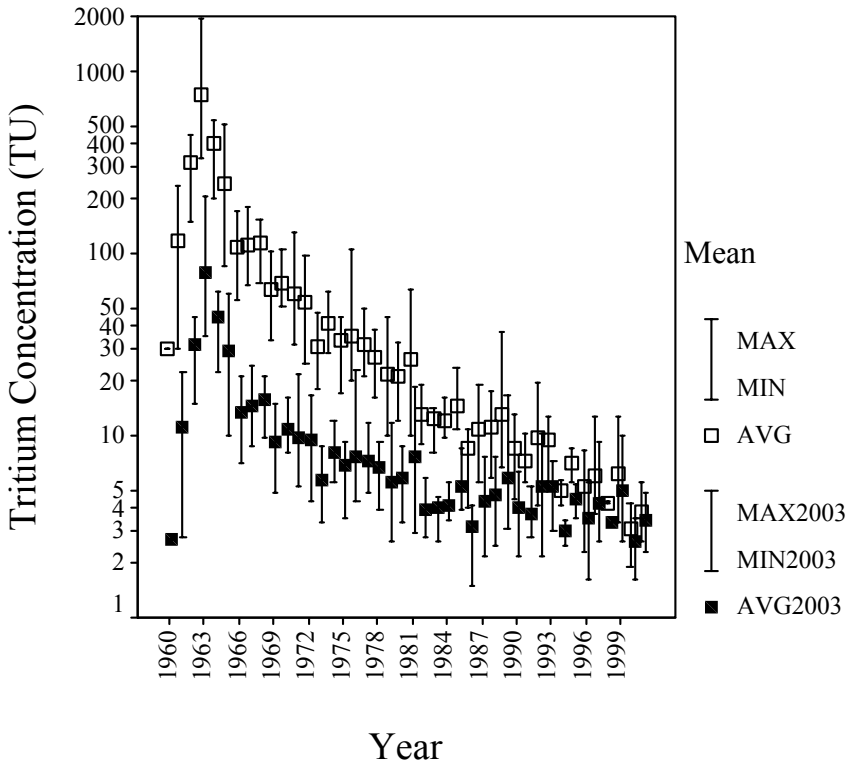

Appendix 7: Rainfall stations details (data taken from GNIP and ISOHIS (2002)).

Station Name	**Country**	**Latitude (N)**	**Longitude (E)**	**Altitude (m)**
Amman airport	Jordan	31° 58' 48"	35° 55' 48"	850
Amman-WAJ	Jordan	31° 57' 27"	35° 50' 53"	900
Azraq	Jordan	31° 51' 0"	36° 49' 0"	533
Deir Alla	Jordan	35° 53' 0"	32° 11' 0"	-224
Queen Alia	Jordan	31° 40' 0"	35° 59' 0"	715
Ar Rabba	Jordan	31° 12' 0"	35° 45' 0"	970
Ras Munif	Jordan	32° 22' 0"	35° 45' 0"	1150
Shoubak	Jordan	30° 16' 12"	35° 34' 48"	1300
Walla	Jordan	31° 43' 12"	35° 47' 0"	785
Beer Sheeva	Israel	31° 13' 48"	34° 46' 48"	270
Haar Kna'an	Israel	32° 0' 0"	34° 49' 12"	30
Bet Daggan	Israel	32° 58' 12"	35° 30' 0"	964

Appendix 8: The Helium and Neon isotope analysis and the Weise plot calculations of the selected thermal waters.

A	B	C	D	E	F	G	H	i	J	k	L	M	N
sample no.	Well Name	Analysis.	Extractions-nr.	Factor	Elevation of infiltration	Temp. of infiltration	^{3}Heon peak	^{4}He on peak	on ^{4}He QMS	on ^{20}Ne	on ^{22}Ne	on ^{20}Ne SMS	^{3}He Nml/kg
1	El-Mokhybeh	1	5824	9.17	500	16	33018	2.38737	0.935256	0.270717	0.0257785	0.0114305	1.49693E-09
1	El-Mokhybeh	2	5824	10.3	500	16	30818	2.20332	0.859485	0.247143	0.0235561	0.0104732	1.5634E-09
5	Waqas	1	5822	35.56	500	16	17985.5	1.53149	0.598425	0.0789897	0.00775058	0.00330123	3.11405E-09
18	TA1	1	5823	540	500	16	2822.33	3.41526	1.32999	0.00643469	0.00145741	0.00042518	7.4353E-09
18	TA1	2	5823	540	500	16	2765.1	3.40439	1.32238	0.00648363	0.00118333	0.00043223	7.28285E-09
19	TA2	1	5831	540	500	16	2835.88	3.35974	1.30905	0.00615924	0.00114366	0.000408117	7.49078E-09
19	TA2	2	5831	540	500	16	2850.65	3.41036	1.32942	0.00601278	0.000967838	0.000405545	7.53794E-09
Equilibrium with air, for 500 m, 16°C					500	16							
Crust													

O	P	Q	R	S	T	U	V	W	X	Y	Z
^{4}He Nml/kg	^{4}He QMS Nml/kg	^{3}He Nml/g	^{4}He Nml/g	Ne total QMS Nml/g	^{20}Ne/^{22}Ne	Ne-shareto the calculation from ^{20}Ne and ^{22} Ne	^{20}Ne QMS Nml/g	^{22}Ne QMS Nml/g	^{20}Ne/^{22}Ne	Ne ex mL/g	Ne excess %
						= T + 1					
0.000564125	0.000566055	1.49693E-12	5.64125E-07	2.10688755E-07	10.50	11.50165836	1.92370636E-07	1.83181198E-08	10.501658	2.64315448E-08	14.34
0.000582836	0.000583556	1.56339961E-12	5.82836E-07	2.15625587E-07	10.49	11.49167732	1.96861956E-07	1.87636305E-08	10.491677	3.13683762E-08	17.02
0.00138618	0.001406143	3.11405E-12	1.38618E-06	2.36910371E-07	10.19	11.19145664	2.15741512E-07	2.11688593E-08	10.191457	5.26531603E-08	28.58
0.047216903	0.046948419	7.43530374E-12	4.72169E-05	2.94047237E-07	4.42	5.41515428	2.39746432E-07	5.43008050E-08	4.415154	1.09790026E-07	59.59
0.04706056	0.046678023	7.28285E-12	4.70606E-05	2.96229604E-07	5.48	6.47913938	2.50509086E-07	4.57205172E-08	5.479139	1.11972393E-07	60.77
0.046576692	0.046370169	7.49078E-12	4.65767E-05	2.82476608E-07	5.39	6.38555165	2.38239771E-07	4.42368371E-08	5.385552	9.82193975E-08	53.31
0.047323609	0.047105646	7.53794E-12	4.73236E-05	2.75821778E-07	6.21	7.21258930	2.37580064E-07	3.82417141E-08	6.212589	9.15645671E-08	49.69
		5.94E-14	4.36322E-08	1.842572E-07			1.67173727E-07	1.70835E-08	9.785693316	0	0

Appendix 4.8 (Continue): The Helium and Neon isotope analysis and the Weise plot calculations of the selected thermal waters.

AA	AB	AC	AD	AE	AF	AG	AH	AL	AJ
^{20}Ne excess mL/g	^{20}Ne excess %	air excess mL/g = 20Ne total/20Ne in air [ppmVol] - or how much additional air has been dissoluted	^{4}He-air excess ml/g = air excess * 4H in air [ppmVol] - or how much Helium the additional air volume contains	^{4}He solubility mg/L under given p-T conditions	^{4}He excess ml/g	^{4}He excess Anteile	^{3}He/^{4} He measured	^{3}He-air excess ml/g = ^{4}He-air excess * ^{3}He/^{4}He ratio in air	^{3}He/^{4}He solubility in water
		AA/0.00001645	AC*0.00000522					1.384E-06	1.384E-06
2.51969082E-08	15.07	1.53172694E-03	7.99561464E-09	4.36322E-08	5.124973E-07	1.174586E+01	2.653536E-06	1.10659E-14	1.360915E-06
2.96882290E-08	17.76	1.80475556E-03	9.42082402E-09	4.36322E-08	5.297826E-07	1.214202E+01	2.682403E-06	1.30384E-14	1.360915E-06
4.85677842E-08	29.05	2.95244889E-03	1.54117832E-08	4.36322E-08	1.327136E-06	3.041648E+01	2.246496E-06	2.13299E-14	1.360915E-06
7.25727043E-08	43.41	4.41171455E-03	2.30291499E-08	4.36322E-08	4.715024E-05	1.080631E+03	1.574712E-07	3.18723E-14	1.360915E-06
8.33353589E-08	49.85	5.06597927E-03	2.64444118E-08	4.36322E-08	4.699048E-05	1.076969E+03	1.547549E-07	3.65991E-14	1.360915E-06
7.10660436E-08	42.51	4.32012423E-03	2.25510485E-08	4.36322E-08	4.651051E-05	1.065969E+03	1.608267E-07	3.12107E-14	1.360915E-06
7.04063363E-08	42.12	4.28002044E-03	2.23417067E-08	4.36322E-08	4.725764E-05	1.083092E+03	1.592849E-07	3.09209E-14	1.360915E-06
0	0	0	0	4.36322E-08	0.000000E+00	0	1.360915E-06	0	1.360915E-06
									Crust

AK	AL	AM	AN	AO	AP	AQ	AR
$^{3}He_{gem}$-$^{3}He_{air}$ / $^{4}He_{gem}$-$^{4}He_{air}$	$^{4}He_{equilibrium}$ / $^{4}He_{excess}$	Ne/He	delta ^{3}He	Tritium	^{3}He tritiugen ml/g	^{3}He-TU [TU]	$T_{M\,[years]}$
	AE/(R-AD)				5.93797E-14	2.49000E-15	
2.65355E-06	7.845683E-02	0.37220515	91.729457	0.3±0.3	1.42648033E-12	5.72884E+02	122.17
2.68242E-06	7.609179E-02	0.36950308	93.815222	0.3±0.3	1.49098152E-12	5.98788E+02	122.96
2.24651E-06	3.183043E-02	0.16848240	62.31909	0.1±0.3	3.03333950E-12	1.21821E+03	142.81
1.57471E-07	9.245300E-04	0.006263198	-88.622021	0±0.3	7.34405172E-12	2.94942E+03	163.67
1.54754E-07	9.276703E-04	0.006346233	-88.818291	0±0.3	7.18687166E-12	2.88629E+03	163.28
1.60826E-07	9.372346E-04	0.006091774	-88.379575	0±0.3	7.40018492E-12	2.97196E+03	163.80
1.59284E-07	9.224310E-04	0.005855387	-88.490972	0±0.3	7.44763770E-12	2.99102E+03	163.92
1.36092E-06	1.000000E+00	4.22296278			0	0	
2.00E-08	0.0001						

.

Appendix 9: The results of the Kolmogorov-Smirnov test for normality.

Variable	**Significant**	**Normal/Asymmetrical**
Tempreature	0.434	Normal
EC	0.017	Asymmetrical
TDS	0.019	Asymmetrical
pH	0.086	Normal
Ca	0.000	Asymmetrical
Mg	0.011	Asymmetrical
Na	0.022	Asymmetrical
K	0.002	Asymmetrical
Cl	0.040	Asymmetrical
SO_4	0.000	Asymmetrical
HCO_3	0.001	Asymmetrical
NO_3	0.000	Asymmetrical
PO_4	0.038	Asymmetrical
NH_4	0.160	Normal
SiO_2	0.261	Normal

Appendix 10: The relation strength between the different studied variables based on Spearman correlation coefficient.

		T	EC	TDS	PH	Ca	Mg	Na	K	Cl	SO_4	HCO_3	NO_3	PO_4	NH_4	SiO_2
T	Correlation Coefficient	1.000														
	Sig. (2-tailed)	.														
	N	46														
EC	Correlation Coefficient	.082	1.000													
	Sig. (2-tailed)	.588	.													
	N	46	46													
TDS	Correlation Coefficient	.082	1.000**	1.000												
	Sig. (2-tailed)	.588	.	.												
	N	46	46	46												
pH	Correlation Coefficient	-.097	-.174	-.174	1.000											
	Sig. (2-tailed)	.523	.248	.248	.											
	N	46	46	46	46											
Ca	Correlation Coefficient	-.053	.941**	.941**	-.210	1.000										
	Sig. (2-tailed)	.727	.000	.000	.162	.										
	N	46	46	46	46	46										
Mg	Correlation Coefficient	-.017	.770**	.770**	-.201	.837**	1.000									
	Sig. (2-tailed)	.911	.000	.000	.181	.000	.									
	N	46	46	46	46	46	46									
Na	Correlation Coefficient	.130	.950**	.950**	-.157	.823**	.583**	1.000								
	Sig. (2-tailed)	.389	.000	.000	.297	.000	.000	.								
	N	46	46	46	46	46	46	46								
K	Correlation Coefficient	.034	.946**	.946**	-.215	.850**	.589**	.964**	1.000							
	Sig. (2-tailed)	.823	.000	.000	.152	.000	.000	.000	.							
	N	46	46	46	46	46	46	46	46							
Cl	Correlation Coefficient	.122	.952**	.952**	-.200	.832**	.631**	.973**	.947**	1.000						
	Sig. (2-tailed)	.419	.000	.000	.182	.000	.000	.000	.000	.						
	N	46	46	46	46	46	46	46	46	46						
SO_4	Correlation Coefficient	.079	.921**	.921**	-.222	.868**	.705**	.908**	.911**	.875**	1.000					
	Sig. (2-tailed)	.604	.000	.000	.138	.000	.000	.000	.000	.000	.					
	N	46	46	46	46	46	46	46	46	46	46					

Appendix 10 (continue): The relation strength between the different studied variables based on Spearman correlation coefficient.

		T	EC	TDS	PH	Ca	Mg	Na	K	Cl	SO_4	HCO_3	NO_3	PO_4	NH_4	SiO_2
HCO_3	Correlation Coefficient	-.247	.539**	.539**	-.158	.699**	.731**	.360*	.426**	.300*	.555**	1.000				
	Sig. (2-tailed)	.098	.000	.000	.293	.000	.000	.014	.003	.043	.000	.				
	N	46	46	46	46	46	46	46	46	46	46	46				
NO_3	Correlation Coefficient	-.164	.539**	.539**	-.069	.511**	.406**	.478**	.499**	.576**	.349*	.169	1.000			
	Sig. (2-tailed)	.277	.000	.000	.647	.000	.005	.001	.000	.000	.017	.262	.			
	N	46	46	46	46	46	46	46	46	46	46	46	46			
PO_4	Correlation Coefficient	.234	-.187	-.187	-.078	-.177	-.107	-.170	-.227	-.139	-.274	-.143	.286	1.000		
	Sig. (2-tailed)	.117	.214	.214	.605	.239	.481	.258	.130	.358	.065	.343	.054	.		
	N	46	46	46	46	46	46	46	46	46	46	46	46	46		
NH_4	Correlation Coefficient	.554**	-.401**	-.401**	-.190	-.376**	-.280	-.367*	-.417**	-.365*	-.407**	-.295*	-.268	.544**	1.000	
	Sig. (2-tailed)	.000	.006	.006	.206	.010	.060	.012	.004	.013	.005	.047	.072	.000	.	
	N	46	46	46	46	46	46	46	46	46	46	46	46	46	46	
SiO_2	Correlation Coefficient	.504**	.109	.109	.299*	.008	-.119	.207	.124	.165	.215	-.277	-.255	-.267	.193	1.000
	Sig. (2-tailed)	.000	.470	.470	.043	.959	.431	.167	.410	.273	.151	.062	.088	.073	.199	.
	N	46	46	46	46	46	46	46	46	46	46	46	46	46	46	46

* Correlation is significant at the 0.01 level (2-tailed)

Appendix 11: Results of Mann-Whitney test, comparison between the means of the first and the second sampling campaign (significant level of 0.05).

Variable	Significance level
Temperature	0.742
EC	0.767
TDS	0.767
pH	0.956
Ca	0.468
Mg	0.416
Na	0.860
K	0.531
Cl	0.784
SO_4	0.869
CO_3	1.000
HCO_3	0.138
NO_3	0.921
PO_4	0.499
NH_4	0.876
SiO_2	0.362

Appendix 12: Results of Mann-Whitney test, comparison between the means of the upper aquifer (B2/A7) thermal water analysis and the lower sandstone aquifer thermal water analysis (significant level of 0.05).

Variable	Significance level
Temperature	0.099
EC	0.088
TDS	0.088
pH	0.489
Ca	0.908
Mg	0.137
Na	0.003
K	0.005
Cl	0.001
SO_4	0.222
CO_3	1.000
HCO_3	0.002
NO_3	0.025
PO_4	0.163
NH_4	0.648
SiO_2	0.447

Appendix 13: Comparison between the means of the suggested five groups (A1a, A1b, A2a, A2b and B) based on the Mann-Whitney test (α = 0.05).

T	A_{1a}	A_{1b}	A_{2a}	A_{2b}	B
A_{1a}	---	0.465*	0.317*	0.770*	0.051
A_{1b}		---	0.175*	0.617*	1.000*
A_{2a}			---	0.862*	0.098*
A_{2b}				---	0.157*
B					---

EC	A_{1a}	A_{1b}	A_{2a}	A_{2b}	B
A_{1a}	---	0.054	0.003	0.143*	0.055
A_{1b}		---	0.002	0.134*	0.046
A_{2a}			---	0.117*	0.034
A_{2b}				---	0.221*
B					---

TDS	A_{1a}	A_{1b}	A_{2a}	A_{2b}	B
A_{1a}	---	0.054	0.003	0.143*	0.055
A_{1b}		---	0.002	0.134*	0.046
A_{2a}			---	0.117*	0.034
A_{2b}				---	0.221*
B					---

pH	A_{1a}	A_{1b}	A_{2a}	A_{2b}	B
A_{1a}	---	0.201*	0.947*	0.380*	0.053
A_{1b}		---	0.814*	1.000*	0.046
A_{2a}			---	0.862*	0.157*
A_{2b}				---	0.221*
B					---

Ca	A_{1a}	A_{1b}	A_{2a}	A_{2b}	B
A_{1a}	---	0.011	0.003	0.143*	0.053
A_{1b}		---	0.010	0.134*	0.046
A_{2a}			---	0.117*	0.034
A_{2b}				---	0.221*
B					---

Mg	A_{1a}	A_{1b}	A_{2a}	A_{2b}	B
A_{1a}	---	0.006	0.008	0.143*	0.053
A_{1b}		---	0.596*	0.134*	0.046
A_{2a}			---	0.117*	0.034
A_{2b}				---	0.221*
B					---

Na	A_{1a}	A_{1b}	A_{2a}	A_{2b}	B
A_{1a}	---	0.715*	0.003	0.143*	0.053
A_{1b}		---	0.001	0.134*	0.046
A_{2a}			---	0.602*	0.157*
A_{2b}				---	0.221*
B					---

K	A_{1a}	A_{1b}	A_{2a}	A_{2b}	B
A_{1a}	---	0.584*	0.003	0.143*	0.053
A_{1b}		---	0.001	0.134*	0.046
A_{2a}			---	0.602*	0.034
A_{2b}				---	0.221*
B					---

Cl	A_{1a}	A_{1b}	A_{2a}	A_{2b}	B
A_{1a}	---	0.855*	0.003	0.143*	0.053
A_{1b}		---	0.001	0.134*	0.046
A_{2a}			---	0.117*	0.034
A_{2b}				---	1.000*
B					---

SO_4	A_{1a}	A_{1b}	A_{2a}	A_{2b}	B
A_{1a}	---	1.000*	0.003	0.143*	0.053
A_{1b}		---	0.003	0.317*	0.046
A_{2a}			---	0.117*	0.034
A_{2b}				---	0.221*
B					---

HCO_3	A_{1a}	A_{1b}	A_{2a}	A_{2b}	B
A_{1a}	---	0.006	0.053	0.143*	0.053
A_{1b}		---	0.195*	0.134*	0.046
A_{2a}			---	0.602*	0.034
A_{2b}				---	0.221*
B					---

NO_3	A_{1a}	A_{1b}	A_{2a}	A_{2b}	B
A_{1a}	---	1.000*	0.456*	0.025	0.016
A_{1b}		---	0.414*	0.014	0.009
A_{2a}			---	0.025	0.016
A_{2b}				---	1.000*
B					---

PO_4	A_{1a}	A_{1b}	A_{2a}	A_{2b}	B
A_{1a}	---	0.054	0.026	0.756*	0.844*
A_{1b}		---	0.952*	0.130*	0.399*
A_{2a}			---	0.109*	0.469*
A_{2b}				---	1.000*
B					---

NH_4	A_{1a}	A_{1b}	A_{2a}	A_{2b}	B
A_{1a}	---	0.410*	0.590*	0.380*	0.108*
A_{1b}		---	0.953*	0.617*	0.088*
A_{2a}			---	0.860*	0.138*
A_{2b}				---	0.157*
B					---

SiO_2	A_{1a}	A_{1b}	A_{2a}	A_{2b}	B
A_{1a}	---	0.522*	0.014	0.770*	0.245*
A_{1b}		---	0.068*	0.317*	0.096*
A_{2a}			---	0.117*	0.034
A_{2b}				---	1.000*
B					---

All values (except the ones that have * sign) indicate that there are significant difference between the means of the corresponding groups for the considered parameter

Appendix 14: Descriptive statistics of the four groups that resulted from the cluster analysis.

1.Group A_{1a}

	N	Minimum	Maximum	Mean	Std. Deviation
Tempreature	6	36.0500	45.3500	41.2250	3.8533
EC(µs/cm)	6	539.0000	1006.0000	695.8330	185.1023
TDS(mg/l)	6	350.3500	653.9000	452.2917	120.3165
PH	6	6.6050	7.1150	6.8325	0.1766
Ca (mg/l)	6	44.5890	72.5448	56.0786	11.7097
Mg (mg/l)	6	13.5528	28.0781	19.6810	5.1860
Na (mg/l)	6	29.3120	105.5820	56.1722	29.1436
K (mg/l)	6	1.7204	12.2188	5.0504	3.9488
Cl (mg/l)	6	49.6324	159.5319	87.6539	39.2095
SO_4 (mg/l)	6	40.8126	90.9865	53.6964	18.9428
HCO_3 (mg/l)	6	143.4801	328.8041	207.8465	66.4467
NO_3 (mg/l)	6	0.0000	0.0000	0.0000	0.0000
PO_4 (mg/l)	6	0.0010	0.0080	0.0032	0.0024
NH_4 (mg/l)	6	0.0000	0.5150	0.2863	0.2056
SiO_2(mg/l)	6	16.8500	22.8500	19.9250	2.1693

2. Group A_{1b}

	N	Minimum	Maximum	Mean	Std. Deviation
Tempreature	6	35.1500	52.5500	41.1000	7.4852
EC(µs/cm)	6	725.0000	1419.5000	982.5830	258.7940
TDS(mg/l)	6	471.2500	922.6750	638.6792	168.2161
PH	6	6.6350	7.1150	6.9075	0.1655
Ca (mg/l)	6	63.1260	115.2300	82.7652	19.3405
Mg (mg/l)	6	28.0781	45.7028	35.2495	6.2085
Na (mg/l)	6	30.2320	117.2490	61.3067	30.9158
K (mg/l)	6	3.1085	11.1044	5.8585	2.9633
Cl (mg/l)	6	31.9062	201.8974	101.0668	60.2338
SO_4 (mg/l)	6	46.0700	152.9269	87.9843	41.0520
HCO_3 (mg/l)	6	257.3479	338.2778	315.4251	29.8955
NO_3 (mg/l)	6	0.0000	0.0000	0.0000	0.0000
PO_4 (mg/l)	6	0.0000	0.0030	0.0013	0.0012
NH_4 (mg/l)	6	0.0000	0.5495	0.2187	0.2127
SIO_2 (mg/l)	6	16.7500	30.7000	22.2667	4.7726

3.Group A_2

	N	Minimum	Maximum	Mean	Std. Deviation
Tempreature	10	35.2000	61.5000	46.9950	7.9649
EC(µs/cm)	10	1400.0000	3815.0000	2447.4500	780.4524
TDS(mg/l)	10	910.0000	2479.7500	1590.0300	508.3370
PH	10	6.2550	7.8450	6.9180	0.5114
Ca (mg/l)	10	81.0618	268.7364	139.0576	53.1558
Mg (mg/l)	10	20.9674	129.2077	47.4957	31.1870
Na (mg/l)	10	162.3440	472.4450	296.3147	122.9454
K (mg/l)	10	13.9978	41.8370	28.6017	10.0822
Cl (mg/l)	10	276.6989	1114.5970	562.7929	277.1290
SO_4 (mg/l)	10	126.0315	217.9734	173.8745	34.5366
HCO_3 (mg/l)	10	152.6580	572.1004	303.8559	137.5254
NO_3 (mg/l)	10	0.0000	3.0000	0.3800	1.0440
PO_4 (mg/l)	10	0.0000	0.0040	0.0015	0.0010
NH_4 (mg/l)	10	0.0000	0.9650	0.2812	0.2971
SIO_2 (mg/l)	10	18.1000	31.7500	25.7700	4.6389

4. Group B

	N	Minimum	Maximum	Mean	Std. Deviation
Tempreature	2	37.3500	37.3500	37.3500	0.0000
EC(µs/cm)	2	6465.0000	10375.0000	8420.0000	2764.7875
TDS(mg/l)	2	4137.6000	6640.0000	5388.8000	1769.4640
PH	2	6.3200	6.5250	6.4225	0.1450
Ca (mg/l)	2	634.2660	720.4380	677.3520	60.9328
Mg (mg/l)	2	105.1408	123.9810	114.5609	13.3221
Na (mg/l)	2	449.4550	1280.5430	864.9988	587.6683
K (mg/l)	2	135.4229	148.7364	142.0796	9.4141
Cl (mg/l)	2	982.0072	1839.9340	1410.9706	606.6459
SO_4 (mg/l)	2	910.3530	1253.1710	1081.7620	242.4089
HCO_3 (mg/l)	2	1104.4435	1500.0495	1302.2465	279.7357
NO_3 (mg/l)	2	0.0000	5.0000	2.3700	3.1940
PO_4 (mg/l)	2	0.0010	0.0040	0.0025	0.0021
NH_4 (mg/l)	2	0.0000	0.0000	0.0000	0.0000
SIO_2 (mg/l)	2	16.7000	18.8500	17.7750	1.5203

Appendix 15: Kruskal-Wallis test results applied on the four groups that resulted from the cluster analysis.

Variable	Significance level	Groups similarity
Temperature	0.204	S
EC	0.000	D
TDS	0.000	D
pH	0.211	S
Ca	0.000	D
Mg	0.005	D
Na	0.001	D
K	0.000	D
Cl	0.001	D
SO_4	0.001	D
HCO_3	0.005	D
NO_3	0.011	D
PO_4	0.167	S
NH_4	0.288	S
SiO_2	0.040	D

Appendix 16: Comparison between the means of the four groups (A1a, A1b, A2 and B) based on the Mann-Whitney test ($\alpha = 0.05$).

T	**A_{1a}**	**A_{1b}**	**A2**	**B**
A_{1a}	---	0.465*	0.327*	0.051
A_{1b}		---	0.175*	1.000*
A2			---	0.085*
B				---

EC	**A_{1a}**	**A_{1b}**	**A2**	**B**
A_{1a}	---	0.045	0.002	0.053
A_{1b}		---	0.002	0.046
A2			---	0.032
B				---

TDS	**A_{1a}**	**A_{1b}**	**A2**	**B**
A_{1a}	---	0.045	0.002	0.053
A_{1b}		---	0.002	0.046
A2			---	0.032
B				---

pH	**A_{1a}**	**A_{1b}**	**A2**	**B**
A_{1a}	---	0.201*	0.806*	0.053
A_{1b}		---	0.828*	0.046
A2			---	0.133*
B				---

Ca	**A_{1a}**	**A_{1b}**	**A2**	**B**
A_{1a}	---	0.011	0.002	0.053
A_{1b}		---	0.007	0.046
A2			---	0.032
B				---

Mg	**A_{1a}**	**A_{1b}**	**A2**	**B**
A_{1a}	---	0.006	0.006	0.053
A_{1b}		---	0.416*	0.046
A2			---	0.086*
B				---

Na	**A_{1a}**	**A_{1b}**	**A2**	**B**
A_{1a}	---	0.715*	0.002	0.053
A_{1b}		---	0.001	0.046
A2			---	0.133*
B				---

K	**A_{1a}**	**A_{1b}**	**A2**	**B**
A_{1a}	---	0.584*	0.002	0.053
A_{1b}		---	0.001	0.046
A2			---	0.032
B				---

Cl	**A_{1a}**	**A_{1b}**	**A2**	**B**
A_{1a}	---	0.855*	0.002	0.053
A_{1b}		---	0.001	0.046
A2			---	0.053
B				---

SO_4	**A_{1a}**	**A_{1b}**	**A2**	**B**
A_{1a}	---	1.000*	0.002	0.053
A_{1b}		---	0.003	0.046
A2			---	0.032
B				---

HCO_3	**A_{1a}**	**A_{1b}**	**A2**	**B**
A_{1a}	---	0.006	0.037	0.053
A_{1b}		---	0.129*	0.046
A2			---	0.032
B				---

NO_3	**A_{1a}**	**A_{1b}**	**A2**	**B**
A_{1a}	---	1.000	0.301*	0.016
A_{1b}		---	0.258*	0.009
A2			---	0.041
B				---

PO_4	**A_{1a}**	**A_{1b}**	**A2**	**B**
A_{1a}	---	0.054	0.047	0.844*
A_{1b}		---	0.698*	0.399*
A2			---	0.512*
B				---

NH_4	**A_{1a}**	**A_{1b}**	**A2**	**B**
A_{1a}	---	0.410*	0.497*	0.108*
A_{1b}		---	0.870*	0.088*
A2			---	0.119*
B				---

SiO_2	**A_{1a}**	**A_{1b}**	**A2**	**B**
A_{1a}	---	0.522*	0.027	0.245*
A_{1b}		---	0.143*	0.096*
A2			---	0.053
B				---

All values (except the ones that have * sign) indicate that there are significant difference between the means of the corresponding groups for the considered parameter

Appendix 17: The calculated geothermometers for the thermal waters along the Dead Sea Transform.

THERMOMETER		Amorphous Silica	Cristobalite Alpha	Cristobalite Beta	Chalcedony	Quartz	Quartz steam loss	K/Mg	Na/K	Na/K	Na/K	Na/K	Na-K-Ca	Na-K-Ca Mg corrected	Isotope SO4-H2O	Isotope SO4-H2O
Reference		Fournier 1977	Fournier 1977	Fournier 1977	Fournier 1977	Fournier 1977	Fournier 1977	Giggenbach 1983	Fournier 1973	Truesdell 1976	Fournier & Potter 19	Fournier 1979	Fournier 1979	Fournier 1979	Lloyd 1968	Kusakabe 1975
Range		0-250	0-250	0-250	0-250	0-250	0-250			100-275		100-275	100-350	100-350	100-200	
1	EL-Mokhybeh	-50	14	-30	31	63	69	63	174	204	230	210	143	36	244	131
	Remarks												Beta = 1/3	R = 38.3	alpha = 1.0111	alpha = 1.0111
2	El-Hmmeh/Maqla	-36	30	-15	49	80	84	54	178	206	232	212	157	45	143	65
	Reamarks												Beta = 1/3	R = 33.6	alpha = 1.0191	alpha = 1.0191
3	El-Hammeh/Bajeh	-48	16	-28	33	65	71	59	218	223	265	241	161	36	183	92
	Reamarks												Beta = 1/3	R = 37.9	alpha = 1.0153	alpha = 1.0153
4	North Shuneh hot	-44	21	-23	39	71	75	67	125	183	187	172	128	22	167	81
	Remarks												Beta = 1/3	R = 48.7	alpha = 1.0168	alpha = 1.0168
5	Waqas	-48	16	-28	33	65	70	67	187	210	240	219	144	24	172	85
	Remarks												Beta = 1/3	R = 45.5	alpha = 1.0163	alpha = 1.0163
6	Abu-Zyad	-46	18	-26	35	67	72	51	215	222	263	240	176	41	141	63
	Remarks												Beta = 1/3	R = 35.5	alpha = 1.0194	alpha = 1.0194
7	Abu-Thableh	-50	14	-30	31	63	69	55	167	201	224	205	155	43	195	100
	Remarks												Beta = 1/3	R = 34.5	alpha = 1.0143	alpha = 1.0143
8	Abu El-Zeeghan/1	-51	12	-32	29	61	67	41	363	281	371	334	232	91	125	52
	Remarks												Beta = 1/3	R = 22.5	alpha = 1.0213	alpha = 1.0213
9	Abu El-Zeeghan/2	-55	8	-36	24	57	63	38	202	216	252	230	193	100	132	57
	Remarks												Beta = 1/3	R = 17.9	alpha = 1.0204	alpha = 1.0204
10	Al-Kafreen	-55	8	-36	25	57	63	59	201	216	252	229	157	31	224	118
	Remarks												Beta = 1/3	R = 40.3	alpha = 1.0124	alpha = 1.0124
11	Zara/Istraha	-40	26	-19	44	75	79	45	184	208	237	217	174	46	171	84
	Remarks												Beta = 1/3	R = 33.2	alpha = 1.0164	alpha = 1.0164
12	Zara/Maghara	-40	25	-20	43	75	79	43	189	210	242	221	176	57	166	81
	Remarks												Beta = 1/3	R = 28.9	alpha = 1.0168	alpha = 1.0168

Appendix 17 (Continue): The calculated geothermometers for the thermal waters along the Dead Sea Transform.

THERMOMETER		Amorphous Silica	Cristobalite Alpha	Cristobalite Beta	Chalcedony	Quartz	Quartz steam loss	K/Mg	Na/K	Na/K	Na/K	Na/K	Na-K-Ca	Na-K-Ca Mg corrected	Isotope SO4-H2O	Isotope SO4-H2O
Reference		Fournier 1977	Fournier 1977	Fournier 1977	Fournier 1977	Fournier 1977	Fournier 1977	Giggenbach 1983	Fournier 1973	Truesdell 1976	Fournier & Potter 19	Fournier 1979	Fournier 1979	Fournier 1979	Lloyd 1968	Kusakabe 1975
Range		0-250	0-250	0-250	0-250	0-250	0-250			100-275		100-275	100-350	100-350	100-200	
13	El-Seel El-Hami	-35	32	-14	50	82	85	43	185	209	239	218	170	60	182	92
	Remarks												Beta = 1/3	R = 27.7	alpha = 1.0154	alpha = 1.0154
14	Tal El-Rojom	-35	31	-14	50	81	85	43	177	205	232	212	167	65	152	71
	Remarks												Beta = 1/3	R = 26.	alpha = 1.0182	alpha = 1.0182
15	Ma'in/El-Mabkhara	-41	24	-21	42	73	78	41	174	204	230	210	176	61	178	89
	Remarks												Beta = 1/3	R = 27.8	alpha = 1.0157	alpha = 1.0157
16	Ma'in/El-Ameer	-43	22	-23	40	71	76	43	171	203	227	208	175	47	169	82
	Remarks												Beta = 1/3	R = 32.7	alpha = 1.0166	alpha = 1.0166
17	Ma'in/El-Shallal	-37	29	-16	48	79	83	41	164	200	221	202	173	54	164	79
	Remarks												Beta = 1/3	R = 30.1	alpha = 1.0170	alpha = 1.0170
18	TA1	-52	11	-33	27	60	66	56	194	213	246	224	173	27	183	92
	Remarks												Beta = 1/3	R = 42.7	alpha = 1.0153	alpha = 1.0153
19	TA2	-53	11	-33	27	60	66	47	202	216	252	230	169	50	167	81
	Remarks												Beta = 1/3	R = 31.5	alpha = 1.0167	alpha = 1.0167
20	Iben Hammad	-55	8	-35	25	57	63	51	168	202	224	205	152	45	171	84
	Remarks												Beta = 1/3	R = 33.7	alpha = 1.0163	alpha = 1.0163
21	Burbyta	-45	19	-25	37	68	73	54	170	203	227	207	146	48	213	111
	Remarks												Beta = 1/3	R = 32.4	alpha = 1.0131	alpha = 1.0131
22	Afra/Sawna	-48	16	-28	33	65	70	68	136	188	197	181	124	32	202	104
	Remarks												Beta = 1/3	R = 41.9	alpha = 1.0139	alpha = 1.0139
23	Afra/Maqla	-48	16	-28	33	65	70	65	106	175	170	156	114	47	234	125
	Remarks												Beta = 1/3	R = 35.1	alpha = 1.0117	alpha = 1.0117

Appendix 18: Saturation Indices of the average chemical analysis calculated by means of PhreeqC.

	Phase	Anhydrite	Aragonite	Artinite	Brucite	Calcite	Chalcedony	Chrysotile	Clinoenstatite	$CO_2(g)$	Cristobalite	Diopside	Dolomite	Dolomite(d)	Epsomite	Forsterite	Gypsum	$H_2(g)$	$H_2S(g)$	Halite	Huntite	Hydromagnesite	Magadiite	Magnesite	Mirabilite	Nahcolite	Natron
	Form	$CaSO_4$	$CaCO_3$	$MgCO_3:Mg(OH)_2:3H_2O$	$Mg(OH)_2$	$CaCO_3$	SiO_2	$Mg_3Si_2O_5(OH)_4$	$MgSiO_3$	CO_2	SiO_2	$CaMgSi_2O_6$	$CaMg(CO_3)_2$	$CaMg(CO_3)_2$	$MgSO_4:7H_2O$	Mg_2SiO_4	$CaSO_4:2H_2O$	H_2	H_2S	NaCl	$CaMg_3(CO_3)_4$	$Mg_5(CO_3)_4OH)_2:4H_2O$	$NaSi_7O_{13}(OH)_3:3H_2O$	$MgCO_3$	$Na_2SO_4:10H_2O$	$NaHCO_3$	Na2CO3:10H2O
1	El-Mokhybeh	-2.14	0	-6.37	-5.05	0.14	-0.05	-4.58	-3.21	-1.55	-0.04	-3.64	0.32	-0.19	-4.69	-8.34	-1.97	-22.21	-66.76	-7.3	-3.59	-13.21	-5.72	-0.42	-8.57	-4.67	-10.14
2	El-Hmmeh/Maqla	-1.54	0	-6.38	-5.01	0.2	0.1	-4.32	-3.04	-1.45	0.11	-3.26	0.37	-0.13	-4.23	-8.12	-1.39	-22.01	-65.75	-6.3	-3.53	-13.21	-4.07	-0.43	-7.39	-4.27	-9.47
3	El-Hammeh/Bajeh	-1.83	-0	-6.98	-5.5	-0	-0.02	-5.84	-3.63	-1.3	0	-4.45	-0	-0.52	-4.38	-9.21	-1.66	-21.71	-63.95	-6.9	-4.27	-14.34	-5.69	-0.59	-8.1	-4.55	-10.15
4	North Shuneh hot	-1.69	-0	-5.81	-4.47	0.03	-0.14	-3.77	-2.8	-1.2	-0.15	-3.26	0.33	-0.11	-4.34	-7.3	-1.64	-21.68	-65.93	-6.7	-3.15	-12.05	-5.16	-0.27	-8.46	-4.6	-10.45
5	Waqas	-2.13	-0	-5.89	-4.57	0.08	-0.16	-3.95	-2.91	-1.3	-0.16	-3.37	0.38	-0.08	-4.74	-7.53	-2.04	-21.9	-66.83	-7.7	-3.15	-12.2	-5.88	-0.28	-9.39	-4.9	-10.93
6	Abu-Zyad	-1.34	0	-6.54	-5.2	0.21	-0.13	-5.76	-3.5	-0.71	-0.13	-4.38	0.48	0.02	-4.13	-8.75	-1.26	-21.14	-62.56	-5.9	-3.12	-12.96	-5.3	-0.32	-7.41	-3.94	-9.59
7	Abu-Thableh	-1.47	0	-7.11	-5.72	0.14	-0.04	-6.55	-3.87	-0.99	-0.02	-4.88	0.24	-0.27	-4.08	-9.68	-1.3	-21.41	-62.21	-6	-3.82	-14.18	-5.53	-0.49	-6.96	-3.92	-9.2
8	Abu El-Zeeghan/1	-0.51	0	-7.53	-6.21	0.46	-0.08	-8.21	-4.41	-0.3	-0.07	-5.76	0.67	0.17	-3.4	-10.7	-0.36	-20.61	-57.98	-5.1	-3.18	-14.29	-5.65	-0.39	-5.73	-3.26	-8.58
9	Abu El-Zeeghan/2	-0.42	1	-7.05	-5.93	0.78	-0.13	-7.45	-4.18	-0.39	-0.11	-5.16	1.18	0.68	-3.44	-10.2	-0.27	-21.03	-59.98	-4.4	-2.28	-13.23	-5.33	-0.2	-4.75	-2.7	-7.38
10	Al-Kafreen	-1.94	-1	-7.93	-6.03	-0.5	-0.12	-7.63	-4.26	-1.19	-0.1	-5.76	-0.9	-1.38	-4.44	-10.4	-1.77	-21.25	-61.62	-6.9	-5.94	-16.51	-6.63	-0.99	-8.13	-4.67	-10.51
11	Zara/Istraha	-1.56	0	-6.09	-4.67	0.13	0.03	-3.56	-2.79	-1.7	0.03	-2.82	0.26	-0.22	-4.26	-7.52	-1.43	-22.25	-67.25	-5.6	-3.68	-13	-3.97	-0.46	-6.77	-4.1	-8.89
12	Zara/Maghara	-1.49	0	-6.08	-4.69	0.25	0.01	-3.7	-2.83	-1.58	0.01	-2.83	0.43	-0.05	-4.29	-7.58	-1.36	-22.18	-67.02	-5.5	-3.41	-12.84	-4	-0.41	-6.76	-4	-8.81
13	El-Seel El-Hami	-1.55	-1	-7.77	-5.36	-0.6	-0.08	-6.61	-3.67	-1.01	-0.1	-4.73	-1.4	-1.77	-4.67	-9.05	-1.56	-20.8	-62.24	-5.9	-6.79	-16.96	-4.39	-1.28	-7.88	-4.57	-10.61
14	Tal El-Rojom	-1.61	0	-5.08	-3.78	0.42	0.06	-0.91	-1.87	-2.35	0.06	-0.86	0.69	0.21	-4.5	-5.71	-1.49	-23.22	-72.36	-5.8	-2.95	-11.55	-3.2	-0.32	-7.13	-4.42	-8.89
15	Ma'in/El-Mabkhara	-1.25	-0	-7.48	-5.36	-0.3	-0.19	-6.92	-3.78	-0.58	-0.21	-5.02	-0.8	-1.17	-4.41	-9.15	-1.29	-20.5	-60.94	-5.2	-5.55	-15.7	-4.75	-0.97	-7.1	-3.94	-9.81
16	Ma'in/El-Ameer	-1.4	-0	-6.82	-5.12	-0.1	-0.1	-5.52	-3.4	-1.07	-0.1	-4.18	-0.2	-0.63	-4.23	-8.57	-1.33	-21.3	-63.45	-5.2	-4.44	-14.23	-4.52	-0.65	-6.62	-3.85	-9.06
17	Ma'in/El-Shallal	-1.45	1	-3.78	-3.11	0.94	0.03	1	-1.23	-2.34	0.03	0.28	1.86	1.38	-4.25	-4.4	-1.34	-23.68	-74.67	-5.1	-0.5	-8.31	-2.78	0.32	-6.35	-3.84	-7.73
18	TA1	-1.5	0	-5.66	-4.52	0.25	-0.17	-3.62	-2.84	-1.43	-0.17	-3.14	0.69	0.21	-4.08	-7.42	-1.39	-21.74	-65.31	-5.2	-2.63	-11.64	-5.39	-0.16	-7.12	-4.09	-9.14
19	TA2	-1.85	-1	-7.63	-5.62	-0.4	-0.17	-6.87	-3.94	-1.26	-0.16	-5.1	-0.9	-1.33	-4.62	-9.62	-1.73	-21.38	-63.24	-6.4	-5.93	-16.26	-6.04	-1.04	-7.79	-4.5	-10.14
20	Iben Hammad	-2.16	-1	-7.51	-5.59	-0.4	-0.14	-6.5	-3.86	-1.48	-0.13	-4.9	-0.8	-1.26	-4.81	-9.53	-2	-21.75	-64.63	-6.7	-5.8	-16.05	-6.19	-0.99	-8.01	-4.59	-10.06
21	Burbyta	-2.26	-1	-8.55	-6.12	-0.8	-0.03	-7.94	-4.28	-1.36	-0.02	-5.74	-1.7	-2.22	-4.98	-10.5	-2.12	-21.19	-62.16	-7.1	-7.74	-18.55	-5.77	-1.48	-8.62	-5	-11.02
22	Afra/Sawna	-2.21	-1	-6.88	-5.05	-0.4	-0.13	-5.18	-3.34	-1.52	-0.13	-4.11	-0.6	-1.11	-4.85	-8.44	-2.11	-21.74	-65.63	-7.3	-5.3	-14.88	-5.96	-0.83	-9.27	-5.16	-11.22
23	Afra/Maqla	-2.23	-1	-7.37	-5.32	-0.5	-0.13	-5.98	-3.61	-1.48	-0.13	-4.52	-0.9	-1.41	-4.99	-8.99	-2.13	-21.62	-65	-7.2	-6.03	-16.01	-5.91	-1.05	-9.02	-5.05	-11.04

Appendix 19: Species distribution of the four groups: A_{1a}, A_{1b}, A_2 and B calculated by means of PhreeqC.

1. Group A_{1a}

	Species	Molality	Activity	Log Molality	Log Activity	Log Gamma
	H+	1.83E-07	1.68E-07	-6.738	-6.776	-0.038
	OH-	6.61E-08	5.98E-08	-7.18	-7.224	-0.044
	H2O	5.55E+01	1.00E+00	1.744	0	0
C(4)		4.02E-03				
	HCO3-	2.96E-03	2.69E-03	-2.529	-2.571	-0.041
	CO2	1.01E-03	1.01E-03	-2.996	-2.995	0.001
	CaHCO3+	3.17E-05	2.88E-05	-4.499	-4.541	-0.041
	MgHCO3+	1.64E-05	1.49E-05	-4.785	-4.828	-0.043
	NaHCO3	3.51E-06	3.52E-06	-5.455	-5.454	0.001
	CO3-2	1.10E-06	7.52E-07	-5.958	-6.124	-0.165
	CaCO3	1.06E-06	1.06E-06	-5.975	-5.974	0.001
	MgCO3	3.39E-07	3.39E-07	-6.47	-6.469	0.001
	NaCO3-	3.60E-08	3.26E-08	-7.444	-7.487	-0.043
Ca		1.32E-03				
	Ca+2	1.23E-03	8.40E-04	-2.91	-3.076	-0.166
	CaSO4	5.43E-05	5.44E-05	-4.265	-4.265	0.001
	CaHCO3+	3.17E-05	2.88E-05	-4.499	-4.541	-0.041
	CaCO3	1.06E-06	1.06E-06	-5.975	-5.974	0.001
	CaOH+	9.19E-10	8.32E-10	-9.037	-9.08	-0.043
Cl		2.69E-03				
	Cl-	2.69E-03	2.43E-03	-2.571	-2.614	-0.043
H(0)		3.96E-25				
	H2	1.98E-25	1.99E-25	-24.703	-24.702	0.001
K		1.36E-04				
	K+	1.35E-04	1.22E-04	-3.869	-3.912	-0.043
	KSO4-	3.10E-07	2.81E-07	-6.509	-6.551	-0.043
	KOH	2.53E-12	2.53E-12	-11.597	-11.596	0.001
Mg		7.41E-04				
	Mg+2	6.88E-04	4.73E-04	-3.162	-3.325	-0.163
	MgSO4	3.59E-05	3.59E-05	-4.445	-4.444	0.001
	MgHCO3+	1.64E-05	1.49E-05	-4.785	-4.828	-0.043
	MgCO3	3.39E-07	3.39E-07	-6.47	-6.469	0.001
	MgOH+	1.13E-08	1.02E-08	-7.947	-7.99	-0.043
Na		2.57E-03				
	Na+	2.57E-03	2.33E-03	-2.591	-2.633	-0.042
	NaSO4-	4.18E-06	3.78E-06	-5.379	-5.422	-0.043
	NaHCO3	3.51E-06	3.52E-06	-5.455	-5.454	0.001
	NaCO3-	3.60E-08	3.26E-08	-7.444	-7.487	-0.043
	NaOH	9.16E-11	9.18E-11	-10.038	-10.037	0.001
O(0)		0.00E+00				
	O2	0.00E+00	0.00E+00	-42.977	-42.976	0.001
S(-2)		0.00E+00				
	H2S	0.00E+00	0.00E+00	-62.606	-62.605	0.001
	HS-	0.00E+00	0.00E+00	-62.779	-62.823	-0.044
	S-2	0.00E+00	0.00E+00	-68.797	-68.965	-0.167
S(6)		5.72E-04				
	SO4-2	4.77E-04	3.24E-04	-3.321	-3.489	-0.168
	CaSO4	5.43E-05	5.44E-05	-4.265	-4.265	0.001
	MgSO4	3.59E-05	3.59E-05	-4.445	-4.444	0.001
	NaSO4-	4.18E-06	3.78E-06	-5.379	-5.422	-0.043
	KSO4-	3.10E-07	2.81E-07	-6.509	-6.551	-0.043
	HSO4-	5.83E-09	5.28E-09	-8.234	-8.277	-0.043
Si		3.32E-04				
	H4SiO4	3.31E-04	3.32E-04	-3.48	-3.479	0.001
	H3SiO4-	3.23E-07	2.92E-07	-6.491	-6.534	-0.043
	H2SiO4-2	1.76E-13	1.19E-13	-12.755	-12.926	-0.171

2. Group A_{1b}

	Species	Molality	Activity	Log Molality	Log Activity	Log Gamma
	H+	1.37E-07	1.24E-07	-6.863	-6.907	-0.044
	OH-	9.10E-08	8.08E-08	-7.041	-7.093	-0.052
	H2O	5.55E+01	1.00E+00	1.744	0	0
C(4)		6.41E-03				
	HCO3-	5.03E-03	4.49E-03	-2.299	-2.347	-0.049
	CO2	1.25E-03	1.25E-03	-2.904	-2.902	0.001
	CaHCO3+	7.69E-05	6.88E-05	-4.114	-4.163	-0.049
	MgHCO3	4.98E-05	4.44E-05	-4.303	-4.353	-0.05
	NaHCO3	5.97E-06	5.98E-06	-5.224	-5.223	0.001
	CaCO3	3.42E-06	3.43E-06	-5.466	-5.465	0.001
	CO3-2	2.66E-06	1.70E-06	-5.575	-5.769	-0.195
	MgCO3	1.37E-06	1.37E-06	-5.865	-5.863	0.001
	NaCO3-	8.43E-08	7.50E-08	-7.074	-7.125	-0.05
Ca		2.07E-03				
	Ca+2	1.88E-03	1.20E-03	-2.726	-2.921	-0.195
	CaSO4	1.08E-04	1.08E-04	-3.967	-3.966	0.001
	CaHCO3+	7.69E-05	6.88E-05	-4.114	-4.163	-0.049
	CaCO3	3.42E-06	3.43E-06	-5.466	-5.465	0.001
	CaOH+	1.80E-09	1.61E-09	-8.744	-8.794	-0.05
Cl		2.85E-03				
	Cl-	2.85E-03	2.53E-03	-2.545	-2.596	-0.052
H(0)		2.17E-25				
	H2	1.08E-25	1.09E-25	-24.965	-24.964	0.001
K		1.50E-04				
	K+	1.50E-04	1.33E-04	-3.826	-3.877	-0.052
	KSO4-	4.78E-07	4.25E-07	-6.321	-6.372	-0.05
	KOH	3.70E-12	3.71E-12	-11.431	-11.43	0.001
Mg		1.45E-03				
	Mg+2	1.31E-03	8.44E-04	-2.883	-3.074	-0.191
	MgSO4	8.92E-05	8.95E-05	-4.05	-4.048	0.001
	MgHCO3	4.98E-05	4.44E-05	-4.303	-4.353	-0.05
	MgCO3	1.37E-06	1.37E-06	-5.865	-5.863	0.001
	MgOH+	2.78E-08	2.47E-08	-7.556	-7.607	-0.05
Na		2.67E-03				
	Na+	2.66E-03	2.37E-03	-2.576	-2.626	-0.05
	NaSO4-	6.03E-06	5.37E-06	-5.22	-5.27	-0.05
	NaHCO3	5.97E-06	5.98E-06	-5.224	-5.223	0.001
	NaCO3-	8.43E-08	7.50E-08	-7.074	-7.125	-0.05
	NaOH	1.26E-10	1.26E-10	-9.9	-9.899	0.001
O(0)		0.00E+00				
	O2	0.00E+00	0.00E+00	-42.454	-42.452	0.001
S(-2)		0.00E+00				
	H2S	0.00E+00	0.00E+00	-63.771	-63.77	0.001
	HS-	0.00E+00	0.00E+00	-63.805	-63.857	-0.052
	S-2	0.00E+00	0.00E+00	-69.671	-69.868	-0.197
S(6)		9.17E-04				
	SO4-2	7.13E-04	4.52E-04	-3.147	-3.344	-0.198
	CaSO4	1.08E-04	1.08E-04	-3.967	-3.966	0.001
	MgSO4	8.92E-05	8.95E-05	-4.05	-4.048	0.001
	NaSO4-	6.03E-06	5.37E-06	-5.22	-5.27	-0.05
	KSO4-	4.78E-07	4.25E-07	-6.321	-6.372	-0.05
	HSO4-	6.12E-09	5.45E-09	-8.213	-8.264	-0.05
Si		3.71E-04				
	H4SiO4	3.70E-04	3.72E-04	-3.431	-3.43	0.001
	H3SiO4-	4.97E-07	4.42E-07	-6.304	-6.354	-0.05
	H2SiO4-2	3.87E-13	2.43E-13	-12.413	-12.615	-0.202

3. GroupA2

	Species	Molality	Activity	Log Molality	Log Activity	Log Gamma
	H+	1.38E-07	1.21E-07	-6.86	-6.918	-0.058
	OH-	9.80E-08	8.28E-08	-7.009	-7.082	-0.073
	H2O	5.55E+01	9.99E-01	1.744	0	0
C(4)		6.09E-03				
	HCO3-	4.79E-03	4.10E-03	-2.32	-2.387	-0.067
	CO2	1.11E-03	1.11E-03	-2.956	-2.953	0.003
	CaHCO3+	1.03E-04	8.81E-05	-3.988	-4.055	-0.067
	MgHCO3+	5.38E-05	4.57E-05	-4.27	-4.34	-0.07
	NaHCO3	2.51E-05	2.52E-05	-4.601	-4.598	0.003
	CaCO3	4.47E-06	4.50E-06	-5.349	-5.346	0.003
	CO3-2	2.96E-06	1.59E-06	-5.529	-5.798	-0.269
	MgCO3	1.44E-06	1.45E-06	-5.842	-5.839	0.003
	NaCO3-	3.82E-07	3.25E-07	-6.419	-6.489	-0.07
Ca		3.48E-03				
	Ca+2	3.13E-03	1.68E-03	-2.505	-2.774	-0.269
	CaSO4	2.41E-04	2.43E-04	-3.618	-3.615	0.003
	CaHCO3+	1.03E-04	8.81E-05	-3.988	-4.055	-0.067
	CaCO3	4.47E-06	4.50E-06	-5.349	-5.346	0.003
	CaOH+	2.72E-09	2.31E-09	-8.566	-8.636	-0.07
Cl		1.59E-02				
	Cl-	1.59E-02	1.35E-02	-1.799	-1.871	-0.073
H(0)		2.05E-25				
	H2	1.03E-25	1.03E-25	-24.989	-24.986	0.003
K		7.33E-04				
	K+	7.29E-04	6.16E-04	-3.137	-3.21	-0.073
	KSO4-	3.71E-06	3.15E-06	-5.431	-5.501	-0.07
	KOH	1.76E-11	1.77E-11	-10.755	-10.752	0.003
Mg		1.96E-03				
	Mg+2	1.74E-03	9.53E-04	-2.759	-3.021	-0.262
	MgSO4	1.60E-04	1.62E-04	-3.795	-3.792	0.003
	MgHCO3+	5.38E-05	4.57E-05	-4.27	-4.34	-0.07
	MgCO3	1.44E-06	1.45E-06	-5.842	-5.839	0.003
	MgOH+	3.37E-08	2.86E-08	-7.473	-7.543	-0.07
Na		1.29E-02				
	Na+	1.28E-02	1.09E-02	-1.892	-1.961	-0.069
	NaSO4-	4.66E-05	3.96E-05	-4.332	-4.402	-0.07
	NaHCO3	2.51E-05	2.52E-05	-4.601	-4.598	0.003
	NaCO3-	3.82E-07	3.25E-07	-6.419	-6.489	-0.07
	NaOH	5.94E-10	5.98E-10	-9.226	-9.223	0.003
O(0)		0.00E+00				
	O2	0.00E+00	0.00E+00	-42.412	-42.409	0.003
S(-2)		0.00E+00				
	HS-	0.00E+00	0.00E+00	-63.678	-63.752	-0.073
	H2S	0.00E+00	0.00E+00	-63.679	-63.676	0.003
	S-2	0.00E+00	0.00E+00	-69.478	-69.752	-0.274
S(6)		1.81E-03				
	SO4-2	1.36E-03	7.23E-04	-2.866	-3.141	-0.275
	CaSO4	2.41E-04	2.43E-04	-3.618	-3.615	0.003
	MgSO4	1.60E-04	1.62E-04	-3.795	-3.792	0.003
	NaSO4-	4.66E-05	3.96E-05	-4.332	-4.402	-0.07
	KSO4-	3.71E-06	3.15E-06	-5.431	-5.501	-0.07
	HSO4-	9.98E-09	8.49E-09	-8.001	-8.071	-0.07
Si		4.30E-04				
	H4SiO4	4.29E-04	4.32E-04	-3.368	-3.365	0.003
	H3SiO4-	6.20E-07	5.27E-07	-6.208	-6.278	-0.07
	H2SiO4-2	5.68E-13	2.97E-13	-12.246	-12.527	-0.281

4.Group B

	Species	Molality	Activity	Log Molality	Log Activity	Log Gamma
	H+	4.58E-07	3.78E-07	-6.34	-6.423	-0.083
	OH-	3.46E-08	2.64E-08	-7.461	-7.578	-0.118
	H2O	5.55E+01	9.98E-01	1.744	-0.001	0
C(4)		3.43E-02				
	HCO3-	1.96E-02	1.54E-02	-1.709	-1.811	-0.103
	CO2	1.29E-02	1.32E-02	-1.891	-1.881	0.01
	CaHCO3+	1.28E-03	1.01E-03	-2.894	-2.997	-0.103
	MgHCO3+	3.32E-04	2.60E-04	-3.479	-3.586	-0.107
	NaHCO3	2.47E-04	2.52E-04	-3.608	-3.598	0.01
	CaCO3	1.61E-05	1.65E-05	-4.794	-4.784	0.01
	CO3-2	4.93E-06	1.92E-06	-5.307	-5.718	-0.411
	MgCO3	2.57E-06	2.63E-06	-5.59	-5.58	0.01
	NaCO3-	1.33E-06	1.04E-06	-5.878	-5.984	-0.107
Ca		1.70E-02				
	Ca+2	1.30E-02	5.11E-03	-1.885	-2.291	-0.406
	CaSO4	2.69E-03	2.75E-03	-2.571	-2.561	0.01
	CaHCO3+	1.28E-03	1.01E-03	-2.894	-2.997	-0.103
	CaCO3	1.61E-05	1.65E-05	-4.794	-4.784	0.01
	CaOH+	2.86E-09	2.24E-09	-8.543	-8.65	-0.107
Cl		4.00E-02				
	Cl-	4.00E-02	3.06E-02	-1.398	-1.514	-0.116
H(0)		1.98E-24				
	H2	9.89E-25	1.01E-24	-24.005	-23.995	0.01
K		3.65E-03				
	K+	3.59E-03	2.75E-03	-2.445	-2.561	-0.116
	KSO4-	6.69E-05	5.24E-05	-4.174	-4.281	-0.107
	KOH	2.46E-11	2.51E-11	-10.61	-10.6	0.01
Mg		4.74E-03				
	Mg+2	3.52E-03	1.44E-03	-2.454	-2.842	-0.389
	MgSO4	8.87E-04	9.08E-04	-3.052	-3.042	0.01
	MgHCO3+	3.32E-04	2.60E-04	-3.479	-3.586	-0.107
	MgCO3	2.57E-06	2.63E-06	-5.59	-5.58	0.01
	MgOH+	1.76E-08	1.38E-08	-7.754	-7.861	-0.107
Na		3.78E-02				
	Na+	3.71E-02	2.91E-02	-1.431	-1.537	-0.106
	NaSO4-	5.02E-04	3.92E-04	-3.3	-3.406	-0.107
	NaHCO3	2.47E-04	2.52E-04	-3.608	-3.598	0.01
	NaCO3-	1.33E-06	1.04E-06	-5.878	-5.984	-0.107
	NaOH	4.95E-10	5.07E-10	-9.305	-9.295	0.01
O(0)		0.00E+00				
	O2	0.00E+00	0.00E+00	-44.402	-44.392	0.01
S(-2	**)**	0.000e+00\par				
	H2S	0.00E+00	0.00E+00	-58.156	-58.147	0.01
	HS-	0.00E+00	0.00E+00	-58.6	-58.718	-0.118
	S-2	0.00E+00	0.00E+00	-64.791	-65.214	-0.422
S(6)		1.13E-02				
	SO4-2	7.18E-03	2.69E-03	-2.144	-2.57	-0.426
	CaSO4	2.69E-03	2.75E-03	-2.571	-2.561	0.01
	MgSO4	8.87E-04	9.08E-04	-3.052	-3.042	0.01
	NaSO4-	5.02E-04	3.92E-04	-3.3	-3.406	-0.107
	KSO4-	6.69E-05	5.24E-05	-4.174	-4.281	-0.107
	HSO4-	1.27E-07	9.90E-08	-6.898	-7.004	-0.107
Si		2.98E-04				
	H4SiO4	2.97E-04	3.04E-04	-3.527	-3.517	0.01
	H3SiO4-	1.52E-07	1.19E-07	-6.819	-6.926	-0.107
	H2SiO4-2	5.70E-14	2.14E-14	-13.244	-13.671	-0.427

Appendix 20: Input files for the inverse modelling of the four groups: A_{1a}, A_{1b}, A_2 and B calculated by means of PhreeqC.

1. Group A_{1a}

```
SOLUTION 1  Rain Water
        units   mmol/l
        pH      7
        temp    25
        Ca      0.14695
        Mg      0.03935
        Na      0.1372
        Cl      0.1289
        Alkalinity      0.1517999  as HCO3
        S       0.1244
        K       0.0197
SOLUTION 2  A1a
        units   mmol/l
        pH      6.776
        pe      4
        density 1
        temp    25
        redox   pe
        Ca      1.316991
        Mg      0.7404361
        Na      2.571988
        K       0.1354987
        Si      0.3315028
        Cl      2.686656
        Alkalinity      3.010343  as HCO3
        S       0.5713334
 INVERSE_MODELING 1
        -solutions      1  2
        -uncertainty 0.002
        -Range
        -phases
                Calcite
                Gypsum
      CO2(g)
                Dolomite
                Quartz
                Halite  dissolve
                K-feldspar
                Kx
                Nax
                Cax2
PHASES
Halite
      NaCl = Na+ + Cl-
      log_k   1.582
End
```

2. Group A_{1b}

```
SOLUTION 1  Rain Water
        units   mmol/l
        pH      7
        temp    25
        Ca      0.14695
        Mg      0.03935
        Na      0.1372
        Cl      0.1289
        Alkalinity      0.1517999  as HCO3
        S       0.1244
        K       0.0197
SOLUTION 2  A1b
        units   mmol/l
        pH      6.907
        pe      4
        density 1
        temp    25
        redox   pe
        Ca      2.064995
        Mg      1.44998
        Na      2.666664
        K       0.149821
        Si      0.3705558
        Cl      2.850726
        Alkalinity      5.170223  as HCO3
        S       0.9159657
 INVERSE_MODELING 1
        -solutions      1  2
        -uncertainty 0.002
        -Range
        -phases
                Calcite
                Gypsum
      CO2(g)
                Dolomite
                Quartz
                Halite  dissolve
                K-feldspar
                Kx
                Nax
                Cax2
PHASES
Halite
      NaCl = Na+ + Cl-
      log_k   1.582
End
```

3. Group A_2

```
SOLUTION 1  Rain Water
        units   mmol/l
        pH      7
        temp    25
        Ca      0.14695
        Mg      0.03935
        Na      0.1372
        Cl      0.1289
        Alkalinity      0.1517999  as HCO3
        S       0.1244
        K       0.0197
SOLUTION 2  A2
        units   mmol/l
        pH      6.918
        pe      4
        density 1
        temp    25
        redox   pe
        Ca      3.469501
        Mg      1.95375
        Na      12.88885
        K       0.7315
        Si      0.4288567
        Cl      15.87434
        Alkalinity      4.980591  as HCO3
        S       1.81009
 INVERSE_MODELING 1
        -solutions      1  2
        -uncertainty 0.002
        -Range
        -phases
      Calcite
                Gypsum
                CO2(g)
      Dolomite
                Quartz
                Halite  dissolve
                K-feldspar
                Kx
                Nax
                Cax2
PHASES
Halite
      NaCl = Na+ + Cl-
      log_k   1.582

End
```

4. Group B

```
SOLUTION 1  Rain Water
        units   mmol/l
        pH      7
        temp    25
        Ca      0.14695
        Mg      0.03935
        Na      0.1372
        Cl      0.1289
        Alkalinity      0.1517999  as HCO3
        S       0.1244
        K       0.0197
SOLUTION 2  B
        units   mmol/l
        pH      6.4225
        pe      4
        density 1
        temp    25
        redox   pe
        Ca      16.9
        Mg      4.712497
        Na      37.62497
        K       3.633734
        Si      0.2958063
        Cl      39.79832
        Alkalinity      21.34146  as HCO3
        S       11.26178
 INVERSE_MODELING 1
        -solutions      1  2
        -uncertainty 0.005
        -Range
        -phases
     Calcite
                Gypsum
                CO2(g)
      Dolomite
                Quartz
                Halite  dissolve
                K-feldspar
                Kx
                Nax
                Cax2
PHASES
Halite
      NaCl = Na+ + Cl-
      log_k   1.582

End
```

Appendix 21: Chemical analysis of Al-Hammam spring and its average after El-Naser (1991).

Parameter	**Value**			**Average**
Date	Jan.72[1]	Dec.88	May.89	
T (^{o}C)	-	27	29	28
EC (μs/cm)	3150	3420	3250	3273
PH	-	6.35	6.45	6.40
Ca (meq/l)	13.10	15.88	14.82	14.60
Mg (meq/l)	4.10	4.61	4.18	4.30
Na (meq/l)	17.50	15.59	15.18	16.05
K (meq/l)	1.13	1.21	1.38	1.24
Cl (meq/l)	13.90	13.69	14.06	13.97
HCO_3 (meq/l)	8.09	8.61	8.74	8.48
SO_4 (meq/l)	13.73	14.9	14.56	14.40
NO_3 (meq/l)	-	0.02	0.02	0.02

[1]Source: Water Quality in Jordan (1979).

Appendix 22: Chemical analysis of Rasun, Ain Diek, El-Qantarah, Ain Jarash, El Maghasil, Nu'aymeh, Yarmouk University #1, Aurjan Foga, Et Teis springs and wells and their average. The Tempreature in (^{o}C), the EC in (µs/cm) while the chemical constituents are in (meq/l) after El-Naser (1991).

Parameters	**Rasun spring[r]**	**Ain Diek[r]**	**El-Qantarah[r]**	**Ain Jarash[r]**	**El Magahsil[r]**	**Nu'aymeh Mun #1**	**Yarmouk Uni.#1**	**Aurjan Foga**	**Et Teis**	**Average**
Date	-	-	-	-	-	Dec.89	Dec.89	Dec.89	Dec.89	-
T (^{o}C)	17.9	-	-	-	-	22	22	18	18	20
EC (µs/cm)	660	608	624	590	500	565	610	690	600	605
pH	7.44	7.8	7.9	7.20	7.27	7.35	7.45	7.03	7.54	7.44
Ca (meq/l)	4.57	3.84	3.94	4.08	3.6	3.28	3.6	4.32	4.22	3.94
Mg (meq/l)	1.17	1.65	1.18	0.94	0.66	1.63	1.9	1.66	0.82	1.29
Na (meq/l)	0.7	0.7	0.9	0.65	0.6	0.95	0.8	0.76	0.43	0.72
K (meq/l)	0.07	0.08	0.23	0.10	0.00	0.05	0.05	0.04	0.02	0.07
Cl (meq/l)	0.78	0.8	1.08	0.58	0.56	1.03	1	1.10	0.74	0.85
HCO_3 (meq/l)	5.13	4.75	4.24	4.72	3.94	4.25	4.7	5.25	4.73	4.63
SO_4 (meq/l)	0.06	0.1	0.1	0.18	0.16	0.25	0.2	0.11	0.10	0.14
NO_3 (meq/l)	0.41	0.49	0.86	0.52	0.18	0.35	0.4	0.22	0.17	0.4

[r] Source: Rimawi (1985).

Appendix 23: The Ionic ratios of the samples of both the upper aquifer (B2/A7) and the lower sandstone aquifer (Zarqa and Kurnub).

No.	Well/spring	Na/Cl	Ca/Cl	Mg/Cl	Mg/Ca	Ca/SO_4	SO_4/Cl	Na/Ca	K/Cl	Ca/SO_4+HCO_3	HCO_3/Cl	EC(µs/cm)
1	EL-Mokhybeh	1.29	1.29	0.83	0.64	3.64	0.36	0.99	0.07	0.31	3.85	772.5
2	El-Hmmeh/Maqla	0.90	0.50	0.27	0.53	1.81	0.28	1.77	0.05	0.41	0.94	1419.5
3	El-Hammeh/Bajeh	0.78	0.80	0.51	0.63	2.67	0.30	0.98	0.06	0.37	1.85	1036
4	North Shuneh hot well	0.92	0.56	0.54	0.98	1.60	0.35	1.65	0.03	0.31	1.47	1094.5
5	Waqas well	1.46	1.75	1.50	0.86	3.28	0.53	0.83	0.09	0.27	6.00	725
6	Abu-Zyad Well	0.93	0.49	0.29	0.59	2.14	0.23	1.89	0.07	0.37	1.10	2185
7	Abu-Thableh	0.90	0.51	0.28	0.55	2.25	0.22	1.79	0.05	0.39	1.08	1967
8	Abu El-Zeeghan/1	0.71	0.57	0.18	0.32	1.67	0.34	1.24	0.13	0.57	0.65	6465
9	Abu El-Zeeghan/2	1.07	0.35	0.08	0.24	1.38	0.25	3.10	0.07	0.48	0.47	10375
10	Al-Kafreen well	0.85	0.68	0.48	0.70	2.18	0.31	1.25	0.06	0.36	1.59	848
11	Zara/Istraha	0.88	0.20	0.11	0.56	1.46	0.14	4.43	0.05	0.46	0.30	2027
12	Zara/Maghara	0.86	0.22	0.10	0.46	1.79	0.12	3.95	0.05	0.50	0.31	2285
13	El-Seel El-Hami	0.88	0.23	0.10	0.43	1.53	0.15	3.83	0.05	0.52	0.29	1400
14	Tal El-Rojom	0.87	0.23	0.09	0.39	1.53	0.15	3.80	0.05	0.57	0.25	1550.5
15	Maain/El-Mabkhara	0.92	0.16	0.07	0.45	1.57	0.10	5.71	0.05	0.49	0.23	3100
16	Maain/El-Ameer	0.92	0.15	0.09	0.56	1.46	0.10	6.07	0.05	0.45	0.23	3075
17	Maain/ElShallal	0.95	0.14	0.07	0.50	1.34	0.10	6.77	0.05	0.44	0.21	3070
18	TA1	0.42	0.21	0.17	0.79	5.11	0.04	1.98	0.03	1.24	0.13	3815
19	TA2	1.02	0.38	0.19	0.50	1.82	0.21	2.67	0.07	0.38	0.80	1006
20	Iben Hammad	1.16	0.45	0.25	0.54	2.29	0.20	2.55	0.06	0.32	1.23	753
21	Burbyta	0.90	0.51	0.26	0.50	2.43	0.21	1.77	0.05	0.40	1.08	539
22	Afra/Sawna	0.66	0.64	0.47	0.74	2.74	0.23	1.03	0.02	0.38	1.46	560.5
23	Afra/Maqla	0.87	0.62	0.34	0.55	2.82	0.22	1.40	0.02	0.38	1.41	544

Appendix 24: The chemical signatures of the thermal waters compared to the Dead Sea signatures.

No.	Name of the spring/well	Mg/Ca	HCO3/Cl	Na/Cl
1	EL-Mokhybeh	0.39	6.62	0.83
2	El-Hmmeh/Maqla	0.32	1.63	0.58
3	El-Hammeh/Bajeh	0.38	3.18	0.51
4	North Shuneh hot well	0.59	2.53	0.60
5	Waqas well	0.52	10.33	0.95
6	Abu-Zyad Well	0.36	1.89	0.60
7	Abu-Thableh	0.33	1.86	0.59
8	Abu El-Zeeghan/1	0.20	1.12	0.46
9	Abu El-Zeeghan/2	0.15	0.82	0.70
10	Al-Kafreen well	0.43	2.74	0.55
11	Zara/Istraha	0.34	0.51	0.57
12	Zara/Maghara	0.28	0.53	0.56
13	El-Seel El-Hami	0.26	0.50	0.57
14	Tal El-Rojom	0.24	0.43	0.56
15	Ma'in/El-Mabkhara	0.27	0.39	0.60
16	Ma'in/El-Ameer	0.34	0.40	0.60
17	Ma'in/ElShallal	0.30	0.37	0.62
18	TA1	0.48	0.23	0.27
19	TA2	0.30	1.38	0.66
20	Iben Hammad	0.33	2.11	0.75
21	Burbyta	0.30	1.85	0.58
22	Afra/Sawna	0.45	2.51	0.43
23	Afra/Maqla	0.33	2.43	0.57

Appendix 25: Thermal waters classification based on the total hardness.

No.	Well/Spring	TH	Classification
1	EL-Mokhybeh	296.48	Hard
2	El-Hmmeh/Maqla	440.07	Very Hard
3	El-Hammeh/Bajeh	392.48	Very Hard
4	North Shuneh hot	380.52	Very Hard
5	Waqas well	292.37	Hard
6	Abu-Zyad Well	668.27	Very Hard
7	Abu-Thableh	612.32	Very Hard
8	Abu El-Zeeghan/1	2093.99	Very Hard
9	Abu El-Zeeghan/2	2232.17	Very Hard
10	Al-Kafreen well	306.69	Very Hard
11	Zara/Istraha	404.79	Very Hard
12	Zara/Maghara	468.16	Very Hard
13	El-Seel El-Hami	288.62	Hard
14	Tal El-Rojom	316.16	Very Hard
15	Ma'in/El-Mabkhara	501.44	Very Hard
16	Ma'in/El-Ameer	506.55	Very Hard
17	Ma'in/ElShallal	455.86	Very Hard
18	TA1	1201.59	Very Hard
19	TA2	258.31	Hard
20	Iben Hammad	202.78	Hard
21	Burbyta	167.04	Hard
22	Afra/Sawna	214.70	Hard
23	Afra/Maqla	186.02	Hard

Appendix 26: Jordanian drinking water Standards

1. The Parameters that have Aesthetic effect:

Parameters	Permissible level	Maximum permissible level
	(mg/l)	(mg/l)
PH	6.5-8.5	-
TDS	500	1500
NH_4	0.5	0.5
Al	0.1	0.2
Mn	0.1	0.2
Fe	0.3	1
Cu	1	1.5
Zn	3	5
Na	200	400
Cl	200	500
SO_4	200	500

Appendix 26 (continue): Jordanian drinking water Standards

2. The Parameters that have a health significance:

Parameters	**Permissible level**
	(mg/l)
As	0.01
Pb	0.01
CN	0.07
Cd	0.003
Cr	0.05
Ba	1.5
Se	0.05
B	2
Hg	0.002
Ag	0.1
Ni	0.07
Sb	0.005
F	2
NO_2	2
NO_3	50 *

* allowed until 70mg/l when no better water resource is available

Appendix 27: World Health Organization (WHO) guidelines for drinking water:

1. The parameters that have aesthetic effect:

Parameters	**WHO guidelines (1996) (mg/l)**
TDS	1000
Na	200
K	12
Cl	250
SO_4	250
NO_3	50
Hardness	500
Fe	0.3
Mn	0.1
Cu	1
Zn	3

Appendix 27 (continue): World Health Organization (WHO) guidelines for drinking water:

2. The parameters that have a health significance:

Parameter	WHO guidelines (1996) (mg/l)
Pb	0.01
As	0.01
Cr	0.05
Cd	0.003
Ni	0.02
F	1.5

Appendix 28: Thermal waters classification based on the salinity (EC) values.

No.	Well/Spring	Level
1	EL-Mokhybeh	C3
2	El-Hmmeh/Maqla	C3
3	El-Hammeh/Bajeh	C3
4	North Shuneh hot well	C3
5	Waqas well	C2
6	Abu-Zyad Well	C3
7	Abu-Thableh	C3
8	Abu El-Zeeghan/1	C4
9	Abu El-Zeeghan/2	C4
10	Al-Kafreen well	C3
11	Zara/Istraha	C3
12	Zara/Maghara	C4
13	El-Seel El-Hami	C3
14	Tal El-Rojom	C3
15	Ma'in/El-Mabkhara	C4
16	Ma'in/El-Ameer	C4
17	Ma'in/El-Shallal	C4
18	TA1	C4
19	TA2	C3
20	Iben Hammad	C3
21	Burbyta	C2
22	Afra/Sawna	C2
23	Afra/Maqla	C2

Appendix 29: Thermal waters classification based on the soluble sodium percent (SSP).

No.	Well/Spring	SSP	Water class
1	EL-Mokhybeh	24.24	Good
2	El-Hmmeh/Maqla	37.96	Good
3	El-Hammeh/Bajeh	24.38	Good
4	North Shuneh hot well	30.17	Good
5	Waqas well	19.25	Excellent
6	Abu-Zyad Well	39.02	Good
7	Abu-Thableh	37.73	Good
8	Abu El-Zeeghan/1	35.48	Good
9	Abu El-Zeeghan/2	57.16	Permissible
10	Al-Kafreen well	28.14	Good
11	Zara/Istraha	60.01	Doubtfull
12	Zara/Maghara	59.01	Permissible
13	El-Seel El-Hami	58.73	Permissible
14	Tal El-Rojom	59.06	Permissible
15	Ma'in/El-Mabkhara	67.57	Doubtful
16	Ma'in/El-Ameer	67.12	Doubtful
17	Ma'in/ElShallal	70.29	Doubtful
18	TA1	37.05	Good
19	TA2	48.71	Permissible
20	Iben Hammad	46.48	Permissible
21	Burbyta	38.23	Good
22	Afra/Sawna	23.54	Good
23	Afra/Maqla	31.65	Good

Appendix 30: Thermal waters classification based on the sodium adsorption ratio (SAR).

No.	Well/Spring	SAR	Level
1	EL-Mokhybeh	1.05	S1
2	El-Hmmeh/Maqla	2.43	S1
3	El-Hammeh/Bajeh	2.19	S1
4	North Shuneh hot well	1.63	S1
5	Waqas well	0.77	S1
6	Abu-Zyad Well	3.08	S1
7	Abu-Thableh	2.85	S1
8	Abu El-Zeeghan/1	4.27	S1
9	Abu El-Zeeghan/2	11.80	S2
10	Al-Kafreen well	1.28	S1
11	Zara/Istraha	5.70	S1
12	Zara/Maghara	5.87	S1
13	El-Seel El-Hami	4.56	S1
14	Tal El-Rojom	4.86	S1
15	Ma'in/El-Mabkhara	8.85	S1
16	Ma'in/El-Ameer	8.73	S1
17	Ma'in/ElShallal	9.63	S1
18	TA1	3.84	S1
19	TA2	2.86	S1
20	Iben Hammad	2.35	S1
21	Burbyta	1.52	S1
22	Afra/Sawna	0.87	S1
23	Afra/Maqla	1.23	S1

Appendix 31: Thermal water classification based on the Wilcox diagram.

No.	Well/Spring	Water class
1	EL-Mokhybeh	C3-S1
2	El-Hmmeh/Maqla	C3-S1
3	El-Hammeh/Bajeh	C3-S1
4	North Shuneh hot well	C3-S1
5	Waqas well	C3-S1
6	Abu-Zyad Well	C3-S1
7	Abu-Thableh	C3-S1
8	Abu El-Zeeghan/1	Out of range
9	Abu El-Zeeghan/2	Out of range
10	Al-Kafreen well	C3-S1
11	Zara/Istraha	C3-S2
12	Zara/Maghara	C4-S2
13	El-Seel El-Hami	C3-S1
14	Tal El-Rojom	C3-S2
15	Ma'in/El-Mabkhara	C4-S3
16	Ma'in/El-Ameer	C4-S3
17	Ma'in/ElShallal	C4-S3
18	TA1	C4-S2
19	TA2	C3-S1
20	Iben Hammad	C3-S1
21	Burbyta	C2-S1
22	Afra/Sawna	C2-S1
23	Afra/Maqla	C2-S1

Appendix 32: recommended maximum concentrations of trace elements in irrigation water (Ayers and Westcot 1994).

Element	**Recommended Maximum Concentration (mg/l)**	**Remarks**
Al(aluminium)	5.0	Can cause non-productivity in acid soils (pH < 5.5), but more alkaline soils at pH > 7.0 will precipitate the ion and eliminate any toxicity.
As (arsenic)	0.10	Toxicity to plants varies widely, ranging from 12 mg/l for Sudan grass to less than 0.05 mg/l for rice.
Be (beryllium)	0.10	Toxicity to plants varies widely, ranging from 5 mg/l for kale to 0.5 mg/l for bush beans.
Cd (cadmium)	0.01	Toxic to beans, beets and turnips at concentrations as low as 0.1 mg/l in nutrient solutions. Conservative limits recommended due to its potential for accumulation in plants and soils to concentrations that may be harmful to humans.
Co (cobalt)	0.05	Toxic to tomato plants at 0.1 mg/l in nutrient solution. Tends to be inactivated by neutral and alkaline soils.
Cr (chromium)	0.10	Not generally recognized as an essential growth element. Con-servative limits recommended due to lack of knowledge on its toxicity to plants.
Cu (copper)	0.20	Toxic to a number of plants at 0.1 to 1.0 mg/l in nutrient solutions.
F (fluoride)	1.0	Inactivated by neutral and alkaline soils.
Fe (iron)	5.0	Not toxic to plants in aerated soils, but can contribute to soil acidification and loss of availability of essential phosphorus and molybdenum. Overhead sprinkling may result in unsightly deposits on plants, equipment and buildings.
Li (lithium)	2.5	Tolerated by most crops up to 5 mg/l; mobile in soil. Toxic to citrus at low concentrations (<0.075 mg/l). Acts similarly to boron.
Mn (manganese)	0.20	Toxic to a number of crops at a few-tenths to a few mg/l, but usually only in acid soils.
Mo (molybdenum)	0.01	Not toxic to plants at normal concentrations in soil and water. Can be toxic to livestock if forage is grown in soils with high concentrations of available molybdenum.
Ni (nickel)	0.20	Toxic to a number of plants at 0.5 mg/l to 1.0 mg/l; reduced toxicity at neutral or alkaline pH.
Pd (lead)	5.0	Can inhibit plant cell growth at very high concentrations.
Se (selenium)	0.02	Toxic to plants at concentrations as low as 0.025 mg/l and toxic to livestock if forage is grown in soils with relatively high levels of added selenium. An essential element to animals but in very low concentrations.
Ti (titanium)	----	Effectively excluded by plants; specific tolerance unknown.
V (vanadium)	0.10	Toxic to many plants at relatively low concentrations.

Appendix 33: Thermal waters classification based on the Langlier saturation index (LSI).

No.	Well/Spring	PH	PHs	ΔpH	Water Agresivity
1	EL-Mokhybeh	7.12	7.03	0.09	Balanced
2	El-Hmmeh/Maqla	7.02	6.89	0.13	Balanced
3	El-Hammeh/Bajeh	6.87	6.88	-0.01	Balanced
4	North Shuneh hot	6.85	6.83	0.02	Balanced
5	Waqas well	6.96	6.92	0.04	Balanced
6	Abu-Zyad Well	6.58	6.47	0.11	Balanced
7	Abu-Thableh	6.72	6.64	0.08	Balanced
8	Abu El-Zeeghan/1	6.32	6.08	0.24	Scale forming
9	Abu El-Zeeghan/2	6.53	6.11	0.42	Scale forming
10	Al-Kafreen well	6.64	6.91	-0.27	Aggressive
11	Zara/Istraha	7.14	7.05	0.09	Balanced
12	Zara/Maghara	7.1	6.92	0.18	Balanced
13	El-Seel El-Hami	6.41	6.77	-0.36	Aggressive
14	Tal El-Rojom	7.62	7.26	0.36	Scale forming
15	Ma'in/El-Mabkhara	6.26	6.43	-0.17	Balanced
16	Ma'in/El-Ameer	6.66	6.72	-0.06	Balanced
17	Ma'in/ElShallal	7.85	7.06	0.79	Scale forming
18	TA1	6.88	6.70	0.18	Balanced
19	TA2	6.7	6.95	-0.25	Aggressive
20	Iben Hammad	6.89	7.13	-0.24	Aggressive
21	Burbyta	6.61	7.13	-0.52	Aggressive
22	Afra/Sawna	6.88	7.14	-0.26	Aggressive
23	Afra/Maqla	6.82	7.13	-0.31	Aggressive

Appendix 34: Thermal waters description based on the saturation index (SI) and the recommended treatment.

No.	Well/Spring	SI Calcite	Description	General recommendation
1	EL-Mokhybeh	0.14	Near balanced	No treatment
2	El-Hmmeh/Maqla	0.20	Near balanced	No treatment
3	El-Hammeh/Bajeh	-0.02	Near balanced	No treatment
4	North Shuneh hot well	0.03	Near balanced	No treatment
5	Waqas well	0.08	Near balanced	No treatment
6	Abu-Zyad Well	0.21	Near balanced	No treatment
7	Abu-Thableh	0.14	Near balanced	No treatment
8	Abu El-Zeeghan/1	0.46	Some faint coating	Probably no treatment
9	Abu El-Zeeghan/2	0.78	Mild scale coating	Treatment my be needed
10	Al-Kafreen well	-0.47	Non-mild corrosion	Probably no treatment
11	Zara/Istraha	0.13	Near balanced	No treatment
12	Zara/Maghara	0.25	Near balanced to some faint coating	Probably no treatment
13	El-Seel El-Hami	-0.63	Non-mild corrosion	Probably no treatment
14	Tal El-Rojom	0.42	Some faint coating	Probably no treatment
15	Ma'in/El-Mabkhara	0.34	Some faint coating	Probably no treatment
16	Ma'in/El-Ameer	-0.10	Near balanced	No treatment
17	Ma'in/ElShallal	0.94	Mild scale coating	Treatment may be needed
18	TA1	0.25	Near balanced to some faint coating	Probably no treatment
19	TA2	-0.41	Non-mild Corrosion	Probably no treatment
20	Iben Hammad	-0.37	Non-mild Corrosion	Probably no treatment
21	Burbyta	-0.84	Mild Corrosion	Treatment my be needed
22	Afra/Sawna	-0.39	Non-mild Corrosion	Probably no treatment
23	Afra/Maqla	-0.48	Non-mild Corrosion	Probably no treatment